VIBRATION AND LOADS IN HINGELESS ROTORS

Volume I - Theoretical Analyses

By G.A. Watts and R.J. London
September 1972

Prepared under Contract No. NAS2-5168 Phase II, by

LOCKHEED-CALIFORNIA COMPANY

Rotary Wing Division
Van Nuys, California

for

U.S. ARMY AIR MOBILITY RESEARCH AND DEVELOPMENT LABORATORY
AMES DIRECTORATE

and

NATIONAL AERONAUTICS AND SPACE ADMINISTRATION
AMES RESEARCH CENTER

SUMMARY

Analytic methods are developed for calculating blade loads and shaft-transmitted vibratory forces in stiff bladed hingeless rotors operating at advance ratios from $\mu = .3$ to $\mu = 2.0$.

Calculated shaft harmonic moments compared well with experimental values when the blade first flap frequency was in the region of two-per-revolution harmonic excitation. Calculated blade bending moment azimuthal distributions due to changes in cyclic pitch agreed well with experiment at radial stations near the blade root at values of the ratio of first flap frequency to rotor rotation rate from 1.5 to 5.0. At stations near the blade tip good agreement was only obtained at the higher values of frequency ratio.

A compendium of experimental shaft transmitted force and blade loads data for two different rotor systems is included in Volume II.

CONTENTS

	Page
SUMMARY	iii
INTRODUCTION	1
SYMBOLS	7
HINGELESS ROTOR TYPES STUDIED	15
Geometry Variations	15
Degrees of Freedom	19
Vertical motions of mass elements	21
In-plane motions of mass elements	30
Kinematic Relationships	37
Vertical motions blade-rotor kinematics	37
In-plane motions blade-rotor kinematics	45
Theoretical Considerations	51
Aerodynamic simplifications	51
In-plane motion of a single blade	56
Flap in-plane inertia coupling	57
High-speed gyroscope	57
Mean aeroelastic derivatives	58
Oscillatory Aeroelastic derivatives	60
Residual forces	62

CONTENTS (cont.)

	Page
VERTICAL MOTIONS EQUATIONS	65
Single Blade Equations of Motion	65
Single blade inertia matrix	66
Single blade centrifugal and structural matrix	68
Single blade aerodynamic matrices	69
Rotor Equations of Motion	73
Rotor equations of motion in rotating axes	73
Transformation to stationary axes	79
Complete Vertical Equations of Motion	82
Body terms	82
Inertia	82
Aerodynamic	84
Gyroscope terms	86
Complete vertical equations	87
IN-PLANE MOTIONS EQUATIONS	89
Single Blade Equations of Motion	90
Blade inertia matrix	91
Blade coriolis matrix	92
Blade centrifugal and structural matrix	93
Blade aerodynamic matrices	95
In-plane Equations of the Rotor	98
Body terms	103
The homogeneous equation	103

CONTENTS (cont.)

	Page
In-plane Forcing Functions	104
In-plane forcing due to vertical motions	105
In-plane forcing due to vertical aerodynamic forces	108
In-plane forcing due to minimum drag coefficient	115
Complete In-plane Equations of Motion	117
SOLUTION OF VERTICAL MOTIONS EQUATIONS	119
General Discussion	119
Why there is no subharmonic response	125
Three- and Four-Blade Rotors	129
Fixed-shaft fixed-swashplate solution	130
Tip path motions	143
Mean aeroelastic derivatives	147
Oscillatory aeroelastic derivatives	180
Fixed shaft, free swashplate	232
Free shaft, free swashplate	239
SOLUTION OF IN-PLANE MOTIONS EQUATIONS	241
Stability of In-plane Motions	241
BLADE LOADS	247
Principles Involved in Blade Loads Determination	247
Blade Flap Bending Moments, 33-Foot Rotor	250
CONCLUDING REMARKS	268
REFERENCES	271

INTRODUCTION

Within the spectrum of VTOL aircraft types there is a class that must have a low downwash velocity for efficient hovering and to avoid excessive disturbance to the surface and persons standing below. It also must possess high speed, long range, and flight characteristics that are not fatiguing to the pilot or passengers even in gusty conditions. It must also possess a low initial cost and inexpensive maintenance to be commercially or militarily viable.

The low downwash velocity in hovering flight demands a low disk loading or large disk area per unit weight. At present this requirement can be met only by large diameter rotors. The need for rotors designed for high forward speed, low drag, rapid highly damped response to control motions, mild response to gusts, and low vibration level has stimulated a search for a simpler, more inherently stable rotor system than found on most helicopters in operation today.

One approach to meeting these requirements has been the development of the "hingeless" rotor. The hingeless rotor differs from those found in most currently flying helicopters in that its blades possess only bearings for feathering motion, which is controlled rather than free, and no flapping or lead-lag hinges. The blades of most conventional helicopters are essentially gimballed near the mast or they may be joined rigidly together and the whole rotor gimballed to the top of the mast (teetering rotors).

Two main advantages of the hingeless or cantilever-bladed rotor are its ability to apply hub moments through the shaft to the body rapidly and of generally greater magnitude than available from articulated rotors, and its making available larger and more appropriately aligned damping forces due to body pitch and roll rotation rates. These potential advantages, of course, have long been appreciated in the helicopter world for the cantilever-bladed rotor. They could not be taken advantage of in the past, however, due to the extreme gust sensitivity of such a system and the extreme and variable cross-coupling of the cyclic and lift producing controls.

With the development, over the past fifteen years, of the directly geared gyroscope-stabilized feathering system, gust sensitivity and controls cross-coupling have been greatly reduced and rapidly responding hingeless rotor helicopters with highly stable body modes have been developed and demonstrated.

The development of the hingeless rotor gyroscope-stabilized system, however, has not been without its problems, most of which stemmed from the lack of significant damping in the blade in-plane modes. As opposed to the flapping modes which are highly damped by aerodynamic forces, the in-plane aerodynamic damping is small. Under near 2P resonant conditions, the in-plane forces and motions can combine with the flapping deflections and forces to nullify the hub moment feedback path to the gyroscope and produce instability. This particular problem has been solved in two ways. First, the in-plane resonance has been kept to a low rotor rpm and tight control has been maintained on the rpm to avoid the dangerous region. The second solution has been to substitute direct hub moment feedback for the hub moment feedback via feathering moments, thus eliminating the in-plane motion sensitive part of the feedback path.

Another in-plane resonance problem occurs in rotors with more than three blades. Pilot-induced oscillations can lead to high stresses in the reactionless modes. These modes are particularly lightly damped since there is no shaft motion present in the mode and therefore no damping from the body. Again, strictly keeping away from the resonance has been the solution.

One more possible consequence of light in-plane damping, which can be avoided by careful distribution of mass and stiffness on either side of the feathering hinge, is flap-lag instability. This is caused by coupling of the in-plane and flap blade modes at high collective pitch and is discussed in detail in Reference 1.

In recognition of the importance of in-plane motion to the development of satisfactory hingeless rotors, the present study has investigated the in-plane behavior of multibladed rotors.

Along with the large mean hub moment capability of the hingeless rotor comes inevitably the capacity to produce large oscillatory hub moments. As long as the advance ratio stays well below $\mu = 1.0$, however, they are normally not significant, except in certain transition flight conditions. But at advance ratio greater than $\mu = 1.0$, the shaft vibration force levels become very important. And since it appears that the next major developments in hingeless rotor vehicles involve flying at advance ratios greater than $\mu = 1.0$, the present study investigated shaft-transmitted vibratory forces due to high advance ratio.

A basic problem in hingeless rotor design is the creation of section structural properties that do not pick up excessive stresses under any operating or transient condition and that at the same time maintain radial mass and stiffness distributions which keep the desired characteristics and avoid instability. In the next generation of hingeless rotor aircraft, expected to operate at reduced rotor rpm and $\mu > 1.0$, this problem is especially acute. Endurance limit stresses must not be exceeded if blades of sufficient life expectancy are to be produced.

Because of the fundamental nature of blade stress determination to advanced rotor design, the azimuthal distribution of blade section flap bending moment were investigated in this study.

The results of these studies are expected to provide a basis for the systematic optimization of the design of the next generation of high speed compound helicopters. This includes the slowed hingeless rotor compound helicopter that cruises at a speed of 300 to 350 knots with the rotor slowed to as little as half the hovering rpm, and is characterized by low rotor lift and advance ratio to $\mu = 1.5$. It also includes, at some future date, the stowable rotor aircraft with the speed of fixed wing aircraft, low rotor lift during conversion, rotor slowed to zero rpm and then stowed within the fuselage.

The specific purposes of this study were as follows:

1. Derive the equations of vertical and in-plane mass element motion for three-and four-blade rotor-body free-flight configurations with gyroscope-stabilized swashplates.

2. Analyze the equations for their steady harmonically forced vibratory response in the form of mean and harmonic aeroelastic shaft-transmitted forces.

3. Analyze the equations for blade section lift and flap bending moment variation with azimuth.

4. Analyze experimental shaft vibratory, and blade load data for three rotors:

   a. A 33-foot 3-blade rotor with a high constant speed gyroscope-stabilized swashplate and fixed shaft.

   b. A 7.5-foot 4-blade rotor with fixed shaft and swashplate.

   c. The 35-foot 4-blade rotor of the XH-51A compound helicopter in free flight with a rotor speed gyro-stabilized swashplate and the shaft restrained by the free body.

5. Compare theory and experiment.

6. Parameter range for which the study is valid is as follows:

   a. Stiff bladed rotors $P > 1.3$.

   b. High advance ratio $\mu > .3$.

   c. Subcritical advancing tip $M_{1_{90}} < .85$.

Phase I of this study (References 2, 3, and 4) investigated the vertical motions equations of the 33-foot 3-blade rotor. The mean hub and swashplate moment and thrust mean aeroelastic derivatives were calculated, neglecting the effects of the harmonic differential equation coefficients as is the practice with conventional articulated rotors at low advance ratio. Good agreement was obtained with experiment at low values of advance ratio. Cyclic pitch to trim hub and swashplate moments to zero, control effectiveness, and stability of the gyro-stabilized system were also investigated and reasonable agreement found with experiment.

Equations of flapping motion, including aerodynamics, were found for the 7.5-foot rotor by Sissingh and Kuczynski in References 5 and 6. The mean aeroelastic derivatives of hub moment with respect to cyclic and

collective pitch and angle-of-attack were calculated, including effects of blade mean, first and second harmonic response. Good agreement was obtained with experiment.

Effects of induced inflow and first and second blade flapping modes were investigated by Ormiston and Peters in Reference 7. This study showed the necessity of including more than one flap mode if the ratio of flap frequency to rotor rotational frequency was less than 1.3. It also showed the large influence of induced inflow at advance ratio $\mu < .3$ and also that significant effects of induced flow existed at all advance ratio.

The necessity of including the rotor and gyroscope degrees of freedom in the equations of motion of the total airframe is shown by Heimbold and Griffith in Reference 8.

Blade section aerodynamic lift and flap and in-plane bending moments presented by Bartsch in Reference 9, Volumes I and II, and comparison with comprehensive method results by Sweers, in Volume III, for flight tests of the XH-51A compound helicopter, form a data base for assessing the validity of the current formulation in the modest μ, low flap frequency range.

Deckert and Mc Cloud analyzed 33-foot rotor data in Reference 10 and discovered that hub moments produced by cyclic pitch approach zero as rotor rpm and advance ratio approach zero and infinity respectively, thereby precluding their use in trimming mean hub moments. They also showed that small values of cyclic pitch were useful, at high advance ratio, in reducing shaft vibration.

The experimental testing of the 33-foot 3-blade rotor analyzed under this contract took place in the NASA-Ames Research Center 40 by 80 foot wind tunnel. The maximum wind speed attained was 120 knots and advance ratios of $\mu = .4, .5, .8, 1.1$, and 2.0 were tested over ranges of rotor rpm.

Four mass and stiffness configurations of the 7.5-foot 4-blade rotor were tested in the U. S. Army Air Mobility R and D Laboratory, Ames Directorate 7 by 10 foot wind tunnel. The advance ratio range extended from .29 to 1.75 and flap frequency ratio extended from P = 1.22 to 2.32.

Flight testing of the XH-51A compound helicopter was performed by the Lockheed-California Company, Rotary Wing Division.

The equations of motion derived in this study were programmed on the IBM 360 digital computer, and the CPS (Conversational Programming System) terminal was employed in the analysis of the experimental data.

In the design of compound helicopters for flight to advance ratios greater than unity ($\mu > 1.0$) elimination of shaft-transmitted vibratory forces and the control of blade stress excursions are expected to be the main tasks. This study has indicated the nature and causes of these two phenomena and provided a straightforward analytic tool for their prediction. The groundwork has therefore been laid for the invention of devices, such as harmonic swashplate control, and optimization of design for the minimization of flight loads and vibrations in advanced hingeless rotor helicopters.

It is also possible, with vibration and loads calculable at extreme values of design and flight operation parameters, that refinements in the methods may be made which will allow calculations in the realm of the conventional helicopter.

SYMBOLS

Symbols and matrices employed in the vertical motions equations are shown first. Those required for the in-plane equations follow, and subscripts common to both systems complete the section.

b	number of blades	
b.m.	blade flap bending moment	ft-lb
B	tip loss factor	
c	blade chord	ft
C_l	blade root cutout fraction	
C_m	hub pitch moment coefficient	$\frac{M}{\rho(\Omega R)^2 \pi R^3}$
C_ℓ	hub roll moment coefficient	$\frac{L}{\rho(\Omega R)^2 \pi R^3}$
C_{m_θ}	swashplate pitch moment coefficient	$\frac{M_\theta}{\rho(\Omega R)^2 \pi R^3}$
C_{ℓ_ϕ}	swashplate roll moment coefficient	$\frac{M_\phi}{\rho(\Omega R)^2 \pi R^3}$
C_T	thrust coefficient	$\frac{T}{\rho(\Omega R)^2 \pi R^2}$
c_{ℓ_α}	blade section lift curve slope	
C_R	feathering friction	ft-lb/rad/sec
C_S	swashplate damping	ft-lb/rad/sec
D	drag	lb
F_N	jet engine thrust	lb

H	blade flap generalized force	
H_{δ_o}, H_{δ_θ}, H_{δ_ϕ}	rotor flap generalized force	
I_b	blade flap moment of inertia	slugs ft^2
I_o	blade moment of inertia about the quarter chord	slugs ft^2
I_G	gyroscope diametral moment of inertia	slugs ft^2
I_{XX}, I_{YY}	airframe pitch and roll moments of inertia	slugs ft^2
k	mechanical advantage blades to swashplate	
K_s	swashplate spring	ft-lb/rad
L	lift	lb
L	hub rolling moment	ft-lb
M	hub pitch moment	ft-lb
m	blade mass distribution	slugs/ft
$M_{\delta_o\delta_o}$, $M_{\delta_\theta\delta_\theta}$, $M_{\delta_\phi\delta_\phi}$	rotor flap generalized mass	
M_θ	swashplate pitch moment	ft-lb
M_ϕ	swashplate roll moment	ft-lb
n	n^{th} flapping mode	
p	p^{th} blade	
P	ratio of blade first flap frequency to rotor rotation rate	
p.m.	blade pitch moment about the quarter chord	ft-lb

q	dynamic pressure	lb/ft^2
r	radial distance from shaft centerline	ft
R	rotor radius	ft
t	time	seconds
T	thrust	lb
V	forward speed	ft/sec
V	blade root shear	lb
W	airframe gross weight	lb
x, y, z	rotor rotating axes	
X, Y, Z	stationary axes	
α	angle-of-attack	deg or rad
β	blade linear flap angle	deg or rad
β_o	rotor precone	deg or rad
γ	fraction of critical damping	
γ	blade Lock number	$\rho \frac{c_{\ell_\alpha} cR^4}{I_b}$
δ	blade parabolic mode tip deflection	ft
$\delta_o, \delta_\theta, \delta_\phi, \delta_d$	rotor flapping mode deflection	ft
θ	swashplate tilt	rad
θ_o	collective pitch	deg or rad
$\theta_{.75R}$	collective pitch at three quarter radius	deg or rad
θ_t	blade twist rate	rad/ft
$\theta_{c/4}$ (or θ_p)	blade pitch about the quarter chord	rad
θ_f	blade feathering pitch	rad

θ_{1c}, θ_{1s}	cyclic pitch	deg or rad
Θ	rotor-airframe pitch angle	rad
Λ	blade forward sweep	deg or rad
μ	advance ratio	
ρ	air density	slugs/ft^3
σ	solidity	
ϕ	swashplate roll tilt	rad
Φ	rotor-airframe roll angle	rad
ψ	azimuth position of rotor	deg or rad
ψ_p	position of p^{th} blade relative to blade 1	rad
ψ_o	cant angle	deg or rad
ω_δ	blade first flap frequency	rad/sec
Ω	rotor rotation rate	rad/sec
Ω_G	gyroscope rotation rate	rad/sec

Matrices

$[A]$	aerodynamic stiffness, rotating axes
$[A_R]$	aerodynamic damping, rotating axes
$[AF]$	aerodynamic forcing, rotating axes
$[B]$	aerodynamic stiffness, stationary axes
$[B_R]$	aerodynamic damping, stationary axes
$[CF]$	centrifugal and structural

$[D]$	transformation, rotor to blade freedoms
$[Da]$	damping
$[E]$	centrifugal and structural, stationary axes
$[F]$	forcing matrix, stationary axes
$\left[\frac{\partial F_b}{\partial \eta}\right]$	rate of change of blade force with blade deflection
$[I]$	inertia
$[I_{body}]$	airframe inertia
$[J_{body}]$	airframe aerodynamic stiffness
$[J_{\dot{}_{body}}]$	airframe aerodynamic damping
$[J_{RR_{body}}]$	airframe acceleration aerodynamics
$[S]$	centrifugal and structural, stationary axes
$[T]$	transformation from stationary to rotating axes
$\{f\}$	forcing angles
$\{\beta\}$	rotor degrees of freedom
$\{\eta\}$	blade degrees of freedom

Additional symbols employed in the in-plane motions equations:

a.f.	blade axial force	lb
c_{d_o}	minimum drag coefficient	
e	pivot radial position	ft

F_{ip}	blade in-plane force	lb
H_{ζ_o}, H_{ζ_θ}, H_{ζ_ϕ}	rotor in-plane mode generalized force	
$I_{b_{shaft}}$	blade moment of inertia about the shaft	slugs ft^2
$I_{b_{pivot}}$	blade moment of inertia about the pivot	slugs ft^2
I_R	hub moment of inertia	slugs ft^2
J_b, K_b, J_{e_b}, K_{e_b}	blade inertia parameters	
K_y	body lateral spring to ground	lb/ft
K_x	body longitudinal spring to ground	lb/ft
L_p	lift on p^{th} blade	lb
M_b	blade mass	slugs
M_R	hub mass	slugs
n.f.	blade normal force	lb
N	rotor yawing moment	ft-lb
p.t.	blade pivot torsion	ft-lb
$r_{c.g.}$	blade center of gravity radial distance	ft
s.t.	blade shaft torsion	ft-lb
u	blade normal displacement	ft
v	blade axial displacement	ft
x	longitudinal displacement	ft
X	longitudinal force	lb

y	lateral displacement	ft
Y	lateral force	lb
ζ	blade rotation about its pivot	rad
ζ_o, ζ_y, ζ_n, ζ_d	rotor mode deflection	rad
κ	ratio of inclination of blade in-plane principle axis to feathering pitch	
ν	blade rotation about the shaft	rad
ω_{ip}	blade non-rotating undamped natural frequency	rad/sec
[COR]	Coriolis force matrix	

Subscripts

0, 1c, 1s, 2c, 2s	harmonic component
c/4	about the quarter-chord
d	differential collective mode
f	feathering
g	gust
ℓ	lift
n	normal to blade leading edge
n	n^{th} mode or harmonic
p	p^{th} blade
1, 2 ,..., p ,..., b	blade numbering sequence
r	rotating axis system
.75R	blade three-quarter radius

xy	in-plane equations or in-plane rotating axes
XY	in-plane stationary axis system
z	vertical equations or vertical system rotating axes
Z	vertical system, stationary axes

Less frequently used symbols are defined in the text.

HINGELESS ROTOR TYPES STUDIED

In this report a set of stiff-bladed hingeless rotors operating at high advance ratio is considered. Its selection was based on the desire to study rotors that could be employed in future vehicle concepts. Therefore, those aspects of the advanced helicopter design that cross into the well-understood areas of conventional helicopters, such as hover and low advance ratio flight, are not studied.

This philosophy crystallized into the consideration of rotors which could be applied to the two following types of vehicle:

1. Slowed hingeless rotor winged compound helicopter
2. Stowable rotor aircraft

These considerations resulted in the decision to study only the high advance ratio flight range $.3 < \mu \leqslant \infty$; and rotor blades with flapping stiffness in the range $1.3 < P \leqslant \infty$. It further resulted in limiting the flight regions to low lift values and subcritical advancing blade tip Mach numbers.

The blades, experimentally investigated, had inoptimum structure and therefore low Lock numbers, but this is not considered to restrict the applicability of the theory correlation.

Because the rotors were of the hingeless type, the minimum number of blades considered was three. Four-blade rotors were also extensively studied. The theoretical derivations were extended to any number of blades.

Since such rotors can be employed with gyroscope-stabilized feathering systems, blades swept forward of the feathering hinge and corresponding feathering moments and degrees of freedom were considered throughout the analyses.

Geometry Variations

The variations in blade geometry considered in this study are as follows:

Radius	R	ft
Chord	c	ft
Sweep angle	Λ	radians

Cutout fraction	c_1	
Precone	β_o	radians
Twist rate	θ_t	radians/ft

These are illustrated in Figure 1. It should be noted that both the locus of quarter chord points (along the r - axis) and the feathering axis pass through the center of the shaft or center of rotation (the z - axis). In blade configurations in which the quarter chord or hinge lines do not pass exactly through the center of rotation, fictitious hinge lines and quarter chords may be assigned with little loss of precision.

The analyses presented in this report are valid for precone and twist values that do not seriously violate small perturbation values (say up to 10°) and for any value of blade radius. Chord lengths, on the other hand, should not exceed a chord-to-radius ratio of about 1/10 or blade section aerodynamic pitch damping, neglected in the theory, may become significant. Blade torsional deformation, neglected in these analyses, can also result in significant changes in blade airloads should the ratio of aerodynamic moment to torsional rigidity become large enough.

Sweep angle and root cutout values may be of any magnitude.

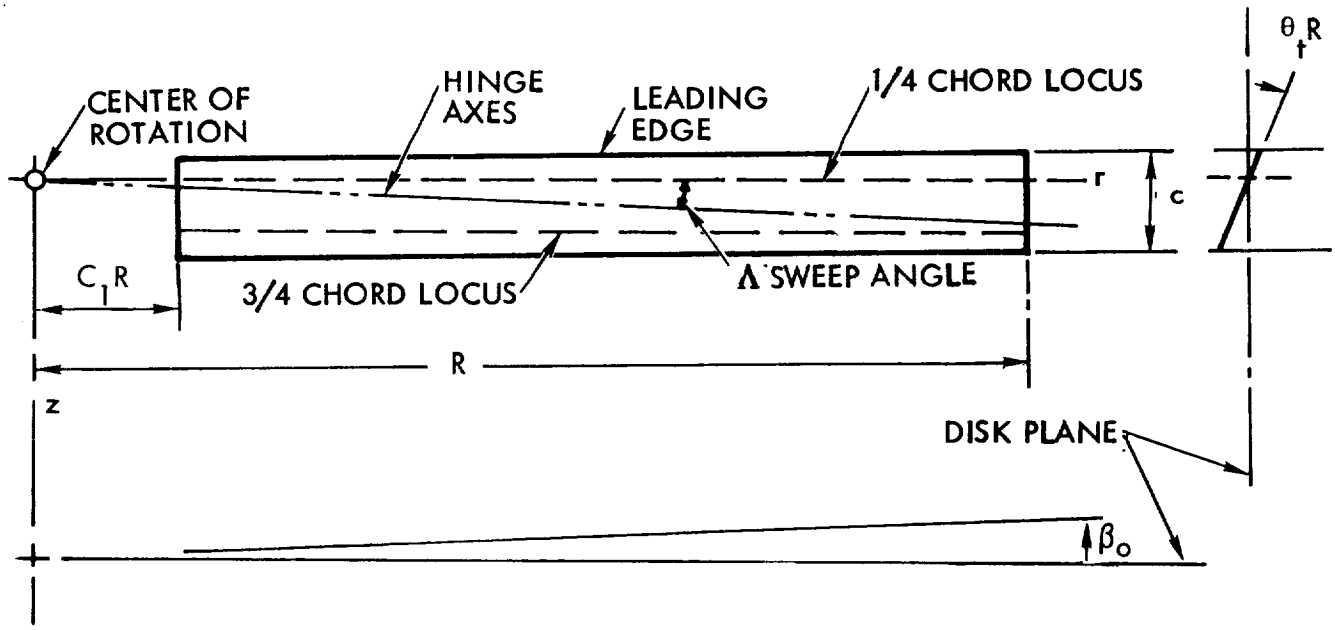

Figure 1. Blade Geometry

The particular equations derived to completion in this report are for three- and four-blade rotors but indications are given at every step as to the procedure to follow to extend the derivation to rotors with 5, 6,.... n blades.

In considering the complete rotor, an axis system rotating with the blades is required to act as a reference for the location of each of the blades. It is denoted by lower case letters. The axis system is selected so that the positive z-axis runs along the shaft upward, in its nominal untilted position. The axes rotate with the rotor but are not attached to it, for the rotor can pitch, roll, plunge, surge, sideslip, and yaw relative to the rotating axis system. The x-axis runs along the nominal position of the number one blade quarter-chord locus, if precone is zero (otherwise normal to the z-axis). The y-axis extends normal to the x, z plane, positive to the right, to form a right-handed axis system.

The blades are numbered in ascending order moving around the rotor in a clockwise direction so that, to an observer on the ground watching the blades go by, the blades would appear in the order 1, 2, 3,..., n, 1, 2, 3,.., The arrangement of blades and rotating (lowercase) axes is shown in Figure 2.

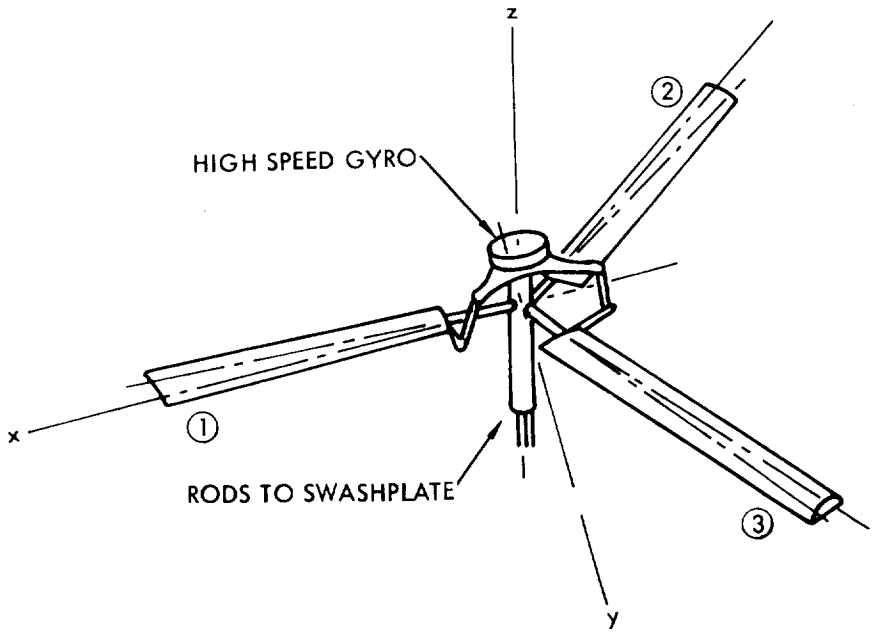

Figure 2. Rotating Axis System and Blade Numbering

The figure also shows schematically the attachment of the blade feathering horns to the swashplate via the stabilization gyroscope, in the general case of this report. Tilting the swashplate, and the parallel gyroscope, causes the blades to feather cyclically. The relationship between swashplate tilt and blade feathering is shown in Figure 3.

Swashplate tilt relative to rotating axes is denoted by θ_r, ϕ_r pitch and roll about the y and x axes respectively. Because of the blade feathering arm and linkage geometry, pitch and roll do not separately produce pure "cyclic pitch" of the blades as is usually the case with articulated rotors. ("cyclic pitch" here is relative to rotating axes.) This slewing around of the gyroscope (and swashplate) relative to the blades is denoted by ψ_o, the cant angle, and is shown in Figure 3. By this definition, most articulated rotors would possess a cant angle of ninety degrees ($\psi_o = 90°$).

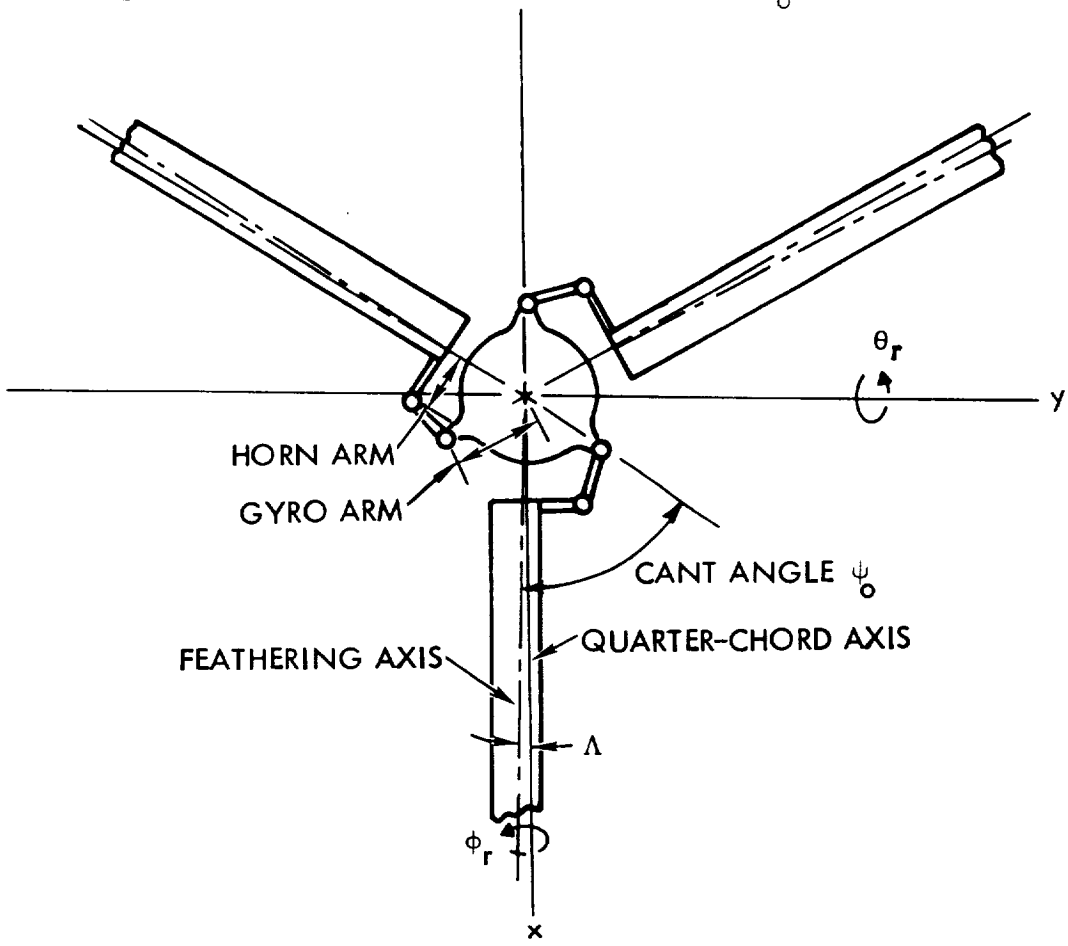

Figure 3. Cant Angle and Mechanical Advantage

Cant angles different from 90° are employed in gyroscope-stabilized hingeless rotors for purposes of free-flight stability. If the shaft is prevented from pitching and rolling, as is the case during wind tunnel testing, the rotor-gyroscope stability is not affected by cant angle. It should be noted that the cant angle is relative to the blade feathering axis. The blade quarter chord leads the feathering axis by the sweep angle.

In order to allow the use of a smaller gyroscope the gyro arm is made shorter than the blade feathering horn arm so that the gyro tilt angle is somewhat greater than the maximum feathering displacement. This is called mechanical advantage.

$$k = \frac{\text{Horn arm}}{\text{Gyro arm}} = \text{Mechanical Advantage}$$

Mechanical advantage is such that values greater than about 1.5 are difficult to achieve mechanically.

Degrees of Freedom

The geometric form of the rotor systems studied in this report has been discussed in the previous section. It was necessary to establish a reference axis system rotating with the rotor in order to describe the blades, linkages. gyroscope, and rotating part of the swashplate. Similarly, in order to discuss the rigid body to which the rotor is attached and the stationary part of the swashplate, it is necessary to establish a second reference axis system that is stationary. Denoted by capital letters, this system employs the same vertical or Z axis as the rotating system. Its X and Y axes, however, do not rotate but remain fixed relative to the earth. (In actual fact they translate with the mean forward speed of the vehicle.) The X or longitudinal axis is positive in the nominal aft direction of the body and the Y axis extends normal to the X, Z plane positive to the right, again forming a right handed system. Both axis systems are shown in Figure 4.

The rotating axes are related to the stationary axes by the rotation angle ψ, which is a function of time. Since the rotation rate is assumed to be constant in these analyses, $\psi = \Omega t$

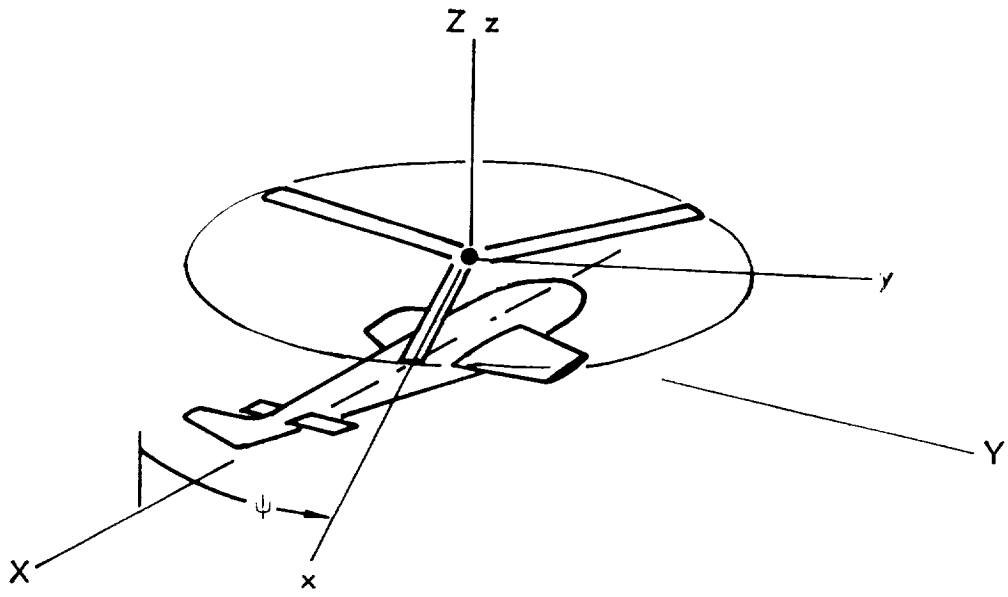

Figure 4. Stationary and Rotating Axes

where Ω = the rotor rotation rate - radians/sec

t = time in seconds.

Perturbational motions of the rotor and shaft, described in terms of degrees of freedom in the rotating axis system, may be transformed to stationary axes. In this form the shaft motions are in a convenient form to include the rigid motions of the vehicle body.

It is clear, therefore, that the degrees of freedom of the system may be described in rotating or stationary axes. (There are some exceptions which will be noted later.) Motions of rotating parts are basically described relative to rotating axes and motions of stationary parts relative to stationary axes. The complete set of motions equations could be described in either coordinate system. In these analyses, however, the rotor alone is described in rotating axes; its equations of motion are transformed to stationary axes and these are combined with the body equations of motion and solved in stationary axes.

Whether thought of relative to rotating or stationary coordinates, the rotor-gyroscope-body motions have been separated into two sets for the purpose of this study; those that produce perturbational motions of the elements of mass essentially in the vertical direction, and those that produce mass element motions essentially in the plane of the rotor disk. The two sets of degrees of freedom can only be separated in the small perturbation motion sense since nonlinear coupling between the two sets becomes significant with increasing blade loads and displacements.

It should be noted that the vertical motions equations are solved completely independently of the in-plane motions equations. The in-plane motion equations forcing functions, however, are produced almost entirely as a by-product of the motions of the vertical equations degrees of freedom and their aerodynamic forcing functions.

The two sets of degrees of freedom will be described separately in the following:

Vertical motions of mass elements. - The degrees of freedom employed in describing those motions of the rotor-gyroscope-body system that are essentially in the vertical direction can be most easily pictured relative to stationary axes (with one exception, discussed later). Figure 5 shows the stationary X, Y, Z axes degrees of freedom of a 5-blade rotor. The set for 3-blade rotors is obtained by deleting the two scalloped disk flapping modes δ_{2c} and δ_{2s}, the reactionless flapping cosine and sine degrees of freedom. For rotors with even numbers of blades 4, 6, ... etc, in addition to the reactionless modes existing in pairs, there is a single reactionless mode, sometimes called the differential collective mode (or degree of freedom). It is characterized by the blades being alternately up and down.

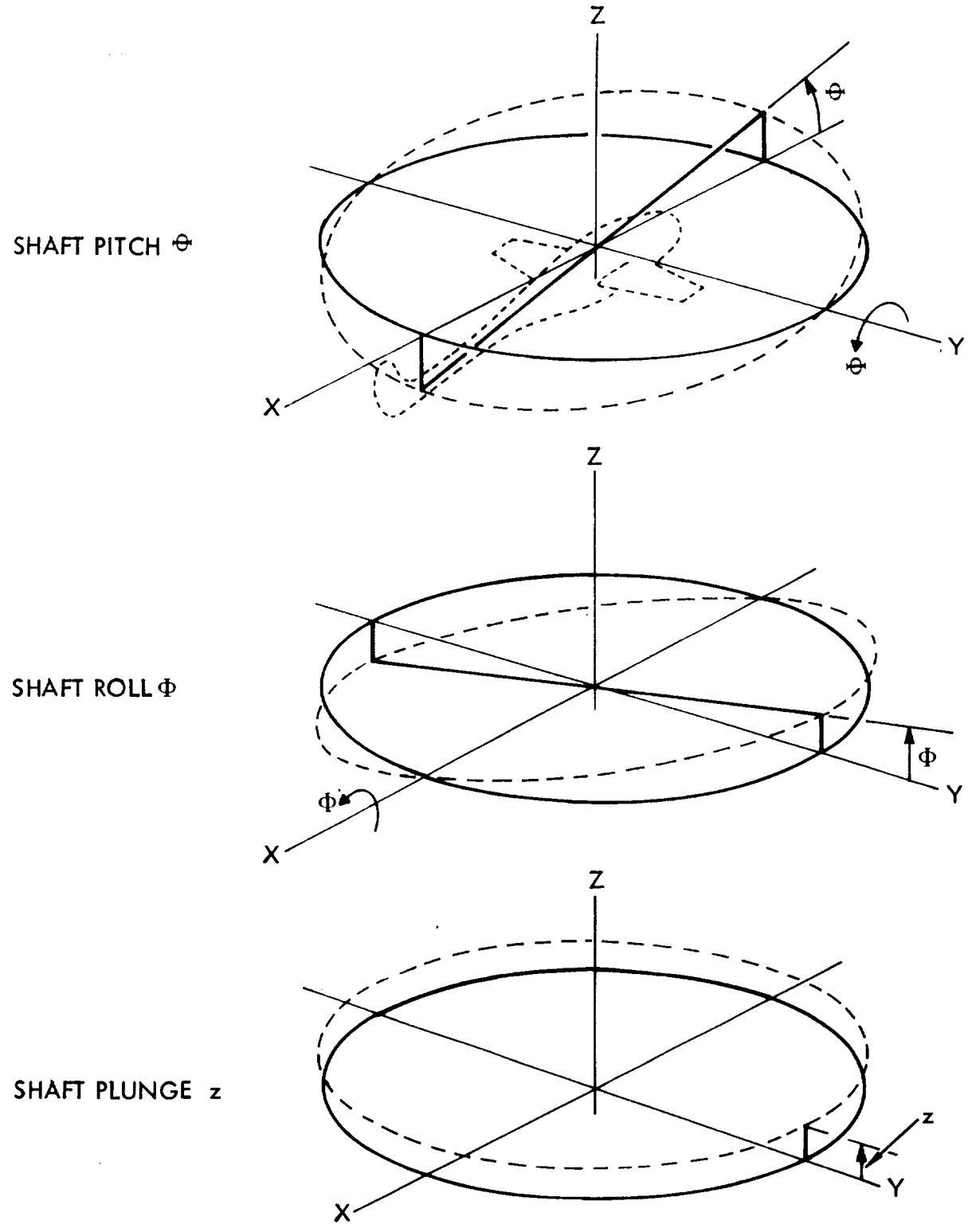

Figure 5. Vertical Motion Degrees of Freedom in Stationary Axes

SWASHPLATE AND
GYROSCOPE PITCH θ

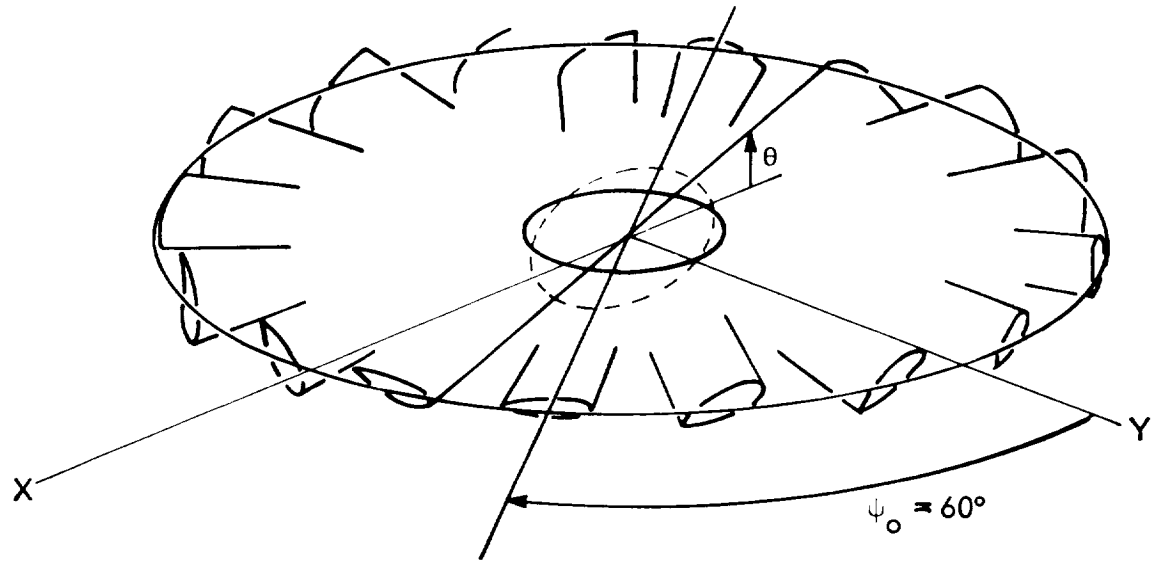

Note: Blade feathering displacements accompanying gyro tilt angles show effect of cant angle ψ_o.

SWASHPLATE AND
GYROSCOPE ROLL ϕ

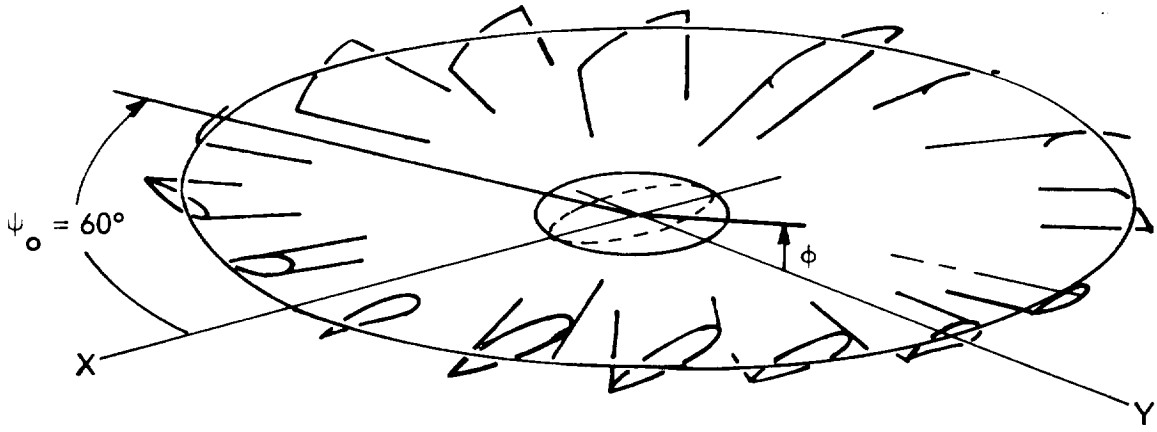

Figure 5. (Continued)

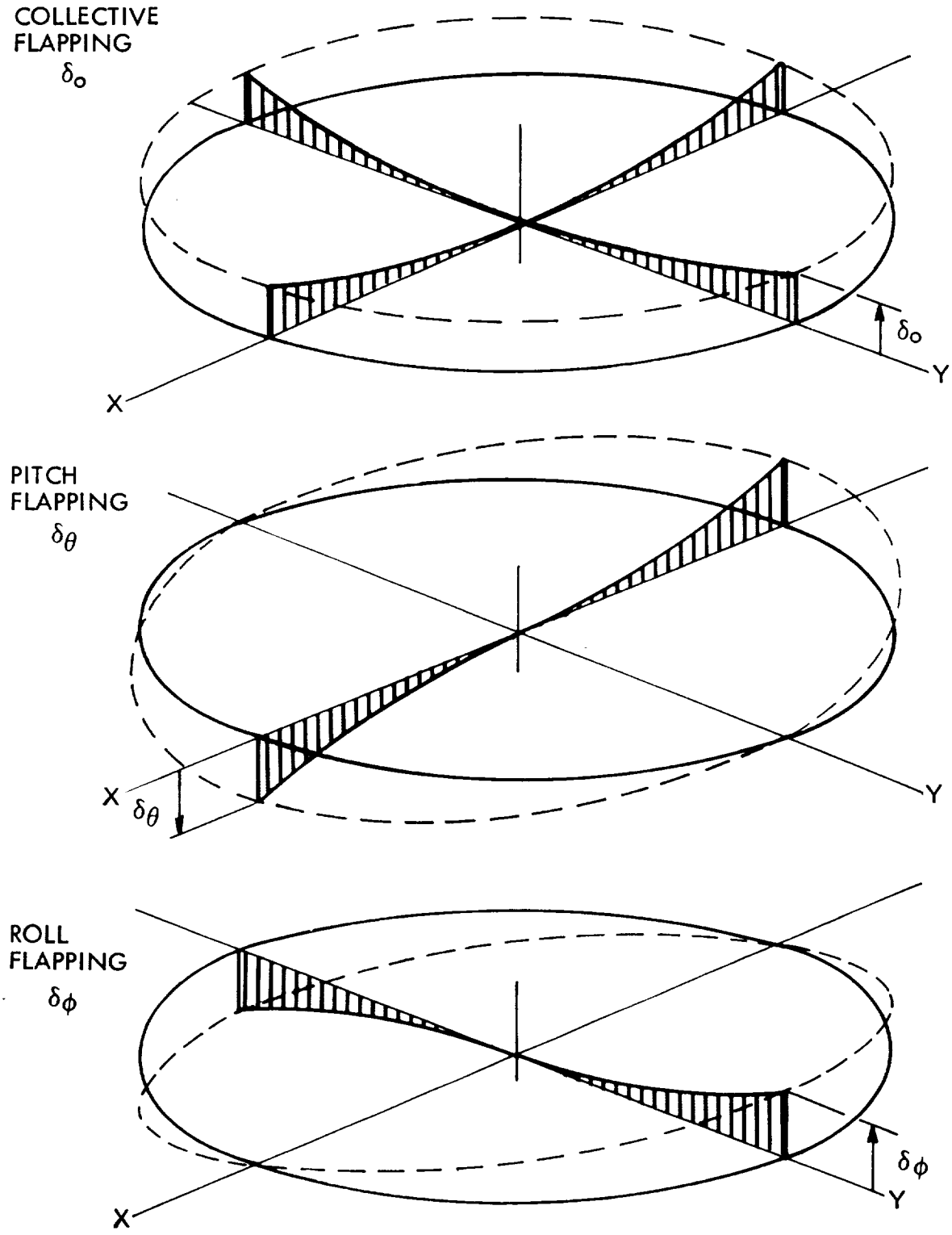

Figure 5. (Continued)

REACTIONLESS FLAPPING
COSINE COMP.

δ_{2c}

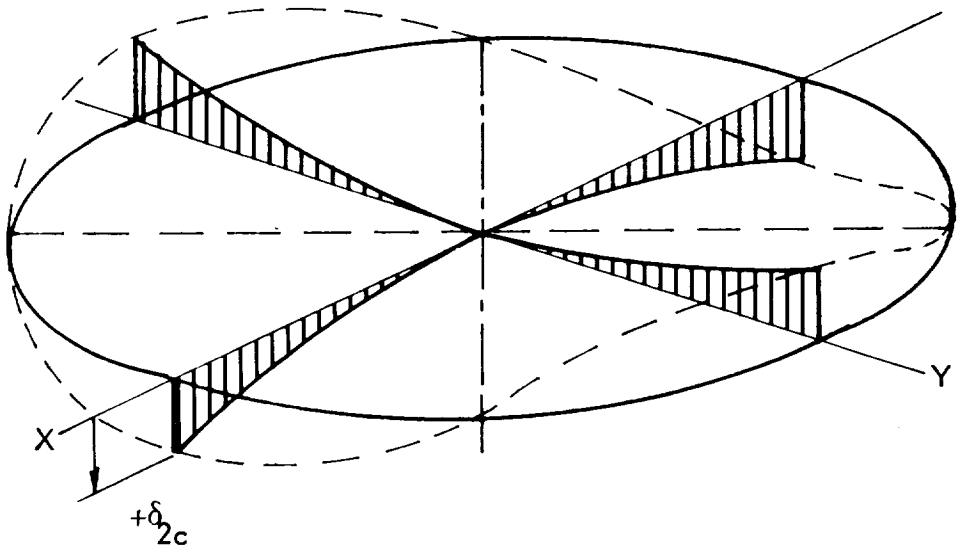

REACTIONLESS FLAPPING
SINE COMP.

δ_{2s}

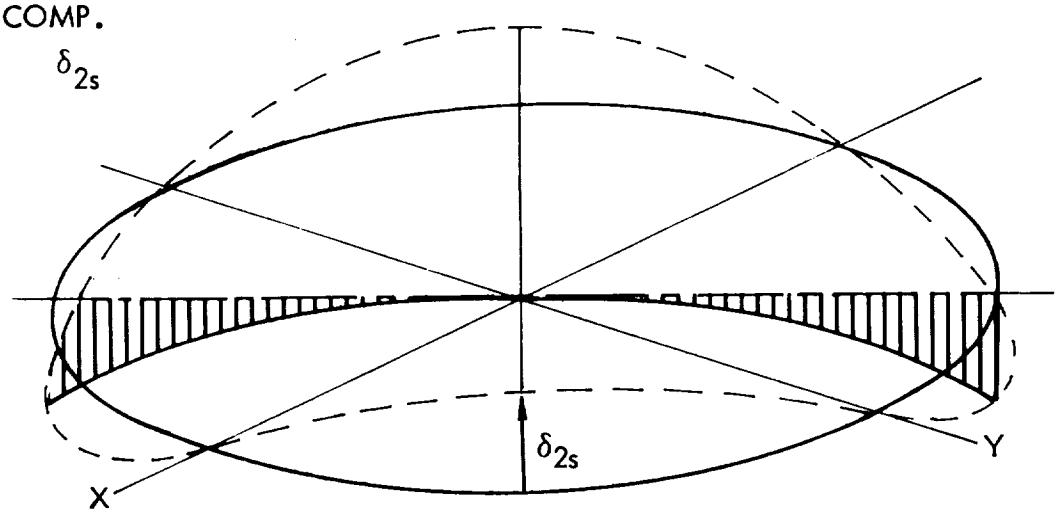

Figure 5. (Concluded)

In this report the degrees of freedom are arranged in vectors in a fixed order to facilitate matrix algebra. For 3-, 4-, and 5-blade rotors the vectors of degrees of freedom in stationary axes are as follows:

3-blade rotor

$$\beta_Z = \begin{Bmatrix} \Theta \\ \Phi \\ z \\ \theta \\ \phi \\ \delta_o \\ \delta_\theta \\ \delta_\phi \end{Bmatrix}$$

4-blade rotor

$$\beta_Z = \begin{Bmatrix} \Theta \\ \Phi \\ z \\ \theta \\ \phi \\ \delta_o \\ \delta_\theta \\ \delta_\phi \\ \delta_d \end{Bmatrix}$$

5-blade rotor

$$\beta_Z = \begin{Bmatrix} \Theta \\ \Phi \\ z \\ \theta \\ \phi \\ \delta_o \\ \delta_\theta \\ \delta_\phi \\ \delta_{2c} \\ \delta_{2s} \end{Bmatrix}$$

NOTE: 1. Subscript Z denotes stationary axes.
2. Subscript d denotes differential collective mode.

The degrees of freedom have been shown in stationary coordinates for the sake of clarity but they, in fact, represent the end product; the form in which they are employed in the equations of motion to be solved.

In order to obtain these degrees of freedom a parallel set in rotating coordinates must be transformed to stationary axes. The rotating axis degrees of freedom employ the same symbols as the stationary axis modes but are differentiated by subscript "r." They look the same as the stationary modes but the mode shapes are relative to the rotating x, y, z axis system and remain undistorted as the rotor rotates or are independent of azimuth (the number one blade lies along the x-axis at all values of azimuthal orientation of the rotor).

The transformation from rotating axis degrees of freedom to stationary axis degrees of freedom must therefore be a function of azimuth or time if the rotation rate is constant.

The transformation for the 5-blade rotor is as follows:

$$\beta_z = \left|T_z\right| \beta_Z$$

z - rotating axes

Z - stationary axes

$$\begin{Bmatrix} \Theta_r \\ \Phi_r \\ z_r \\ \theta_r \\ \phi_r \\ \delta_{o_r} \\ \delta_{\theta_r} \\ \delta_{\phi_r} \\ \delta_{2c_r} \\ \delta_{2s_r} \end{Bmatrix} = \begin{bmatrix} \cos\psi & -\sin\psi & & & & & & & & \\ \sin\psi & \cos\psi & & & & & & & & \\ & & 1 & & & & & & & \\ & & & \cos\psi & -\sin\psi & & & & & \\ & & & \sin\psi & \cos\psi & & & & & \\ & & & & & 1 & & & & \\ & & & & & & \cos\psi & -\sin\psi & & \\ & & & & & & \sin\psi & \cos\psi & & \\ & & & & & & & & \cos 2\psi & -\sin 2\psi \\ & & & & & & & & \sin 2\psi & -\cos 2\psi \end{bmatrix} \begin{Bmatrix} \Theta \\ \Phi \\ z \\ \vartheta \\ \phi \\ \delta_o \\ \delta_\theta \\ \delta_\phi \\ \delta_{2c} \\ \delta_{2s} \end{Bmatrix}$$

For the 3-blade rotor the transformation is as above with the last two rows and columns deleted. For the 4-blade rotor the last row and column are deleted and the lower right corner element $\cos 2\psi$ is replaced by 1.

For aircraft body and gyroscope (or swashplate) angular motion and rotor disk tilt, unit values of displacement in stationary coordinates are equivalent to displacements in rotating coordinates which vary sinusoidally once per revolution with azimuth. For example, a unit value of body pitch in stationary coordinates $\Theta = 1.0$ radian is equivalent to the following sinusoidal variations with azimuth in rotating coordinates:

$$\Theta_r = \Theta \cos\psi$$

$$\Phi_r = \Theta \sin\psi$$

Body plunge, collective flapping and, for the four-blade rotor, the differential collective mode are the same in both coordinate systems.

Constant reactionless flapping displacement in stationary coordinates, however, is equivalent to reactionless flapping in rotating coordinates that varies with the second harmonic of azimuth. For example, if the disk of a 5-blade rotor took up a constant cosine scalloped shape in stationary coordinates, δ_{2c}, the equivalent motion in rotating coordinates varies with azimuth as follows:

$$\delta_{2c_r} = \delta_{2c} \cos 2\psi$$

$$\delta_{2s_r} = \delta_{2c} \sin 2\psi$$

The relationship between rotating and stationary axes vectors of degrees of freedom is also expressed in this report for the sake of conciseness, in vector notation, as follows:

$$\beta_z = \left|T_z\right| \beta_Z$$

z = rotating axes

Z = stationary axes

Although the equations are employed in stationary coordinates, they came into that form through the application of the $\left|T_z\right|$ transformation to the more fundamental equations of motion derived relative to rotating coordinates. It is necessary, therefore, to first develop the equations relative to rotating coordinates or the relationship between the motions and the generalized forces of the rotating degrees of freedom.

The first step in this development is the determination of the kinematic relationship between the motions of the individual blades in their single-blade degrees of freedom and the motions of the complete rotor in its rotating degrees of freedom. The relationship is independent of the azimuthal position of the rotor. This forms the subject of a later section.

Motions of the rotor in its rotating degrees of freedom may be described in terms of the single blade degrees of freedom (shown in Figure 6).

The vertical single blade degrees of freedom may be arranged in a vector to facilitate matrix algebra,

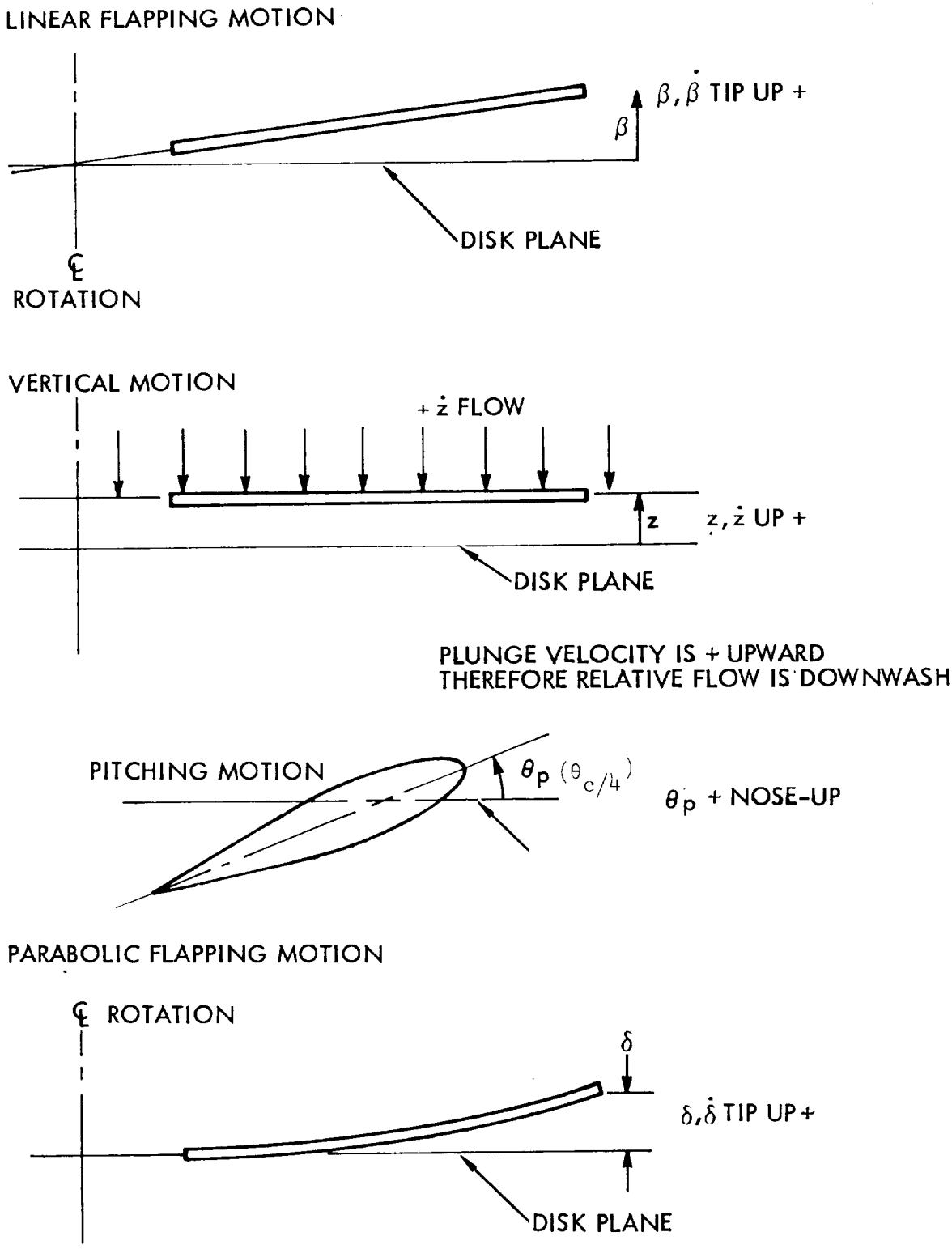

Figure 6. Single Blade Vertical Degrees of Freedom

$$\eta_{z_p} = \begin{Bmatrix} \beta_p \\ z_p \\ \theta_p \\ \delta_p \end{Bmatrix}$$

The pitch, roll, and plunge motions of the rotor disk are composed of the first three blade freedoms: linear flap β, vertical plunge z, and blade feathering θ_p. Gyroscope (and swashplate) pitch and roll are composed of blade feathering and linear flapping (due to the sweep of the feathering hinge). Rotor disk collective, pitch and roll and reactionless flapping modes are all defined in terms of the blade parabolic or first flap structural mode.

The vertical motions equations contain only the first blade dynamic flapping mode.

In-plane motions of mass elements. - The stationary axis degrees of freedom employed to describe rotor motions essentially in the plane of the disk are as shown in Figure 7. The freedoms shown are for a five-blade rotor. Deletion of the cosine and sine reactionless lead-lag freedoms provides the set needed for a three-blade rotor. Four-blade rotors require the addition of one differential collective lead-lag mode to the three-blade set. It is the same in rotating and stationary axes.

The number of blades shown in Figure 7 is arbitrary; the displacements merely show the deflected positions the blades would occupy at that azimuth. It should be noted that positive lead-lag is lead or counterclockwise structural deflections. (This is opposite the convention in Reference 11 but is used since all counterclockwise displacements are to be positive, as is the normal mathematical convention.) At this point, the blade in-plane deflection mode has not been defined.

The in-plane degrees of freedom in stationary axes are arranged in vectors to facilitate matrix algebra, as were the vertical motions freedoms.

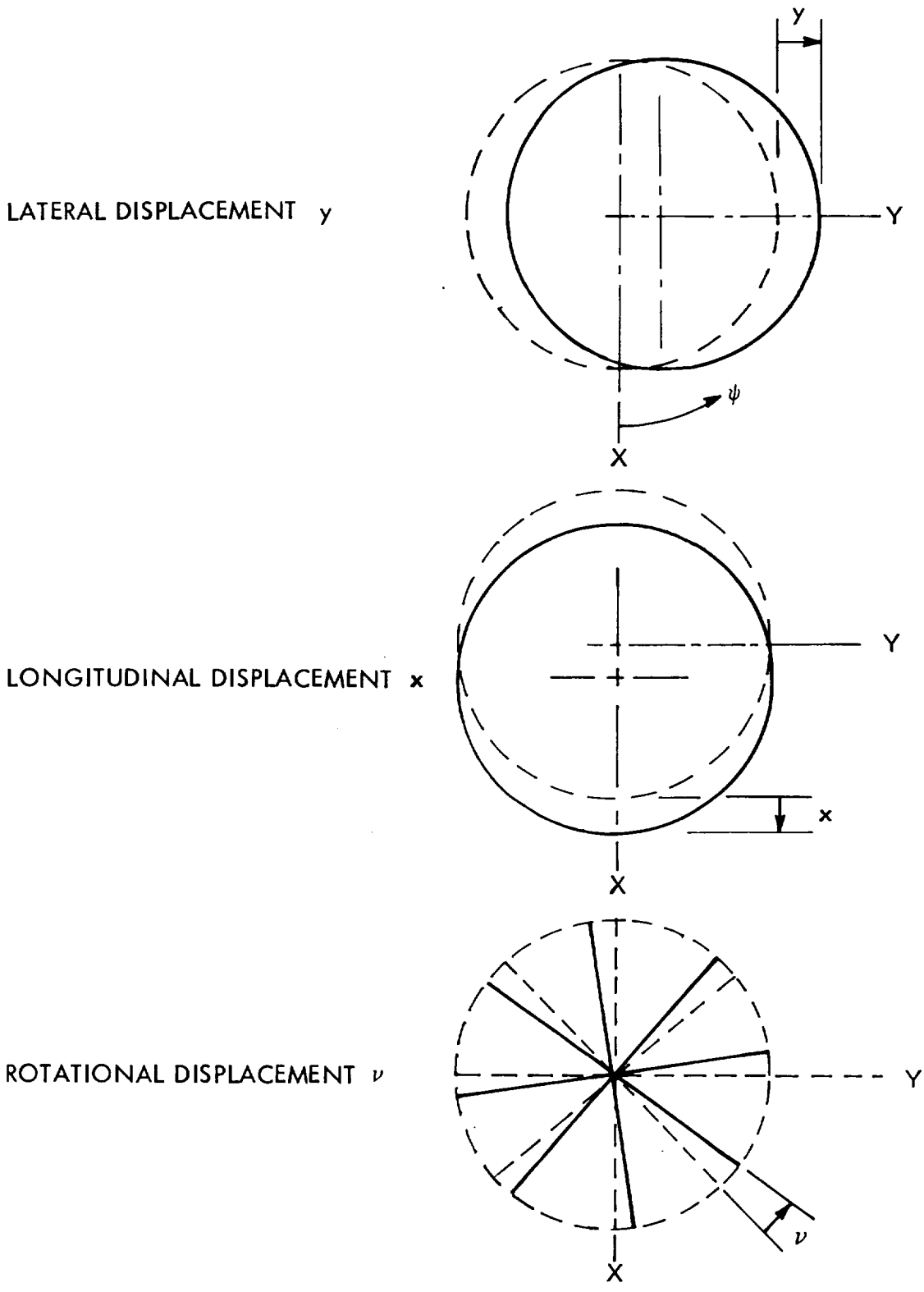

Figure 7. In-Plane Motions Degrees of Freedom in Stationary Axes

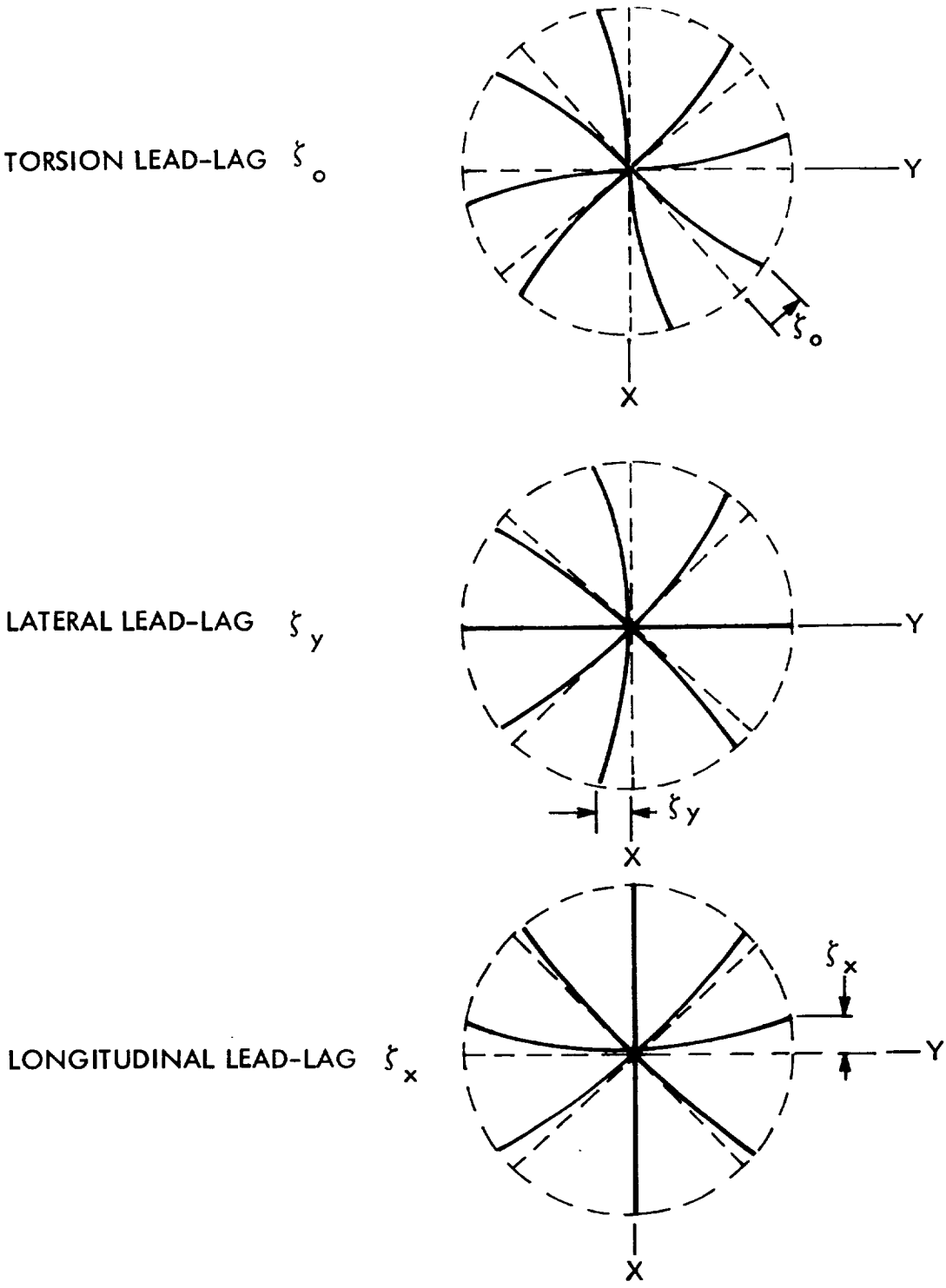

Figure 7. (Continued)

REACTIONLESS LEAD-LAG
COSINE COMPONENT
ζ_{2c}

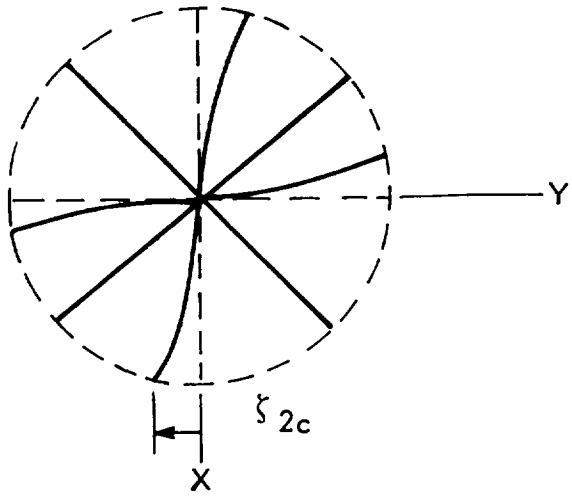

REACTIONLESS LEAD-LAG
SINE COMPONENT
ζ_{2s}

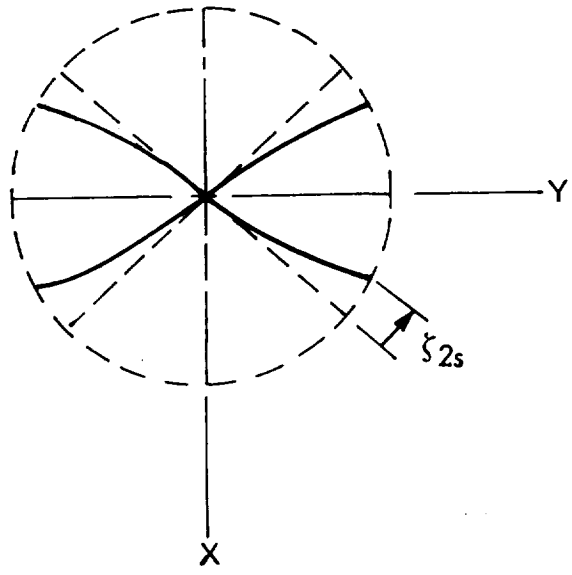

Figure 7. (Concluded)

3-blade rotor

$$\beta_{XY} = \begin{Bmatrix} y \\ x \\ \upsilon \\ \zeta_o \\ \zeta_y \\ \zeta_x \end{Bmatrix}$$

4-blade rotor

$$\beta_{XY} = \begin{Bmatrix} y \\ x \\ \upsilon \\ \zeta_o \\ \zeta_y \\ \zeta_x \\ \zeta_d \end{Bmatrix}$$

5-blade rotor

$$\beta_{XY} = \begin{Bmatrix} y \\ x \\ \upsilon \\ \zeta_o \\ \zeta_y \\ \zeta_x \\ \zeta_{2c} \\ \zeta_{2s} \end{Bmatrix}$$

Compared to the vertical motions degrees of freedom, a motion equivalent to swashplate tilt is missing. The in-plane motions are therefore described by two fewer degrees of freedom than the vertical motions.

The next step is to visualize these modes in axes rotating with the rotor. The lower case x, y label for rotating axes replaces the uppercase X, Y of the stationary axes system but the modes maintain the same shape. The major difference now is that the blades maintain fixed azimuth positions relative to the x, y axes. The x-axis is always directed through the axis of rotation parallel to the number (1) blade quarter chord line and the blades are numbered in ascending order as they pass a fixed azimuth position. The azimuth location of the pth blade relative to number (1) blade is

$$\psi_p = - (p-1) \frac{2\pi}{b}$$

where b is the number of blades.

The rotating axis degrees of freedom employ the same symbols as the stationary axis freedom but differentiated by subscript "r."

Vectors describing the in-plane rotor motions in rotating degrees of freedom may be transformed to stationary axes degrees of freedom by a sine-cosine transformation very similar to the one employed for the vertical motions. For five-blade rotors, the transformation of rotating axes freedoms to stationary axes is as follows:

$$
\begin{Bmatrix} y_r \\ x_r \\ v_r \\ \zeta_{or} \\ \zeta_{yr} \\ \zeta_{xr} \\ \zeta_{2c_r} \\ \zeta_{2s_r} \end{Bmatrix} = \begin{bmatrix} \cos\psi & -\sin\psi & & & & & & \\ \sin\psi & \cos\psi & & & & & & \\ & & 1 & & & & & \\ & & & 1 & & & & \\ & & & & \cos\psi & -\sin\psi & & \\ & & & & \sin\psi & \cos\psi & & \\ & & & & & & \cos 2\psi & -\sin 2\psi \\ & & & & & & \sin 2\psi & \cos 2\psi \end{bmatrix} \begin{Bmatrix} y \\ x \\ v \\ \zeta_o \\ \zeta_y \\ \zeta_x \\ \zeta_{2c} \\ \zeta_{2s} \end{Bmatrix}
$$

For 3-blade rotors, the last two rows and columns are deleted. For 4-blade rotors, 1.0 is added to the lower right corner of the 3-blade motions expanded by one row and column.

The above relationship is also expressed in matrix form as follows:

$$
\theta_{xy} = \left|T_{xy}\right| \theta_{XY}
$$

Vector subscripts
xy - rotating axes
XY - stationary axes

Before the equations of motion in rotating axes can be developed it is necessary to determine the kinematic relationship between motions of individual blades in their single-blade degrees of freedom and the motions of the complete rotor in its degrees of freedom relative to axes rotating with the rotor. This is the subject of a later section.

Motions of the rotor in its rotating degrees of freedom may be described in terms of the single blade degrees of freedom shown in Figure 8. The first flexible mode has been defined to be a straight line lead-lag with an offset pivot. This mode shape was assumed after an inspection of experimental mode shapes for the 33-foot rotor. Examining the reasons for its very close approximation to this shape, it became evident that all hingeless rotors with relatively flexible root sections in-plane and relatively stiff in-plane blade

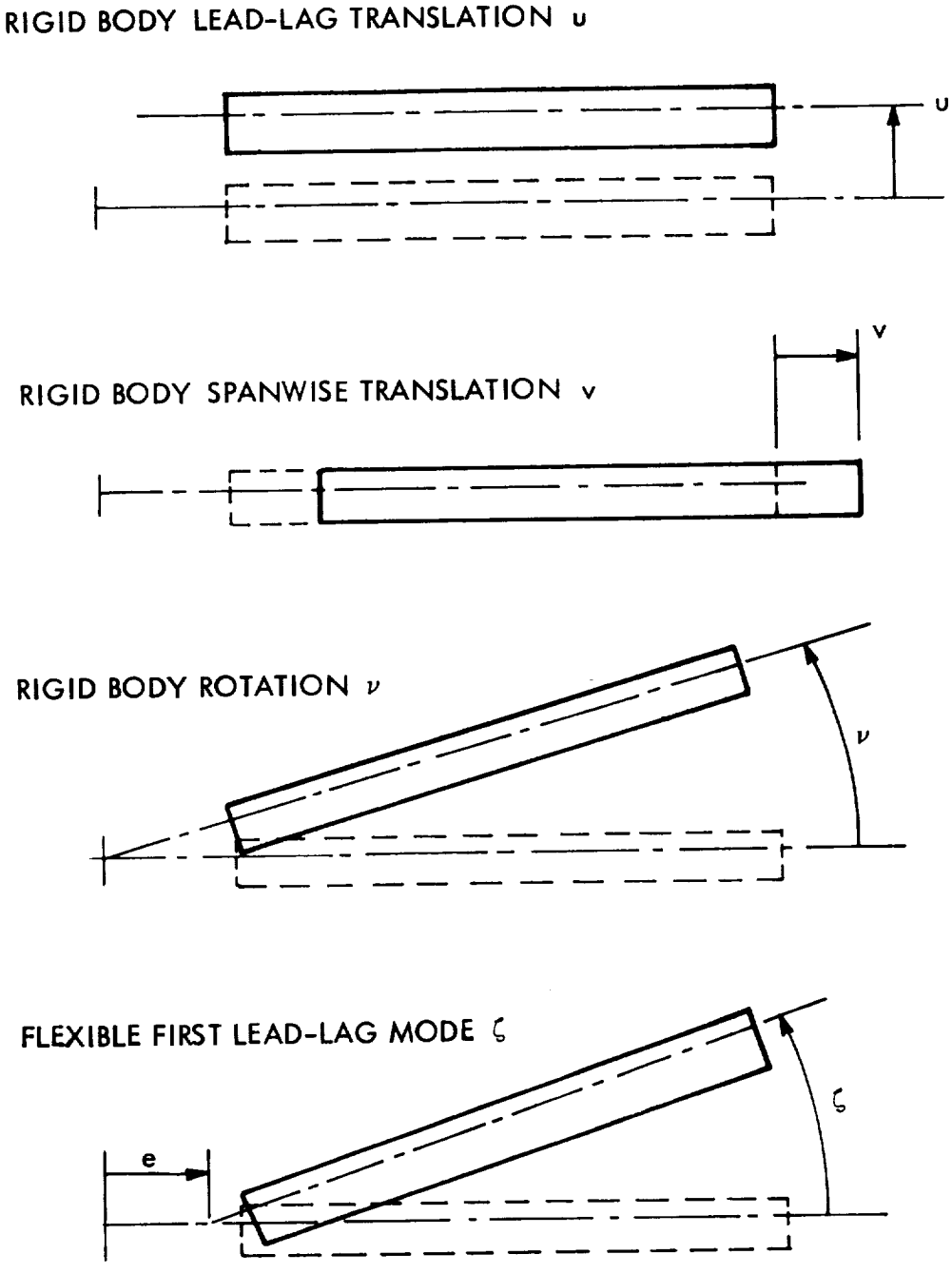

Figure 8. Single Blade In-Plane Degrees of Freedom

stiffness outboard would have shapes of this type. The specific shapes and frequencies, etc., will be discussed in a later section, as they vary with rpm.

The single blade degrees of freedom may be arranged into a vector for matrix operations:

$$\eta_{xy_p} = \begin{Bmatrix} u_p \\ v_p \\ v_p \\ \zeta_p \end{Bmatrix}$$

The rotor in-plane degrees of freedom relative to coordinates rotating with the rotor are composed of the single blade degrees of freedom. The only structural dynamic mode included is the first in-plane lead-lag mode denoted ζ. Higher dynamic modes have not been included in this analysis.

The lateral and longitudinal degrees of freedom y_r and x_r in rotating coordinates are composed only of u and v single blade degrees of freedom. The rotational mode v_r is composed only of the blade rigid body rotation mode v. All the remaining rotor degrees of freedom, relative to rotating axes are lead-lag modes and are composed solely of flexible first lead-lag blade degrees of freedom ζ.

Kinematic Relationships

In this section the rotor degrees of freedom relative to rotating axes are defined in terms of single blade degrees of freedom. The kinematic relationships between the two sets of freedoms, for each set of motions, vertical and in-plane, are expressed as transformation matrices

Sets of degrees of freedom for vertical and in-plane motions are treated separately.

Vertical motions blade-rotor kinematics. - Arranging the single blade degrees of freedom in a vector facilitates the matrix algebra and allows the displacements of the pth blade to be represented by a single symbol η_{z_p}

where

$$\eta_{z_p} = \begin{Bmatrix} \beta_p \\ z_p \\ \theta_p \\ \delta_p \end{Bmatrix}$$

The blade motions may then be expressed conveniently in terms of rotor motions in degrees of freedom relative to rotating axes.

$$\eta_{z_p} = \left[D_{z_p}\right] \beta_z$$

where p indicates the blade number. Rewriting:

$$\begin{Bmatrix} \beta_p \\ z_p \\ \theta_p \\ \delta_p \end{Bmatrix} = \left[D_{z_p}\right] \begin{Bmatrix} \Theta_r \\ \Phi_r \\ z_r \\ \theta_r \\ \phi_r \\ \delta_{o_r} \\ \delta_{\theta_r} \\ \delta_{\phi_r} \\ \delta_{2c_r} \\ \delta_{2s_r} \end{Bmatrix}$$

for a five-blade rotor

where $\left[D_{z_p}\right]$ is:

$$\begin{bmatrix}
\frac{d\beta_p}{d\Theta_r} & \frac{d\beta_p}{d\Phi_r} & \frac{d\beta_p}{dz_r} & \frac{d\beta_p}{d\theta_r} & \frac{d\beta_p}{d\phi_r} & \frac{d\beta_p}{d\delta_{o_r}} & \frac{d\beta_p}{d\delta_{\theta_r}} & \frac{d\beta_p}{d\delta_{\phi_r}} & \frac{d\beta_p}{d\delta_{2c_r}} & \frac{d\beta_p}{d\delta_{2s_r}} \\
\frac{dz_p}{d\Theta_r} & \frac{dz_p}{d\Phi_r} & \frac{dz_p}{dz_r} & \frac{dz_p}{d\theta_r} & \frac{dz_p}{d\phi_r} & \frac{dz_p}{d\delta_{o_r}} & \frac{dz_p}{d\delta_{\theta_r}} & \frac{dz_p}{d\delta_{\phi_r}} & \frac{dz_p}{d\delta_{2c_r}} & \frac{dz_p}{d\delta_{2s_r}} \\
\frac{d\theta_p}{d\Theta_r} & \frac{d\theta_p}{d\Phi_r} & \frac{d\theta_p}{dz_r} & \frac{d\theta_p}{d\theta_r} & \frac{d\theta_p}{d\phi_r} & \frac{d\theta_p}{d\delta_{o_r}} & \frac{d\theta_p}{d\delta_{\theta_r}} & \frac{d\theta_p}{d\delta_{\phi_r}} & \frac{d\theta_p}{d\delta_{2c_r}} & \frac{d\theta_p}{d\delta_{2s_r}} \\
\frac{d\delta_p}{d\Theta_r} & \frac{d\delta_p}{d\Phi_r} & \frac{d\delta_p}{dz_r} & \frac{d\delta_p}{d\theta_r} & \frac{d\delta_p}{d\phi_r} & \frac{d\delta_p}{d\delta_{o_r}} & \frac{d\delta_p}{d\delta_{\theta_r}} & \frac{d\delta_p}{d\theta_{\phi_r}} & \frac{d\delta_p}{d\theta_{2c_r}} & \frac{d\delta_p}{d\theta_{2s_r}}
\end{bmatrix}$$

The next task is to define the motions of the individual blades in terms of those of the rotor, the elements of the matrix. The motions of the blades are relative to the blade line of aerodynamic centers (or quarter chord) projected into a plane normal to the undeflected rotor shaft.

Consider a rotor with b number of blades with the number 1 blade located along the $+x$ axis (the axes rotate with the rotor). The position of the locus of aerodynamic centers of blade p is located at:

$$\psi_p = -(p-1)\frac{2\pi}{b}$$

which is an important relationship in determining blade motion relative to rotor motion.

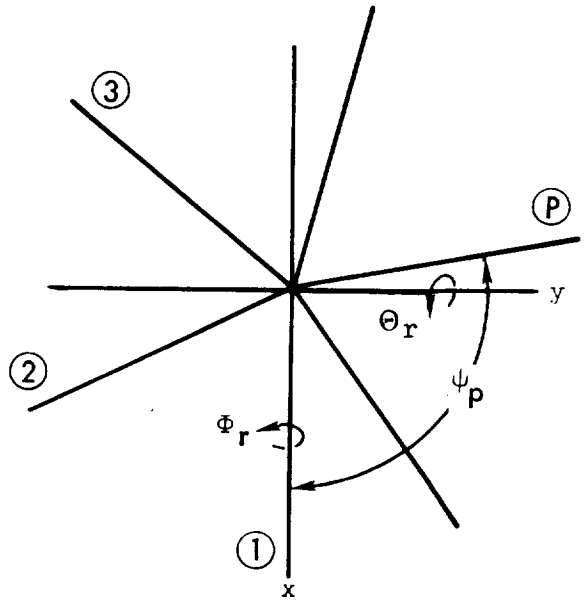

Blade motion due to shaft motion - Blade rigid flapping and pitching about the aerodynamic center are the only blade motions resulting from shaft pitch and roll displacements.

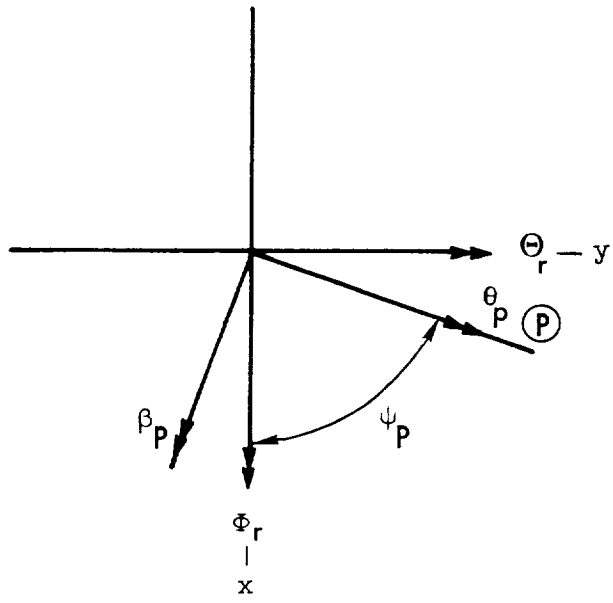

The rigid flapping of an arbitrary blade p due to shaft motion is:

$$\beta_p = - \Theta_r \cos \psi_p + \Phi_r \sin \psi_p$$

$$\beta_p = - \Theta_r \cos (p-1) \frac{2\pi}{b} - \Phi_r \sin (p-1) \frac{2\pi}{b}$$

The pitching of blade p due to shaft motion is:

$$\theta_p = \Theta_r \sin \psi_p + \Phi_r \cos \psi_p$$

$$\theta_p = - \Theta_r \sin (p-1) \frac{2\pi}{b} + \Phi_r \cos (p-1) \frac{2\pi}{b}$$

Rotor plunge motion produces only blade plunge motion. For a blade p, the relationship is merely: $z_p = z$.

In matrix notation the blade motion due to shaft motion is:

$$\begin{Bmatrix} \theta_p \\ z_p \\ \theta_p \\ \delta_p \end{Bmatrix} = \begin{bmatrix} -\cos(p-1)\frac{2\pi}{b} & -\sin(p-1)\frac{2\pi}{b} & 0 \\ 0 & 0 & 1 \\ -\sin(p-1)\frac{2\pi}{b} & \cos(p-1)\frac{2\pi}{b} & 0 \\ 0 & 0 & 0 \end{bmatrix} \begin{Bmatrix} \Theta_r \\ \Phi_r \\ z_r \end{Bmatrix}.$$

where $p = 1, \ldots, b$.

Blade motion due to gyro motion: Gyro pitching and rolling motion causes blade pitching and flapping relative to the blade quarter chord axis. In order to resolve the gyro motions into blade motions, define the axes x_b and y_b:

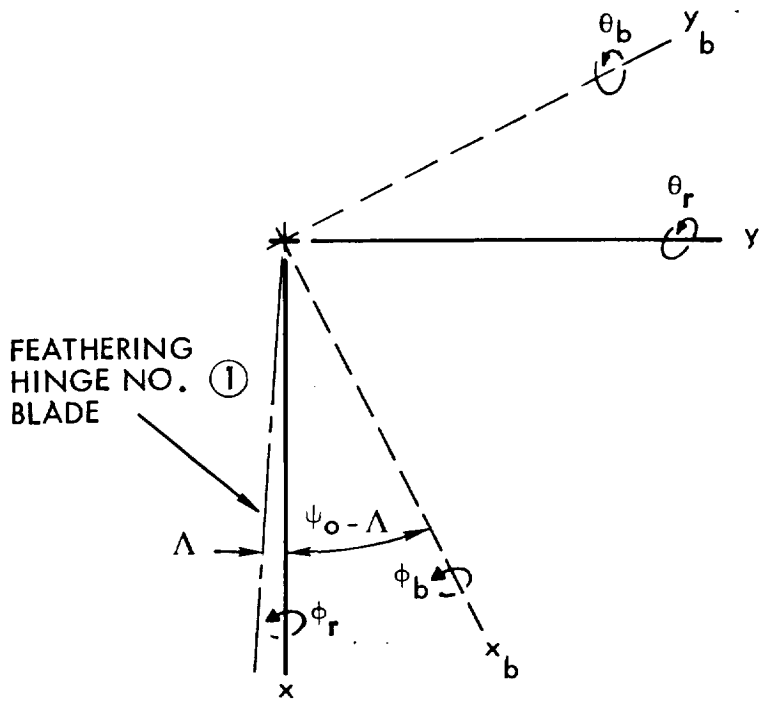

where:

$$\begin{Bmatrix} \theta_b \\ \phi_b \end{Bmatrix} = \begin{bmatrix} \cos(\psi_o - \Lambda) & -\sin(\psi_o - \Lambda) \\ \sin(\psi_o - \Lambda) & \cos(\psi_o - \Lambda) \end{bmatrix} \begin{Bmatrix} \theta_r \\ \phi_r \end{Bmatrix}$$

Positive values for θ_b and ϕ_b swashplate deflections produce positive blade feathering angles at $\psi = 180°$ and $90°$ respectively. Note that the blade feathering axis is located behind the quarter chord axis by the angle Λ. However, the azimuth position is measured relative to the quarter chord axis.

With the above in mind, the feathering angle of a blade located at ψ_p is:

$$\theta_{f_p} = \frac{1}{k}\left[-\theta_b \cos \psi_p + \phi_b \sin \psi_p\right]$$

$$\theta_{f_p} = -\frac{1}{k}\theta_b \cos (p-1)\frac{2\pi}{b} - \frac{1}{k}\phi_b \sin (p-1)\frac{2\pi}{b}$$

or in matrix notation:

$$\left\{\theta_{f_p}\right\} = -\frac{1}{k}\left[\cos (p-1)\frac{2\pi}{b} \qquad \sin (p-1)\frac{2\pi}{b}\right]\begin{Bmatrix}\theta_b\\ \phi_b\end{Bmatrix}$$

where k is the gyro to blades mechanical advantage.

The relationship between blade feathering about the feathering axis to pitching and flapping relative to the quarter chord axis is:

$$\begin{Bmatrix}\beta_p\\ \theta_p\end{Bmatrix} = \begin{Bmatrix}\sin \Lambda\\ \cos \Lambda\end{Bmatrix}\left\{\theta_{f_p}\right\}$$

Now the motions about the quarter chord can be expressed in terms of the swashplate angles θ_r and ϕ_r:

$$\begin{Bmatrix}\beta_p\\ \theta_p\end{Bmatrix} = -\frac{1}{k}\begin{Bmatrix}\sin \Lambda\\ \cos \Lambda\end{Bmatrix}\left[\cos (p-1)\frac{2\pi}{b} \quad \sin (p-1)\frac{2\pi}{b}\right]\begin{bmatrix}\cos (\psi_o - \Lambda) & -\sin (\psi_o - \Lambda)\\ \sin (\psi_o - \Lambda) & \cos (\psi_o - \Lambda)\end{bmatrix}\begin{Bmatrix}\theta_r\\ \phi_r\end{Bmatrix}$$

therefore:

$$\begin{bmatrix} \frac{d\beta_p}{d\theta_r} & \frac{d\beta_p}{d\phi_r} \\ \\ \frac{d\theta_p}{d\theta_r} & \frac{d\theta_p}{d\phi_r} \end{bmatrix} = -\frac{1}{k} \begin{Bmatrix} \sin\Lambda \\ \\ \cos\Lambda \end{Bmatrix} \begin{bmatrix} \cos(p-1)\frac{2\pi}{b} & \sin(p-1)\frac{2\pi}{b} \end{bmatrix} \begin{bmatrix} \cos(\psi_o - \Lambda) & -\sin(\psi_o - \Lambda) \\ \\ \sin(\psi_o - \Lambda) & \cos(\psi_o - \Lambda) \end{bmatrix}$$

and:

$$\begin{Bmatrix} \beta_p \\ \\ z_p \\ \\ \theta_p \\ \\ \delta_p \end{Bmatrix} = \begin{bmatrix} \frac{d\beta_p}{d\theta_r} & \frac{d\beta_p}{d\phi_r} \\ \\ 0 & 0 \\ \\ \frac{d\theta_p}{d\theta_r} & \frac{d\theta_p}{d\phi_r} \\ \\ 0 & 0 \end{bmatrix} \begin{Bmatrix} \theta_r \\ \\ \phi_r \end{Bmatrix}$$

Blade motion due to rotor flexible flapping motion: Blade flapping displacements are limited to the first flap mode, various combinations of which make up the rotor flapping modes. In rotating coordinates, the number of rotor modes will then equal the number of blades. A 2-blade rotor would have a collective and a pitch (or roll) flapping mode; whereas a 3-blade rotor would have both pitch and roll flapping modes, plus the collective mode. A 4-blade rotor would additionally have a self-balancing rotor mode, which would produce no inertial forces in the earth-fixed axes system. A 5-blade rotor would have two self-balancing modes.

For example, the modes of a 4-blade rotor would be as follows:

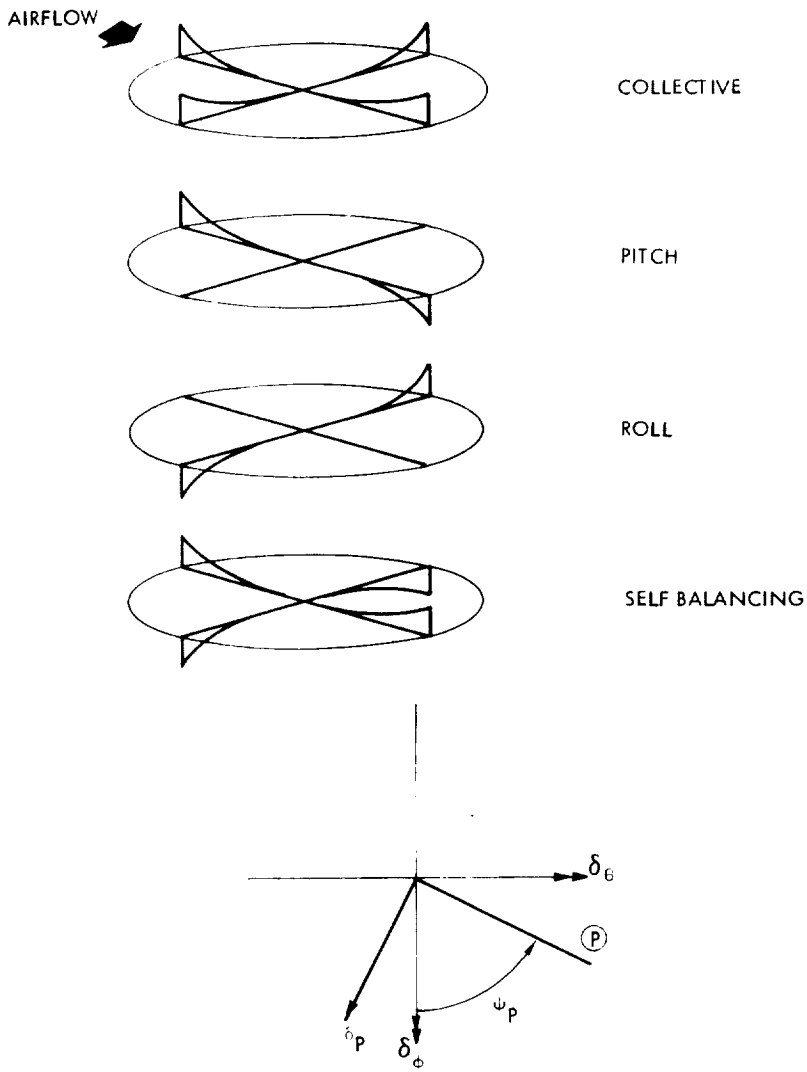

The relationship between the rotor flapping modes and the flapping of a blade at ψ_p is:

$$\delta_p = - \delta_{n\theta_r} \cos n \psi_p + \delta_{n\phi_r} \sin n \psi_p$$

$$\delta_p = - \delta_{n\theta_r} \cos n (p-1) \frac{2\pi}{b} - \delta_{n\phi_r} \sin n (p-1) \frac{2\pi}{b}$$

For rotors with an even number of blades:

$n = 1, \ldots, 0.5b$

For rotors with an odd number of blades:

$n = 1, \ldots, 0.5 (b-1)$.

where n is a number representing the harmonic shape of the mode relative to the axes rotating with the rotor. For example, n = 1 represents rotor disk tilting relative to the shaft; n = 2 represents a scalloped shape for the rotor tips with two lobes up and two down regardless of the number of blades.

Substituting the required values of n yields the modes. Thus:

$$\delta_p = -\delta_{\theta_r} \cos (p-1)\frac{2\pi}{b} - \delta_{\phi_r} \sin (p-1)\frac{2\pi}{b} \qquad n = 1$$

$$\delta_p = -\delta_{2c_r} \cos 2(p-1)\frac{2\pi}{b} - \delta_{2s_r} \sin 2(p-1)\frac{2\pi}{b} \qquad n = 2$$

$$\vdots$$

$$\delta_p = -\delta_{nc_r} \cos n(p-1)\frac{2\pi}{b} - \delta_{ns_r} \sin n(p-1)\frac{2\pi}{b}$$

In addition, the collective mode will be:

$$\delta_p = \delta_o$$

In matrix form:

$$\begin{Bmatrix} \beta_p \\ z_p \\ \theta_p \\ \delta_p \end{Bmatrix} = \begin{bmatrix} 0 & 0 & 0 & \cdots & 0 \\ 0 & 0 & 0 & \cdots & 0 \\ 0 & 0 & 0 & \cdots & 0 \\ 1 & -\cos (p-1)\frac{2\pi}{b} & -\sin (p-1)\frac{2\pi}{b} & \cdots & -\sin n(p-1)\frac{2\pi}{b} \end{bmatrix} \begin{Bmatrix} \delta_{o_r} \\ \delta_{\theta_r} \\ \delta_{\phi_r} \\ \vdots \\ \delta_{nc_r} \\ \delta_{ns_r} \end{Bmatrix}$$

In summary, the transformation matrix relating blade motions of the degrees of freedom in rotating axes are as shown on the following page for the five-blade rotor:

In-plane motions blade-rotor kinematics - With the in-plane displacements of the pth blade represented by the vector:

$$
\begin{Bmatrix} \theta_p \\ z_p \\ \theta_p \\ \xi_p \end{Bmatrix} = \begin{bmatrix} -\cos(p-1)\frac{2\pi}{b} & -\sin(p-1)\frac{2\pi}{b} & 0 & \frac{d\theta_p}{d\theta_r} & \frac{d\theta_p}{d\phi_r} & 0 \\ 0 & 0 & 1 & 0 & 0 & 0 \\ -\sin(p-1)\frac{2\pi}{b} & \cos(p-1)\frac{2\pi}{b} & 0 & \frac{d\theta_p}{d\theta_r} & \frac{d\theta_p}{d\phi_r} & 0 \\ 0 & 0 & 0 & 0 & 0 & 1 \end{bmatrix} \begin{Bmatrix} \Theta_r \\ z_r \\ \theta_r \\ \phi_r \\ \delta_{o_r} \\ \delta_{\theta_r} \\ \delta_{\phi_r} \\ \delta_{2c_r} \\ \delta_{2s_r} \end{Bmatrix}
$$

$$
\begin{Bmatrix} z_p \\ \xi_p \end{Bmatrix} = \begin{bmatrix} 0 & 0 & 0 & 0 & 0 & -\cos(p-1)\frac{2\pi}{b} & -\sin(p-1)\frac{2\pi}{b} & -\cos 2(p-1)\frac{2\pi}{b} & -\sin 2(p-1)\frac{2\pi}{b} \\ 0 & 0 & 0 & 0 & 0 & -\sin(p-1)\frac{2\pi}{b} & \cos(p-1)\frac{2\pi}{b} & -\sin 2(p-1)\frac{2\pi}{b} & \cos 2(p-1)\frac{2\pi}{b} \end{bmatrix} \begin{Bmatrix} z_r \\ \theta_r \\ \phi_r \\ \delta_{o_r} \\ \delta_{\theta_r} \\ \delta_{\phi_r} \\ \delta_{2c_r} \\ \delta_{2s_r} \end{Bmatrix}
$$

$$\eta_{xy_p} = \begin{Bmatrix} u_p \\ v_p \\ v_p \\ \delta_p \end{Bmatrix}$$

the relationship between the dispacements of degrees of freedom of the rotor relative to rotating axes and the displacements of the pth blade may be expressed as follows:

$$\eta_{xy_p} = \left[D_{xy_p} \right] \quad \theta_{xy}$$

where θ_{xy} is the vector of displacements of the rotor degrees of freedom relative to rotating axes.

Determination of the elements of the $\left[D_{xy_p} \right]$ matrix, or the pth blade motions that occur due to the motions of each of the rotor degrees of freedom follows.

DUE TO UNIT y DISPLACEMENT:

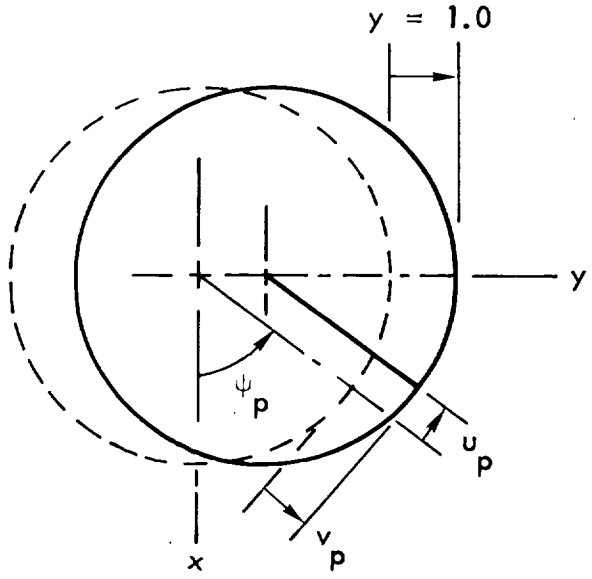

FOR THE P TH BLADE

$u_p = \cos \psi_p$

$v_p = \sin \psi_p$

WHERE $\psi_p = -(p-1)\frac{2\pi}{b}$

DUE TO UNIT x DISPLACEMENT:

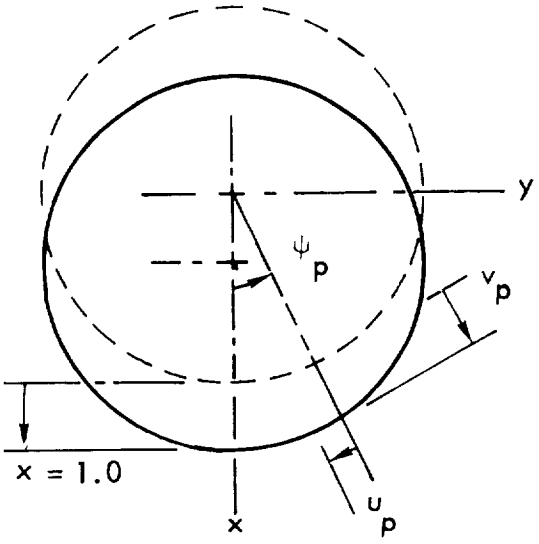

FOR THE P TH BLADE OF A "b" BLADED ROTOR

$u_p = -\text{SIN}\ \psi_p$

$v_p = \text{COS}\ \psi_p$

DUE TO UNIT ν DISPLACEMENT:

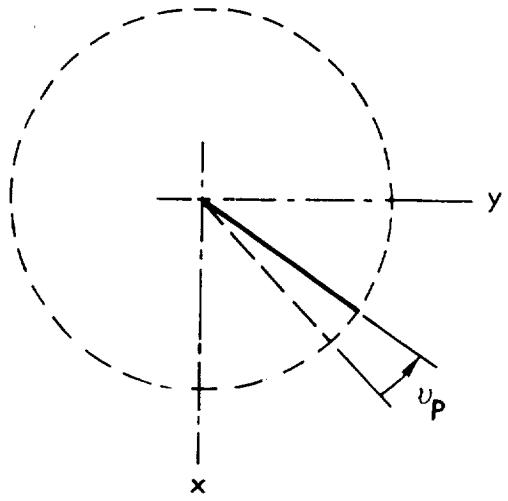

$v_p = 1.0$

DUE TO UNIT ζ_o DISPLACEMENT:

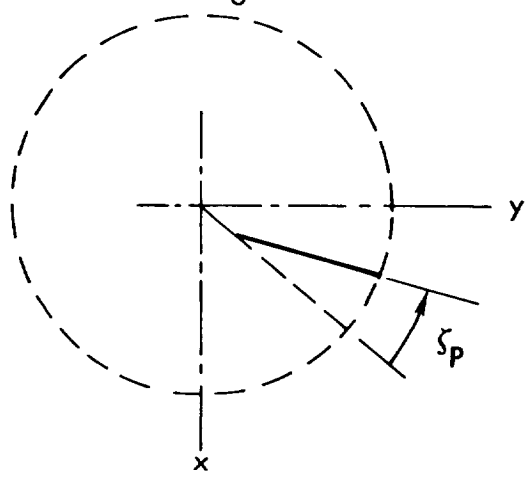

$\zeta_p = 1.0$

Due to unit ζ_y displacement:

$$\zeta_p = - \cos \psi_p$$

Due to unit ζ_x displacement:

$$\zeta_p = \sin \psi_p$$

Due to unit ζ_{2c} displacement:

$$\zeta_p = - \cos 2 \psi_p$$

Due to unit ζ_{2s} displacement:

$$\zeta_p = + \sin 2 \psi_p$$

If more than five blades are employed in the rotor design, then a general expression for blade displacement due to unit reactionless mode displacements can be used.

For unit reactionless mode dispacements ζ_{mc} and ζ_{ms}, where m = 1, 2...n

$n = \frac{b}{2}$ for even numbers of blades

In-plane motions - Relationship between the motions of the pth blade and the motions of the rotor in-plane degrees of freedom relative to rotating axes

$$\eta_{xy_p} = \left[D_{xy_p}\right] \beta_{xy}$$

$$\begin{Bmatrix} u_p \\ v_p \\ v_p \\ \zeta_p \end{Bmatrix} = \begin{bmatrix} \cos\psi_p & -\sin\psi_p & & \\ \sin\psi_p & \cos\psi_p & & \\ & & 1.0 & \\ & & & 1.0 - \cos\psi_p \quad \sin\psi_p \quad -\cos 2\psi_p \quad \sin 2\psi_p \cdots \cos n\psi_p \quad \sin n\psi_p \end{bmatrix}$$

ELEMENTS NOT SHOWN ARE ZERO

$$\begin{Bmatrix} y_r \\ x_r \\ v_r \\ \zeta_{o_r} \\ \zeta_{y_r} \\ \zeta_{x_r} \\ \zeta_{2c_r} \\ \zeta_{2s_r} \\ \vdots \\ \zeta_{nc_r} \\ \zeta_{ns_r} \end{Bmatrix}$$

and $n = \frac{b-1}{2}$ for odd numbers of blades

b = number of blades

the displacements of the pth blade become

$$\zeta_p = - \cos m\psi_p$$

$$\zeta_p = \sin m\psi_p$$

Theoretical Considerations

Some of the physical elements of the rotor-gyroscope-body system or the forces on, or motions of them, were simplified for the sake of clarifying the behavior of the complete system. The chosen simplifications did not greatly distort the completed result and the reasons for this are discussed in this section.

Those aspects of the system elements simplified included: rotor aerodynamics, blade section aerodynamics, radial flow effects at blade tips, in-plane components of aerodynamic lift forces, in-plane motion of a single blade, blade flap to in-plane inertia coupling,and the high-speed gyroscope physical representation. The ranges of system parameters over which the simplifications are expected to be valid are indicated.

Some concepts useful in understanding the behavior or hingeless rotors are also discussed. These include mean rotor aeroelastic derivatives, the composition of the hub force two-component vibration derivatives, residual forces and how these may be trimmed by the application of cyclic pitch.

Aerodynamic Simplifications. - Flight at advance ratio greater than $\mu = 0.7$ has not been studied very extensively, up to this time. Therefore, the present study should be considered exploratory in nature. The simplest concepts which yield approximately correct answers have been used.

In this study of the basic behavior of hingeless rotor systems, the mathematical models representing them have been shorn of all but the most essential considerations. Some of the effects eliminated would have contributed significantly to the magnitudes of the final answers at certain critical conditions,

but including them would have obscured the fundamental behavior of the system (and more comprehensive methods are available for the purpose of producing accurate quantitative results).

Some of the simplifications are as follows:

Linear aerodynamics: The present tests have been limited to conditions which do not seriously violate aerodynamic linearily. Allowing the use of linear aerodynamic theory opens the door to straightforward techniques for estimating such things as radial lift induction effects, effects of downwash from previous blade passages and unsteady aerodynamics. Only one of these effects has been investigated in this study. The main consequence, however, of aerodynamic linearity is that superposition of the effects of angle changes, for example: control angle, angle of attack, and precone may be calculated independently of each other and summed up to yield the correct answer.

Aerodynamics is expected to be linear as long as the combined section angle-of-attack remains less than, say, 10 degrees. During the conversion phase of flight of a stowable rotor aircraft and high-speed flight of slowed rotor compound helicopters, the nominal rotor lift is small so that blade angles-of-attack are well below stall limits in areas of significant dynamic pressure. In addition, over most of the conversion, tip speeds are well below the speed of sound.

In the formulation of the equations of motion the inertia and structural forces are also kept within the linear range, except for in-plane forcing functions, so that the theory of systems of linear ordinary differential equations, with harmonic coefficients, can be employed.

Rotor-induced inflow: At high advance ratio, if induced inflow is assumed uniform over the disk, its value is very small. Even though uniform inflow is generally considered a poor approximation, it is expected that at very high advance ratio even the nonuniform induced inflow effects are negligible; therefore, it has been completely ignored in this report.

Advance ratio effects: With any forward speed at all there is a region just to the left of the rotor mast where the net flow proceeds past the airfoil sections from the trailing edge to the leading edge. It is small at

low advance ratio and approaches 50% of the disk as the advance ratio approaches infinity. Effects of reverse velocity have been explicitly accounted for. The blade trailing edge has become the new "leading edge" and section aerodynamic centers have been assumed shifted to the three quarter chord locus and local lift curve slope has been reduced.

Another ramification of advance ratio is that it controls the geometry of the vortex patterns shed by the individual blades. At low advance ratio the vortex structure and attendant downwash from many blade passages accumulates over the rotor disk and drifts slowly downstream causing large induced downwash over the disk concentrating toward its aft edge. However, at high advance ratio, the tip vortices stream almost straight downstream from the blade tips so that downwash cannot accumulate. This is why induced downwash at high advance ratio has been assumed to be negligible.

At azimuths remote from 90 and 270 degrees at high advance ratio, the flow approaches the blade obliquely. In the disk aft semicircle the flow meets the blade flowing obliquely outboard. In the disk forward semicircle, it meets the blade flowing obliquely inboard. Wind tunnel tests have shown that resolving the flow into components parallel to the blade and normal to it, ignoring the radial component, and treating the blade section immersed in the normal component as two-dimensional flow, yields a close approximation to the measured pressure distribution and lift at the section (Reference 12). This principle has been used extensively for reducing the drag of wings of airplanes flying at transonic Mach numbers. In addition, recent tests have shown that the primary effect of spanwise flow is to increase the maximum lift before stall on the section and not to change the lift curve slope or linearity (Reference 13).

At high advance ratio, radial flow acting on the tips of slender blades at a local angle-of-attack, creates some lift. If the rotor angle-of-attack were zero, the blades in the forward semi-disk would still present a local angle-of-attack due to precone. A simplified analysis showed that even at an advance ratio as high as $\mu = 2.0$ the effects on aeroelastic derivatives of blade tip lift were dwarfed by blade loads induced by flow normal to the leading edge. Blade tip slender-body lift due to radial flow was therefore not included in these analyses.

Unsteady aerodynamics: The primary effect of unsteady aerodynamics can be seen by examining the growth of lift on a blade section after a sudden change in angle-of-attack. Lift growth is given by Wagner in terms of numbers of chords travelled (Reference 14). Lift starts at 50% of maximum and grows to 90% within 6 chords travelled. In a rotor with blades of small chord the lift becomes 90% of steady state in a small fraction of the rotor tip perimeter resulting in effectively steady-state conditions being reached within less than 10% of total azimuthal travel if the forward speed were zero. At high advance ratio the tip velocity at $\psi = 90°$ is greater than ΩR so the lift would grow to steady state in somewhat smaller azimuthal displacement. In the reverse flow region, the opposite would be true and a much longer azimuthal travel would be required to attain a near steady-state condition. Unsteady effects would cause some deviation from the results expected with steady aerodynamics, especially in the reverse flow region but there the low dynamic pressure makes the lift sensitivity small so the effect would be lost in the total aerodynamic derivative. The net effect of unsteady aerodynamics is not expected to reduce the effective blade section lift-curve slope by more than a few percent. For this reason unsteady aerodynamics is not expected to change the basic characteristics of solutions found without it and was not included in these analyses.

Blade lift radial induction effects: - The most significant effect of radial induction is loss of lift near the blade tip. This effect depends on the aspect ratio of the lifting surface. The blades of typical rotors have aspect ratios greater than ten. For such high aspect ratios the tip effect is hardly noticeable inboard of about 80% of the radius, and can be approximately accounted for by assuming the blade to be smaller in radius by a factor B ($B \approx 0.97$ in these analyses) than it is.

A second effect is a small reduction in lift over the whole blade. This may be accounted for by reducing the local lift curve slope slightly. A reduction factor of .95 was found to be appropriate for the 33-ft rotor. The lift at a section with the above corrections depends only on the local dynamic pressure normal to the leading edge and the normal angle-of-attack at the section. This is also known as strip theory.

In-plane component of blade lift: In the formulation of the in-plane equations of motion of the blades-hub mass system, it is assumed that all mass motions are in the plane of the disk. In actual fact the principal axis of the blade in-plane motions of the three-quarter radius section, for example, are not normal to and parallel to the disk plane but are at a small angle to the reference plane.

It is, therefore, important to calculate the component of section aerodynamic lift in the direction of the in-plane principal axis even though it continuously changes direction with azimuth. So long as these in-plane equation external forces are calculated in the actual direction of the in-plane modes they may be applied to the planar equations without introducing significant error.

The blade section lift force is predominantly in the vertical direction so that the in-plane component magnitude is controlled by the sine of the small angle between the in-plane principal axis and the relative wind vecotr component normal to the blade leading edge. This assumes that the blade section resultant force is perpendicular to the wind velocity vecotr and may be justified by examining a section of a blade with local angle of attack applied to it. The lift and drag are available from section theory and experiment (Reference 12).

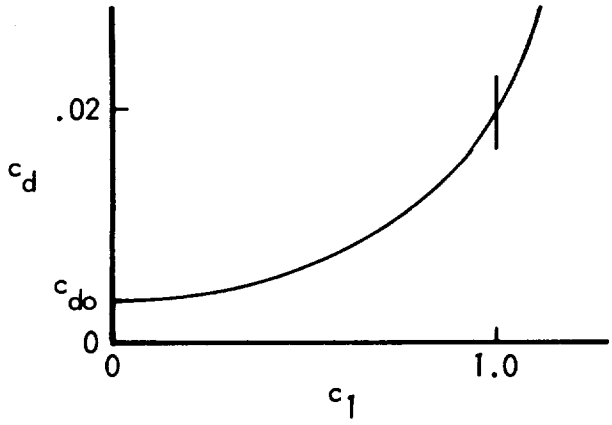

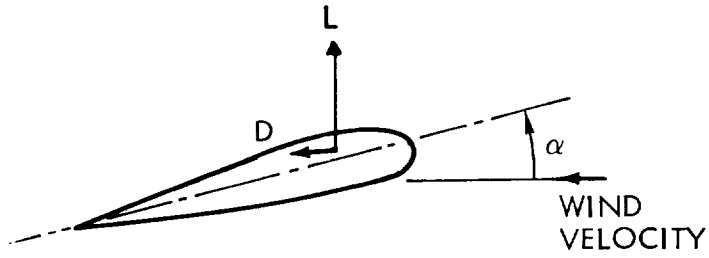

The drag is very small and parallel to the wind vector, it is at $c_l = 1.0$, for example, 2% of the lift or $c_d = .02$. This causes about a 1.0° change in the resultant vector from the position of the lift vector alone. If the c_{d_o}

or drag at zero lift is considered separately, then the resultant is less than 1/2 degree from the section lift vector, which is uniquely defined to be perpendicular to the wind vector. In forcing the blades in the in-plane principal axis direction the effective plane of the in-plane motion may vary by angles of the order of 10° or more from the wind direction. The error caused by eliminating the section drag due to lift, therefore, will be virtually negligible in determining the in-plane aerodynamic external forces.

In-plane motion of a single blade. - In an actual cantilever blade with no root motion, the flap and in-plane motions are coupled. The blade still possesses modes that are primarily flap motion or in-plane motion but each has some component of the other.

At some feathering pitch, near zero, the two first cantilever modes, characterized by motions at the three-quarter radius, for example, will be uncoupled: pure flap and pure in-plane. The inclination of the principal axis will be zero.

At zero rpm, if the hub inboard of the feathering hinge is very stiff so that most of the blade flexibility is outboard, then the structural principal axis and the flap-in-plane mode vibration principal axes follow the feathering pitch rotation. This is the case for the 33-ft rotor. If the hub inboard of the feathering hinge is flexible and the blade outboard very stiff then the principal axis does not rotate as the blade feathers. Most rotors in service approach this condition.

At high rpm centrifugal forces come into play. They produce a large effective stiffness resisting displacements normal to the disk plane and a small effective stiffness resisting displacements in the plane of the disk, the latter proportional to effective in-plane pivot offset. The principal axis of the centrifugal stiffnesses are not affected by blade feathering pitch. For example, the flap in-plane principal axes for an articulated rotor are always parallel and perpendicular to the disk plane and independent of blade feathering pitch.

Centrifugal stiffening acting in conjunction with flap and in-plane structural stiffnesses generates a new principal axis which rotates in proportion to feathering pitch with a factor of proportionally either greater or less than unity. In these analyses the factor is denoted by the symbol κ.

Flap-in-plane inertia coupling. - The in-plane blade-hub mass equations of motion were written as though all mass motions took place in the disk plane normal to the shaft. The vertical motions equation were written as though all masses moved only in the vertical direction. Under these conditions no coupling between vertical motions and in-plane motions would exist.

If a rotor possessed no precone or twist and its collective pitch and angle-of-attack were zero it would satisfy these conditions for small cyclic pitch applications.

The 7.5-foot rotor, studied experimentally, essentially met these requirements even though it was operated at significant values of collective pitch and angle-of-attack. Even though the blades of the 33 foot rotor were twisted and preconed it is felt to have approximately met the requirements because it was tested only at zero angle of attack and a collective pitch, at the three-quarter radius, of $\theta_{.75R} = 1.5°$. Also, the blades of both rotors were stiffer than those in use in most flying hingeless rotor helicopters.

The vertical motions equations were forced by large, easily calculated, linearly independent aerodynamic and centrifugal external forces. The resulting response was stable and well behaved.

The forcing functions for the in-plane equations, however, were nonlinear functions of the vertical equations external forces and response motions and were small in magnitude. The in-plane response was lightly damped and, near resonance, of large magnitude.

High-speed gyroscope. - The high-speed gyroscope, in these analyses, was mounted so that it always remained parallel to the swashplate. Slop and elastic distortion in the linkages attaching its housing to the blade feathering horns was assumed to be zero.

The gyroscope itself was assumed to have no vertical depth; all its mass was assumed to be concentrated into a flat disk. With its diametral inertia, or moment of inertia about an axis lying in the disk, denoted by I_G, its unforced equations of motion in stationary axis were:

$$\begin{bmatrix} I_G & 0 \\ 0 & I_G \end{bmatrix} \begin{Bmatrix} \ddot{\theta} \\ \ddot{\phi} \end{Bmatrix} + \begin{bmatrix} 0 & -2\Omega_G I_G \\ 2\Omega_G I_G & 0 \end{bmatrix} \begin{Bmatrix} \dot{\theta} \\ \dot{\phi} \end{Bmatrix} = 0$$

where Ω_G is the gyro rotation rate in radians per second

Mean aeroelastic derivatives. - If the shaft of a hingeless rotor were fixed so that its response motions were zero and it was then given prescribed steady rigid body displacements and velocities so that steady aerodynamic states existed at the rotor, then the rotor would attain steady oscillating deformed shapes under the action of the motion-induced airloads and gyroscopic forces. It would also develop steady mean and oscillating forces at the hub.

The mean aeroelastic derivatives are the rates of change of each mean hub force component with respect to each change in shaft displacement and velocity. Derivatives may also be found if the change in each mean force component due to unit changes in each control system displacement and basic geometric shape such as twist and precone is given.

Mean aeroelastic derivatives are often used in conjunction with the six degree of freedom rigid body equations of motion for helicopter overall stability analyses in much the same way as wing aeroelastic derivatives are used in fixed wing aircraft stability analyses.

The mean and oscillatory aeroelastic derivatives may be calculated using the rotor alone vertical motions equations, which in this study possess numbers of degrees of freedom equal to the number of blades. The aerodynamic coefficients of the differential equations or the ratio of change of generalized force per unit displacement or velocity of each degree of freedom must first be calculated. The coefficients are divided into two classes: response coefficients and forcing coefficients. Response coefficients represent the aerodynamic forces produced by motions of the degrees of freedom. Forcing coefficients represent those aerodynamic forces produced external to the dynamic system by gust angle-of-attack, rotor preconing, and blade twist and by swashplate collective, which is not a degree of freedom in this analysis.

TWIST SHAPE PARAMETER

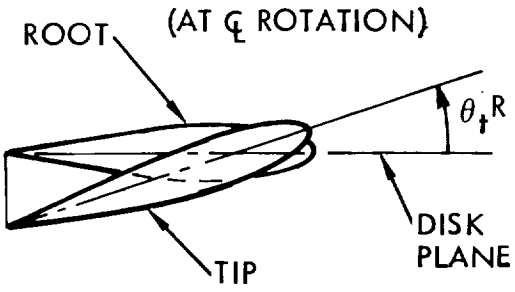

+ twist is nose up and it is measured from zero at the root (℄ rotation). It should be noted that θ_t is a rate of change of twist angle per unit span; therefore $\theta_{tip} = \theta_t R$.

COLLECTIVE DISPLACEMENT

Not a degree of freedom but collective forces are used in forcing derivatives.

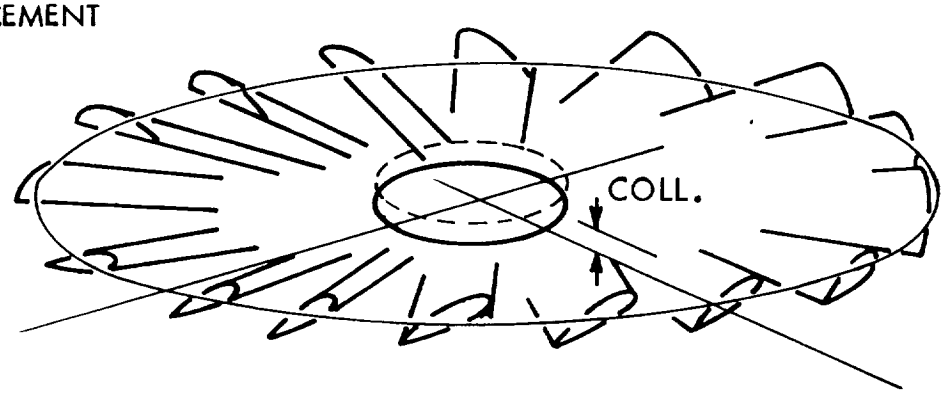

The main difference between aerodynamic derivatives of fixed wing and rotary wing aircraft is that the rotary wing derivatives or coefficients possess, as well as a mean value, parts which vary periodically with time (or azimuth). In the case of the forcing derivatives, these merely add steady oscillatory components to steady-state conditions. But the periodic parts of the response coefficients alter the basic mathematics of the differential equations.

The coefficients, analogous to the rigid wing derivatives of fixed wing aircraft, relate the rotor forces, moments, and generalized forces to the displacements and velocities in the various rotor degrees of freedom. The coefficients are employed in equations relative to an earth-fixed axis system, but are serially derived in this report from blade forces due to blade motions through full rotor coefficients in rotating axes to the final fixed axes values. Coefficients may be found for rotors with three to five blades.

An examination of the stationary axis coefficients showed them to consist of mean values, independent of rotor azimuth, and harmonic components at fre-frequencies of integer multiples of the number of blades times the rotor rotational rate. The lowest frequency multiples of the three- and four-blade rotors were 3P and 4P respectively, and were much larger in magnitude than that of the higher multiples of rotor frequency. For this reason only the amplitudes of the lowest frequency components, along with the mean value, were kept in the analyses. The phase of the harmonic components, remained essentially unchanged except at values of $1/\mu$ approaching zero.

The mean aeroelastic derivatives based on rotor alone equations of motion, including aerodynamic coefficients just described, are displayed in vector diagrams where changes in two moment or force components take place with respect to one controllable motion. For example, the variation in hub pitch and roll moment per unit cyclic pitch aeroelastic derivatives, with blade stiffness and advance ratio, is shown as a map of hub moment vector change.

Oscillatory aeroelastic derivatives. - The oscillatory components of the aeroelastic derivatives, relative to stationary coordinates, consist primarily of first harmonic, $b\Omega$, frequency; where b is number of blades and Ω the rotor rotation frequency. (Higher harmonic forces are very small and are not studied in this report.)

The $b\Omega$ harmonic variations of hub and swashplate moment and shaft shear execute fixed ellipsoidal patterns in a vector diagram such as that used to display mean derivatives. The ellipse may be flat or circular or have any aspect ratio between these limits and its major axis may be oriented in any azimuth. For example, the shaft shear oscillatory forces produced by a 3-blade rotor in stationary axis may be described as the following function of azimuth, where Y and X are lateral and fore-aft forces respectively.

$$Y = Y_{3c} \cos 3\psi + Y_{3s} \sin 3\psi$$

$$X = X_{3c} \cos 3\psi + X_{3s} \sin 3\psi$$

This resolution of the forces may be transformed into rotating coordinates to yield the two constant amplitude components, 2P and 4P, of vibration which had combined to form the 3P ellipse in stationary axis.

$$Y_R = A \cos 2\psi + B \sin 2\psi + C \cos 4\psi - D \sin 4\psi$$

$$X_R = B \cos 2\psi - A \sin 2\psi + D \cos 4\psi + C \sin 4\psi$$

In rotating coordinates the force vector consists of two constant amplitude parts one advancing at two per revolution (2P) and the other regressing at four per revolution (4P). These two force components fully describe the oscillatory forces, whether in rotating or stationary coordinates.

If the two components are kept separate and transformed back into stationary coordinates, each keeps its same advancing or regressing character but, of course, changes back to 3P frequency.

$$Y = A \cos 3\psi + B \sin 3\psi + C \cos 3\psi - D \sin 3\psi$$

$$X = B \cos 3\psi - A \sin 3\psi + D \cos 3\psi + C \sin 3\psi$$

The two vector components are shown in Figure 9.

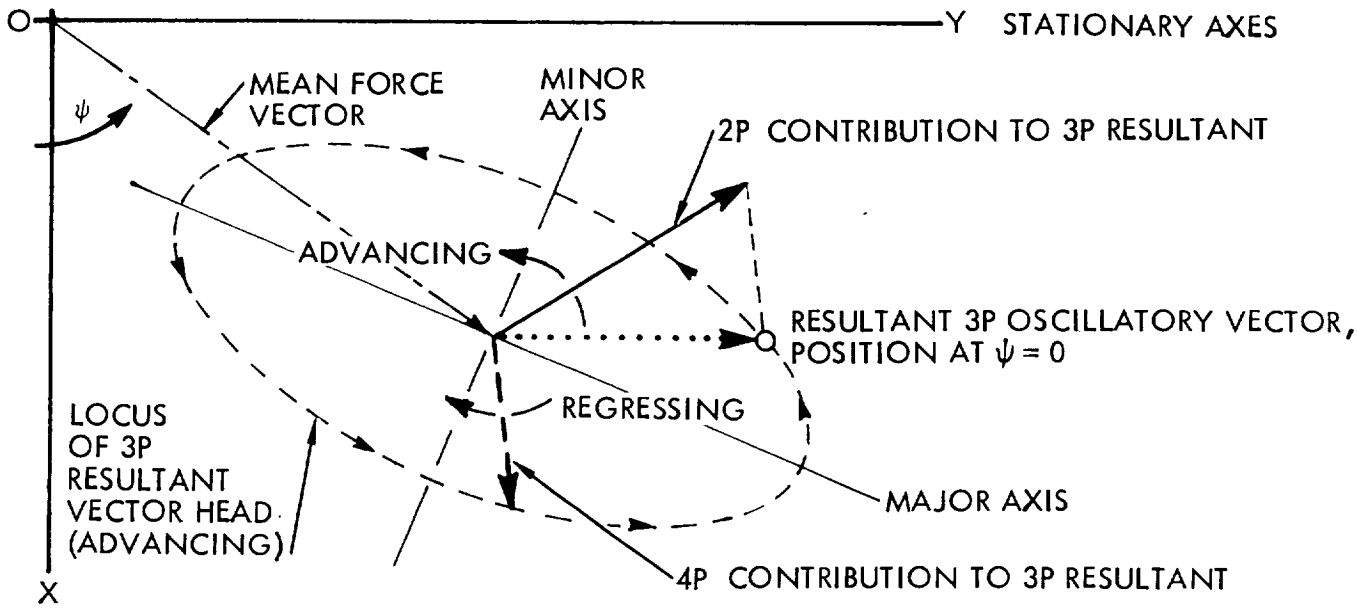

Figure 9. Three-Blade Rotor Shaft Shear Force Variation With Time

The 3P two-dimensional moment or force vibration may therefore be completely described in terms of its advancing and regressive components by specifying the amplitude and azimuthal heading, or the Y and X components, of each at a particular instant of time or rotor azimuth position. In this report the vibration components are described at rotor azimuth $\psi = 0$, that is, with the number 1 blade pointed aft along the X-axis.

It is clear that the Y and X force components of each of the advancing and regressing components of the 3P vibration at $\psi = 0$ are given by the following:

2P Contribution

$$Y_{2p} = A = \frac{Y_{3c} - X_{3s}}{2}$$

$$X_{2p} = B = \frac{X_{3c} + Y_{3s}}{2}$$

4P Contribution

$$Y_{4p} = C = \frac{Y_{3c} + X_{3s}}{2}$$

$$X_{4p} = D = \frac{X_{3c} - Y_{3s}}{2}$$

The complete specification of oscillatory aeroelastic derivatives of shaft two-dimensional forces follows the rules of shaft shear:

$$\frac{\partial \left(Y_{2p}, X_{2p} ; Y_{4p}, X_{4p} \right)}{\partial \left(\theta_{1c}, \theta_{1s}, \theta_{o}, \alpha \right)}$$

Residual forces. - The concept of residual forces facilitates the discussion of experimental results. In a rotor wind tunnel experiment only the following parameters may be controlled and varied: cyclic and collective pitch θ_c, θ_s, θ_o and angle-of-attack α. It is therefore only possible to obtain experimental aeroelastic derivatives of hub forces and moments and blade forces with respect to these parameters.

In rotors with precone, blade twist, and camber, there are "residual forces" with the controls neutral, i.e., with $\theta_c = \theta_s = \theta_o = \alpha = 0$. Knowledge of the residual mean and oscillatory forces coupled with the mean and oscillatory aeroelastic derivatives allows the recreation of all test conditions and extrapolation and interpolation of them. In particular, cyclic pitch required to trim hub moments to zero may be found, and these are displayed to indicate the center of cyclic pitch variation during the tests. In addition, cyclic pitch to trim swashplate meoments or any 2P or 4P vibration component to zero could be determined from this data, if desired.

It should be noted that the residual forces for the 7.5-ft-diameter rotor are zero. It should also be noted that since no systematic variation of collective pitch or angle-of-attack were made in the 33-ft rotor tests, the contributions of the small values existing during the tests are added to the residual forces. Because of the large cyclic pitch required to trim out the effects of twist and precone on the 33-ft rotor it was not possible to actually test at zero cyclic pitch under all rpm-forward speed conditions without overloading the rotor. At these test conditions the residual forces may not be realistic, since they were obtained by extrapolation of a best fit plane through the experimental data, and at the high rotor forces at zero cyclic pitch nonlinear effects may be important.

VERTICAL MOTIONS EQUATIONS

Equations of motion are derived for a free flying rotary wing aircraft having three body degrees of freedom, a main rotor with an arbitrary number of blades (b), and a control gyro on the main rotor with two degrees of freedom. The body degrees of freedom are restricted to pitch, roll, and plunge; the gyro degrees of freedom to pitch and roll only. Only one bending mode is used for each individual rotor blade. Its shape is parabolic and in many cases (in particular for a stoppable rotor vehicle) is a good approximation of the first vertical or "flapwise" blade bending mode.

The derivation first develops the equations of motion of each single blade in its own axis system rotating with the rotor. The equations, in four degrees of freedom, contain matrices of inertia; centrifugal, structural, and aerodynamic coefficients.

Next, the independent sets of equations, one for each blade, are coupled together and transformed into equations of motion of the total rotor, still in rotating coordinates. Coefficients representing swashplate springs and dampers and rotor elastic mode structural damping are then added.

Following this, the equations in rotating coordinates are transformed into stationary coordinates where the gyroscope, swashplate stationary axis springs, and dampers and body terms are added to complete the homogenous linear ordinary differential equations.

Lastly, the external forces applied to the system are calculated. These forcing functions, occupying the RHS of the equations, are caused by control motions or forces, precone, twist, and angle-of-attack.

Single Blade Equations of Motion

The single blade forced linear ordinary differential equations of motion establish the condition of dynamic equilibrium between the external generalized forces and those produced by motions of the blade degrees of freedom. They consist of sums of the products of coefficients and motions as follows:

$$\left[I_b\right] \ddot{\eta}_z + \left[CF_b\right] \eta_z - \left[\frac{\partial F_b}{\partial \dot{\eta}} (\psi)\right] \dot{\eta}_z - \left[\frac{\partial F_b}{\partial \eta} (\psi)\right] \eta_z = \left[\frac{\partial F_b}{\partial \text{Fixed}}_{\text{geom}}\right] \left\{\begin{matrix}\text{Fixed}\\ \text{geom}\end{matrix}\right\}$$

where

$$\eta_z = \left\{\begin{matrix} \beta \\ z \\ \theta_{c/4} \\ \delta \end{matrix}\right\} \quad \text{and} \quad \left\{\begin{matrix}\text{fixed}\\ \text{geom}\end{matrix}\right\} = \left\{\begin{matrix} \beta_o \\ \theta_o \\ \theta_t \\ \dot{z}_g \end{matrix}\right\}$$

β_o — rotor precone

θ_o — rotor collective

θ_t — blade twist rate

$\dot{z}_g$ — gust angle-of-attack factored by forward speed

and the square matrices represent the following

$\left[I_b\right]$ — Blade inertia

$\left[CF_b\right]$ — Centrifugal and structural stiffness

$\left[\frac{\partial F_b}{\partial \dot{\eta}} (\psi)\right]$ — Aerodynamic damping

$\left[\frac{\partial F_b}{\partial \eta} (\psi)\right]$ — Aerodynamic stiffness

$\left[\frac{\partial F_b}{\partial \text{Fixed}}_{\text{geom}}\right]$ — Blade aerodynamic and centrifugal forcing

Single blade inertia matrix. - The single blade inertia matrix represents the relationship between accelerations in the degrees of freedom and generalized forces on the degrees of freedom due to the accelerations.

$$\begin{Bmatrix} \text{b.m.} \\ V \\ \text{p.m.} \\ H \end{Bmatrix} = - \left[I_b\right] \begin{Bmatrix} \ddot{\beta} \\ \ddot{z} \\ \ddot{\theta}\, c/_4 \\ \ddot{\delta} \end{Bmatrix}$$

Note: The minus sign merely indicates the presence of the forces on the RHS of the equation in this expression.

The blade generalized forces are as follows:

b.m. Blade root bending moment at the center of rotation, ft lb.

V Blade root shear at the center of rotation, lb.

p.m. Pitch moment about the blade quarter chord, ft lb.

H Blade flapping generalized force, lb.

The $\left[I_b\right]$ matrix therefore is defined as follows:

$$\left[I_b\right] = \begin{bmatrix} \frac{\partial \text{b.m.}}{\partial \ddot{\beta}} & \frac{\partial \text{b.m.}}{\partial \ddot{z}} & \frac{\partial \text{b.m.}}{\partial \ddot{\theta}\, c/_4} & \frac{\partial \text{b.m.}}{\partial \ddot{\delta}} \\ \frac{\partial V}{\partial \ddot{\beta}} & \frac{\partial V}{\partial \ddot{z}} & \frac{\partial V}{\partial \ddot{\theta}\, c/_4} & \frac{\partial V}{\partial \ddot{\delta}} \\ \frac{\partial \text{p.m.}}{\partial \ddot{\beta}} & \frac{\partial \text{p.m.}}{\partial \ddot{z}} & \frac{\partial \text{p.m.}}{\partial \ddot{\theta}\, c/_4} & \frac{\partial \text{p.m.}}{\partial \ddot{\delta}} \\ \frac{\partial H}{\partial \ddot{\beta}} & \frac{\partial H}{\partial \ddot{z}} & \frac{\partial H}{\partial \ddot{\theta}\, c/_4} & \frac{\partial H}{\partial \ddot{\delta}} \end{bmatrix}$$

For blades with mass centroids of sections distributed along the quarter chord line, mass distribution given by $\frac{dm}{dr}(r)$ and a local pitching moment of inertia of the blade about the quarter chord of I_o, the above matrix becomes:

$$\left[I_b\right] = \begin{bmatrix} \int_r r^2 \frac{dm}{dr}\, dr & \int_r r \frac{dm}{dr}\, dr & 0 & \int_r \left(\frac{r}{R}\right)^2 r\, \frac{dm}{dr}\, dr \\ \int_r r \frac{dm}{dr}\, dr & \int_r \frac{dm}{dr}\, dr & 0 & \int_r \left(\frac{r}{R}\right)^2 \frac{dm}{dr}\, dr \\ 0 & 0 & I_o & 0 \\ \int_r \left(\frac{r}{R}\right)^2 r\, \frac{dm}{dr}\, dr & \int_r \left(\frac{r}{R}\right)^2 \frac{dm}{dr}\, dr & 0 & \int_r \left(\frac{r}{R}\right)^4 \frac{dm}{dr}\, dr \end{bmatrix}$$

The matrix is symmetric.

Single blade centrifugal and structural matrix. - The single blade centrifugal and structural matrix relates the generalized single blade forces to displacements of the single blade degrees of freedom.

$$\begin{Bmatrix} \text{b.m.} \\ V \\ \text{p.m.} \\ H \end{Bmatrix} = -\left[\text{C.F.}_b\right] \begin{Bmatrix} \beta \\ z \\ \theta_{c/4} \\ \delta \end{Bmatrix}$$

Note: Minus sign indicates terms are on RHS of equations.

The matrix is therefore defined as follows:

$$\left[CF_b\right] = \begin{bmatrix} \frac{\partial \text{b.m.}}{\partial \beta} & \frac{\partial \text{b.m.}}{\partial z} & \frac{\partial \text{b.m.}}{\partial \theta_{c/4}} & \frac{\partial \text{b.m.}}{\partial \delta} \\ \frac{\partial V}{\partial \beta} & \frac{\partial V}{\partial z} & \frac{\partial V}{\partial \theta_{c/4}} & \frac{\partial V}{\partial \delta} \\ \frac{\partial \text{p.m.}}{\partial \beta} & \frac{\partial \text{p.m.}}{\partial z} & \frac{\partial \text{p.m.}}{\partial \theta_{c/4}} & \frac{\partial \text{p.m.}}{\partial \delta} \\ \frac{\partial H}{\partial \beta} & \frac{\partial H}{\partial z} & \frac{\partial H}{\partial \theta_{c/4}} & \frac{\partial H}{\partial \delta} \end{bmatrix}$$

The centrifugal part of the matrix may be formed from the inertia matrix by factoring moments of inertia by Ω^2 and making the second row and column zero. The structural part of the term $\frac{dH}{d\delta}$ is obtained by substituting the natural frequency squared, ω_δ^2, for the rotational frequency squared, Ω^2, in the product with the flapping generalized mass.

$$\left[CF_b\right] = \Omega^2 \begin{bmatrix} \int_r r^2 \frac{dm}{dr}\, dr & 0 & 0 & \int_r \left(\frac{r}{R}\right)^2 r\, \frac{dm}{dr}\, dr \\ 0 & 0 & 0 & 0 \\ 0 & 0 & I_o & 0 \\ \int_r \left(\frac{r}{R}\right)^2 r\, \frac{dm}{dr}\, dr & 0 & 0 & \left(\frac{\omega_\delta}{\Omega}\right)^2 \int_r \left(\frac{r}{R}\right)^4 \frac{dm}{dr}\, dr \end{bmatrix}$$

Single blade aerodynamic matrices. - There are three single blade aerodynamic matrices. They relate root bending moment, shear, quarter-chord pitching moment, and flap generalized force, to the velocities and displacements of the degrees of freedom and to the fixed geometric shape parameters of the blade.

The two response aerodynamic matrices are:

$$\left[\frac{\partial F_b}{\partial \eta}(\psi)\right] \quad \text{and} \quad \left[\frac{\partial F_b}{\partial \dot{\eta}}(\psi)\right]$$

and the forcing aerodynamic derivatives in matrix form are:

$$\left[\frac{\partial F_b}{\partial \text{ Fixed geom}}(\psi)\right]$$

The two response matrices are similar in form to the centrifugal and inertia matrices except terms in each are functions of azimuth. For example, the aerodynamic damping matrix is as follows:

$$\left[\frac{\partial F_b}{\partial \dot{\eta}}(\psi)\right] = \begin{bmatrix} \frac{\partial b.m.}{\partial \dot{\beta}}(\psi) & \frac{\partial b.m.}{\partial \dot{z}}(\psi) & \frac{\partial b.m.}{\partial \dot{\theta} c/_4}(\psi) & \frac{\partial b.m.}{\partial \dot{\delta}}(\psi) \\ \frac{\partial V}{\partial \dot{\beta}}(\psi) & \frac{\partial V}{\partial \dot{z}}(\psi) & \frac{\partial V}{\partial \dot{\theta} c/_4}(\psi) & \frac{\partial V}{\partial \dot{\delta}}(\psi) \\ \frac{\partial p.m.}{\partial \dot{\beta}}(\psi) & \frac{\partial p.m.}{\partial \dot{z}}(\psi) & \frac{\partial p.m.}{\partial \dot{\theta} c/_4}(\psi) & \frac{\partial p.m.}{\partial \dot{\delta}}(\psi) \\ \frac{\partial H}{\partial \dot{\beta}}(\psi) & \frac{\partial H}{\partial \dot{z}}(\psi) & \frac{\partial H}{\partial \dot{\theta} c/_4}(\psi) & \frac{\partial H}{\partial \dot{\delta}}(\psi) \end{bmatrix}$$

The forcing matrix, on the other hand, is not square. It has four rows, one for each generalized force, and columns equalling the number of rotor and blade fixed geometry descriptive elements. The fixed shapes considered in this analysis have been: rotor precone θ_o, rotor collective pitch θ_o, blade twist rate θ_t, and gust vertical velocity $\dot{z}_g$.

In addition to aerodynamic forcing functions, the forcing matrix contains terms due to centrifugal force acting on rotor blade linear flapping due to precone and collective pitch.

The combined aerodynamic and centrifugal forcing matrix is as follows:

$$\left[\frac{\partial F_b}{\partial \begin{matrix}\text{Fixed}\\ \text{geom}\end{matrix}}(\psi)\right] = \left[\begin{matrix} \frac{\partial b.m.}{\partial \theta_o}(\psi) & \frac{\partial b.m.}{\partial \theta_o}(\psi) & \frac{\partial b.m.}{\partial \theta_t}(\psi) & \frac{\partial b.m.}{\partial \dot{z}_g} \\ \frac{\partial V}{\partial \theta_o}(\psi) & \frac{\partial V}{\partial \theta_o}(\psi) & \frac{\partial V}{\partial \theta_t}(\psi) & \frac{\partial V}{\partial \dot{z}_g}(\psi) \\ \frac{\partial p.m.}{\partial \theta_o}(\psi) & \frac{\partial p.m.}{\partial \theta_o}(\psi) & \frac{\partial p.m.}{\partial \theta_t} & \frac{\partial p.m.}{\partial \dot{z}_g} \\ \frac{\partial H}{\partial \theta_o}(\psi) & \frac{\partial H}{\partial \theta_o}(\psi) & \frac{\partial H}{\partial \theta_t}(\psi) & \frac{\partial H}{\partial \dot{z}_g}(\psi) \end{matrix}\right] + \left[CF_b\right] \left[\begin{matrix} 1 & \sin\Lambda & 0 & 0 \\ 0 & 0 & 0 & 0 \\ 0 & \cos\Lambda & 0 & 0 \\ 0 & 0 & 0 & 0 \end{matrix}\right]$$

The elements of the aerodynamic matrices are evaluated at closely spaced intervals of azimuth. They represent values of root b.m., shear, quarter-chord pitch moment, and flap generalized force due to each of the displacements and velocities of the degrees of freedom and also the fixed geometric shapes, and are found by integrating aerodynamic forces radially. These aerodynamic coefficients are functions of advance ratio μ and tip speed dynamic pressure, $2\, q_{tip} = \rho(\Omega R)^2$, as well as, of course, the rotor blade detailed geometry.

Aerodynamic strip theory is used. That is, the flow relative to the blade is resolved into components parallel to the blade quarter-chord line and normal to it, section dynamic pressure is based on the normal component $q_n = \frac{\rho}{2} V_n^2$, and the angle-of-attack of the section α_n is measured between the normal component and the blade chord line. The effects of the radial flow component parallel to the blade are ignored. The section lift is given as

$$d\ell = c_{\ell_\alpha} \cdot \alpha_n\, q_n\, c\, dr$$

where c_{ℓ_α} = section lift curve slope

c = section chord, ft

dr = increment in radius, ft

Induced inflow and unsteady aerodynamics have been neglected and tip losses accounted for by the tip loss factor B.

The distributions of lift due to blade motions and geometric shapes are integrated radially so as to yield the four generalized blade forces b.m., V, p.m., and H at closely spaced intervals of azimuth. This gives the elements of the three matrices as functions of azimuth.

The effects of the reverse velocity region were explicitly accounted for. The aerodynamic center of the blade was assumed to shift to the three-quarter chord point.

In the three matrices there are only three types of section angle-of-attack; they are due to: section pitch, radial slope, and section velocity:

section pitch $\begin{cases} \theta_{c/4} \\ \theta_o \\ \theta_t \end{cases}$

radial slope $\begin{cases} \beta \\ \delta \\ \beta_o \end{cases}$

section velocity $\begin{cases} \dot{\beta} \\ \dot{\delta} \\ \dot{z} \end{cases}$

The increments of lift in the radial direction for each type of angle-of-attack are as follows:

Section pitch: $\alpha_n = \theta_{c/4} + \theta_o + \theta_t \, r$

$$d\ell = c_{\ell_\alpha} \cdot \alpha_n \frac{\rho}{2} (\Omega r + V \sin \psi)^2 \, c\,dr$$

This expression applies in the advancing flow region. In the reverse velocity region the sign of the lift increment reverses.

Radial slope: $\text{slope (radians)} = \beta_o + \beta + \left(\frac{2r}{R^2}\right)\delta$

$$\alpha_n = \frac{-(\text{slope})\ V \cos\psi}{(\Omega r + V \sin\psi)}$$

$$d\ell = c_{\ell_\alpha}\ (-\text{slope})\ V \cos\psi\ \frac{\rho}{2}\ (\Omega r + V \sin\psi)\ c\,dr$$

This expression applies in advancing flow. The sign changes in the reverse velocity region.

Section velocity: $\text{velocity} = r\dot{\beta} + \left(\frac{r}{R}\right)^2 \dot{\delta} + \dot{z}$

$$\alpha_n = -\frac{\text{velocity}}{(\Omega r + V \sin\psi)}$$

$$d\ell = c_{\ell_\alpha}\ (-\text{velocity})\ \frac{\rho}{2}\ (\Omega r + V \sin\psi)\ c\,dr$$

And again the sign changes in the reverse velocity region.

The radial distribution of the lift increment $d\ell$ at each azimuth position is then factored by the mode shapes of the four modes to yield the aerodynamic derivatives. The four mode shapes are (1) linear flapping, (2) vertical displacement, (3) pitch moment arm about the quarter-chord line, and (4) parabolic flapping.

$$\text{b.m.} = \int_r r\,\frac{d\ell}{dr}\,dr$$

$$V = \int_r \frac{d\ell}{dr}\,dr$$

$$\text{p.m.} = \int_r \left(c - \frac{c}{4}\right)\frac{d\ell}{dr}\,dr \quad \text{(reverse velocity region only)}$$

$$H = \int_r \left(\frac{r}{R}\right)^2 \frac{d\ell}{dr}\,dr$$

The above integrations at each of a large number of azimuthal positions become the aerodynamic derivatives for the single blade.

Rotor Equations of Motion

The single blade equations would permit the calculation of the independent motions of each blade unrestrained at its root by the shaft or by attachment to the other blades through the gyroscope. In this section, the restraints, offered by the shaft to vertical and tilting motions and by the other blades (through the swashplate) to feathering motions, are applied to the three independent blade equations causing them to be transformed into the equations of motion of the complete rotor in rotating coordinates.

Following the transformation to rotor degrees of freedom in rotating axes, the swashplate rotating damping and rotor flapping structural damping terms are added. The rotor equations are then in a form to be transformed to stationary axes.

Once in stationary coordinates, stationary damping, springs, and gyroscope terms are added to the swashplate and the body equations of motion, complete with pitch, plunge, and roll inertia and aerodynamic terms, are added to the rotor equations of motion.

Transformation of blade external forcing functions due to precone, twist, collective, and angle of attack through rotor rotating coordinates and adding swashplate control moments or displacements and body residual forces and moments complete the rotor airframe equations of motion.

Rotor equations of motion in rotating axes. - The pth single blade motions are represented by the vector:

$$\eta_{z_p} = \begin{Bmatrix} \theta_p \\ z_p \\ \theta_p \\ \delta_p \end{Bmatrix}$$

For a three-blade rotor, for example, there would be a corresponding vector for all blades

$$\eta_z = \begin{Bmatrix} \eta_{z_1} \\ \eta_{z_2} \\ \eta_{z_3} \end{Bmatrix}$$

and it would contain 12 components, or degrees of freedom.

It is possible to write the equation of all three independent blade motions together as follows:

$$\begin{bmatrix} I_b & & \\ & I_b & \\ & & I_b \end{bmatrix} \begin{Bmatrix} \ddot{\eta}_{z_1} \\ \ddot{\eta}_{z_2} \\ \ddot{\eta}_{z_3} \end{Bmatrix} + \begin{bmatrix} CF_b & & \\ & CF_b & \\ & & CF_b \end{bmatrix} \begin{Bmatrix} \eta_{z_1} \\ \eta_{z_2} \\ \eta_{z_3} \end{Bmatrix} - \begin{bmatrix} \frac{\partial F_b}{\partial \dot{\eta}_1} & & \\ & \frac{\partial F_b}{\partial \dot{\eta}_2} & \\ & & \frac{\partial F_b}{\partial \dot{\eta}_3} \end{bmatrix} \begin{Bmatrix} \dot{\eta}_{z_1} \\ \dot{\eta}_{z_2} \\ \dot{\eta}_{z_3} \end{Bmatrix}$$

$$\begin{bmatrix} \frac{\partial F_b}{\partial \eta_1} & & \\ & \frac{\partial F_b}{\partial \eta_2} & \\ & & \frac{\partial F_b}{\partial \eta_3} \end{bmatrix} \begin{Bmatrix} \eta_{z_1} \\ \eta_{z_2} \\ \eta_{z_3} \end{Bmatrix} = \begin{bmatrix} \frac{\partial F_b}{\partial \text{ fixed geom}} 1 \\ \frac{\partial F_b}{\partial \text{ fixed geom}} 2 \\ \frac{\partial F_b}{\partial \text{ fixed geom}} 3 \end{bmatrix} \begin{Bmatrix} \text{fixed} \\ \text{geom} \end{Bmatrix}$$

It has been shown in the section on kinematics that blade displacements are related to rotor displacements in rotating coordinates by:

$$\eta_{z_p} = \left[D_{z_p} \right] \beta_z$$

Therefore the vector of all blade displacements is related to the rotor motions by:

$$\begin{Bmatrix} \eta_{z_1} \\ \eta_{z_2} \\ \eta_{z_3} \end{Bmatrix} = \begin{bmatrix} D_{z_1} \\ D_{z_2} \\ D_{z_3} \end{bmatrix} \beta_z \quad \text{or} \quad \eta_z = \left[D_z\right] \beta_z$$

and since the relationship between blade motions and rotor motions is purely kinematic, then:

$$\dot{\eta}_z = \left[D_z\right] \dot{\beta}_z$$

$$\ddot{\eta}_z = \left[D_z\right] \ddot{\beta}_z$$

On the other hand, the transpose of the $\left[D_z\right]$ matrix relates the generalized forces applied to the rotor degrees of freedom to the generalized forces on the individual blades.

$$\begin{Bmatrix} M_r \\ L_r \\ T_r \\ M_{\theta_r} \\ M_{\phi_r} \\ H_{\delta_{o_r}} \\ H_{\delta_{\theta_r}} \\ H_{\delta_{\phi_r}} \end{Bmatrix} = \left[D_z\right]^T \begin{Bmatrix} b.m._1 \\ V_1 \\ p.m._1 \\ H_1 \\ \hline b.m._2 \\ V_2 \\ p.m._2 \\ H_2 \\ \hline b.m._3 \\ V_3 \\ p.m._3 \\ H_3 \end{Bmatrix}$$

Generalized Rotor Forces in Rotating Axes

where M_r = Rotor pitch moment ft lb

L_r = Rotor roll moment ft lb

T_r = Rotor thrust lb

M_{θ_r} = Swashplate pitch moment ft lb

M_{ϕ_r} = Swashplate roll moment ft lb

$H_{\delta_{\circ r}}$ = Rotor collective flapping generalized force lb

$H_{\delta_{\theta_r}}$ = Rotor pitch flapping generalized force lb

$H_{\delta_{\phi_r}}$ = Rotor roll flapping generalized force lb.

The two properties of the $\left[D_z\right]$ matrix permit the three uncoupled rotor blade equations of motion to be transformed into equations of motion of the overall rotor degrees of freedom in rotating coordinates.

$$\left[D_z\right]^T \begin{bmatrix} I_b & & \\ & I_b & \\ & & I_b \end{bmatrix} \left[D_z\right] \begin{Bmatrix} \ddot{\Theta} \\ \ddot{\Phi} \\ \ddot{z} \\ \ddot{\theta} \\ \ddot{\phi} \\ \ddot{\delta}_o \\ \ddot{\delta}_\theta \\ \ddot{\delta}_\phi \end{Bmatrix} + \left[D_z\right]^T \begin{bmatrix} CF_b & & \\ & CF_b & \\ & & CF_b \end{bmatrix} \left[D_z\right] \begin{Bmatrix} \Theta \\ \Phi \\ z \\ \theta \\ \phi \\ \delta_o \\ \delta_\theta \\ \delta_\phi \end{Bmatrix}$$

$$\left[D_z\right]^T \begin{bmatrix} \frac{\partial F_b}{\partial \eta_1}(\psi) & & \\ & \frac{\partial F_b}{\partial \eta_2}(\psi) & \\ & & \frac{\partial F_b}{\partial \eta_3}(\psi) \end{bmatrix} \left[D_z\right] \begin{Bmatrix} \dot{\Theta} \\ \dot{\Phi} \\ \dot{z} \\ \dot{\theta} \\ \dot{\phi} \\ \dot{\delta}_o \\ \dot{\delta}_\theta \\ \dot{\delta}_\phi \end{Bmatrix} - \left[D_z\right]^T \begin{bmatrix} \frac{\partial F_b}{\partial \eta_1}(\psi) & & \\ & \frac{\partial F_b}{\partial \eta_2}(\psi) & \\ & & \frac{\partial F_b}{\partial \eta_3}(\psi) \end{bmatrix} \left[D_z\right] \begin{Bmatrix} \Theta \\ \Phi \\ z \\ \theta \\ \phi \\ \delta_o \\ \delta_\theta \\ \delta_\phi \end{Bmatrix}$$

$$= \left[D_z\right]^T \begin{bmatrix} \frac{\partial F_b}{\partial \text{ f.g. } 1} \\ \frac{\partial F_b}{\partial \text{ f.g. } 2} \\ \frac{\partial F_b}{\partial \text{ f.g. } 3} \end{bmatrix} \begin{Bmatrix} \text{fixed} \\ \text{geom.} \end{Bmatrix}$$

Rotor equations in rotating coordinates may be written more concisely as follows:

$$\left[I\right] \ddot{\beta}_z + \left[S\right] \beta_z - \left[A_R\ (\psi)\right] \dot{\beta}_z - \left[A\ (\psi)\right]\ \beta_z = \left[A.F.\ (\psi)\right] \begin{Bmatrix} \beta_o \\ \theta_o \\ \theta_t \\ z_g \end{Bmatrix}$$

The $[AF\ (\psi)]$ matrix contains aerodynamic forcing functions, primarily, but it also includes centrifugal collective generalized forces due to precone, β_o, and collective pitch, θ_o.

Rotating damping, C_R, due to feathering friction, and rotor flapping structural damping, γ_δ, may be conveniently added at this point. They form a mechanical damping matrix relating rotor degree of freedom generalized forces to velocities of the degrees of freedom

$$\{\text{generalized forces}\} = \left[D_a\right] \dot{\beta}_z$$

$\left[D_a\right]$ a diagonal matrix is defined as follows:

$$\left[Da\right] = \begin{bmatrix} 0 & 0 & 0 & 0 & 0 & 0 & 0 & 0 & 0 \\ 0 & 0 & 0 & 0 & 0 & 0 & 0 & 0 & 0 \\ 0 & 0 & 0 & 0 & 0 & 0 & 0 & 0 & 0 \\ 0 & 0 & 0 & C_R & 0 & 0 & 0 & 0 & 0 \\ 0 & 0 & 0 & 0 & C_R & 0 & 0 & 0 & 0 \\ 0 & 0 & 0 & 0 & 0 & 2\gamma_\delta \omega_\delta M_{\delta_o} \delta_o & 0 & 0 & \\ 0 & 0 & 0 & 0 & 0 & 0 & 0 & 2\gamma_\delta \omega_\delta M_{\delta_\theta} \delta_\theta & 0 \\ 0 & 0 & 0 & 0 & 0 & 0 & 0 & 0 & 2\gamma_\delta \omega_\delta M_{\delta_\phi} \delta_\phi \end{bmatrix}$$

The final equations of the rotor relative to rotating coordinates are as follows:

$$\left[I\right] \ddot{\beta}_z + \left[Da\right] \dot{\beta}_z + \left[S\right] \beta_z - \left[A_R\ (\psi)\right] \dot{\beta}_z - \left[A\ (\psi)\right] \beta_z = \left[A.F.\ (\psi)\right] f$$

where

$$f = \begin{Bmatrix} \beta_o \\ \theta_o \\ \theta_t \\ \dot{z}_g \end{Bmatrix}$$

Transformation to stationary axes. - The transformation matrix relating the rotor rotating degrees of freedom, β_z, to the rotor stationary axes degrees of freedom, β_Z, and discussed earlier, is $\left[T_z\right]$.

$$\beta_z = \left[T_z\right] \beta_Z$$

The transpose of the transformation matrix supplies the relationship between the generalized forces on the degrees of freedom in stationary coordinates to the generalized forces on the rotating axes degrees of freedom.

$$\left\{\text{Generalized Forces}_Z\right\} = \left[T_z\right]^T \left\{\text{Generalized Forces}_z\right\}$$

The transformation and its derivatives and transpose supply the means of transforming the equations of rotor motions from rotating to stationary axes.

The derivatives of the relationships between rotating and stationary degrees of freedom are as follows:

$$\dot{\beta}_z = \left[T_z\right] \dot{\beta}_Z + \left[\dot{T}_z\right] \beta_Z$$

$$\ddot{\beta}_z = \left[T_z\right] \ddot{\beta}_Z + 2 \left[\dot{T}_z\right] \dot{\beta}_Z + \left[\ddot{T}_z\right] \beta_Z$$

The equations of motion in rotating axes may then be transformed to stationary axes in the same fashion as equations of blade motion were transformed into equations of rotor motion. The full transformation process is written out and then the abbreviations permitted by rotational symmetry are shown:

$$\left[T_z\right]^T [I]\left\{\left[T_z\right] \ddot{\beta}_Z + 2 \left[\dot{T}_z\right] \dot{\beta}_Z + \left[\ddot{T}_z\right] \beta_Z\right\}$$

$$+ \left[T_z\right]^T [Da]\left\{\left[T_z\right] \dot{\beta}_Z + \left[\dot{T}_z\right] \beta_Z\right\} + \left[T_z\right]^T [S] \left[T_z\right] \beta_Z$$

$$- \left[T_z\right]^T \left[A_R\right] \left\{\left[T_z\right] \dot{\beta}_Z + \left[\dot{T}_z\right] \beta_Z\right\} - \left[T_z\right]^T [A] \left[T_z\right] \beta_Z$$

$$= \left[T_z\right]^T [A.F.] \; f$$

The derivatives of the transformation matrix consist of derivatives of the elements of the matrix. For example, $\left[\dot{T}_z\right]$ is as follows:

$$\left[\dot{T}_z\right] = \Omega \begin{bmatrix} -\sin\Omega t & -\cos\Omega t & 0 & 0 & 0 & 0 & 0 & 0 \\ \cos\Omega t & -\sin\Omega t & 0 & 0 & 0 & 0 & 0 & 0 \\ 0 & 0 & 0 & 0 & 0 & 0 & 0 & 0 \\ 0 & 0 & 0 & -\sin\Omega t & -\cos\Omega t & 0 & 0 & 0 \\ 0 & 0 & 0 & \cos\Omega t & -\sin\Omega t & 0 & 0 & 0 \\ 0 & 0 & 0 & 0 & 0 & 0 & 0 & 0 \\ 0 & 0 & 0 & 0 & 0 & 0 & -\sin\Omega t & -\cos\Omega t \\ 0 & 0 & 0 & 0 & 0 & 0 & \cos\Omega t & -\sin\Omega t \end{bmatrix}$$

and similarly for $\left[\ddot{T}_z\right]$.

The inertia, centrifugal and damping aspects of the rotor are all rotationally symmetric and are independent of rotor azimuth position ψ or Ωt. For this reason transformation of the matrices describing them to stationary axes can be simplified by employing the values of the transformation, its derivatives and its transpose at $\psi = 0$. The same result would be obtained if transformation matrices at any other values of azimuth had been employed. The transformation matrices at $\psi = 0$ are as follows:

$$\left[T_z(o)\right] = \left[T_z(0)\right]^T = \begin{bmatrix} 1 & 0 & 0 & 0 & 0 & 0 & 0 & 0 \\ 0 & 1 & 0 & 0 & 0 & 0 & 0 & 0 \\ 0 & 0 & 1 & 0 & 0 & 0 & 0 & 0 \\ 0 & 0 & 0 & 1 & 0 & 0 & 0 & 0 \\ 0 & 0 & 0 & 0 & 1 & 0 & 0 & 0 \\ 0 & 0 & 0 & 0 & 0 & 1 & 0 & 0 \\ 0 & 0 & 0 & 0 & 0 & 0 & 1 & 0 \\ 0 & 0 & 0 & 0 & 0 & 0 & 0 & 1 \end{bmatrix}$$

$$\left[\dot{T}_z\ (o)\right] = \Omega \begin{bmatrix} 0 & -1 & 0 & 0 & 0 & 0 & 0 & 0 \\ 1 & 0 & 0 & 0 & 0 & 0 & 0 & 0 \\ 0 & 0 & 0 & 0 & 0 & 0 & 0 & 0 \\ 0 & 0 & 0 & 0 & -1 & 0 & 0 & 0 \\ 0 & 0 & 0 & 1 & 0 & 0 & 0 & 0 \\ 0 & 0 & 0 & 0 & 0 & 0 & 0 & 0 \\ 0 & 0 & 0 & 0 & 0 & 0 & 0 & -1 \\ 0 & 0 & 0 & 0 & 0 & 0 & 1 & 0 \end{bmatrix}$$

$$\left[\ddot{T}_z\ (\psi)\right] = -\ \Omega^2 \begin{bmatrix} 1 & 0 & 0 & 0 & 0 & 0 & 0 & 0 \\ 0 & 1 & 0 & 0 & 0 & 0 & 0 & 0 \\ 0 & 0 & 0 & 0 & 0 & 0 & 0 & 0 \\ 0 & 0 & 0 & 1 & 0 & 0 & 0 & 0 \\ 0 & 0 & 0 & 0 & 1 & 0 & 0 & 0 \\ 0 & 0 & 0 & 0 & 0 & 0 & 0 & 0 \\ 0 & 0 & 0 & 0 & 0 & 0 & 1 & 0 \\ 0 & 0 & 0 & 0 & 0 & 0 & 0 & 1 \end{bmatrix}$$

The $\left[T_z\ (0)\right]$, $\left[\dot{T}_z\ (0)\right]$ and $\left[\ddot{T}_z\ (0)\right]$ are employed in transforming the inertia, centrifugal and structural, and damping matrices to stationary coordinates. The transformation and derivatives varying with azimuth $\left[T_z\ (\psi)\right]$ and $\left[\dot{T}_z\ (\psi)\right]$, however, must be employed in transforming the aerodynamic matrices to stationary coordinates since they vary with azimuth.

Including the simplifications, the rotor equations in stationary axes become:

$$[I]\ \ddot{\beta}_z + \left[2\ [I]\ \left[\dot{T}_z\right] + [Da]\right] \dot{\beta}_z + \left[[I]\ \left[\ddot{T}_z\right] + [Da]\ \left[\dot{T}_z\right] + [S]\right] \beta_z$$

$$- \left[T_z\ (\psi)\right]^T \left[A_R\right]\left[T_z\ (\psi)\right]\ \dot{\beta}_z - \left[T_z\ (\psi)\right]^T \left[\left[A_R\right]\left[\dot{T}_z\ (\psi)\right] + [A]\left[T_z(\psi)\right]\right] \beta_z$$

$$= \left[T_z\ (\psi)\right]^T\ [AF]\ f$$

To the equations of motion of the rotor in stationary coordinates must be added terms for swashplate springs and dampers to ground. The swashplate rotationally symmetric spring and damper terms are as follows:

$$\begin{bmatrix} C_s & 0 \\ 0 & C_s \end{bmatrix} \begin{Bmatrix} \dot{\theta} \\ \dot{\phi} \end{Bmatrix} + \begin{bmatrix} K_s & 0 \\ 0 & K_s \end{bmatrix} \begin{Bmatrix} \theta \\ \phi \end{Bmatrix} = 0$$

The final rotor equations in stationary axes including the above terms are as follows:

$$[I]\ \ddot{\beta}_z + [C]\ \dot{\beta}_z + [E]\ \beta_z - \left[B_R\right]\ \dot{\beta}_z - [B]\ \beta_z = [F]\ f$$

and the matrices contain terms of the following kind:

$[I]$	Inertia
$[C]$	Mechanical damping and gyroscopic
$[E]$	Mechanical stiffness
$[B_R]$	Aerodynamic damping, function of azimuth
$[B]$	Aerodynamic stiffness, function of azimuth
$[F]$	Forcing functions

Complete Vertical Equations of Motion

The rotor equations and forcing functions have been derived in stationary coordinates in the previous section. The gyroscopic terms are shown on page 58. In this section the body inertia and aerodynamic coefficients are derived and combined with the rotor and gyroscopic equations to form the left-hand side of the equations or the homogenous differential equations.

It should be noted that the term "body" refers to the complete non-rotating configuration to which the rotor is attached. It includes the body, nacelle, wing, and tail.

The rotor forcing functions, the body forces and moments existing at zero angle-of-attack and swashplate control moments are combined to form the right-hand side of the complete equations or the forcing functions.

Body Terms. - The body terms consist of inertia forces due to acceleration of the three body degrees of freedom pitch, roll, and plunge, and aerodynamic terms due to acceleration, velocity, and displacement of the degrees of freedom. In addition, there are body steady forcing terms due to c.g. offset, aerodynamic forces at zero shaft angle-of-attack, due to gust angle-of-attack and jet engine thrust.

Inertia. - The equations of motion of the rotor were derived with the coordinate axes assumed to pass through the center of gravity. With the c.g. on the shaft centerline, Z forces (lift) produced no pitch or roll moments about the c.g.

It is now required to modify the equations to accept changes in c.g. position both fore and aft, and laterally. (The XH-51A(C) has a fairly wide lateral c.g. range due to vehicle asymmetry.)

In aircraft work it is standard practice to consider the coordinate axes to pass through the c.g. and the aerodynamic terms are altered to suit changing c.g. positions. In the case of the helicopter, it appears to be simpler to leave the axes unchanged and modify the inertia matrix to suit the changing c.g. position.

The following figure illustrates the changes:

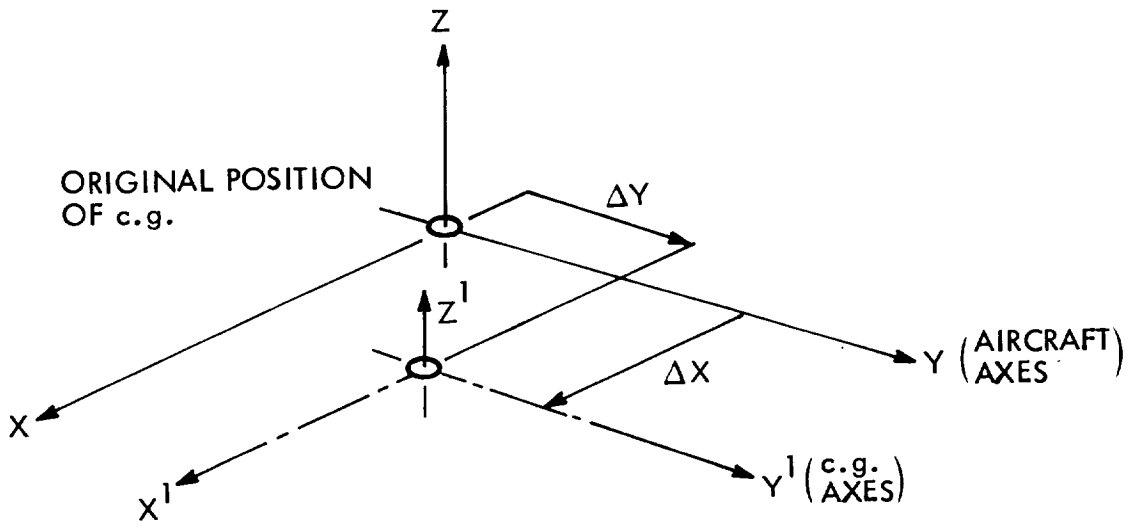

About the c.g. axes (X', Y') the inertia forces are as follows:

$$\begin{bmatrix} I_{Y'Y'} & & \\ & I_{X'X'} & \\ & & M \end{bmatrix} \begin{Bmatrix} \ddot{\theta}' \\ \ddot{\Phi}' \\ \ddot{Z}' \end{Bmatrix} = \begin{Bmatrix} M_{Y'Y'} \\ M_{X'X'} \\ Z' \end{Bmatrix}$$

Moments about the aircraft axes (X, Y) are related to moments about the c.g. axes as follows:

$$\begin{Bmatrix} M_{YY} \\ M_{XX} \\ Z \end{Bmatrix} = \begin{bmatrix} 1.0 & 0 & -\Delta X \\ 0 & 1.0 & +\Delta Y \\ 0 & 0 & 1.0 \end{bmatrix} \begin{Bmatrix} M_{Y'Y'} \\ M_{X'X'} \\ Z' \end{Bmatrix} \qquad (1)$$

By the transpose rule the c.g. axis motions must be related to the aircraft axes motions by

$$\begin{Bmatrix} \ddot{\theta}' \\ \ddot{\Phi}' \\ \ddot{Z}' \end{Bmatrix} = \begin{bmatrix} 1.0 & 0 & -\Delta X \\ 0 & 1.0 & \Delta Y \\ 0 & 0 & 1.0 \end{bmatrix}^T \begin{Bmatrix} \ddot{\theta} \\ \ddot{\Phi} \\ \ddot{Z} \end{Bmatrix}$$

Substituting for $\begin{Bmatrix} \ddot{\theta}' \\ \ddot{\Phi}' \\ \ddot{Z}' \end{Bmatrix}$ in equation (1) and then transforming the moments

to aircraft axes by equation (2) yields

$$\begin{Bmatrix} M_{YY} \\ M_{XX} \\ Z \end{Bmatrix} = \begin{bmatrix} 1.0 & 0 & -\Delta X \\ 0 & 1.0 & \Delta Y \\ 0 & 0 & 1.0 \end{bmatrix} \begin{bmatrix} I_{Y'Y'} & & \\ & I_{X'X'} & \\ & & M \end{bmatrix} \begin{bmatrix} 1.0 & 0 & 0 \\ 0 & 1.0 & 0 \\ -\Delta X & \Delta Y & 1.0 \end{bmatrix} \begin{Bmatrix} \ddot{\theta} \\ \ddot{\Phi} \\ \ddot{Z} \end{Bmatrix}$$

and this yields

$$\begin{Bmatrix} M_{YY} \\ M_{XX} \\ Z \end{Bmatrix} = \begin{bmatrix} I_{Y'Y'} + M\Delta X^2 & -M\Delta X\Delta Y & -M\Delta X \\ -M\Delta X\Delta Y & I_{X'X'} + M\Delta Y^2 & M\Delta Y \\ -M\Delta X & M\Delta Y & M \end{bmatrix} \begin{Bmatrix} \ddot{\theta} \\ \ddot{\Phi} \\ \ddot{Z} \end{Bmatrix}$$

$$= \left[I_{body}\right] \ddot{\beta}_Z$$

Thus, with pitch and roll moments of inertia about the c.g. axes called $I_{Y'Y'}$ and $I_{X'X'}$ and the mass of the body (but not blades) called M and with the displacements of the c.g. relative to the shaft-centered aircraft axes called Δx and Δy, the inertia terms of the aircraft body are as shown above.

Aerodynamic. - The aerodynamic terms in the airframe equations of motion are as follows for the unforced system:

$$\begin{bmatrix} 0 & 0 & \frac{1}{V} M_{\dot{\alpha}} \\ 0 & 0 & 0 \\ 0 & 0 & 0 \end{bmatrix} \begin{Bmatrix} \ddot{\theta} \\ \ddot{\phi} \\ \ddot{z} \end{Bmatrix} + \begin{bmatrix} -\left(M_q + M_{\dot{\alpha}}\right) & 0 & \frac{1}{V} M_{\alpha} \\ 0 & -Lp & 0 \\ 0 & 0 & -\frac{1}{V} Z_{\alpha} \end{bmatrix} \begin{Bmatrix} \dot{\theta} \\ \dot{\phi} \\ \dot{z} \end{Bmatrix} + \begin{bmatrix} -M_{\alpha} & 0 & 0 \\ 0 & 0 & 0 \\ Z_{\alpha} & 0 & 0 \end{bmatrix} \begin{Bmatrix} \theta \\ \phi \\ z \end{Bmatrix} = 0$$

$$\left[J_{RR_{body}}\right] \ddot{\beta}_Z + \left[J_{R_{body}}\right] \dot{\beta}_Z + \left[I_{body}\right] \beta_Z = 0$$

Some small aerodynamic coupling terms may also exist but they have been ignored.

Before these equations can be added to the complete rotor equations (those which include the forcing terms on the RHS), the forcing and balancing wing-body-tail-nacelle terms must be added to the RHS of the above equations.

It should be noted that the signs of the aerodynamic terms are such as to convert them from aircraft axes to helicopter axes. Therefore, the aerodynamic terms have been derived according to aircraft sign conventions.

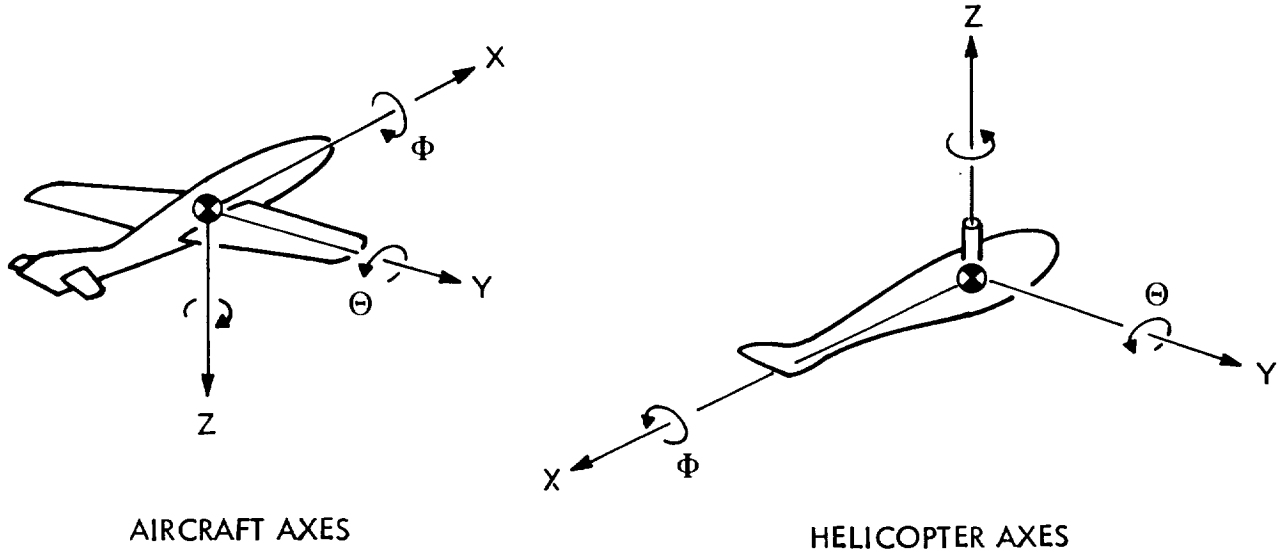

AIRCRAFT AXES

HELICOPTER AXES

Both are right-hand systems.

The RHS terms consist of gravitational attractive forces, gust angle-of-attack forces, aerodynamic pitch, roll, and lift forces at $\alpha_{rotor} = 0$, the change in body forces due to jet engine thrust, and a force correction term due to rotor downwash and to correct balance error.

$$= \Delta x_{c.g.} nW + M_{\alpha} \cdot \alpha_{gust} + M_{\alpha = 0} + \frac{dM}{dF_N} \cdot F_N + \Delta M_o \ (q*, \text{error})$$

$$= -\Delta y_{c.g.} nW - L_{\alpha} \cdot \alpha_{gust} - L_{\alpha = 0} - \frac{dL}{dF_N} \cdot F_N - \Delta L_o \ (q*, \text{error})$$

$$= - \quad nW - Z_{\alpha} \cdot \alpha_{gust} - Z_{\alpha = 0} - \frac{dZ}{dF_N} \cdot F_N - \Delta Z_o \ (q^*, \text{ error})$$

$$= \left\{F_{body}\right\} \quad *\text{Refers to downwash correction}$$

The body aerodynamic derivatives and zero shaft angle forces and moments are found by conventional aircraft methods for configurations with large bodies, wings, and tails.

Gyroscope terms. - Absolute gyroscope motions, or motions relative to the earth, consist of tilt relative to the airframe θ, ϕ combined with tilt of the airframe Θ, Φ.

$$\text{absolute gyroscope tilt} = \begin{Bmatrix} \Theta \\ \Phi \end{Bmatrix} + \begin{Bmatrix} \theta \\ \phi \end{Bmatrix}$$

Absolute gyroscope tilt can be written in a more convenient form,

$$\begin{Bmatrix} \Theta \\ \Phi \end{Bmatrix} + \begin{Bmatrix} \theta \\ \phi \end{Bmatrix} = \begin{bmatrix} 1 & 0 & 1 & 0 \\ 0 & 1 & 0 & 1 \end{bmatrix} \begin{Bmatrix} \Theta \\ \Phi \\ \theta \\ \phi \end{Bmatrix}$$

When accelerated or given a tilting velocity, the gyroscope generates body and swashplate moments as follows:

$$\begin{bmatrix} I_G & 0 & I_G & 0 \\ 0 & I_G & 0 & I_G \\ I_G & 0 & I_G & 0 \\ 0 & I_G & 0 & I_G \end{bmatrix} \begin{Bmatrix} \ddot{\Theta} \\ \ddot{\Phi} \\ \ddot{\theta} \\ \ddot{\phi} \end{Bmatrix} + \begin{bmatrix} 0 & -2\,\Omega I_G & 0 & -2\,\Omega I_G \\ 2\,\Omega I_G & 0 & 2\,\Omega I_G & 0 \\ 0 & -2\,\Omega I_G & 0 & -2\,\Omega I_G \\ 2\,\Omega I_G & 0 & 2\,\Omega I_G & 0 \end{bmatrix} \begin{Bmatrix} \dot{\Theta} \\ \dot{\Phi} \\ \dot{\theta} \\ \dot{\phi} \end{Bmatrix} = \begin{Bmatrix} M \\ L \\ M_{\theta} \\ M_{\phi} \end{Bmatrix}$$

The left-hand side terms are added to the rotor body differential equations to account for the effects of the gyroscope.

Complete vertical equations. - The complete equations of vertical mass element motion with forcing functions consist of rotor equations, body equations, and gyroscopic equations. The complete set is as follows:

$$\left[I + I_{body} + J_{RR\ body} + I_G\right] \ddot{\beta}_Z + \left[C + J_{R\ body} + C_G\right] \dot{\beta}_Z + \left[E + J_{body}\right] \beta_Z - \left[B_R(\psi)\right] \dot{\beta}_Z - \left[B(\psi)\right] \beta_Z = \left[F(\psi)\right] \{f\} + \left\{F_{body}\right\} + \{cm\}$$

Swashplate control moments $\{c.m.\}$ have been added. They are applied in a vector with all elements zero but the M_θ and M_ϕ swashplate moments. External control moments may be applied to the free swashplate through them for "closed loop" operation.

The equations represent the free flight of a feathering feedback gyroscope-stabilized hingeless rotor compound helicopter.

IN-PLANE MOTIONS EQUATIONS

Equations of motion of the rotor blade - hub mass system in the plane of the disk or the plane normal to the shaft are derived. The system is free in the disk plane, or constrained by springs to ground. The hub mass may translate longitudinally and laterally and it may rotate relative to the rotating axes. Each blade is assumed attached to the hub at a pivot point located at a fraction of the tip radius from the shaft. The distance depends on the blade elastic dynamic in-plane mode shape. The blade in-plane motion about the pivot is assumed to be rigid.

The number of degrees of freedom in the system is three for the body freedoms and one for each blade; i.e., 6 for the three-blade rotor and 7 for one with four blades. The rotor elastic degrees of freedom are collective (or all blades together to give a shaft torque) lateral, longitudinal, and the reactionless or differential collective or scissors mode.

The derivation first develops the equations of motion of a single blade in its axis system rotating with the rotor. The equations, in four degrees of freedom, contain matrices of the following coefficients: inertia or acceleration terms, coriolis or velocity terms, centrifugal and structural or displacement terms, and aerodynamic velocity and displacement terms. The response aerodynamic terms are assumed to depend on the blade section drag coefficient at zero lift and are very weak. The periodic parts may be ignored without significantly affecting the blade response. This assumption reduces the equations of blade motion to linear ordinary differential equations with constant coefficients.

The individual blade degrees of freedom are then constrained to take up only those motions permitted by the overall rotor degrees of freedom. The relationship has been discussed in the section on kinematics. The transpose of the kinematic relationship matrix is then allowed to act on the individual blade generalized forces so as to gather them into generalized forces on the overall rotor degrees of freedom. In this way the three or four sets of individual blade equations of motion are transformed into a single set of equations of motion of the whole rotor in rotating axes. Terms are then added to account for the mass and moment of inertia of the hub and blade structural damping.

Following this, the equations are transformed into stationary coordinates where non-rotating body mass and springs to ground (if tunnel mounted) are added to complete the homogeneous or left-hand side of the differential equations.

The in-plane equations forcing functions or forces external to the homogeneous set are next derived. The major portion of these forces is produced by forces on, and motions of the degrees of freedom of the vertical motion equations. The remaining small portion comes from the azimuthal variation of blade section drag.

The major forcing functions are divided into two parts: vertical motions induced and vertical aerodynamics induced types.

The in-plane forces caused by blade vertical motions come about because in actual fact blade element masses also move slightly in the radial direction as they take up vertical deflections. These small radial displacements and velocities cause in-plane centrifugal and coriolis forces - which are considered to be external to the in-plane equations.

Essentially vertical section air forces actually have small components in the plane of the disk and in the direction of the principal axis of blade lead-lag motions. These components are carefully calculated to produce the other major portion of the in-plane forcing function.

Single Blade Equations of Motion

The single blade freedoms are discussed in the section on in-plane motions of mass elements. The vector of dispacement of the degrees of freedom of the pth blade is:

$$\eta_{xy_p} = \begin{Bmatrix} u_p \\ v_p \\ \upsilon_p \\ \zeta_p \end{Bmatrix}$$

The homogenous differential equations of the in-plane motions of a single blade are as follows:

$$\left|I_p\right| \ \ddot{\eta}_{xy_p} + \left|COR_p\right| \ \dot{\eta}_{xy_p} + \left|CF_p\right| \ \eta_{xy_p}$$

$$- \left|A_{R_p}\right| \ \dot{\eta}_{xy_p} - \left|A_p\right| \ \eta_{xy_p} = 0$$

where the square matrices represent the following:

$\left\|I_p\right\|$	Blade inertia
$\left\|COR_p\right\|$	Coriolis coefficients
$\left\|CF_p\right\|$	Centrifugal and structural stiffness
$\left\|A_{R_p}\right\|$	Blade aerodynamic damping
$\left\|A_p\right\|$	Blade aerodynamic stiffness

Forcing functions are treated in a later section.

Blade inertia matrix. - The blade inertia matrix represents the relationship between accelerations in the degrees of freedom and generalized forces on the degrees of freedom due to the acceleration.

$$\begin{Bmatrix} n.f._p \\ a.f._p \\ s.t._p \\ p.t._p \end{Bmatrix} = - \left|I_p\right| \begin{Bmatrix} \ddot{u}_p \\ \ddot{v}_p \\ \ddot{v}_p \\ \ddot{\zeta}_p \end{Bmatrix}$$

Note: Minus shows terms on R.H.S.

The blade generalized forces are:

n.f. Normal force acting on blade, or pivot shear, lb

a.f. Axial force acting on blade, or pivot tension, lb

s.t. Shaft torque, or root in-plane bending moment, ft lb

p.t. Pivot torque, or in-plane moment at pivot, ft lb

The $\left|I_p\right|$ matrix represents the rate of change of generalized force per unit acceleration. For example the (1,1) element is $\frac{\partial n.f.}{\partial \ddot{u}}$. The complete matrix is as follows:

$$\left|I_p\right| = \begin{bmatrix} M_b & 0 & M_b r_{c.g.} & M_b (r_{c.g.} - e) \\ 0 & M_b & 0 & 0 \\ M_b r_{c.g.} & 0 & I_{b_{shaft}} & I_b - e M_b r_{c.g.} \\ M_b (r_{c.g.} - e) & 0 & I_{b_{shaft}} - e M_b r_{c.g.} & I_{b_{pivot}} \end{bmatrix}$$

The $\left|I_p\right|$ matrix is symmetrical.

M_b = Blade mass = $\int_e^R \frac{dm}{dr}\, dr$

Note: e = pivot offset in feet.

$r_{c.g.}$ = Center of gravity of blade measured from center of rotation

$$r_{c.g.} = \frac{1}{M_b} \int_e^R \frac{dm}{dr}\, dr$$

$I_{b_{shaft}}$ = Moment of inertia of the blade about shaft centerline

$I_{b_{pivot}}$ = Moment of inertia of the blade about the pivot

Blade coriolis matrix. - The coriolis matrix relates blade generalized forces to velocities of the blade degrees of freedom.

$$\begin{Bmatrix} n.f._p \\ a.f._p \\ s.t._p \\ p.t._p \end{Bmatrix} = - \left[COR_p\right] \begin{Bmatrix} u_p \\ v_p \\ v_p \\ \zeta_p \end{Bmatrix}$$

Note: Negative indicates R.H.S.

$$\left[COR_p\right] = 2\Omega \begin{bmatrix} 0 & -M_b & 0 & 0 \\ M_b & 0 & M_b r_{c.g.} & M_b (r_{c.g.} - e) \\ 0 & -M_b r_{c.g.} & 0 & 0 \\ 0 & -M_b (r_{c.g.} - e) & 0 & 0 \end{bmatrix}$$

The coriolis matrix is anti-symmetric.

Blade centrifugal and structural matrix. - The centrifugal matrix relates generalized forces to displacements of the degrees of freedom and includes blade structural stiffness effects as well as rotating mass effects.

$$\begin{Bmatrix} \text{n.f.}_p \\ \text{a.f.}_p \\ \text{s.t.}_p \\ \text{p.t.}_p \end{Bmatrix} = - \left[CF_p\right] \begin{Bmatrix} u_p \\ v_p \\ v_p \\ \zeta_p \end{Bmatrix}$$

Note: Negative indicates R.H.S.

$$\left[CF_p\right] = \begin{bmatrix} \frac{d\ \text{n.f.}}{du} & \frac{d\ \text{n.f.}}{dv} & \frac{d\ \text{n.f.}}{dv} & \frac{d\ \text{n.f.}}{d\zeta} \\ \frac{d\ \text{a.f.}}{du} & \frac{d\ \text{a.f.}}{dv} & \frac{d\ \text{a.f.}}{dv} & \frac{d\ \text{a.f.}}{d\zeta} \\ \frac{d\ \text{s.t.}}{du} & \frac{d\ \text{s.t.}}{dv} & \frac{d\ \text{s.t.}}{dv} & \frac{d\ \text{s.t.}}{d\zeta} \\ \frac{d\ \text{p.t.}}{du} & \frac{d\ \text{p.t.}}{dv} & \frac{d\ \text{p.t.}}{dv} & \frac{d\ \text{p.t.}}{d\zeta} \end{bmatrix}$$

Matrix for one blade only.

$$\left[CF_p\right] = \begin{bmatrix} \Omega^2 M_b & 0 & \Omega^2 M_b\, r_{c.g.} & \Omega^2 M_b (r_{c.g.} - e) \\ 0 & \Omega^2 M_b & 0 & 0 \\ \Omega^2 M_b\, r_{c.g.} & 0 & 0 & 0 \\ \Omega^2 M_b\, (r_{c.g.} - e) & 0 & 0 & -\Omega^2 \left[I_{b_{shaft}} - \left(I_{b_{pivot}} + M_b\, e r_{c.g.} \right) \right] - \omega_{ip_{\Omega=0}}^2 I_{b_{pivot}} \end{bmatrix}$$

The terms are all self-evident except perhaps $\frac{d\ \text{p.t.}}{d\zeta}$ and $\frac{d\ \text{n.f.}}{d\zeta}$.

Their derivations are as follows:

Forces due to ζ:

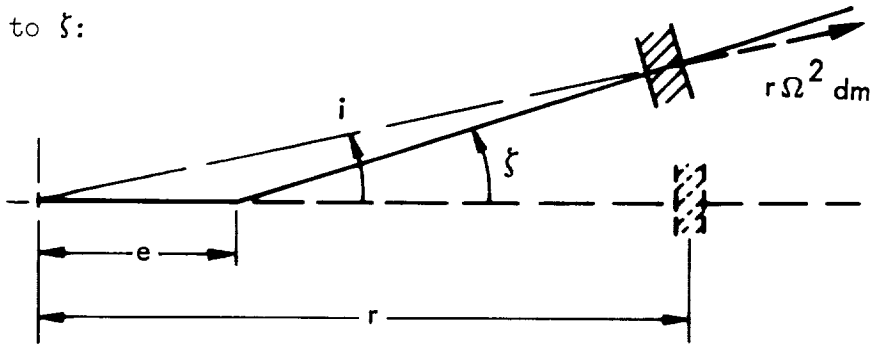

There are two types of forces produced by ζ. The force normal to the undeformed position of the blade

$$\frac{d^2\ n.f.}{d\zeta dr} = r\ \Omega^2\ \frac{dm}{dr} \sin i$$

and the force normal to the deformed blade needed to obtain pivot torque

$$\frac{d^2\ (n.f.)}{d\zeta dr}\ d = r\ \Omega^2\ \frac{dm}{dr} \sin (\zeta - i)$$

Now it may be noted that $\zeta(r - e) = ir$ so that $i = \zeta\ (1 - \frac{e}{r})$ and

$\zeta - i = \frac{e}{r}\ \zeta$. Employing these two relationships and for ζ and i small

$$\frac{d^2\ n.f.}{d\zeta dr} = r\ \Omega^2\ \frac{dm}{dr}\ (1 - \frac{e}{r})$$

$$= \Omega^2\ \frac{dm}{dr}\ (r - e)$$

and $\frac{d^2(n.f.)}{d\zeta dr}\ d = r\ \Omega^2\ \frac{dm}{dr}\ \frac{e}{r}$

$= - e\ \Omega^2\ \frac{dm}{dr}$ and the minus sign denotes a retarding force to forward rotation about the pivot.

The two derivatives with respect to ζ are therefore

$$\frac{d\ n.f.}{d\zeta} = \Omega^2 \int_e^R (r - e)\ \frac{dmdr}{dr} = \Omega^2\ M_b\ (r_{c.g.} - e)$$

$$\frac{d\ p.t.}{d\zeta} = -\Omega^2 \int_e^R e\ (r - e)\ \frac{dm}{dr}\ dr$$

or

$$= \Omega^2 \int_e^R (r - e)\ (r - e)\ \frac{dm}{dr}\ dr - \Omega^2 \int_e^R r(r - e)\ \frac{dm}{dr}\ dr$$

$$= +\Omega^2 \left[I_{b_{pivot}} - I_{b_{shaft}} + e\ M_b\ r_{c.g.} \right]$$

$$= -\Omega^2 \left[I_{b_{shaft}} - \left(I_{b_{pivot}} + M_b\ e\ r_{c.g.} \right) \right]$$

It should be noted that the above is not exactly analogous to the $\frac{dH}{d\zeta}$ term of the vertical blade motion equations. It is, therefore, not possible to include structural stiffness in exactly the same way. In the in-plane formulation the pivot spring is always the same: k_ζ ft lb/radian. Its value, therefore, will not change with rpm. At zero rpm or $\Omega = 0$, the in-plane frequency is given by

$$\omega_{i.p.} = \sqrt{\frac{k_\zeta}{I_{b_{pivot}}}}$$

so that

$$k_\zeta = \omega_{i.p.}^2\ I_{b_{pivot}}$$

$$\frac{d\ p.t.}{d\zeta} = -\left[I_{b_{shaft}} - \left(I_{b_{pivot}} + M_b\ e\ r_{c.g.} \right) \right] \Omega^2 - \left(\omega_{i_{p_{\Omega = 0}}} \right)^2 I_{b_{pivot}}.$$

Blade aerodynamic matrices. - For the purposes of this study all aerodynamic forces caused by in-plane displacements of the blade will be assumed to be zero.

$$\left| A_p \right| = 0$$

The only in-plane aerodynamic force which is not related to the essentially vertical aerodynamic forces is the c_{d_o} or section drag at zero lift. Abbot and Von Doenhoff indicate the c_{d_o} of the NACA 0012 airfoil to be .006. For purposes of this study, to account for roughness and to partially compensate the missing $\frac{dc_d}{dc_l^2}$ an effective value of $c_{d_o} = .011$ will be used. (This figure suggested by N.B. Gorenberg.)

It is now possible to approximate the aerodynamic forces due to blade in-plane motions. It will be assumed that the only forces on the blades due to blade motions will be due to c_{d_o}.

The blade aerodynamic damping motion $\left[A_{R_p}\right]$ is as shown on the following page.

Calculation of the elements of the blade aerodynamic damping matrix is straight forward. The derivation of the $\frac{\partial \text{ p.t.}}{\partial \dot{\zeta}}$ term will be shown as an example.

Aerodynamic drag (or negative force) per unit radius due to unit $\dot{\zeta}$ velocity is as follows:

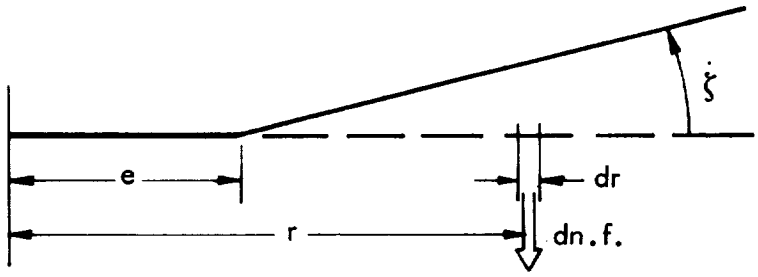

Due to minimum drag coefficient c_{d_o} the rate of change of normal force per unit radius is:

$$\frac{d\ n.f.}{dr} = - c_{d_o} \frac{1}{2} \rho \left(\Omega r + V \sin \psi + \dot{\zeta}(r-e)\right)^2 c + c_{d_o} \frac{1}{2} \rho \left(\Omega r + V \sin \psi\right)^2 c$$

$$= - c_{d_o} \frac{1}{2} \rho \left[(\Omega r + V \sin \psi)^2 + 2(\Omega r + V \sin \psi)\ \dot{\zeta}(r-e)\right.$$

$$\left. + \dot{\zeta}^2 (r-e)^2\right] c + c_{d_o} \frac{1}{2} \rho \left(\Omega r + V \sin \psi\right)^2 c$$

but $\dot{\zeta}^2 (r-e)^2$ is negligibly small compared to the other terms.

$$\frac{d\ n.f.}{dr} = - c_{d_o} \frac{1}{2} \rho \left[2\ \dot{\zeta}(\Omega r + V \sin \psi)\ (r-e)\right] c$$

$$\frac{d^2\ n.f.}{d\zeta\, dr} = - c_{d_o} \rho c\ (r-e)\ (\Omega r + V \sin \psi)$$

Single blade aerodynamic damping matrix:

$$\left|A_{R_P}\right| =$$

$$-c_{d_o}\rho c \begin{bmatrix} (R-e)\left[\frac{\Omega}{2}(R+e)\,V\sin\psi\right] & 0 & \left(\frac{R^3}{3}\Omega+\frac{R^2V}{2}\sin\psi\right) & R^2\left(\frac{R}{3}-\frac{e}{2}\right)\Omega+\left(\frac{R^2}{2}-eR\right)V\sin\psi \\ 0 & 0 & 0 & 0 \\ \left(\frac{R^3}{3}\Omega+\frac{R^2}{2}V\sin\psi\right) & 0 & \left(\frac{R^4\Omega}{4}+\frac{R^3V}{3}\sin\psi\right) & \left(\frac{R^4}{4}-\frac{R^3e}{3}\right)\Omega+\left(\frac{R^3}{3}-\frac{R^2e}{2}\right)V\sin\psi \\ \left[R^2\left(\frac{R}{3}-\frac{e}{2}\right)\Omega+\left(\frac{R^2}{2}-Re\right)V\sin\psi\right] & 0 & \left(\frac{R^4}{4}-\frac{R^3e}{3}\right)\Omega+\left(\frac{R^3}{3}-\frac{R^2e}{2}\right)V\sin\psi & \left(\frac{R^4}{4}-2e\,\frac{R^3}{3}+\frac{e^2R^2}{2}\right)\Omega+\left(\frac{R^3}{3}-2e\,\frac{R^2}{2}+e^2\right)V\sin\psi \end{bmatrix}$$

This matrix is symmetrical.

and the derivative $\frac{d\ p.t.}{d\dot{\zeta}}$ becomes:

$$\frac{d\ p.t.}{d\dot{\zeta}} = -c_{d_o}\ \rho c \int_e^R (r-e)\ (r-e)\ (\Omega r + V \sin\psi)\ dr$$

$$= -c_{d_o}\ \rho c \left[\Omega R^2\left(\frac{R^2}{4} - 2e\ \frac{R}{3} + \frac{e^2}{2}\right) + \left(\frac{R^3}{3} - 2e\frac{R^2}{2} + e^2\right)V \sin\psi\right]$$

In-plane Equations of the Rotor

Once the single blade equations of motion are available, they may be assembled into a single uncoupled matrix. First, form the vector of all single blade displacements:

$$\eta_{xy} = \begin{Bmatrix} \eta_{xy_1} \\ \eta_{xy_2} \\ \eta_{xy_3} \end{Bmatrix} \quad \text{for a three-bladed rotor}$$

The equations of motion of the three uncoupled blades become:

$$\begin{bmatrix} I_1 & & \\ & I_2 & \\ & & I_3 \end{bmatrix} \begin{Bmatrix} \ddot{\eta}_{xy_1} \\ \ddot{\eta}_{xy_2} \\ \ddot{\eta}_{xy_3} \end{Bmatrix} + \begin{bmatrix} COR_1 & & \\ & COR_2 & \\ & & COR_3 \end{bmatrix} \begin{Bmatrix} \dot{\eta}_{xy_1} \\ \dot{\eta}_{xy_2} \\ \dot{\eta}_{xy_3} \end{Bmatrix}$$

$$+ \begin{bmatrix} CF_1 & & \\ & CF_2 & \\ & & CF_3 \end{bmatrix} \begin{Bmatrix} \eta_{xy_1} \\ \eta_{xy_2} \\ \eta_{xy_3} \end{Bmatrix} - \begin{bmatrix} A_{R_1} & & \\ & A_{R_2} & \\ & & A_{R_3} \end{bmatrix} \begin{Bmatrix} \dot{\eta}_{xy_1} \\ \dot{\eta}_{xy_2} \\ \dot{\eta}_{xy_3} \end{Bmatrix} = 0$$

The displacement derivatives assumed to be zero were not included.

The equation may now be transformed into rotor coordinates employing the relationship between blade and rotor coordinates derived in the kinematics section, namely:

$$\eta_{xy_p} = \left[D_{xy_p}\right] \beta_{xy}$$

or expand to three blades

$$\eta_{xy} = \begin{bmatrix} D_{xy_1} \\ D_{xy_2} \\ D_{xy_3} \end{bmatrix} \beta_{xy} \quad \text{or} \quad \eta_{xy} = \left[D_{xy}\right] \beta_{xy}$$

and since the relationship is kinematic

$$\dot{\eta}_{xy} = \left[D_{xy}\right] \dot{\beta}_{xy}$$

and

$$\ddot{\eta}_{xy} = \left[D_{xy}\right] \ddot{\beta}_{xy}$$

and employing the transpose of the $\left[D_{xy}\right]$ matrix for the purpose of gathering up single blade generalized forces and converting them into generalized forces applied to the rotor degrees of freedom. The transpose relationship is as follows:

$$\begin{Bmatrix} Y_r \\ X_r \\ N_r \\ H_{\zeta_{o_r}} \\ H_{\zeta_{y_r}} \\ H_{\zeta_{x_r}} \end{Bmatrix} = \left[D_{xy}\right]^T \begin{Bmatrix} n.f._1 \\ a.f._1 \\ s.t._1 \\ p.t._1 \\ \text{- - - - -} \\ n.f._2 \\ a.f._2 \\ s.t._2 \\ p.t._2 \\ \text{- - - - -} \\ n.f._3 \\ a.f._3 \\ s.t._3 \\ p.t._3 \end{Bmatrix}$$

where the generalized rotor forces in rotating coordinates are as follows:

Y_r Lateral force, lb

X_r Longitudinal force, lb

N_r Yawing force, ft lb

$H_{\zeta_{o_r}}$ Collective lead-lag generalized force, lb

$H_{\zeta_{y_r}}$ Lateral lead-lag generalized force, lb

$H_{\zeta_{x_r}}$ Longitudinal lead-lag generalized force, lb

These two properties of the $\left[D_{xy}\right]$ transformation matrix allow the three uncoupled sets of single blade equations to be transformed into rotor equations of motion as follows:

$$\left[D_{xy}\right]^T \begin{bmatrix} I_1 & & \\ & I_2 & \\ & & I_3 \end{bmatrix} \left[D_{xy}\right] \ddot{\beta}_{xy} + \left[D_{xy}\right]^T \begin{bmatrix} COR_1 & & \\ & COR_2 & \\ & & COR_3 \end{bmatrix} \left[D_{xy}\right] \dot{\beta}_{xy}$$

$$+ \left[D_{xy}\right]^T \begin{bmatrix} CF_1 & & \\ & CF_2 & \\ & & CF_3 \end{bmatrix} \left[D_{xy}\right] \beta_{xy} - \left[D_{xy}\right]^T \begin{bmatrix} A_{R_1} & & \\ & A_{R_2} & \\ & & A_{R_3} \end{bmatrix} \left[D_{xy}\right] \dot{\beta}_{xy} = 0$$

With the equations written in this form it then becomes possible to include rotating hub mass terms and blade structural damping terms. The terms for the rotating hub motions and rotor elastic mode structural damping are as follows and may be combined directly with the rotor equations in rotating coordinates:

$$\begin{bmatrix} M_R & & & & & \\ & M_R & & & & \\ & & I_R & & & \\ & & & 0 & & \\ & & & & 0 & \\ & & & & & 0 \end{bmatrix} \begin{Bmatrix} \ddot{y}_r \\ \ddot{x}_r \\ \ddot{v}_r \\ \ddot{\zeta}_o \\ \ddot{\zeta}_y \\ \ddot{\zeta}_x \end{Bmatrix} + \begin{bmatrix} 0 & -2\Omega M_R & 0 & & & \\ 2\Omega M_R & 0 & 0 & & & \\ 0 & 0 & 0 & & & \\ & & & 2\gamma\omega M_{\zeta o\zeta o} & & \\ & & & & 2\gamma\omega M_{\zeta y\zeta y} & \\ & & & & & 2\gamma\omega M_{\zeta x\zeta x} \end{bmatrix} \begin{Bmatrix} \dot{y}_r \\ \dot{x}_r \\ \dot{v}_r \\ \dot{\zeta}_o \\ \dot{\zeta}_y \\ \dot{\zeta}_x \end{Bmatrix}$$

$$\begin{bmatrix} \Omega^2 M_R & 0 & 0 & 0 & 0 & 0 \\ 0 & \Omega^2 M_R & 0 & 0 & 0 & 0 \\ 0 & 0 & 0 & 0 & 0 & 0 \\ 0 & 0 & 0 & 0 & 0 & 0 \\ 0 & 0 & 0 & 0 & 0 & 0 \\ 0 & 0 & 0 & 0 & 0 & 0 \end{bmatrix} \begin{Bmatrix} y_r \\ x_r \\ v_r \\ \zeta_o \\ \zeta_y \\ \zeta_x \end{Bmatrix} = 0$$

The hub inertia terms and the rotor structural damping terms are defined as follows:

M_R	Hub mass, slugs
I_R	Hub polar moment of inertia, slugs ft^2
γ	Fraction of critical damping
ω	Natural frequency of mode at rpm, radians/second
$M_{\zeta o\zeta o}$, $M_{\zeta y\zeta y}$, $M_{\zeta x\zeta x}$	Generalized masses of rotor collective, lateral and longitudinal lead-lag degrees of freedom.

And the combined equations may be written more concisely as:

$$\left[I_{xy}\right] \ddot{\beta}_{xy} + \left[COR_{xy}\right] \dot{\beta}_{xy} + \left[CF_{xy}\right] \beta_{xy} - \left[A_{R_{xy}}\right] \dot{\beta}_{xy} = 0$$

In a similar way to the transformation from blade to rotor coordinates the equations may be transformed to stationary axes by employing the transformation relation between rotating and stationary axes and remembering that it is a function of time so that:

$$\beta_{xy} = \left[T_{xy}\right] \beta_{XY}$$

$$\dot{\beta}_{xy} = \left[T_{xy}\right] \dot{\beta}_{XY} + \left[\dot{T}_{xy}\right] \beta_{XY}$$

$$\ddot{\beta}_{xy} = \left[T_{xy}\right] \ddot{\beta}_{XY} + 2\left[\dot{T}\right] \dot{\beta}_{XY} + \left[\ddot{T}\right] \beta_{XY}$$

The transpose which relates the generalized forces in stationary axes to those in rotating is as follows:

$$GF_{XY} = \left[T_{xy}\right]^T GF_{xy}$$

or

$$\begin{Bmatrix} Y \\ X \\ N \\ H_{\zeta_o} \\ H_{\zeta_y} \\ H_{\zeta_x} \end{Bmatrix} = \left[T_{xy}\right]^T \begin{Bmatrix} Y_r \\ X_r \\ N_r \\ H_{\zeta_{or}} \\ H_{\zeta_{yr}} \\ H_{\zeta_{xr}} \end{Bmatrix}$$

The rotor and hub equations in stationary axes become:

$$\left[T_{xy}\right]^T \left[I_{xy}\right] \left[T_{xy}\right] \ddot{\beta}_{XY} + \left[\left[T_{xy}\right]^T \left[COR_{xy}\right] \left[T_{xy}\right] + 2 \left[T_{xy}\right]^T \left[I_{xy}\right] \left[\dot{T}_{xy}\right]\right] \dot{\beta}_{XY}$$
$$+ \left[\left[T_{xy}\right]^T \left[CF_{xy}\right] \left[T_{xy}\right] + \left[T_{xy}\right]^T \left[COR_{xy}\right] \left[\dot{T}_{xy}\right] + \left[T_{xy}\right]^T \left[I_{xy}\right] \left[\ddot{T}_{xy}\right]\right] \beta_{XY}$$
$$- \left[T_{xy}\right]^T \left[A_{R_{xy}}\right] \left[T_{xy}\right] \dot{\beta}_{XY} - \left[T_{xy}\right]^T \left[A_{R_{xy}}\right] \left[\dot{T}_{xy}\right] \beta_{XY} = 0$$

And with the appropriate simplifications due to rotational symmetry the equations become, through the use of $\left[T_{xy}\right]$, $\left[\dot{T}_{xy}\right]$ and $\left[\ddot{T}_{xy}\right]$ at $\psi = 0$,

$$\left[I_{xy}\right] \ddot{\beta}_{XY} + \left[\left[COR_{xy}\right] + 2 \left[I_{xy}\right] \left[\dot{T}_{xy}\right]\right] \dot{\beta}_{XY}$$
$$+ \left[\left[CF_{xy}\right] + \left[COR_{xy}\right] \left[\dot{T}_{xy}\right] + \left[I_{xy}\right] \left[\ddot{T}_{xy}\right]\right] \beta_{XY}$$
$$- \left[T_{xy}\right] \left[A_{R_{xy}}\right] \left[T_{xy}\right] \dot{\beta}_{XY} - \left[T_{xy}\right] \left[A_{R_{xy}}\right] \left[\dot{T}_{xy}\right] \beta_{XY} = 0$$

Body terms. - Terms for the body mass and spring restraint to the tunnel are combined with the rotor equations.

The shaft may translate laterally "y" and longitudinally "x" or rotate "υ." No other degrees of freedom involve motions of the shaft. Masses of shaft or body attached to it therefore can cause inertia forces only in acting on those degrees of freedom, the forces Y, X, N.

In the case of the N force the shaft is presumed to be torsionally unrestrained by the transmission and engine - as though it were fluid coupled. The engine applies a mean torque, only, to the shaft and free torsional oscillations of the shaft are allowed.

The Y and X forces due to accelerations $\ddot{x}$ and $\ddot{y}$ will be due to the mass and moments of inertia of the helicopter body.

It is assumed that effective non-rotating masses exist in the plane of the disk. One resists lateral accelerations and the other longitudinal. Their magnitudes are different because they are based on rolling and pitching moments of inertia of the body as well as the body mass.

Springs restraining the shaft against lateral and longitudinal motions are also employed. The terms for body or shaft inertia and springs may be combined with the rotor terms and are as follows:

$$\begin{bmatrix} M_y & 0 & 0 \\ 0 & M_x & 0 \\ 0 & 0 & 0 \end{bmatrix} \begin{Bmatrix} \ddot{y} \\ \ddot{x} \\ \ddot{\upsilon} \end{Bmatrix} + \begin{bmatrix} K_y & 0 & 0 \\ 0 & K_x & 0 \\ 0 & 0 & 0 \end{bmatrix} \begin{Bmatrix} y \\ x \\ \upsilon \end{Bmatrix} = 0$$

With the rotor (and rotating hub) removed these equations govern the roll and pitch or, more accurately, the lateral and longitudinal natural frequencies of the model in the wind tunnel.

The homogeneous equation. - Including the body mass and spring terms with the rotor terms yields the full set of homogeneous in-plane equations.

$$\left|I_{XY}\right| \ddot{\beta}_{XY} + \left|COR_{XY}\right| \dot{\beta}_{XY} + \left|CF_{XY}\right| \beta_{XY} - \left|A_{R_{XY}}\right| \dot{\beta}_{XY} - \left|A_{XY}\right| \beta_{XY} = 0$$

In-Plane Forcing Functions

The in-plane forcing functions are produced by vertical motions of the blades and through components of the vertical response and forcing aerodynamics vector. Before discussing the aerodynamic forces causing blade in-plane motions it should be noted that forcing aerodynamics in the in-plane direction are applied to the blades due to collective pitch, angle-of-attack, cyclic pitch, precone, twist, and the flapping deflections and velocities accompanying them. These in-plane components of the essentially vertical aerodynamic forces depend on two considerations:

1. Magnitude of the essentially vertical force
2. Angle between the lift resultant vector and the effective plane of the blade in-plane response.

Because the in-plane velocities are relatively small, of the order of 10 ft/sec or so, they will not significantly alter the magnitude or direction of the forcing aerodynamics.

The vertical motions equations forcing and response aerodynamics combine to yield net local angles-of-attack relative to the flow component normal to the blade leading edge. The local lift force at the blade element, if assumed to be normal to the relative wind at that section (ignoring the drag contribution to the aerodynamic resultant force) has a component in the direction of the in-plane response of that blade -- calculated in these analyses in the vicinity of the blade section at the 3/4 radius.

These in-plane (of the mode) aerodynamic forces along each blade may be factored by the rotor mode shape for that blade, integrated and combined with the similar generalized force contributions from the other blades to yield the in-plane rotor mode generalized force. The generalized force varies with time as the rotor turns through the azimuth and contributes to the forcing of that in-plane mode. The same forces can also be factored by each of the other rotor mode shapes to obtain the generalized forces in all rotor in-plane modes. Body or shaft modes, or degrees of freedom, however, displace in a direction normal to the shaft or vertical axis so their generalized forces must be calculated relative to the disk plane rather than relative to the principal axis of the blade-alone in-plane motion.

Before leaving the aerodynamic in-plane forcing functions it should be noted that there is an aerodynamic contribution that is independent of "z" motion and forces. It is due to the drag coefficient of the section at zero lift c_{d_o}. Its generalized force is considered separately.

In addition to the aerodynamic contribution to the in-plane forcing functions due to rotor response, there are inertia or mass-induced forces due to blade vertical flapping motions. These depend only on the built-in precone angle β_o and the sum of the contributions to the flapping motion of each blade from the rotor flapping degrees of freedom. The in-plane forces are due solely to displacements, velocities, and accelerations in the radial direction of the elements of blade mass distribution. The inertia forces can be factored by in-plane mode shapes to obtain generalized in-plane forces which are then combined with the aerodynamic external generalized forces to yield the net forcing function to the in-plane degrees of freedom.

In-plane forcing due to vertical motions. - The vertical motions degrees of freedom are assumed to provide displacements parallel to the shaft only, in framing the vertical equations of motion. In actual fact, however, elements of blade mass take up small motions in the radial direction when the blade bends vertically in its parabolic mode shape, especially when in the presence of built-in blade precone angle. Figure 10 shows the small inboard (negative) radial displacement "v" that accompanies the vertical displacement "δ" in conjunction with built-in precone β_o

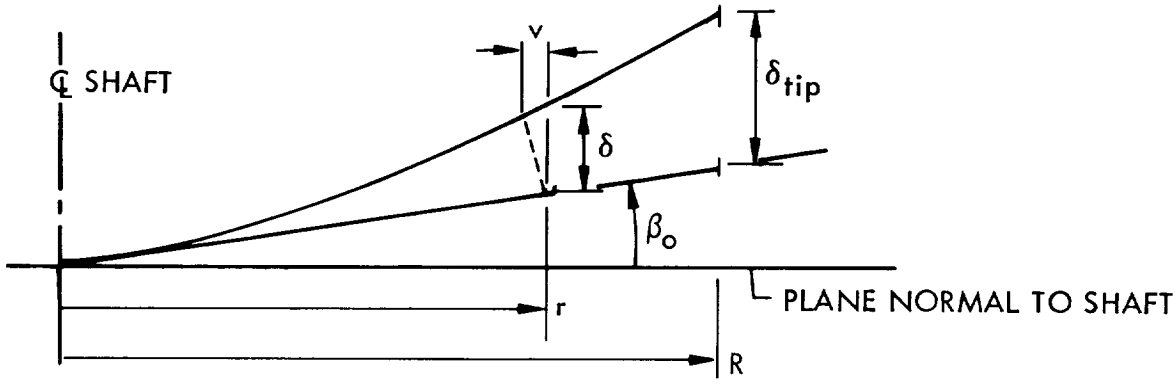

position of blade above plane = $\beta_o r + \delta_{tip} \left(\frac{r}{R}\right)^2$

Figure 10. Blade Radial Displacement Due to Flap Bending

The displacement, velocity, and acceleration of a lump of mass at station "r" due to flapping displacement are as follows:

$$v = -\left[\left(\frac{r}{R}\right)^2 \beta_o + \frac{2}{3}\left(\frac{r}{R}\right)^2 \frac{1}{R}\ \delta_{tip}\right] \delta_{tip}$$

$$\frac{dv}{dt} = -\left[\left(\frac{r}{R}\right)^2 \beta_o + \frac{4}{3}\left(\frac{r}{R}\right)^3 \frac{1}{R}\ \delta_{tip}\right] \dot{\delta}_{tip}$$

$$\frac{d^2v}{dt^2} = -\left(\frac{r}{R}\right)^2 \left[\beta_o + \frac{4}{3}\frac{r}{R^2}\ \delta_{tip}\right] \ddot{\delta}_{tip} - \left(\frac{r}{R}\right)^2 \frac{4}{3}\ \frac{r}{R^2}\ \dot{\delta}_{tip}^{\ 2}$$

The above is the motion of station "r" due to flapping deflection, velocity, and acceleration, in rotating blade axes, and is non-linear.

The non-linearity causes no great difficulty in this analysis since the mass element motions are used only for producing external forces to the linear in-plane equations of motion.

With the radial displacement, velocity, and acceleration of elements of mass of the blades known in terms of tip displacement, velocity, and acceleration it is necessary to find the motions of all blade tips in terms of motions of the rotor degrees of freedom in stationary axes. Then with blade radial motions known in terms of motion of stationary axes degrees of freedom, it is only necessary to find the single blade generalized in-plane forces due to single blade radial motions and collect them by means of the $\left|D_{xy}\right|^T$ matrix and transform these to stationary axes by the $\left|T\right|^T$ matrix. The forces may then be used in conjunction with the aerodynamic forcing functions to find the in-plane response.

The motions of the blade tips are determined from the vertical motions response degrees of freedom by employing the transformation from stationary to rotating axes and from rotor coordinates to blade coordinates, as follows:

$$\eta_z = \left|D_z\right| \left|T_z\right| \beta_z$$

and since β_z is known as a function of time, then $\dot{\eta}_z$ and $\ddot{\eta}_z$ may be obtained by differentiations of the above expression. From η_z, $\dot{\eta}_z$, and $\ddot{\eta}_z$ the required blade tip displacements, velocities, and accelerations may be extracted.

The p^{th} single blade generalized forces due to radial motions may be written in matrix form as:

$$\begin{Bmatrix} \text{n.f.}_p \\ \text{a.f.}_p \\ \text{s.f.}_p \\ \text{p.f.}_p \end{Bmatrix} = \begin{bmatrix} 0 & 0 & \frac{2\Omega\beta_o I_b}{R^2} & \frac{8}{3}\frac{\Omega}{R^4} J_b & 0 & 0 \\ -\frac{\Omega^2\beta_o I_b}{R^2} & -\frac{2}{3}\frac{\Omega^2 J_b}{R^4} & 0 & 0 & \frac{\beta_o I_b}{R^2} & \frac{4}{3} R^4 J_b \\ 0 & 0 & \frac{2\Omega\beta_o J_b}{R^2} & \frac{8}{3}\frac{\Omega K_6}{R^4} & 0 & 0 \\ 0 & 0 & \frac{2\Omega\beta_o}{R^2} J_{e_b} & \frac{8}{3}\frac{\Omega K_{e_b}}{R^4} & 0 & 0 \end{bmatrix} \begin{Bmatrix} \delta_p \\ \delta_p^2 \\ \dot{\delta}_p \\ \delta_p\dot{\delta}_p \\ \ddot{\delta}_p \\ \delta_p\ddot{\delta}_p + \dot{\delta}_p^2 \end{Bmatrix}$$

where $I_b = \int_e^R r^2 \frac{dm}{dr}\, dr$ $\qquad J_{e_b} = \int_e^R r^2 (r-e) \frac{dm}{dr}\, dr$

$J_b = \int_e^R r^3 \frac{dm}{dr}\, dr$ $\qquad K_{e_b} = \int_e^R r^3 (r-e) \frac{dm}{dr}\, dr$

$K_b = \int_e^R r^4 \frac{dm}{dr}\, dr$

and δ_p is the tip deflection of the p^{th} blade, it is a function of azimuth ψ or time Ωt.

The generalized forces on the rotor degrees of freedom in stationary axes are then found by

$$\left|GF_{XY}\right| = \left|T_{xy}\right|^T \left|D_{xy}\right|^T \begin{Bmatrix} \text{n.f.}_1 \\ \text{a.f.}_1 \\ \text{s.t.}_1 \\ \text{p.t.}_1 \\ \text{- - - - -} \\ \text{n.f.}_2 \\ \text{a.f.}_2 \\ \text{s.t.}_2 \\ \text{p.t.}_2 \\ \text{- - - - -} \\ \text{n.f.}_3 \\ \text{d.f.}_3 \\ \text{s.t.}_3 \\ \text{p.t.}_3 \end{Bmatrix}$$

for a 3-bladed rotor.

In-plane forcing due to vertical aerodynamic forces. - Three rotor forces contribute to the in-plane aerodynamic forcing functions, lift or thrust, pitch, and roll hub moments. The blade forces contributing to these three rotor forces are assumed to be concentrated at the blade 3/4 radius. The lift is assumed to be uniform around the azimuth, the pitch and roll moments smooth sinusoidal distributions as shown in Figure 11.

The assumption that rotor pitch and roll moments are applied sinusoidally is a fairly good assumption. Should the forces in fact be applied at a different radial station, the effect on the in-plane forces would be small. For example, if applied at blade tips, the blade forces would be smaller due to increased radius but the in-plane moment would not change significantly because the in-plane moment arm increases to compensate. Should the forces be applied other than sinusoidally, it is unlikely that there would be a significant change in the 1P or 2P components of in-plane force.

The assumption that the lift is applied at the 3/4 radius is fairly good at low advance ratio. At higher advance ratio it could be a poor assumption. If the lift were applied, say, at the blade tips, the in-plane forces would be much larger than if the lift were applied at, say, the 50% station. Furthermore, the lift could be applied in a 2P distribution, or humps at opposite sides of the disk; or it could wander radially as it traversed the azimuth and still be a steady lift.

These assumptions are used here because they simplify the analysis and certain evidence suggests that, in fact, they are not bad for many cases. Aerodynamic forcing is generally a smaller contribution to in-plane generalized forces than are the coriolis forces and, therefore, can afford to be less precise.

These assumptions allow the loading per blade to be written immediately in terms of the Lift T, Pitch Moment M, and Roll Moment L. The lift on the pth blade becomes:

$$L_p = \frac{T}{b} - \frac{2M}{.75Rb} \cos(\psi + \psi_p) + \frac{2L}{.75Rb} \sin(\psi + \psi_p)$$

where p is the pth blade numbered clockwise viewed from above.

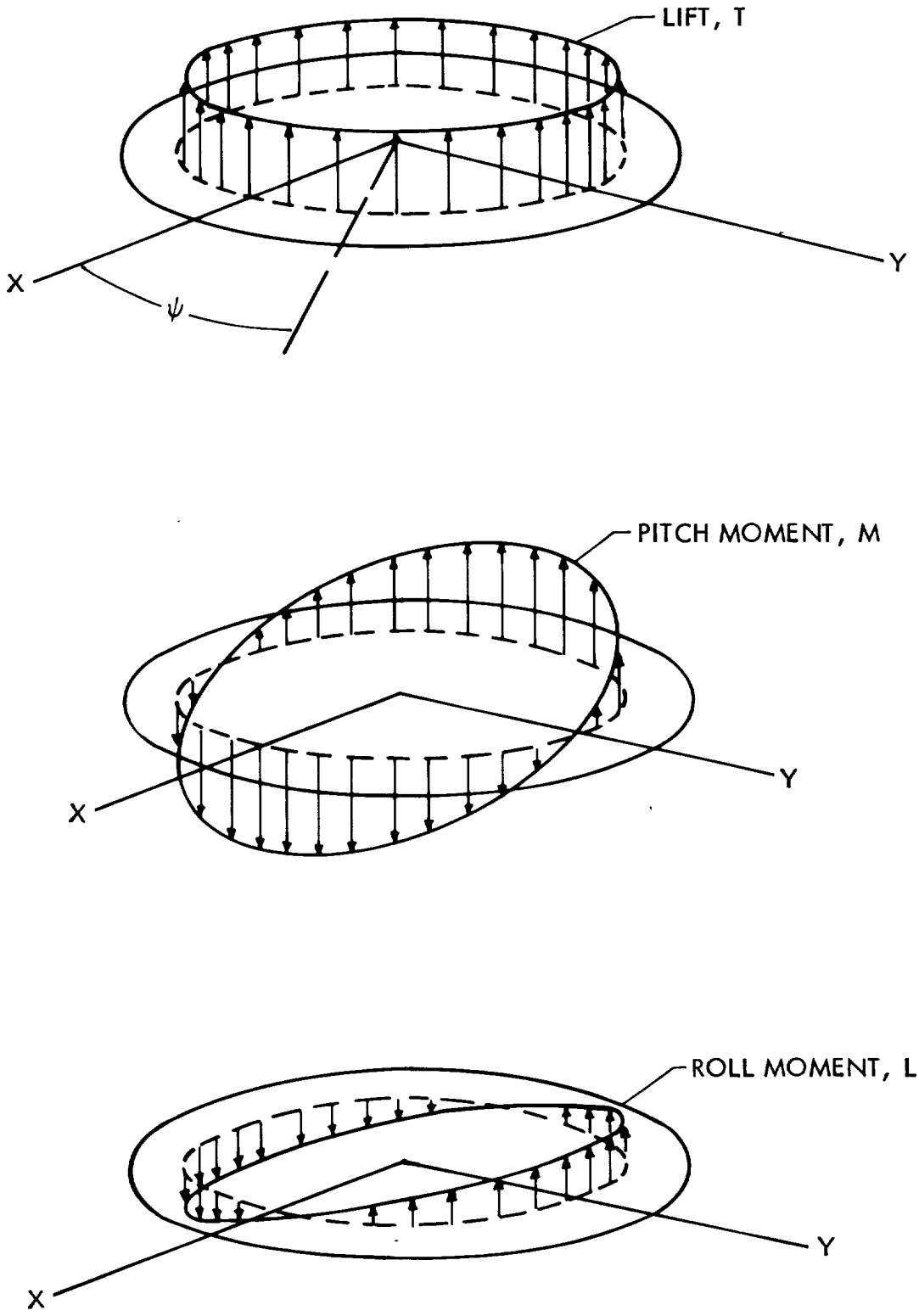

Figure 11. Rotor Vertical Aerodynamic Force Distributions Assumed for Calculating In-Plane Aerodynamic Forcing

With the blade loads specified at each azimuth point, it is only necessary to resolve them into components normal to and parallel to the inclined in-plane mode principal axis to provide the generalized forces for the overall rotor lead-lag modes and to the plane normal to the shaft for overall rotor rigid body modes. For the former, the in-plane axis will be assumed to be inclined proportional to the feathering displacement with the constant of proportionality dependent on the rotor rpm.

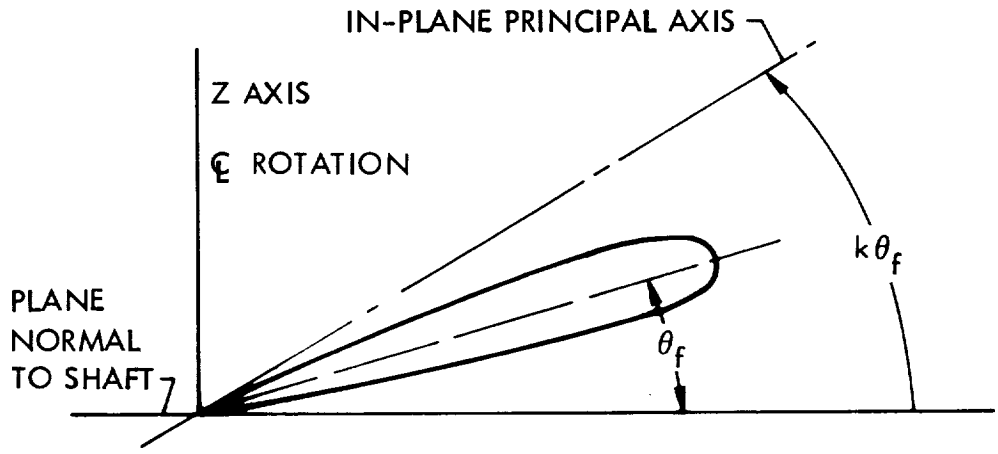

The lift at a section is produced by two classes of angle of attack: Class I - due to rotation of the section relative to the disk plane or shaft, and Class II - due to precone, flap deflection, flap velocity, and pitch, plunge and roll rate of the disk. Only Class II angles-of-attack produce an inclination of the lift vector relative to the shaft axis.

Under the assumption that the c_{d_o} is accounted for separately and the section drag due to section lift is negligible, the lift (and resultant) vector is normal to the flow at infinity relative to the sections.

For Class I angles of attack the lift, therefore, is directed parallel to the shaft axes. Class I angles of attack are:

$$\theta_o,\ \theta_{lc},\ \theta_{ls},\ \text{and}\ \theta_t{}^r$$

With the application of Class II angles-of-attack, even in the presence of Class I lift, the total lift vector is inclined relative to the shaft axis.

The inclination is equal to the sum of the Class II angle contributions at the section. These angles are due to:

$$\beta_o,\ \dot{z},\ \delta_o,\ \delta_\theta,\ \delta_\phi,\ \dot{\theta},\ \dot{\Phi} \text{ in stationary axes.}$$

Contributions to Class II angles-of-attack from rotor flapping velocities in stationary axes $\dot{\delta}_o$, $\dot{\delta}_\Phi$, $\dot{\delta}_\phi$ are neglected in these analyses because only steady cases are considered. Aircraft pitch attitude "θ" effects are included with the $\dot{z}/V$ parameter.

The Class II angle-of-attack at station "r" due to the above is as follows:

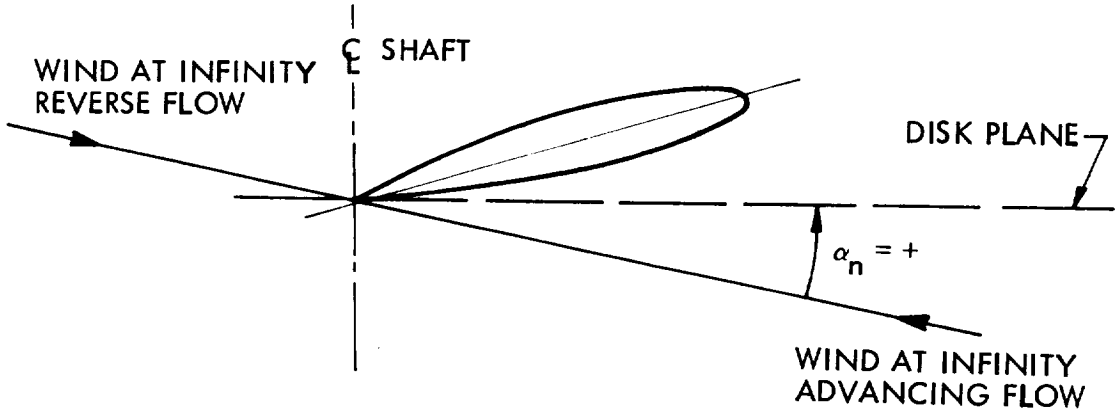

The angle-of-attack is the angle between the wind remote from the section (at infinity) and the chord line regardless of the direction of the wind, advancing or reverse flow. This results in one equation for each contribution which applies in both advancing and reverse velocity regions. The Class II part is that part between the wind at infinity and the plane normal to shaft "α_n."

The basic blade motions and fixed geometry shape that contribute to the Class II angle of attack, obtained from the stationary axes degree of freedom motions, are as follows and depend on the azimuth location of the blade as follows:

β: $$\alpha_n = - \beta \frac{V \cos \psi}{\Omega r + V \sin \psi}$$

$\dot{\beta}$: $$\alpha_n = - \dot{\beta} \frac{r}{\Omega r + V \sin \psi}$$

$\dot{z}$: $$\alpha_n = - \dot{z} \frac{1}{\Omega r + V \sin \psi}$$

δ: $$\alpha_n = - \delta_{tip} \left[\frac{\left(\frac{r}{2R^2} \right) V \cos \psi}{\Omega r + V \sin \psi} \right]$$

$\dot{\delta}$: $$\alpha_n = - \dot{\delta}_{tip} \left[\frac{\left(\frac{r}{R} \right)^2}{\Omega r + V \sin \psi} \right]$$

The net value of α_n due to all Class II contributors then is obtained by factoring the blade motion column matrix by the Class II angle of attack row matrix.

Class II angle-of-attack at station "r" on the pth blade:

$$\alpha_{n_p} = \frac{-1}{\Omega r + V \sin (\psi + \psi_p)} \left[V \cos (\psi + \psi_p) \;\vdots\; \frac{2r}{R^2} V \cos (\psi + \psi_p) \;\vdots\; r \;\vdots\; 1 \;\vdots\; \left(\frac{r}{R} \right)^2 \right] \begin{Bmatrix} \beta_o \\ \delta_p \\ \dot{\beta}_p \\ \dot{z}_p \\ \dot{\delta}_p \end{Bmatrix}$$

In determining the α_{np} the value of radius "r" to use in these analyses is r = .75R (by basic assumption).

It is now possible to calculate the in-plane aerodynamic forcing function. On the pth blade with aerodynamic "normal" forces indicated by "L_p" and the angle-of-attack relative to the vertical axis, or shaft axis called α_{np} and the inclination of the in-plane principal axis given by $\kappa \theta_f$, the in-plane force at the 3/4 blade radius is given by:

In-plane force

$$F_{ip_p} = L_p \sin \left(\alpha_{n_p} + \kappa \theta_f \right)$$

is shown resolved into the in-plane principal axes in Figure 12.

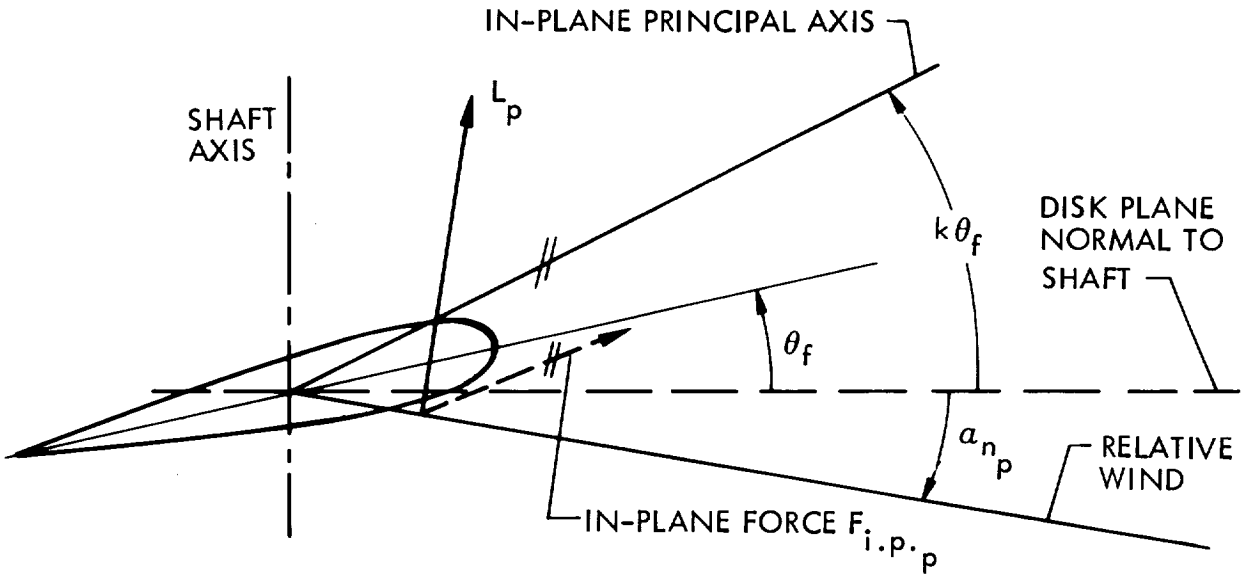

Figure 12. Resolution of Section Lift into Blade In-Plane Principal Axis

It is assumed that $\alpha_{n_p} + \kappa\theta_f$ remains less than 10°, so that

$$\sin(\alpha_{n_p} + \kappa\theta_f) \approx (\alpha_{n_p} + \kappa\theta_f), \text{ and } F_{ip_p} = L_p(\alpha_{n_p} + \kappa\theta_{f_p}).$$

The last piece of information needed to complete the calculation of the F_{ip} is the value of θ_{f_p}. It is obtained from the η_z matrix by abstracting the θ_p, the feathering pitch, and adding it to the collective pitch θ_o and blade twist at the three-quarter radius $\theta_t(.75R)$ so that:

$$\theta_{f_p} = \theta_p + \theta_o + \theta_t(.75R) \text{ so that:}$$

In summary, the expression for F_{ip_p} is as follows:

$$F_{ip} = L_p(\alpha_{n_p} + \kappa\theta_{f_p})$$

where

$$L_p = \left[\frac{T}{b} - \frac{2M}{.75Rb}\cos(\psi + \psi_p) + \frac{2L}{.75Rb}\sin(\psi + \psi_p)\right]$$

$$\alpha_{n_p} = \frac{-1}{\Omega r + V\sin(\psi + \psi_p)}\left[V\cos(\psi + \psi_p)\left|\frac{2r}{R^2}V\cos(\psi + \psi_p)\right|r\left|1\right|\left(\frac{r}{R}\right)^2\right]\begin{Bmatrix}\beta_o\\ \delta_p\\ \dot{\beta}_p\\ \dot{z}_p\\ \dot{\delta}_p\end{Bmatrix}$$

κ = In-plane principal axis factor

$$\theta_{f_p} = \theta_p + \theta_o + .75R\,\theta_t$$

With the in-plane forces on each blade at the 3/4 radius evaluated at closely spaced azimuth positions, it is then necessary to organize these into generalized forces on the blades and collect these into generalized forces on the in-plane degrees of freedom in stationary axes.

It should be noted, however, that in the foregoing discussion the generalized forces on the blade in-plane degrees of freedom were found. This freedom was inclined to the plane normal to the shaft by the angle $\kappa\theta_{f_p}$ and the component of aerodynamic force in that direction was employed in calculating the blade generalized force.

For the rigid body degrees of freedom y, x and υ, however, the blade force component contribution to the generalized forces must be in the plane of the disk normal to the shaft. It is therefore necessary to calculate two F_{ip} one for $\kappa = 0$ and one for κ.

This can be done as follows:

$$\begin{Bmatrix}\text{n.f.}_p\\ \text{a.f.}_p\\ \text{s.t.}_p\\ \text{p.t.}_p\end{Bmatrix} = \begin{Bmatrix}1.0\\ 0\\ .75R\\ 0\end{Bmatrix} F_{ip_{p_{\kappa=0}}} + \begin{Bmatrix}0\\ 0\\ 0\\ .75R-e\end{Bmatrix} F_{ip_\kappa}$$

and for the whole rotor these become:

$$\begin{Bmatrix} GF \\ \beta_{xy} \end{Bmatrix} = \left[T_{xy}\right]^T \left[D_{xy}\right]^T \begin{bmatrix} 1.0 & 0 & 0 & 0 \cdots \\ 0 & 0 & 0 & 0 \cdots \\ .75R & 0 & 0 & 0 \cdots \\ 0 & .75R-e & 0 & 0 \cdots \\ 0 & 0 & 1.0 & 0 \cdots \\ 0 & 0 & 0 & 0 \cdots \\ 0 & 0 & .75R & 0 \cdots \\ \cdot & \cdot & \cdot & .75R-e \cdot \\ \cdot & \cdot & \cdot & \cdot \cdot \cdot \cdot \\ \cdot & \cdot & \cdot & \cdot \cdot \cdot \cdot \\ \cdot & \cdot & \cdot & \cdot \cdot \cdot \cdot \end{bmatrix} \begin{Bmatrix} F_{ip_{1_K}} = 0 \\ F_{ip_{1_K}} \\ F_{ip_{2_K}} = 0 \\ F_{ip_{2_K}} \\ F_{ip_{3_K}} = 0 \\ F_{ip_{3_K}} \\ \cdot \\ \cdot \\ F_{ip_{b_K}} \end{Bmatrix}$$

In-plane forcing due to minimum drag coefficient. - The in-plane forcing function due to blade section minimums drag coefficient c_{d_o} depends on the normal component of dynamic pressure q_n and the blade chord c. For the pth blade,

$$\left(\frac{d\ n.f.}{dr}\right)_p = c_{d_o}\ c\ q_n$$

$$= c_{d_o}\ c\ \frac{\rho}{2} \left[\left(\Omega r + V \sin\left(\psi + \psi_p\right)\right)\right]^2$$

$$n.f. = \int_e^R \frac{d\ n.f.}{dr}\ dr$$

$$a.f. = 0$$

$$s.t. = \int_e^R \frac{d\ n.f.}{dr}\ r\ dr$$

$$p.t. = \int_e^R \frac{d\ n.f.}{dr}\ (r-e)\ dr$$

Form the $\{GF_{blade}\}$ as a column

$$\{GF_{blade}\} = \begin{Bmatrix} n.f._1 \\ a.f._1 \\ s.t._1 \\ p.t._1 \\ \hline n.f._2 \\ a.f._2 \\ s.t._2 \\ p.t._2 \\ \hline \vdots \\ \hline n.f._b \\ a.f._b \\ s.t._b \\ p.t._b \end{Bmatrix}$$

The forcing functions on the stationary axes degrees of freedom are available from

$$\{GF\}_{stationary} = [T_{xy}]^T [D_{xy}]^T \{GF_b\}$$

Complete In-Plane Equations of Motion

The complete set of in-plane differential equations include the homogeneous equations in stationary axes and the forcing functions produced by vertical motions, vertical equations aerodynamic forces, and section drag coefficient.

$$\left[I_{XY}\right] \ddot{\beta}_{XY} + \left[COR_{XY}\right] \dot{\beta}_{XY} + \left[CF_{XY}\right] \beta_{XY}$$

$$- \left[A_{R_{XY}}\right] \dot{\beta}_{XY} - \left[A_{XY}\right] \beta_{XY} = \left\{GF_{XY}\right\} \text{ vertical motions}$$

$$+ \left\{GF_{XY}\right\} \text{vertical aero} + \left\{GF_{XY}\right\} \text{drag coefficient.}$$

SOLUTION OF VERTICAL MOTIONS EQUATIONS

Linear ordinary differential equations of the vertical motions of the rotor-gyroscope-airframe system have been derived in the foregoing section for three-and four-blade rotors. Those coefficients of the equations which depend on aerodynamics vary harmonically with azimuth at frequencies based in the rotation rate of the rotor. The external forcing functions also vary harmonically with azimuth.

In this section the equations are solved for the detailed harmonic or vibratory response of the degrees of freedom. From these and the external forces producing them, the shaft-and swashplate-transmitted vibration forces, the azimuthal variations of tip path displacement and, in the case of the free swashplate, swashplate harmonic tilt displacement wobble are determined. Calculated and experimental results are compared where possible.

General Discussion

The solution of systems of linear ordinary differential equations of motion possessing coefficients which vary harmonically with time is somewhat more complicated than solving equations with constant coefficients. It is the purpose of this section of the report to discuss the logic and methods which permit the solution of such equations for their steady oscillatory response to harmonically varying forcing functions. Such solutions yield shaft-transmitted vibratory loads and blade load histories.

The basic logic will be illustrated by treating the simplest representative system of the type: an undamped single degree of freedom with periodically varying spring stiffness and forced at the period of the spring stiffness oscillation.

Consider the equation:

$$\ddot{w} + (A + B \cos t)\, w = \cos t$$

where A and B are constants and w is the dependent variable. The solution w must contain oscillations associated with the period of the oscillator and the period of the coefficients. Since both are the same, w may be represented by a Fourier series, if subharmonics are excluded. (Later it will be shown that subharmonics cannot exist in a true steady state for these equations).

Let

$$w = a_o + a_{1s} \sin t + a_{1c} \cos t + a_{2s} \sin 2t + a_{2c} \cos 2t + \ldots.$$

then

$$\dot{w} = a_{1s} \cos t - a_{1c} \sin t + 2a_{2s} \cos 2t - 2a_{2c} \sin 2t \ldots\ldots.$$

and

$$\ddot{w} = - a_{1s} \sin t - a_{1c} \cos t - 4a_{2s} \sin 2t - 4a_{2c} \cos 2t \ldots\ldots.$$

substituting w and its derivatives in the equation yields:

$$-a_{1s} \sin t - a_{1c} \cos t - 4a_{2s} \sin 2t - 4a_{2c} \cos 2t \ldots\ldots\ldots\ldots\ldots$$

$$+Aa_o + Aa_{1s} \sin t + Aa_{1c} \cos t + Aa_{2s} \sin 2t + Aa_{2c} \cos 2t \ldots\ldots.$$

$$+Ba_o \cos t + Ba_{1s} \cos t \sin t + Ba_{1c} \cos^2 t + Ba_{2s} \cos t \sin 2t$$

$$+Ba_{2c} \cos t \cos 2t + Ba_{3s} \cos t \sin 3t + Ba_{3c} \cos t \cos 3t$$

$$+Ba_{4s} \cos t \sin 4t + Ba_{4c} \cos t \cos 4t + \ldots\ldots\ldots\ldots\ldots = \cos t$$

It is important to note that each term, in which products of trigonometric functions are found, may be simplified to the sum at two terms of single functions by trigonometric identities so that the above equations may be simplified to:

$$- \sin t\, a_{1s} - \cos t\, a_{1c} - 4 \sin 2t\, a_{2s} - 4 \cos 2t\, a_{2c} \ldots\ldots\ldots\ldots$$

$$Aa_0 + A \sin t\, a_{1s} + A \cos t\, a_{1c} + A \sin 2t\, a_{2s} + A \cos 2t\, a_{2c} \ldots\ldots.$$

$$B \cos t\, a_o + B(\tfrac{1}{2} \sin 2t)\, a_{1s} + B(\tfrac{1}{2} + \tfrac{1}{2} \cos 2t)\, a_{1c} + B(\tfrac{1}{2} \sin 3t$$

$$+ \tfrac{1}{2} \sin t)\, a_{2s} + B(\tfrac{1}{2} \cos 3t + \tfrac{1}{2} \cos t)\, a_{2c} + B(\tfrac{1}{2} \sin 4t + \tfrac{1}{2} \sin 2t)\, a_{3s}$$

$$+ B(\tfrac{1}{2} \cos 4t + \tfrac{1}{2} \cos 2t)\, a_{3c} + B(\tfrac{1}{2} \sin 5t + \tfrac{1}{2} \sin 3t)\, a_{4s}$$

$$+ B(\tfrac{1}{2} \cos 5t + \tfrac{1}{2} \cos 3t)\, a_{4c} \quad \ldots\ldots\ldots\ldots\ldots\ldots\ldots = \cos t$$

All terms in common frequencies are arranged in separate equations in order to permit a solution for the coefficients. Equating coefficients of common frequency:

$$(a_o) \quad (a_{1s}) \quad (a_{1c}) \quad (a_{2s}) \quad (a_{2c}) \quad (a_{3s}) \quad (a_{3c})$$

$$A a_o \qquad \tfrac{1}{2} B\, a_{1c} = 0$$

$$(A-1)\sin t\, a_{1s} \quad \tfrac{1}{2} B \sin t\, a_{2s} = 0$$

$$B \cos t\, a_o \quad (A-1)\cos t\, a_{1c} \quad \tfrac{1}{2} B \cos t\, a_{2c} = \cos t$$

$$B \sin 2t\, a_{1s} \quad (A-4)\sin 2t\, a_{2s} \quad \tfrac{1}{2} B \sin 2t\, a_{3s} = 0$$

$$\tfrac{1}{2} B \cos 2t\, a_{1c} \quad (A-4) \cos 2t\, a_{2c} \quad \tfrac{1}{2} B \cos 2t\, a_{3c} = 0$$

In matrix form this becomes:

$$\begin{bmatrix} A & 0 & B/2 & 0 & 0 & 0 \\ 0 & (A-1) & 0 & B/2 & 0 & 0 \\ B & 0 & (A-1) & 0 & B/2 & 0 \\ 0 & B/2 & 0 & (A-4) & 0 & B/2 \\ 0 & 0 & B/2 & 0 & (A-4) & 0 \end{bmatrix} \begin{Bmatrix} a_o \\ a_{1s} \\ a_{1c} \\ a_{2s} \\ a_{2c} \end{Bmatrix} = \begin{Bmatrix} 0 \\ 0 \\ 1 \\ 0 \\ 0 \end{Bmatrix}$$

It is obvious that the matrix could be extended to any desired number of harmonics by analytic continuation, as in the following example, to four harmonics.

$$\begin{bmatrix} A/2 & 0 & B/2 & 0 & 0 & 0 & 0 & 0 \\ 0 & (A-1) & 0 & B/2 & 0 & 0 & 0 & 0 \\ B/2 & 0 & (A-1) & 0 & B/2 & 0 & 0 & 0 \\ 0 & B/2 & 0 & (A-4) & 0 & B/2 & 0 & 0 \\ 0 & 0 & B/2 & 0 & (A-4) & 0 & B/2 & 0 \\ 0 & 0 & 0 & B/2 & 0 & (A-9) & 0 & B/2 \\ 0 & 0 & 0 & 0 & B/2 & 0 & (A-9) & 0 \\ 0 & 0 & 0 & 0 & 0 & B/2 & 0 & (A-16) \end{bmatrix} \begin{Bmatrix} 2a_o \\ a_{1s} \\ a_{1c} \\ a_{2s} \\ a_{2c} \\ a_{3s} \\ a_{3c} \\ a_{4s} \end{Bmatrix} = \begin{Bmatrix} 0 \\ 0 \\ 1 \\ 0 \\ 0 \\ 0 \\ 0 \\ 0 \end{Bmatrix}$$

It should be noted that the matrix is symmetric and also that the sine and cosine terms are not coupled to one another, thereby allowing the equations to be rewritten as follows:

$$\begin{bmatrix} A/2 & B/2 & & & & & & \\ B/2 & (A-1) & B/2 & & & & & \\ & B/2 & (A-4) & B/2 & & & & \\ & & B/2 & (A-9) & & & & \\ & & & & (A-1) & B/2 & & \\ & & & & B/2 & (A-4) & B/2 & \\ & & & & & B/2 & (A-9) & B/2 \\ & & & & & & B/2 & (A-16) \end{bmatrix} \begin{Bmatrix} 2a_o \\ a_{1c} \\ a_{2c} \\ a_{3c} \\ a_{1s} \\ a_{2s} \\ a_{3s} \\ a_{4s} \end{Bmatrix} = \begin{Bmatrix} 0 \\ 1 \\ 0 \\ 0 \\ 0 \\ 0 \\ 0 \\ 0 \end{Bmatrix}$$

In this particular case a_{1s}, a_{2s}, a_{3s}, a_{4s} ..... = 0. But of more importance the harmonic sines and cosines may be solved for separately. This is a consequence of the absence of velocity dependent terms and does not occur in general.

A property that does generally occur for the helicopter equations, however, is the fact that the forcing functions occur only in the first harmonic. In the case at hand the forcing functions exist only in the first two rows,

i.e., for the mean value and first harmonic. The equations of the higher frequency components are not forced; so high frequency coefficients may be solved for algebraically in terms of low frequency coefficients, so that ultimately the high frequency coefficients may be expressed solely in terms of the two forced coefficients. Choosing the set of equations to the third harmonic allows the property to be illustrated, as follows:

$$\begin{bmatrix} A/2 & B/2 & & \\ B/2 & (A-1) & B/2 & \\ & B/2 & (A-4) & B/2 \\ & & B/2 & (A-9) \end{bmatrix} \begin{Bmatrix} 2a_o \\ a_{1c} \\ a_{2c} \\ a_{3c} \end{Bmatrix} = \begin{Bmatrix} 0 \\ 1 \\ 0 \\ 0 \end{Bmatrix}$$

Eliminate a_{3c} and a_{2c} from the equation as follows:

$$[B/2]\, a_{2c} + [A-9]\, a_{3c} \approx 0$$

if $a_{4c} \approx 0$ (if a_{4c} is neglegible)

$$\therefore \quad a_{3c} = - [A-9]^{-1} [B/2]\, a_{2c}$$

and

$$[B/2]\, a_{1c} + [A-4]\, a_{2c} + [B/2]\, a_{3c} = 0$$

$$[B/2]\, a_{1c} + \left[[A-4] - [B/2][A-9]^{-1} [B/2]\right] a_{2c} = 0$$

$$a_{2c} = - \left[[A-4] - [B/2][A-9]^{-1} [B/2]\right]^{-1} [B/2]\, a_{1c}$$

The equations may then be reduced to two unknowns:

$$\begin{bmatrix} A/2 & B/2 \\ B/2 & \left[[A-1] - [B/2]\left[[A-4] - [B/2][A-9]^{-1}[B/2]\right]^{-1}[B/2]\right] \end{bmatrix} \begin{Bmatrix} 2a_o \\ a_{1c} \end{Bmatrix} = \begin{Bmatrix} 0 \\ 1 \end{Bmatrix}$$

It is interesting to inspect the detailed structure of the (2,2) element

$$\left[[A-1] - [B/2]\left[[A-4] - [B/2][A-9]^{-1}[B/2]\right]^{-1}[B/2]\right]$$

It may be expanded to any number of harmonics "n" by analytic continuation and takes up the general form:

$$\Big[[A-1] - [B/2]\Big[[A-4] - [B/2]\Big[[A-9] \quad \ldots\ldots\ldots\ldots\ldots\ldots\ldots$$
$$\ldots - [B/2]\Big[\big[A - (n-1)^2\big] - [B/2]\big[A-n^2_{\text{cutoff}}\big]^{-1}[B/2]\Big]^{-1}[B/2]\ldots$$
$$\ldots\ldots\ldots\Big]^{-1}[B/2]\Big]^{-1}[B/2]\Big]$$

The value of the (2,2) element converges very rapidly as additional harmonics are included. Generally speaking three or four harmonics give adequate accuracy to the mean and first harmonic term and sometimes to the second. As an example, solve for the harmonic coefficients of

$$\ddot{w} + (A + B \cos t)\ w = \cos t$$

for $A = 2.0, \quad B = 1.0$

First evaluate the (2,2) element with two, three, and then four harmonics at cutoff.

Number of Harmonics Considered	Value of (2,2) Element
2	1.125
3	1.1272
4	1.12727

The equations to solve become a 2 by 2 matrix system as follows:

$$\begin{bmatrix} A/2 & B/2 \\ B/2 & (2,2) \end{bmatrix} \begin{Bmatrix} 2a_o \\ a_{1c} \end{Bmatrix} = \begin{Bmatrix} 0 \\ 1 \end{Bmatrix}$$

and $a_o = -.285$

$a_{1c} = 1.14$

With the mean and first harmonic known, the expanded set of equations may be employed to determine the next few higher harmonics approaching the n cutoff limit, but of course not exceeding it.

$$a_{2c} = .2906$$

$$a_{3c} = .0228$$

The solution of the forced oscillation of the equation then becomes

$$w = -.285 + 1.14 \cos t + .29 \cos 2t + .023 \cos 3t \ldots\ldots\ldots\ldots$$

and is shown in Figure 13.

It is interesting to note that even though no mean force exists a mean displacement of the response occurs. Physically speaking, this is a consequence of the negative excursion of the sinusoidal force acting on a reduced value of stiffness.

This process is important in explaining the large effects on the mean aeroelastic derivatives of including the harmonic coefficients in the vertical motions differential equations at advance ratios greater than unity.

Why there is no subharmonic response. - In postulating a form for the forced response of the system with periodic coefficients the foregoing discussion has shown how the higher harmonic coefficients of the response are coupled together so that, in fact, an infinite series of harmonics exists.

It is logical to consider whether the system does respond also in a subharmonic fashion. This question is answered in a straightforward way. Assume the series to contain subharmonic terms in addition to the superharmonic so that it appears as follows:

$$w = \ldots\ldots a_{\frac{1}{2}s} \sin \tfrac{1}{2}t + a_{\frac{1}{2}c} \cos \tfrac{1}{2}t + a_o + a_{1s} \sin t + a_{1c} \cos t + \ldots\ldots$$

$$\dot{w} = \ldots\ldots \tfrac{1}{2} a_{s/2} \cos t/2 - \tfrac{1}{2} a_{c/2} \sin t/2 + 0 + a_{1s} \cos t - a_{1c} \sin t + \ldots$$

$$\ddot{w} = \ldots -\tfrac{1}{4} a_{s/2} \sin t/2 - \tfrac{1}{4} a_{c/2} \cos t/2 + 0 - a_{1s} \sin t - a_{1c} \cos t + \ldots$$

Substituting displacements, velocities, and accelerations in the differential equations adds the subharmonics to the existing terms. They become:

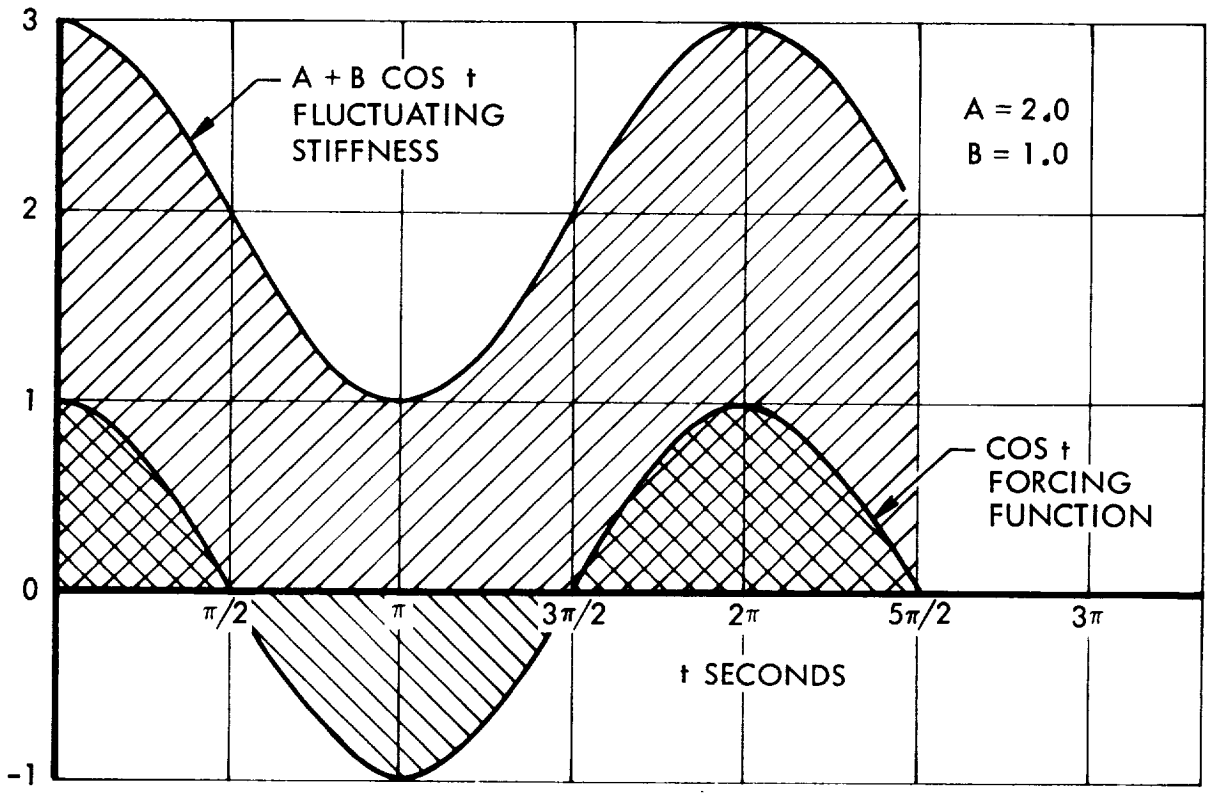

$$\ddot{W} + (A + B \cos t) W = \cos t$$

$$W = -.285 + 1.14 \cos t + .29 \cos 2t + .023 \cos 3t$$

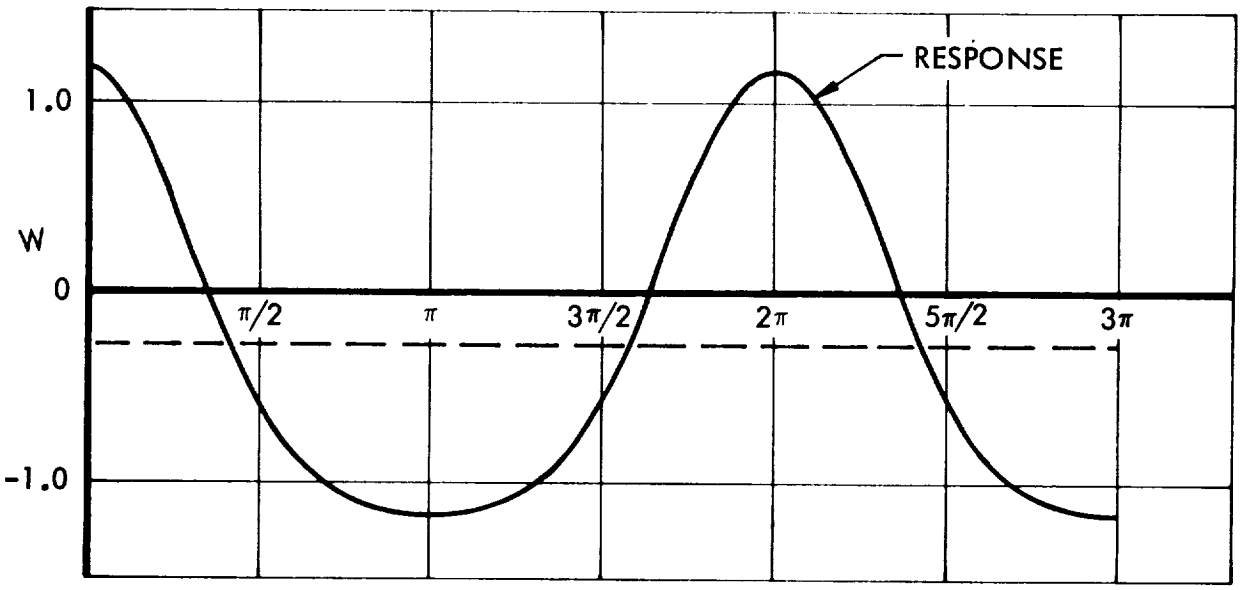

Figure 13. Steady Oscillatory Response of a Forced System With Periodic Stiffness

$$.... - \tfrac{1}{[\,]}\, a_{s/2} \sin t/2 - \tfrac{1}{[\,]}\, a_{c/2} \cos t/2 ....$$

$$.... A\, a_{s/2} \sin t/2 + A\, a_{c/2} \cos t/2 ....$$

$$.... B\, a_{s/2} \cos t \sin t/2 + B\, a_{c/2} \cos t \cos t/2 ....$$

and expanded they are as follows:

$$.... - \tfrac{1}{[\,]}\, a_{s/2} \sin t/2 - \tfrac{1}{[\,]}\, a_{c/2} \cos t/2 ....$$

$$.... + A\, a_{s/2} \sin t/2 + A\, a_{c/2} \cos t/2 ....$$

$$.... + B\, a_{s/2} \left(\tfrac{1}{2} \sin 1.5t - \tfrac{1}{2} \sin t/2\right)$$

$$+ B\, a_{c/2} \left(\tfrac{1}{2} \cos 1.5t + \tfrac{1}{2} \cos t/2\right) ....$$

With all terms assembled together, the matrix becomes:

$$\left[\begin{array}{cccccc|cc}
A/2 & 0 & B/2 & 0 & . & . & & \\
0 & (A-1) & 0 & B/2 & . & . & & \\
B/2 & 0 & (A-1) & 0 & . & . & & \\
0 & B/2 & 0 & (A-4) & . & . & & \\
. & . & . & . & . & . & & \\
. & . & . & . & . & . & & \\
\hline
 & & & & & & \left(A-\frac{1}{4}-\frac{B}{2}\right) & 0 \quad . \; . \\
 & & & & & & 0 & \left(A-\frac{1}{4}+\frac{B}{2}\right) \quad . \; . \\
 & & & & & & . & . \quad . \; .
\end{array}\right]
\left\{\begin{array}{c} 2a_o \\ a_{1s} \\ a_{1c} \\ a_{2s} \\ . \\ . \\ \hline a_{s/2} \\ a_{c/2} \\ . \end{array}\right\}
=
\left\{\begin{array}{c} 0 \\ 0 \\ 1 \\ 0 \\ 0 \\ 0 \\ \hline 0 \\ 0 \\ 0 \end{array}\right\}$$

It is evident that the subharmonics are not coupled to the superharmonics in any way. They could only be excited by being forced separately, and in this problem that subharmonic forcing is absent.

It may be concluded that a linear system forced at the period of its differential equation periodic coefficients possesses superharmonic response by no subharmonic.

It should be noted that the real system may not be strictly linear, and in that case, subharmonic response is a distinct possibility.

Three- and Four-Blade Rotors

The basic method developed in the general discussion will now be applied to rotors having three and four blades. The solutions will be similar except for the inclusion of the rotor reactionless mode in the four-blade solution. This mode, of course, does not exist for a three-blade rotor. The method that follows will be developed primarily with a four-blade rotor in mind, but may be adapted to the three-blade rotor simply by dropping the matrix rows and columns associated with the reactionless mode and converting the 4P terms to 3P.

The nine degree-of-freedom equations in stationary coordinates are as follows:

$$[I]\{\ddot{\beta}\} + \left[[D] + [A_{\dot{\beta}}]\right]\{\dot{\beta}\} + \left[[S] + [A_{\beta}]\right]\{\beta\} = \left[[CF] + [A_F]\right]\{\eta_F\} + \{M\} \quad (1)$$

where the matrices contain the following terms:

$[I]$	inertia
$[D]$	mechanical damping and gyroscopic
$[A_{\beta}]$	aerodynamic stiffness derivatives
$[S]$	structural stiffness
$[A_{\dot{\beta}}]$	aerodynamic damping derivatives
$[CF]$	contains a centrifugal collective flapping force term due to rotor precone
$[A_F]$	aerodynamic derivatives due to fixed angles and blade geometry
$\{M\}$	forces and moments applied to rotor and gyro

In addition to mean values, the aerodynamic derivatives contain terms which are functions of $b\Omega t$, $2b\,\Omega t$, ..., $Nb\Omega t$, where b equals the number of blades. The derivatives that are functions of $2b\Omega t$, ..., $Nb\Omega t$ will be neglected, since their values are small compared with those of the mean and the b per rev harmonic terms.

The four-bladed rotor derivatives also have 2P, 6P, ..., (2 + 4N)P harmonic terms. Those higher than 6P will be neglected as they are relatively small.

Expanding the aerodynamic derivatives in terms of their harmonics while combining structural and mean aerodynamic terms, equation (1) becomes:

$$[I]\{\ddot{\beta}\} + \Big[[E_o] + [E_{2c}]\cos 2\Omega t + [E_{2s}]\sin 2\Omega t + [E_{4c}]\cos 4\Omega t + [E_{4s}]\sin 4\Omega t + [E_{6c}]\cos 6\Omega t + [E_{6s}]\sin 6\Omega t\Big]\{\dot{\beta}\} + \Big[[F_o] + [F_{2c}]\cos 2\Omega t + [F_{2s}]\sin 2\Omega t + [F_{4c}]\cos 4\Omega t + [F_{4s}]\sin 4\Omega t + [F_{6c}]\cos 6\Omega t + [F_{6s}]\sin 6\Omega t\Big]\{\beta\} = \Big[[G_o] + [G_{2c}]\cos 2\Omega t + [G_{2s}]\sin 2\Omega t + [G_{4c}]\cos 4\Omega t + [G_{4s}]\sin 4\Omega t + [G_{6c}]\cos 6\Omega t + [G_{6s}]\sin 6\Omega t\Big]\{\eta_F\} + \{M\} \qquad (2)$$

(For three blades, equation (2) would contain only mean and 3P terms.)

Equation (2) must be solved for β, which is a function of time. Let β be represented by a Fourier series:

$$\beta = \beta_o + \beta_{2c}\cos 2\Omega t + \beta_{2s}\sin 2\Omega t + \beta_{4c}\cos 4\Omega t + \beta_{4s}\sin 4\Omega t + \beta_{6c}\cos 6\Omega t + \beta_{6s}\sin 6\Omega t + \beta_{8c}\cos 8\Omega t + \beta_{8s}\sin 8\Omega t + \beta_{10c}\cos 10\Omega t + \beta_{10s}\sin 10\Omega t + \ldots$$

The series will be truncated at the 14P term. Coefficients of the higher harmonics will be negligible.

Equation (2) will be solved according to whether the swashplate is fixed or free and the vehicle is free flying or has its shaft fixed.

Fixed-shaft, fixed-swashplate solution. - The vector of displacements is as follows:

$$\{\beta\} = \begin{Bmatrix} \Theta \\ \Phi \\ z \\ \theta \\ \phi \\ \delta_o \\ \delta_\theta \\ \delta_\phi \\ \delta_d \end{Bmatrix}$$

where δ_d is the differential collective mode (also known as the reactionless or the self-balancing mode).

For the fixed-shaft fixed-swashplate solution:

$$\ddot{\Theta} = \dot{\Theta} = \Theta = 0$$

$$\ddot{\Phi} = \dot{\Phi} = \Phi = 0$$

$$\ddot{z} = \dot{z} = z = 0$$

$$\ddot{\theta} = \dot{\theta} = 0$$

$$\ddot{\phi} = \dot{\phi} = 0$$

θ and ϕ may take steady nonoscillating specified values. The body degrees of freedom are locked out of the equations. Thus the solution becomes applicable to a vehicle rigidly mounted in a wind tunnel and controlled by displacement inputs to the swashplate.

The displacement vector $\{\beta\}$ may be divided into upper and lower portions:

$$\{\beta\} = \begin{Bmatrix} \Theta \\ \Phi \\ z \\ \theta \\ \phi \\ \hline \delta_o \\ \delta_\theta \\ \delta_\phi \\ \delta_d \end{Bmatrix} = \begin{Bmatrix} \beta_u \\ \hline \beta_\ell \end{Bmatrix}$$

where the given value of $\{\beta_u\}$ is:

$$\{\beta_u\} = \begin{Bmatrix} 0 \\ 0 \\ 0 \\ \theta \\ \phi \end{Bmatrix}$$

It is required to solve for the displacement vector $\{\beta_\ell\}$. However $\{\beta_\ell\}$ is complicated by the reactionless mode. Its coefficients in the differential equations include 2P and 6P components as well as the 0 and 4P expected for the four-blade rotor. But since it is to be a steady oscillatory response, each blade in turn must execute identically the same motion as the blade ahead of it. It is clear, therefore, that hub moments, thrust, swashplate moments,-in fact all data measured relative to the stationary axes-must contain only 0, 4P, 8P, etc, harmonics. This means that the reactionless mode must exercise vigorous 2P, 6P, etc, motion in rotating axes to attain a stationary blade pattern in stationary axes. It should be possible, therefore, in stationary axes, to represent the modal motions selectively as follows rather than to employ all harmonics of all terms simultaneously. Let

$$\{\beta_\ell\} = \begin{Bmatrix} \delta_o \\ \delta_\theta \\ \delta_\phi \\ \hline \delta_d \end{Bmatrix} = \begin{Bmatrix} \beta_{\ell_u} \\ \hline \delta_d \end{Bmatrix}$$

where

$$\{\beta_{\ell_u}\} = \{\delta_u\} = \{\delta_{u_o}\} + \{\delta_{u4c}\} \cos 4\Omega t + \{\delta_{u4s}\} \sin 4\Omega t$$

$$+ \{\delta_{u8c}\} \cos 8\Omega t + \{\delta_{u8s}\} \sin 8\Omega t + \ldots.$$

and

$$\{\delta_d\} = \{\delta_{d2c}\} \cos 2\Omega t + \{\delta_{d2s}\} \sin 2\Omega t + \{\delta_{d6c}\} \cos 6\Omega t$$

$$+ \{\delta_{d6s}\} \sin 6\Omega t + \ldots.$$

By similar reasoning, the last column and bottom rows of the $[A_\beta]$ and $[A_{\dot{\beta}}]$ matrices of equation (1) will contain only 2P and 6P terms of significance (except for the on-diagonal term, which will contain only mean, 4P, and 8P terms of significance). The bottom row of $[A_F]$ in equation (1) will also contain only 2P and 6P terms of importance.

Recalling that

$$\begin{Bmatrix} \Theta \\ \Phi \\ z \\ \theta \\ \phi \\ \hline \delta_o \\ \delta_\theta \\ \delta_\phi \\ \hline \delta_d \end{Bmatrix} = \begin{Bmatrix} \beta_u \\ \hline \delta_u \\ \hline \delta_d \end{Bmatrix}$$

equation (2) may now be rewritten in partitioned form:

$$\begin{bmatrix} I_{11} & I_{12} & I_{13} \\ I_{21} & I_{22} & I_{23} \\ I_{31} & I_{32} & I_{33} \end{bmatrix} \begin{Bmatrix} \ddot{\beta}_u \\ \ddot{\delta}_u \\ \ddot{\delta}_d \end{Bmatrix} + \begin{bmatrix} E_{11} & E_{12} & E_{13} \\ E_{21} & E_{22} & E_{23} \\ E_{31} & E_{32} & E_{33} \end{bmatrix} \begin{Bmatrix} \dot{\beta}_u \\ \dot{\delta}_u \\ \dot{\delta}_d \end{Bmatrix} + \begin{bmatrix} F_{11} & F_{12} & F_{13} \\ F_{21} & F_{22} & F_{23} \\ F_{31} & F_{32} & F_{33} \end{bmatrix} \begin{Bmatrix} \beta_u \\ \delta_u \\ \delta_d \end{Bmatrix}$$

$$= \begin{bmatrix} G_1 \\ G_2 \\ G_3 \end{bmatrix} \{\eta_F\} + \begin{Bmatrix} M_1 \\ M_2 \\ 0 \end{Bmatrix} \qquad (3)$$

The shaded areas contain 2P and 6P and 10P, ... only, all the rest contain 0, 4P, 8P, ...

This is permissible because $I_{13} = I_{31} = I_{23} = I_{32} = 0$ and the products of (2P, 6P ....) x (2P, 6P ....) = 0, 4P, 8P, 12P ....
(2P, 6P ....) x (0, 4P ....) = 2P, 6P, 10P .... For the present solution, the equations simplify to

$$\begin{bmatrix} I_{11} & I_{12} & 0 \\ I_{21} & I_{22} & 0 \\ 0 & 0 & I_{33} \end{bmatrix} \begin{Bmatrix} \ddot{\beta}_u \\ \ddot{\delta}_u \\ \ddot{\delta}_d \end{Bmatrix} + \begin{bmatrix} E_{11} & E_{12} & E_{13} \\ E_{21} & E_{22} & E_{23} \\ E_{31} & E_{32} & E_{33} \end{bmatrix} \begin{Bmatrix} \dot{\beta}_u \\ \dot{\delta}_u \\ \dot{\delta}_d \end{Bmatrix} + \begin{bmatrix} F_{11} & F_{12} & F_{13} \\ F_{21} & F_{22} & F_{23} \\ F_{31} & F_{32} & F_{33} \end{bmatrix} \begin{Bmatrix} \beta_u \\ \delta_u \\ \delta_d \end{Bmatrix}$$

$$= \begin{bmatrix} G_1 \\ G_2 \\ G_3 \end{bmatrix} \{\eta_F\} + \begin{Bmatrix} M_1 \\ M_2 \\ 0 \end{Bmatrix} \qquad (4)$$

Recall that the vector of applied moments in equation (4) is:

$$\{M\} = \begin{Bmatrix} M \\ L \\ T \\ M_\theta \\ M_\phi \end{Bmatrix}$$

$\{M\}$ may be redefined to represent reaction loads (aeroelastic response loads). Thus the vector may be moved to the left-hand side of equation (4) with no change in sign. Additionally, by moving the terms involving the input vector $\{\beta_u\}$ to the right-hand side, equation (4) may be rewritten:

$$\begin{Bmatrix} M \\ 0 \\ 0 \end{Bmatrix} + \begin{bmatrix} I_{12} & 0 \\ I_{22} & 0 \\ 0 & I_{33} \end{bmatrix} \begin{Bmatrix} \ddot{\delta}_u \\ \ddot{\delta}_d \end{Bmatrix} + \begin{bmatrix} E_{12} & E_{13} \\ E_{22} & E_{23} \\ E_{32} & E_{33} \end{bmatrix} \begin{Bmatrix} \dot{\delta}_u \\ \dot{\delta}_d \end{Bmatrix} + \begin{bmatrix} F_{12} & F_{13} \\ F_{22} & F_{23} \\ F_{32} & F_{33} \end{bmatrix} \begin{Bmatrix} \delta_u \\ \delta_d \end{Bmatrix} = \begin{bmatrix} G_1 \\ G_2 \\ G_3 \end{bmatrix} \{\eta_F\} - \begin{bmatrix} F_{11} \\ F_{21} \\ F_{31} \end{bmatrix} \{\beta_u\} \quad (5)$$

Equation (5) may be separated into uncoupled upper and lower halves.

The lower half may be written:

$$\begin{bmatrix} I_{22} & 0 \\ 0 & I_{33} \end{bmatrix} \begin{Bmatrix} \ddot{\delta}_u \\ \ddot{\delta}_d \end{Bmatrix} + \begin{bmatrix} E_{22} & E_{23} \\ E_{32} & E_{33} \end{bmatrix} \begin{Bmatrix} \dot{\delta}_u \\ \dot{\delta}_d \end{Bmatrix} + \begin{bmatrix} F_{22} & F_{23} \\ F_{32} & F_{33} \end{bmatrix} \begin{Bmatrix} \delta_u \\ \delta_d \end{Bmatrix} = \begin{bmatrix} G_2 \\ G_3 \end{bmatrix} \{\eta_F\} - \begin{bmatrix} F_{21} \\ F_{31} \end{bmatrix} \{\beta_u\} \quad (6)$$

This equation is the basis for determining the displacement vectors. Once they are known, the aeroelastic response loads can be found from the upper half of equation (5), which is as follows:

$$\{M\} = -[I_{12}]\{\ddot{\delta}_u\} - \begin{bmatrix} E_{12} & E_{13} \end{bmatrix} \begin{Bmatrix} \delta_u \\ \delta_d \end{Bmatrix} - \begin{bmatrix} F_{12} & F_{13} \end{bmatrix} \begin{Bmatrix} \delta_u \\ \delta_d \end{Bmatrix} + [G_1]\{\eta_F\} - [F_{11}]\{\beta_u\} \quad (7)$$

where the complete right-hand side of the equation is known.

Solution of forced equations of motion: - The problem now is to solve for δ_u and δ_d, starting with equation (6).

$$\delta_u = (\delta_u)_o + \delta_{u_{4c}} \cos 4\Omega t + \delta_{u_{4s}} \sin 4\Omega t + \delta_{u_{8c}} \cos 8\Omega t + \delta_{u_{8s}} \sin 8\Omega t +$$

$$\delta_d = \delta_{d_{2c}} \cos 2\Omega t + \delta_{d_{2s}} \sin 2\Omega t + \delta_{d_{6c}} \cos 6\Omega t + \delta_{d_{6s}} \sin 6\Omega t + \ldots$$

The procedure is tedious but straightforward to solve for the values of the coefficients of the series. Each matrix is expanded in its respective harmonic parts. The series representing the solution is also expanded and products of matrices and solutions are found and all terms of common frequency and phase combined and a truncated solution found. This is shown in detail in the following paragraphs.

First, abbreviate the notation for clarity:

Let

$2\Omega t = t^1$

$2\Omega = \Omega^1$

and

$\delta_u = \beta$

$\delta_d = \delta$

subcripts

$c^1 = 2c$

$s^1 = 2s$

Therefore,

$$\beta = \beta_o + \beta_{2c}1 \cos 2t^1 + \beta_{2s}1 \sin 2t^1 + \beta_{4c}1 \cos 4t^1 + \beta_{4s}1 \sin 4t^1 + \ldots$$

$$\delta = \delta_{1c}1 \cos t^1 + \delta_{1s}1 \sin t^1 + \delta_{3c}1 \cos 3t^1 + \delta_{3s}1 \sin 3t^1 + \ldots$$

and let the matrices be abbreviated.

$E_{22} = M$ $\quad$ $F_{22} = R$

$E_{23} = N$ $\quad$ $F_{23} = S$

$E_{32} = P$ $\quad$ $F_{32} = T$

$E_{33} = Q$ $\quad$ $F_{33} = U$

$$[G_2 \,\vdots\, -F_{21}] = V$$

$$[G_3 \,\vdots\, -F_{31}] = W$$

Then equation (6) becomes:

$$\begin{bmatrix} I_{22} & 0 \\ 0 & I_{33} \end{bmatrix} \begin{Bmatrix} \ddot{\beta} \\ \ddot{\delta} \end{Bmatrix} + \begin{bmatrix} M & N \\ P & Q \end{bmatrix} \begin{Bmatrix} \dot{\beta} \\ \dot{\delta} \end{Bmatrix} + \begin{bmatrix} R & S \\ T & U \end{bmatrix} \begin{Bmatrix} \beta \\ \delta \end{Bmatrix} = \begin{bmatrix} V \\ W \end{bmatrix} \begin{Bmatrix} \eta_F \\ \beta_u \end{Bmatrix} \tag{8}$$

The two components of the vectors and their derivatives are as follows:

$$\ddot{\beta} = \beta_o + \beta_{2c}1 \cdot \cos 2t^1 + \beta_{2s}1 \sin 2t^1 + \beta_{4c}1 \cos 4t^1 + \beta_{4s}1 \sin 4t^1 \ldots$$

$$\dot{\beta} = -2\Omega^1\beta_{2c}1 \sin 2t^1 + 2\Omega^1\beta_{2s}1 \cos 2t^1 - 4\Omega^1\beta_{4c}1 \sin 4t^1 + 4\Omega^1\beta_{4s}1 \sin 4t^1$$

$$\beta = -4\Omega^{1^2}\beta_{2c}1 \cos 2t^1 - 4\Omega^{1^2}\beta_{2s}1 \sin 2t^1 - 16\Omega^{1^4}\beta_{4c}1 \cos 4t^1 \ldots$$

$$- 16\Omega^{1^2}\beta_{4s}1 \sin 4t$$

$$\delta = \delta_{1c}1 \cos t^1 + \delta_{1s}1 \sin t^1 + \delta_{3c}1 \cos 3t^1 + \delta_{3s}1 \sin 3t^1 \ldots$$

$$\dot{\delta} = -\Omega^1\delta_{1c}1 \sin t^1 + \Omega^1\delta_{1s}1 \cos t^1 - 3\Omega^1\delta_{3c}1 \sin 3t^1 + 3\Omega^1\delta_{3s}1 \cos 3t^1$$

$$\ddot{\delta} = -\Omega^{1^2}\delta_{1c} \cos t^1 \ \Omega^{1^2}\delta_{1s}1 \sin t^1 - 9\Omega^{1^2}\delta_{3c}1 \cos 3t^1 - 9\Omega^{1^2}\delta_{3s}1 \sin 3t^1$$

and the matrices become

$$M = M_o + M_{2c}1 \cos 2t^1 + M_{2s}1 \sin 2t^1$$

$$N = N_{1c}1 \cos t^1 + N_{1s}1 \sin t^1 + N_{3c}1 \cos 3t^1 + N_{3s}1 \sin 3t^1$$

$$P = P_{1c}1 \cos t^1 + P_{1s}1 \sin t^1 + P_{3c}1 \cos 3t^1 + P_{3s} \sin 3t^1$$

$$Q = Q_o + Q_{2c}1 \cos 2t^1 + Q_{2s}1 \sin 2t^1$$

For the R, U equations, substitute R, U for M, Q

For the S, T equations, substitute S, T for N, P

The work becomes two matrix equations in the two unknown vectors, β, δ when expanded, in their harmonic components.

Treating the β-Force equation first, matrix by matrix, yields the following expansion from equation (8):

$$
\begin{aligned}
&-4\Omega^{1^2} I_{22}\beta_{2c}1 \cos 2t^1 - 4\Omega^{1^2} I_{22}\beta_{2s}1 \sin 2t^1 - 16\Omega^{1^2} I_{22}\beta_{4c}1 \cos 4t^1 \\
&\qquad - 16\Omega^{1^2} I_{22}\beta_{4s}1 \sin 4t^1 \ldots. \\
&+ \left[M_o + M_{2c}1 \cos 2t^1 + M_{2s}1 \sin 2t^1\right] \left\{-2\Omega^1\beta_{2c}1 \sin 2t^1 + 2\Omega^1\beta_{2s}1 \cos 2t^1 \right. \\
&\qquad \left. -4\Omega^1\beta_{4c}1 \sin 4t^1 + 4\Omega^1\beta_{4s}1 \cos 4t^1 \ldots.\right\} \\
&+ \left[N_{1c}1 \cos t^1 + N_{1s}1 \sin t^1 + N_{3c}1 \cos 3t^1 + N_{3s}1 \sin 3t^1\right] \left\{-\Omega^1\delta_{1c}1 \sin t^1 \right. \\
&\quad \left. + \Omega^1\delta_{1s}1 \cos t^1 - 3\Omega^1\delta_{3c}1 \sin 3t^1 + 3\Omega^1\delta_{3s}1 \cos 3t^1 + \ldots.\right\} \\
&+ \left[R_o + R_{2c}1 \cos 2t^1 + R_{2s}1 \sin 2t^1\right] \left\{\beta_o + \beta_{2c}1 \cos 2t^1 + \beta_{2s}1 \sin 2t^1 \right. \\
&\qquad \left. + \beta_{4c}1 \cos 4t^1 + \beta_{4s}1 \sin 4t^1 + \ldots.\right\} \\
&+ \left[S_{1c}1 \cos t^1 + S_{1s}1 \sin t^1 + S_{3c}1 \cos 3t^1 + S_{3s}1 \sin 3t^1\right] \left\{\delta_{1c}1 \cos t^1 \right. \\
&\quad \left. + \delta_{1s}1 \sin t^1 + \delta_{3c}1 \cos 3t^1 + \delta_{3s}1 \sin 3t^1 + \ldots.\right\} \\
&= \left[V_o + V_{2c}1 \cos 2t^1 + V_{2s}1 \sin 2t^1\right] \begin{Bmatrix} \theta_o \\ \dot{z} \\ \theta \\ \phi \end{Bmatrix} \qquad (9)
\end{aligned}
$$

Treating the δ-Force equations yields, by expanding equation (8):

$$
\begin{aligned}
&I_{33}\left(\Omega^{1^2}\delta_{1c}1 \cos t^1 - \Omega^{1^2}\delta_{1s}1 \sin t^1 - 9\Omega^{1^2}\delta_{3c}1 \cos 3t^1 - 9\Omega^{1^2}\delta_{3s}1 \sin 3t^1\right) \\
&+ \left(P_{1c}1 \cos t^1 + P_{1s}1 \sin t^1 + P_{3c}1 \cos 3t^1 + P_{3s}1 \sin 3t^1\right)\left(-2\Omega^1\beta_{2c} \sin 2t^1\right. \\
&\left. + 2\Omega^1\beta_{2s}1 \cos 2t^1 - 4\Omega^1\beta_{4c}1 \sin 4t^1 + 4\Omega^1\beta_{4s}1 \cos 4t^1 \ldots..\right) \\
&+ \left(Q_o + Q_{2c}1 \cos 2t^1 + Q_{2s}1 \sin 2t^1\right)\left(-\Omega^1\delta_{1c}1 \sin t^1 + \Omega^1\delta_{1s}1 \cos t^1\right. \\
&\left. - 3\Omega^1\delta_{3c}1 \sin 3t^1 + 3\Omega^1\delta_{3s}1 \cos 3t^1 \ldots.\right)
\end{aligned}
$$

$$+ \left(T_{1c}{}^{1} \cos t^{1} + T_{1s}{}^{1} \sin t^{1} + T_{3c}{}^{1} \cos 3t^{1} + T_{3s}{}^{1} \sin 3t^{1}\right) \left(\beta_{o} + \beta_{2c}{}^{1} \cos 2t^{1} + \beta_{2s}{}^{1} \sin 2t^{1} + \beta_{4c}{}^{1} \cos 4t^{1} + \beta_{4s}{}^{1} \sin 4t^{1} \ldots.\right)$$

$$+ \left(J_{o} + U_{2c}{}^{1} \cos 2t^{1} + U_{2s}{}^{1} \sin 2t^{1}\right) \left(\delta_{1c}{}^{1} \cos t^{1} + \delta_{1s}{}^{1} \sin t^{1} + \delta_{3c}{}^{1} \cos 3t^{1} + \delta_{3s}{}^{1} \sin 3t^{1} \ldots\right)$$

$$= \left[W_{1c}{}^{1} \cos t^{1} + W_{1s}{}^{1} \sin t^{1} + W_{3c}{}^{1} \cos 3t^{1} + W_{3s}{}^{1} \sin 3t^{1}\right] \begin{Bmatrix} \theta_{o} \\ \dot{z} \\ \theta \\ \phi \end{Bmatrix} \qquad (10)$$

Expanding the terms of the β-force and δ-force equations and employing trigonometric identities to reduce all terms to harmonic sines and cosines of the first degree allows a set of simultaneous equations relating the coefficients of the Fourier series to be assembled. Each equation of the set contains terms of one harmonic component only. Dividing each equation by its harmonic yields a set which can be truncated and solved for the coefficients, algebraically.

The set of equations may be written in the following order. In all following work the Fourier series is truncated at 14P. This allows the vectors to be described in terms of the following harmonics:

β: β_{o}, β_{2c}, β_{2s}, β_{4c}, β_{4s}, β_{6c}, β_{6s}

δ: δ_{1c}, δ_{1s}, δ_{3c}, δ_{3s}, δ_{5c}, δ_{5s}, δ_{7c}, δ_{7s}

$$
\begin{bmatrix}
A_{11} & A_{12} & A_{13} & A_{14} & A_{15} & A_{16} & A_{17} & 0 & 0 & 0 & 0 & 0 & 0 \\
A_{21} & A_{22} & A_{23} & A_{24} & A_{25} & A_{26} & A_{27} & A_{28} & A_{29} & 0 & 0 & 0 & 0 \\
A_{31} & A_{32} & A_{33} & A_{34} & A_{35} & A_{36} & A_{37} & A_{38} & A_{39} & 0 & 0 & 0 & 0 \\
A_{41} & A_{42} & A_{43} & A_{44} & A_{45} & A_{46} & A_{47} & A_{48} & A_{49} & A_{4,10} & A_{4,11} & 0 & 0 \\
A_{51} & A_{52} & A_{53} & A_{54} & A_{55} & A_{56} & A_{57} & A_{58} & A_{59} & A_{5,10} & A_{5,11} & 0 & 0 \\
A_{61} & A_{62} & A_{63} & A_{64} & A_{65} & A_{66} & A_{67} & A_{68} & A_{69} & A_{6,10} & A_{6,11} & A_{6,12} & A_{6,13} \\
A_{71} & A_{72} & A_{73} & A_{74} & A_{75} & A_{76} & A_{77} & A_{78} & A_{79} & A_{7,10} & A_{7,11} & A_{7,12} & A_{7,13} \\
0 & A_{82} & A_{83} & A_{84} & A_{85} & A_{86} & A_{87} & A_{88} & A_{89} & A_{8,10} & A_{8,11} & A_{8,12} & A_{8,13} \\
0 & A_{92} & A_{93} & A_{94} & A_{95} & A_{96} & A_{97} & A_{98} & A_{99} & A_{9,10} & A_{9,11} & A_{9,12} & A_{9,13} \\
0 & 0 & 0 & A_{10,4} & A_{10,5} & A_{10,6} & A_{10,7} & A_{10,8} & A_{10,9} & A_{10,10} & A_{10,11} & A_{10,12} & A_{10,13} \\
0 & 0 & 0 & A_{11,4} & A_{11,5} & A_{11,6} & A_{11,7} & A_{11,8} & A_{11,9} & A_{11,10} & A_{11,11} & A_{11,12} & A_{11,13} \\
0 & 0 & 0 & 0 & 0 & A_{12,6} & A_{12,7} & A_{12,8} & A_{12,9} & A_{12,10} & A_{12,11} & A_{12,12} & A_{12,13} \\
0 & 0 & 0 & 0 & 0 & A_{13,6} & A_{13,7} & A_{13,8} & A_{13,9} & A_{13,10} & A_{13,11} & A_{13,12} & A_{13,13} \\
0 & 0 & 0 & 0 & 0 & 0 & 0 & A_{14,8} & A_{14,9} & A_{14,10} & A_{14,11} & A_{14,12} & A_{14,13} \\
0 & 0 & 0 & 0 & 0 & 0 & 0 & A_{15,8} & A_{15,9} & A_{15,10} & A_{15,11} & A_{15,12} & A_{15,13}
\end{bmatrix}
\begin{Bmatrix} \xi_o \\ \xi_{1c}^1 \\ \xi_{1s}^1 \\ \xi_{2c}^1 \\ \xi_{2s}^1 \\ \xi_{3c}^1 \\ \xi_{3s}^1 \\ \xi_{4c}^1 \\ \xi_{4s}^1 \\ \xi_{5c}^1 \\ \xi_{5s}^1 \\ \xi_{6c}^1 \\ \xi_{6s}^1 \\ \xi_{7c}^1 \\ \xi_{7s}^1 \end{Bmatrix}
=
\begin{Bmatrix} V_o \\ W_{1c}^1 \\ W_{1s}^1 \\ V_{2c}^1 \\ V_{2s}^1 \\ W_{3c}^1 \\ W_{3s}^1 \\ 0 \\ 0 \\ 0 \\ 0 \\ 0 \\ 0 \\ 0 \\ 0 \end{Bmatrix}
\tag{11}
$$

Combining some of the A_{ij} matrices yields:

$$\left[\begin{array}{c|ccccccc} A_{11} & B_{12} & B_{13} & B_{14} & 0 & 0 & 0 & 0 \\ \hline B_{21} & B_{22} & B_{23} & B_{24} & B_{25} & 0 & 0 & 0 \\ B_{31} & B_{32} & B_{33} & B_{34} & B_{35} & B_{36} & 0 & 0 \\ B_{41} & B_{42} & B_{43} & B_{44} & B_{45} & B_{46} & B_{47} & 0 \\ 0 & B_{52} & B_{53} & B_{54} & B_{55} & B_{56} & B_{57} & B_{58} \\ 0 & 0 & B_{63} & B_{64} & B_{65} & B_{66} & B_{67} & B_{68} \\ 0 & 0 & 0 & B_{74} & B_{75} & B_{76} & B_{77} & B_{78} \\ 0 & 0 & 0 & 0 & B_{85} & B_{86} & B_{87} & B_{88} \end{array}\right] \left\{\begin{array}{c} (\delta_u)_o \\ (\delta_L)_1 \\ (\delta_u)_2 \\ (\delta_L)_3 \\ (\delta_u)_4 \\ (\delta_L)_5 \\ (\delta_u)_6 \\ (\delta_L)_7 \end{array}\right\} = \left\{\begin{array}{c} (F_u)_o \\ (F_L)_1 \\ (F_u)_2 \\ (F_L)_3 \\ 0 \\ 0 \\ 0 \\ 0 \end{array}\right\} \qquad (12)$$

where

$$\left[B_{22}\right] = \left[\begin{array}{cc} A_{22} & A_{23} \\ A_{32} & A_{33} \end{array}\right] \qquad \text{etc.}$$

$$\left[B_{21}\right] = \left[\begin{array}{c} A_{21} \\ A_{31} \end{array}\right] \qquad \text{etc.}$$

$$\left\{(\delta_L)_1\right\} = \left\{\begin{array}{c} \delta_{1c}{}^1 \\ \delta_{1s}{}^1 \end{array}\right\} \quad ; \quad \left\{(\delta_u)_2\right\} = \left\{\begin{array}{c} \beta_{2c}{}^1 \\ \beta_{2s}{}^1 \end{array}\right\} \qquad \text{etc.}$$

By virtue of the zero forcing functions in the 4, 5, ...equations, the matrix may be reduced even further for calculation of the harmonic response, by eliminating the $(\delta_u)_4$, $(\delta_L)_5$, $(\delta_u)_6$, ... terms in the same fashion as shown for the one degree of freedom example. The reduced matrix then becomes:

$$\begin{bmatrix} A_{11} & B_{12} & B_{13} & B_{14} \\ B_{21} & BC_{22} & BC_{23} & BC_{24} \\ B_{31} & BD_{32} & BD_{33} & BD_{34} \\ B_{41} & BE_{42} & BE_{43} & BE_{44} \end{bmatrix} \begin{Bmatrix} (\delta_u)_o \\ (\delta_L)_1 \\ (\delta_u)_2 \\ (\delta_L)_3 \end{Bmatrix} = \begin{Bmatrix} (F_u)_o \\ (F_L)_1 \\ (F_u)_2 \\ (F_L)_3 \end{Bmatrix} \tag{13}$$

and relationships of the following type allow the calculations of the higher harmonic components:

$$\begin{aligned} (\delta_u)_4 &= C_{52}(\delta_L)_1 + C_{53}(\delta_u)_2 + C_{54}(\delta_L)_3 \\ (\delta_L)_5 &= C_{63}(\delta_u)_2 + C_{64}(\delta_L)_3 + C_{65}(\delta_u)_4 \\ (\delta_u)_6 &= C_{74}(\delta_L)_3 + C_{75}(\delta u)_4 + C_{76}(\delta_L)_5 \\ (\delta_L)_7 &= C_{85}(\delta_u)_4 + C_{86}(\delta_L)_5 + C_{87}(\delta u)_6 \end{aligned} \tag{14}$$

where the BC, BD, BE & C_{ij} are determined from values of A_{ij}.

With the responses of the degrees of freedom found, it is possible then to find the thrust, hub moment and swashplate mean and oscillating forces, blade loads, and blade tip motions.

Hub moments, thrust and swashplate moments: - With the motions of the degrees of freedom known it is possible to calculate the forces and their harmonic components $\{M\}$ from equation (7)

$$\begin{aligned} \{M\} = &-\left[I_{12} \;\vdots\; 0\right] \begin{Bmatrix} \ddot{\delta}_u \\ \ddot{\delta}_L \end{Bmatrix} - \left[E_{12} \;\vdots\; E_{13}\right] \begin{Bmatrix} \dot{\delta} \\ \dot{\delta}_L \end{Bmatrix} \\ &- \left[F_{12} \;\vdots\; F_{13}\right] \begin{Bmatrix} \delta_u \\ \delta_L \end{Bmatrix} - \left[F_{11}\right]\{\beta_\mu\} + \left[G_1\right]\{\eta_F\} \end{aligned} \tag{7}$$

and these equations may be expanded in terms of all harmonic components and as before these may be arranged in order of the harmonics. Grouping according to harmonics the equation takes on the following form:

$$\begin{Bmatrix} M_o \\ M_{4c} \\ M_{4s} \\ M_{8c} \\ M_{8s} \\ M_{12c} \\ M_{12s} \end{Bmatrix} = - \begin{bmatrix} D_{11} & D_{12} & D_{13} & \cdots \\ D_{41} & D_{42} & D_{43} & \cdots \\ D_{51} & D_{52} & D_{53} & \cdots \\ D_{81} & D_{82} & D_{83} & \cdots \\ D_{91} & D_{92} & D_{93} & \cdots \\ D_{12,1} & D_{12,2} & D_{12,3} & \cdots \\ D_{13,1} & D_{13,2} & D_{13,3} & \cdots \end{bmatrix} \begin{Bmatrix} \delta_{u_o} \\ \delta_{L_{2c}} \\ \delta_{L_{2s}} \\ \delta_{u_{4c}} \\ \delta_{u_{4s}} \\ - \\ - \\ \delta_{L_{14c}} \\ \delta_{L_{14s}} \end{Bmatrix} - \begin{bmatrix} (F_o)_{11} \\ (F_{4c})_{11} \\ (F_{4s})_{11} \\ 0 \\ 0 \\ 0 \\ 0 \end{bmatrix} \{\beta_u\} + \begin{bmatrix} (G_o)_1 \\ (G_{4c})_1 \\ (G_{4s})_1 \\ 0 \\ 0 \\ 0 \\ 0 \end{bmatrix} \{\eta_F\} \qquad (15)$$

The form of the D's is similar to the A's of the A_{ij} matrix.

Tip path motions. - With the shaft and swashplate both fixed against tilting oscillation, the only motions that occur in the rotor system are the deflection of the blades. This section, therefore, sets out to show what these deflections are over the range of advance ratio μ and flapping stiffness ratio P for which these analyses are expected to be valid.

The calculations were performed employing the Lock number $\gamma = 4.57$ of the 33-foot rotor. The nondimensionalized blade tip deflection δ/R, however, should be valid for any rotor, with any number of blades, if it has the same value of Lock number.

Figures 14 through 16 show the variation of tip deflection as the blade travels the azimuth ψ for those familes of conditions μ = .5, 1.1, and 1.7 with members of each family of flapping stiffness ratios of P = 1.5, 2.0, and 5.0.

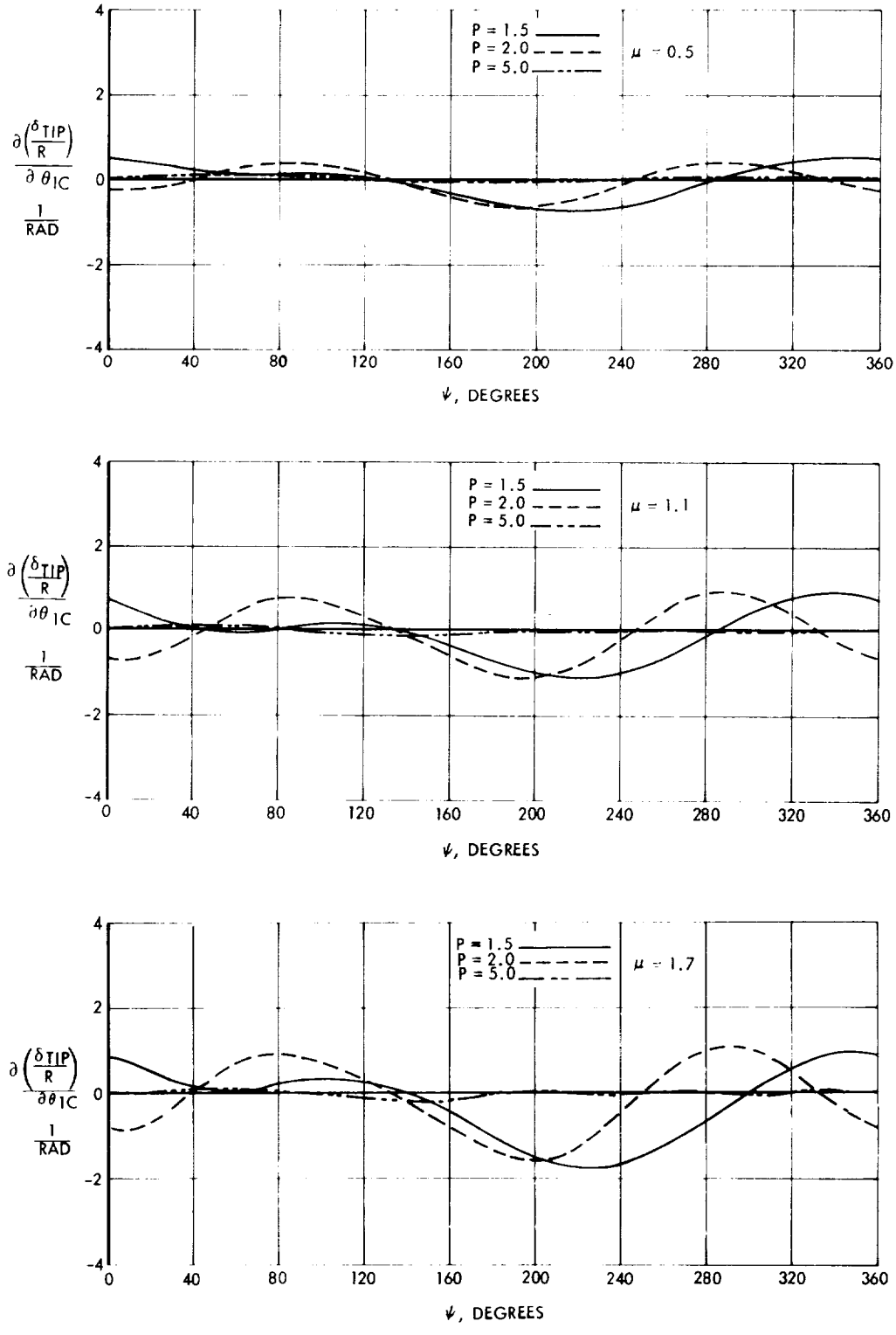

Figure 14. Blade Tip Motion Due to Lateral Cyclic Pitch, Lock Number $\gamma = 4.57$

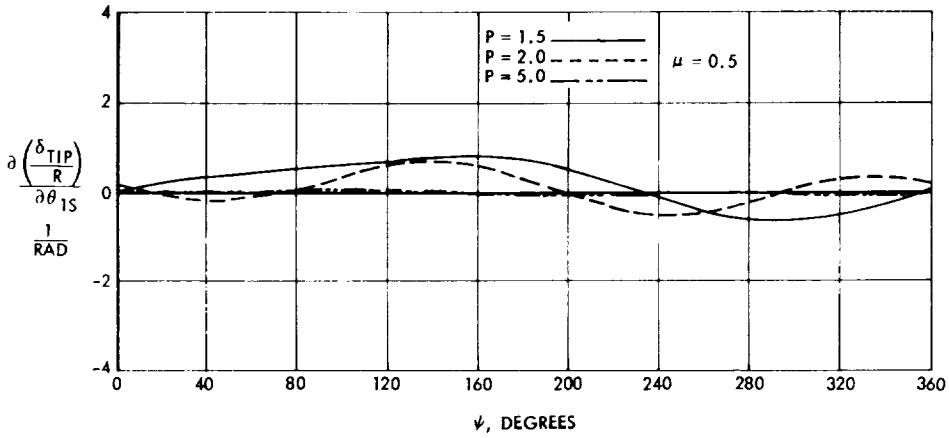

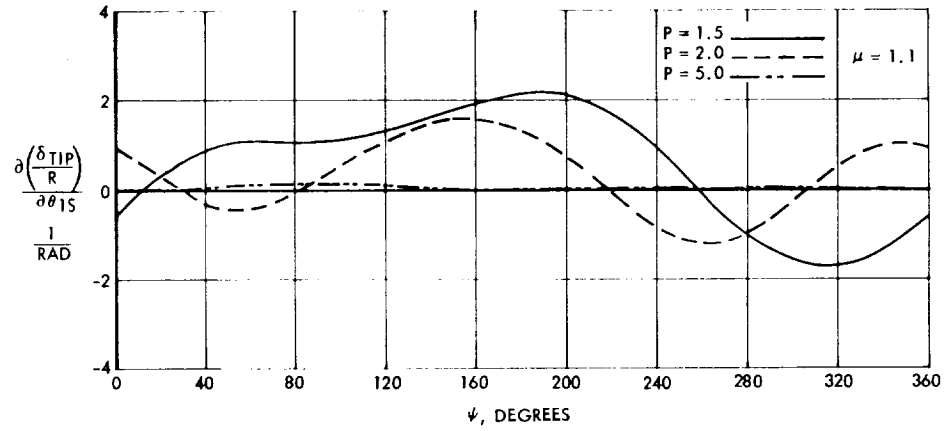

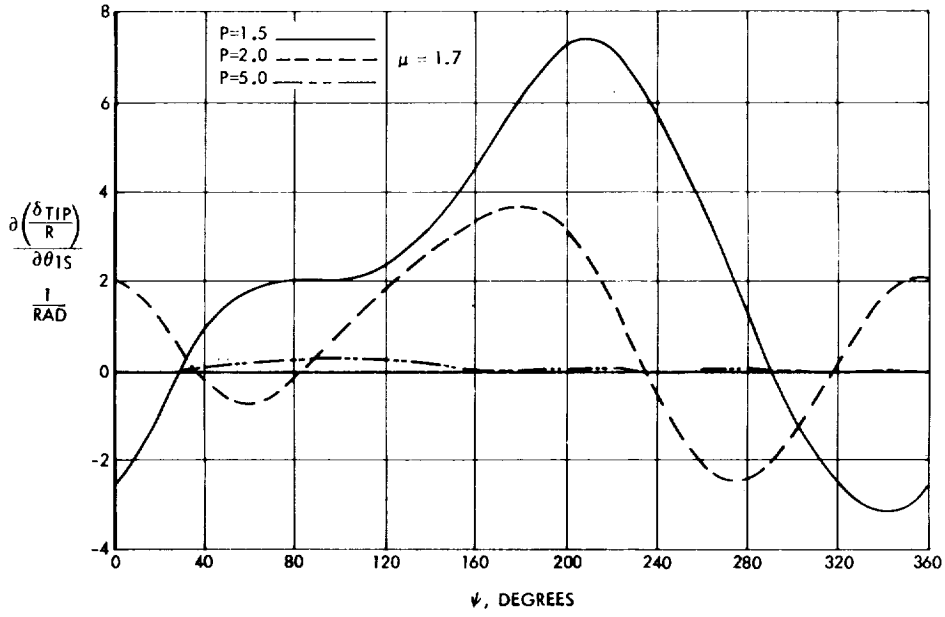

Figure 15. Blade Tip Motion Due to Longitudinal Cyclic Pitch, Lock Number $\gamma = 4.57$

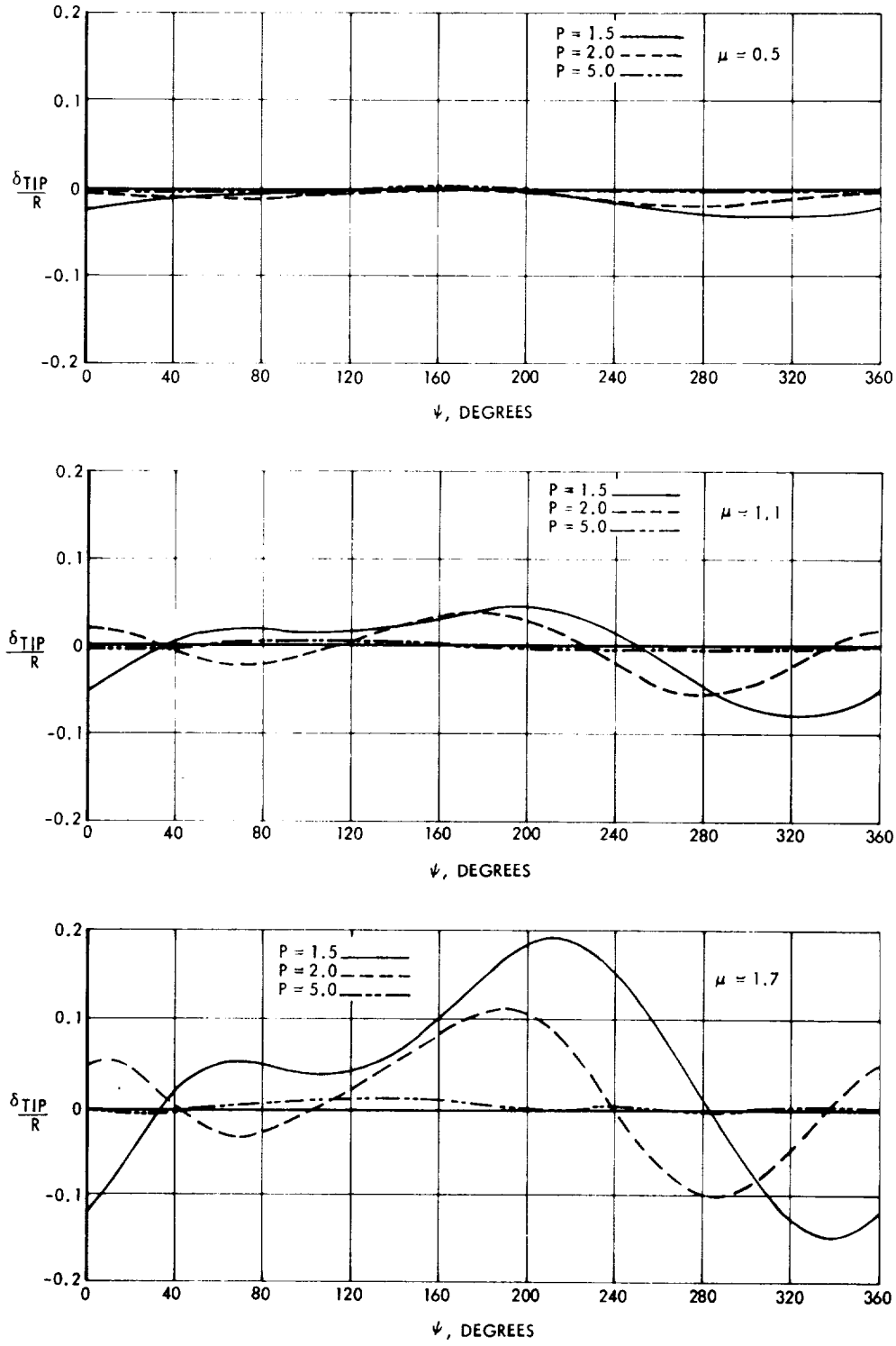

Figure 16. Residual Blade Tip Theoretical Displacement Due to Residual Parameters. β_o=2.25°, $\theta_t R$ = -9.43°, α = 0, θ_{75R} = 1.5°

Figure 14 shows the rate of change of tip path deflection with respect to θ_{1c}, Figure 15 the rate with respect to θ_{1s}, and Figure 16 shows the residual tip path deflection occurring at $\theta_{1c} = \theta_{1s} = 0$ and caused by the blade twist, rotor precone, and the small collective pitch, $\theta_{.75R} = 1.5^{\circ}$, present in the tests of the 33-foot rotor.

Mean aeroelastic derivatives. With the fixed-shaft, fixed-swashplate equations solved for the motions of the blades, it is possible to calculate the shaft-transmitted forces, blade airloads, and flapping bending moments and the input data required for the in-plane equations of motions. This section of the report is concerned only with the mean values of the aeroelastic forces transmitted through the shaft, the mean aeroelastic derivatives.

Mean aeroelastic derivatives of the rotor are commonly used in articulated rotor helicopter stability analyses at low advance ratio. For gyroscope stabilized hingeless rotors, especially at high advance ratio, it is usually not satisfactory to separate overall body motions from those of the rotor gyroscope system. This makes the concept of mean aeroelastic derivatives of limited usefulness in these applications. Certain of the derivatives, however, are easily measured in wind tunnels and provide an excellent reference by which to judge analysis methods. It is for this reason that they are treated here.

Theoretical and experimental values of rotor mean aeroelastic derivatives are shown for the 33-foot three-blade rotor and the 7.5-foot four-blade rotor. First the derivatives of hub moment, swashplate moment, and thrust with respect to cyclic pitch for the 33-foot rotor, are discussed.

The theoretical variation of hub moment coefficient derivatives with advance ratio μ and flap frequency P are shown as vectors in the X, Y plane in Figures 17 and 18. The derivatives are applicable to rotors of any size, numbers of blades, and blade geometry, provided they have the same Lock number ($\gamma = 4.57$) as the 33-foot rotor. Two sets of curves are shown. The heavy lines show the effects of including the harmonic components of the aerodynamic coefficients in the differential equations. The light lines show the effect of leaving them out, as in the common practice with articulated

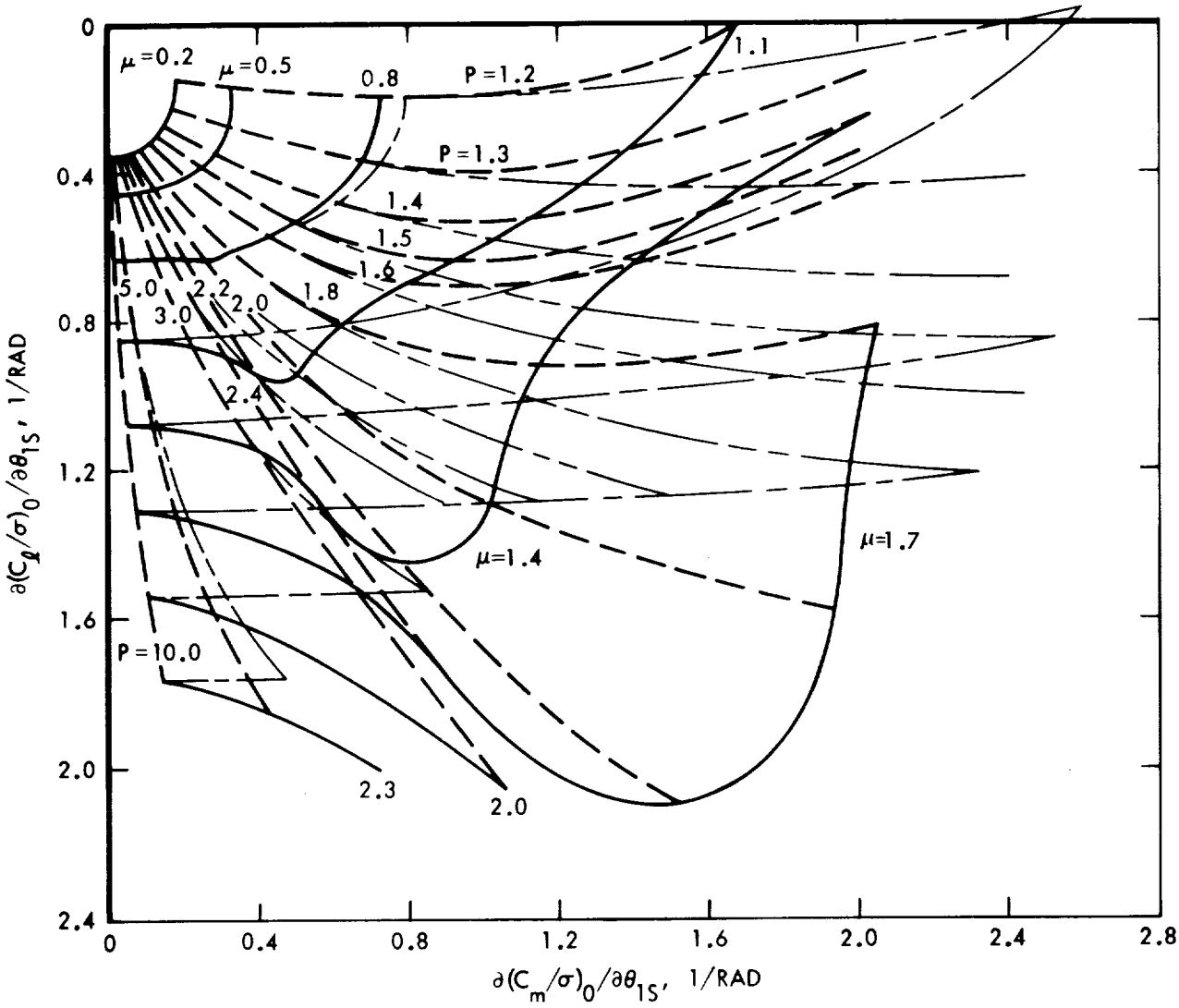

Figure 17. Hub Moment Longitudinal Cyclic Pitch Aeroelastic Derivatives, $\gamma = 4.57$

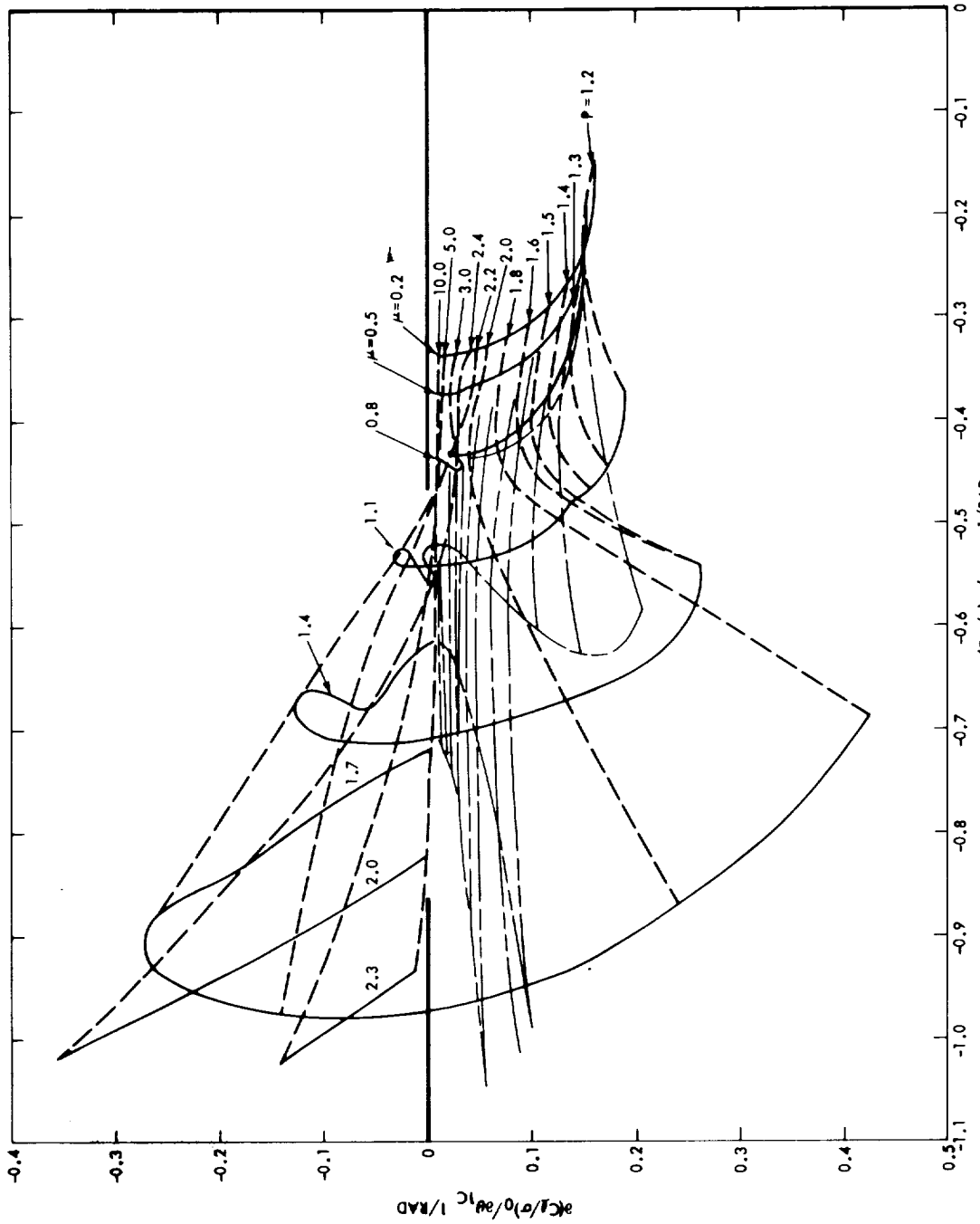

Figure 18. Hub Moment Lateral Cyclic Pitch Aeroelastic Derivatives, $\gamma = 4.57$

rotors at low advance ratio. It is interesting to note that at advance ratios well below unity, $\mu<1.0$, there is little difference between the two sets of curves. This seems to justify the common practice of leaving out the periodic coefficients. At advance ratio greater than unity, $\mu>1.0$, however, the effects of the harmonic components are very large. A large bump develops in the vicinity of P = 2.0, in the derivatives with respect to θ_{ls}, as the advance ratio increases above μ = .8 so that the mean derivatives become much larger with the periodic coefficients included. With $P<1.8$ the effects are large, but the derivatives with periodic coefficients become smaller than their counterparts without periodic parts.

Comparisons of theoretical mean aeroelastic derivatives with the experimental values for the 33-foot rotor are shown in Figures 19 through 22. In these plots the components of the derivative vectors are displayed versus flapping frequency ratio P for tested values of advance ratio. Small corrections have been made to the experimental points to bring them to common values of advance ratio. There is general quantitative agreement between theory and experiment but the fine structure of the variation with P exhibited by the experimental data is not mirrored in the theoretical results. This may be due to too restricted a mathematical representation of the participating vibratory modes in the theory.

In Figure 21, experimental hub pitch moment aeroelastic derivatives due to longitudinal cyclic pitch for the 7.5 foot diameter 4-blade rotor are included with the 33 foot rotor data for comparison. The derivatives are interpolated to produce values at advance ratio μ = 0.5, 0.8, 1.1, and 2.0 and are shown at four values of flap frequency ratio. It is interesting to note that the 7.5 foot 4-blade rotor data at μ = 0.5 and 0.8 compares very favorably with values measured on a rotor of more than four times the diameter, that possesses only three blades and has about half the solidity.

Figure 21 also shows a significant effect due to the blade first flapwise radial mode shape. The 7.5 foot rotor configuration with the stiff flexure gives greater values of pitch derivatives, for the same μ, γ, and P, than does the configuration with the less stiff flexure. The effects of the modal differences seem to increase with advance ratio.

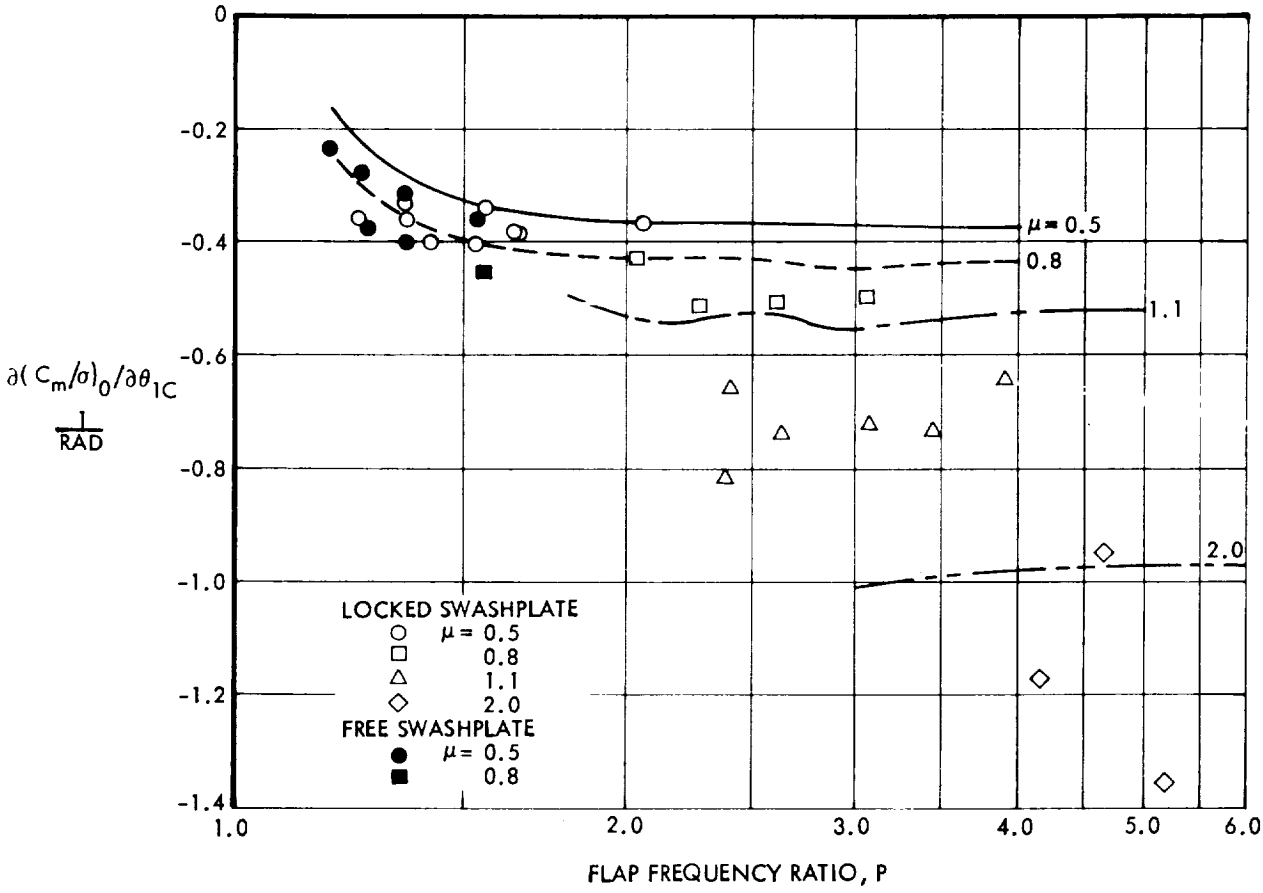

Figure 19. Mean Aeroelastic Derivative of Hub Pitch Moment With Respect to Lateral Cyclic Pitch, $\gamma = 4.57$

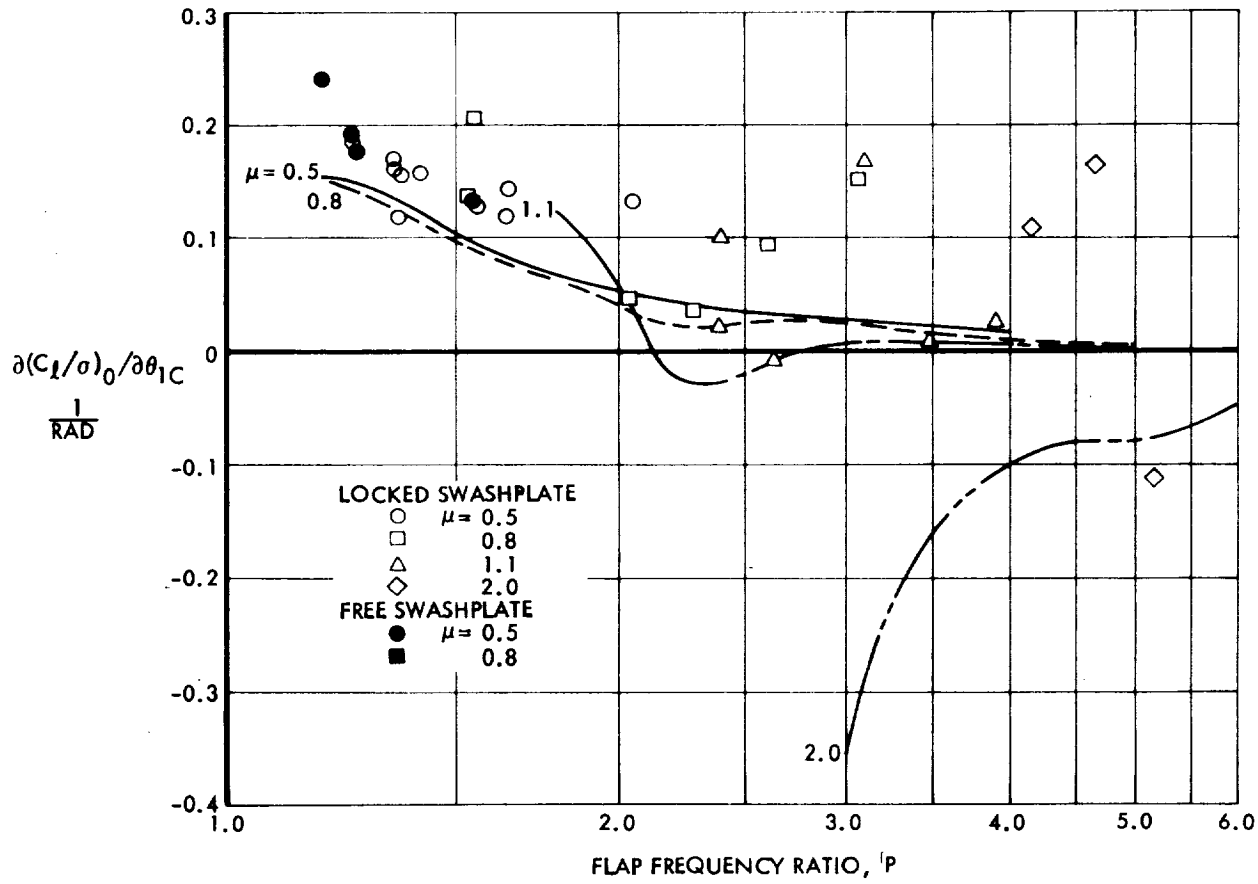

Figure 20. Mean Aeroelastic Derivative of Hub Roll Moment With Respect to Lateral Cyclic Pitch, $\gamma = 4.57$

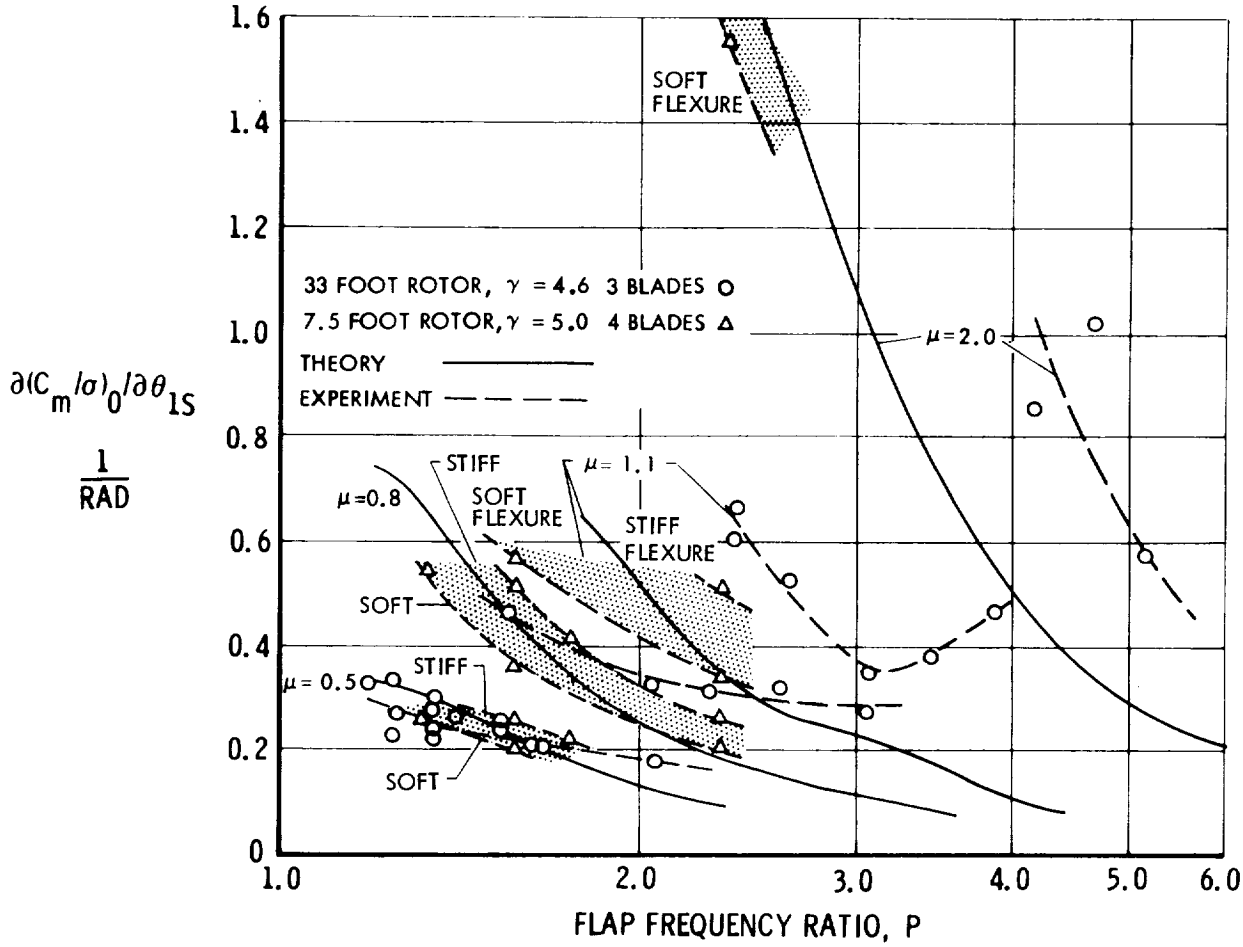

Figure 21. Mean Aeroelastic Derivative of Hub Pitch Moment With Respect to Longitudinal Cyclic Pitch, $\gamma = 4.57$

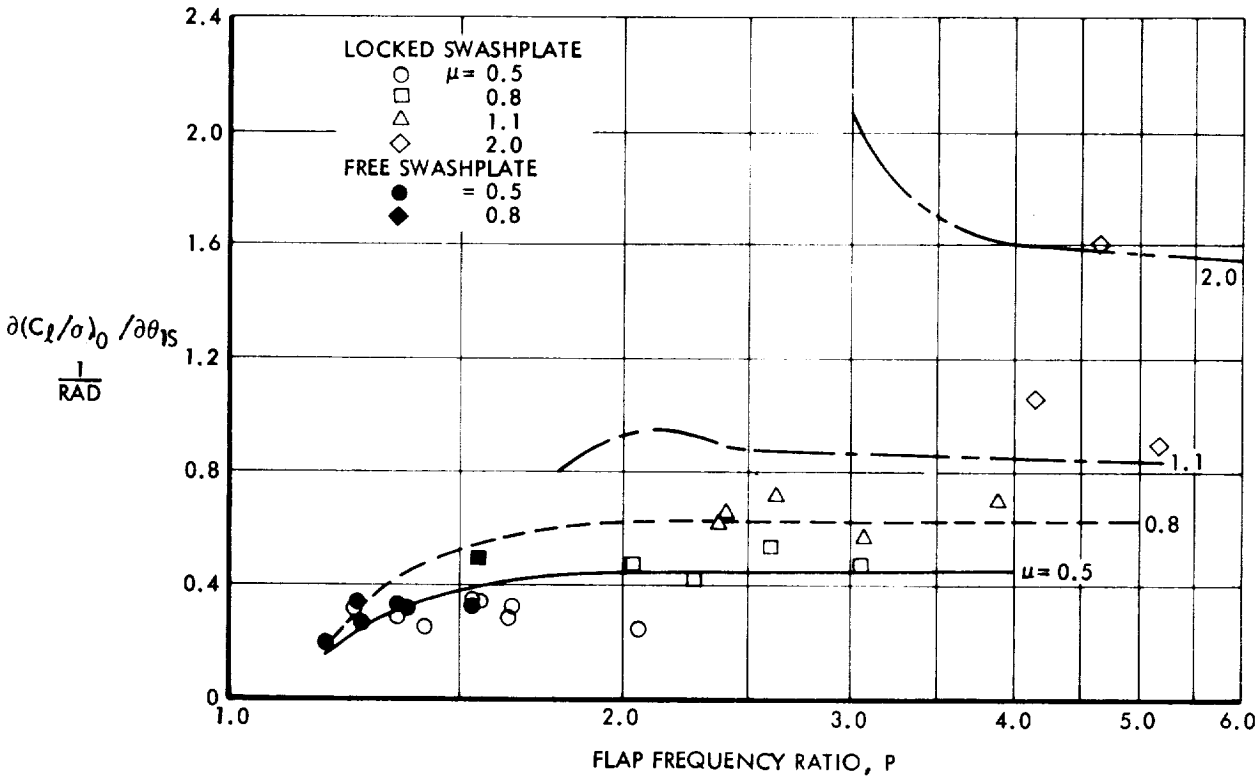

Figure 22. Mean Aeroelastic Derivative of Hub Roll Moment With Respect to Longitudinal Cyclic Pitch, $\gamma = 4.57$

Swashplate moment coefficient mean aeroelastic derivatives with respect to cyclic pitch for the 33-foot rotor are shown plotted in vector form in Figures 23 and 24. It should be noted that in addition to being divided by rotor solidity σ, as were the hub moment coefficient derivatives, the swashplate moment coefficients are divided by the blade sweep angle Λ and factored by the swashplate mechanical advantage k. These further factors serve the purpose of making the derivatives independent of Λ and k at low advance ratio. At high advance ratio the derivatives become a weak function of sweep ratio, $\frac{b\Lambda}{\sigma}$ (or $\pi \frac{\Lambda}{c/R}$), because of reverse velocity effects.

Swashplate mean derivatives variations with P and μ at $\gamma = 4.57$ are similar to those of the hub moments. The effect of the cant angle $\psi_o = 60^\circ$ between the blades and the swashplate is apparent in the approximately 60° counterclockwise skew of the derivatives relative to the hub moment derivatives. As with the hub moment derivatives, deletion of the harmonic components of the coefficients in the differential equations has little effect at advance ratio less than unity and a large effect at values greater than unity.

Comparisons of theoretical swashplate moment coefficient derivatives, calculated with harmonic components included, with values measured experimentally on the 33-foot rotor, are shown in Figures 25 through 28.

As with the hub moment derivatives the vector components are shown versus flap frequency P at particular values of advance ratio μ. Again the agreement between theory and experiment is quantitatively good but the fine structure of the experimental data is not seen in the theory.

The variation of the thrust coefficient C_T/σ with cyclic pitch is shown in Figures 29 and 30 over the range of P and μ for which the theory is expected to be valid. The theory includes the effects of the harmonic components of the aerodynamic derivatives. Agreement between experiment and theory is better for the longitudinal cyclic pitch because of its greater effect.

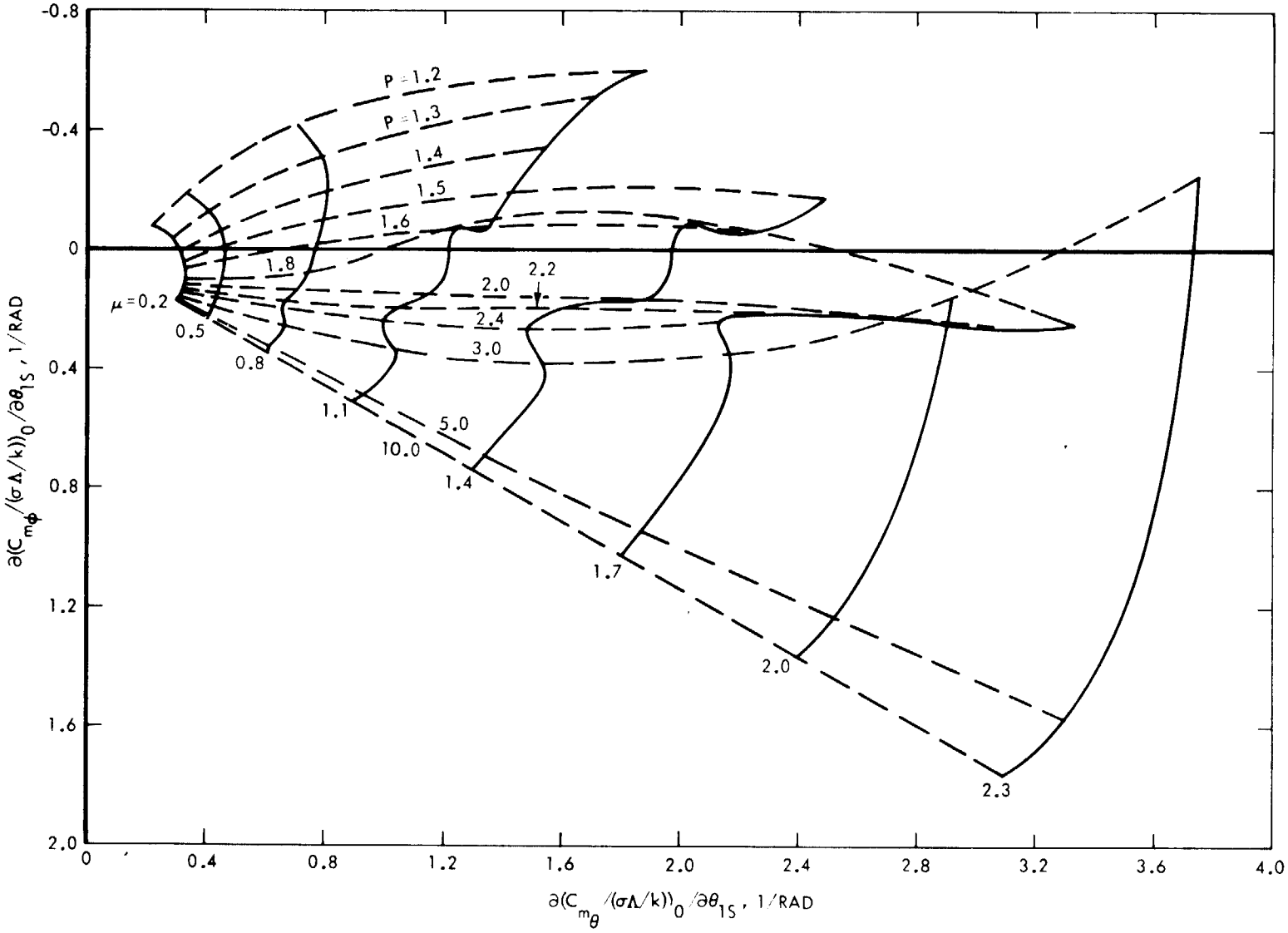

Figure 23. Swashplate Moment Lateral Cyclic Pitch Aeroelastic Derivatives, $\gamma = 4.57$

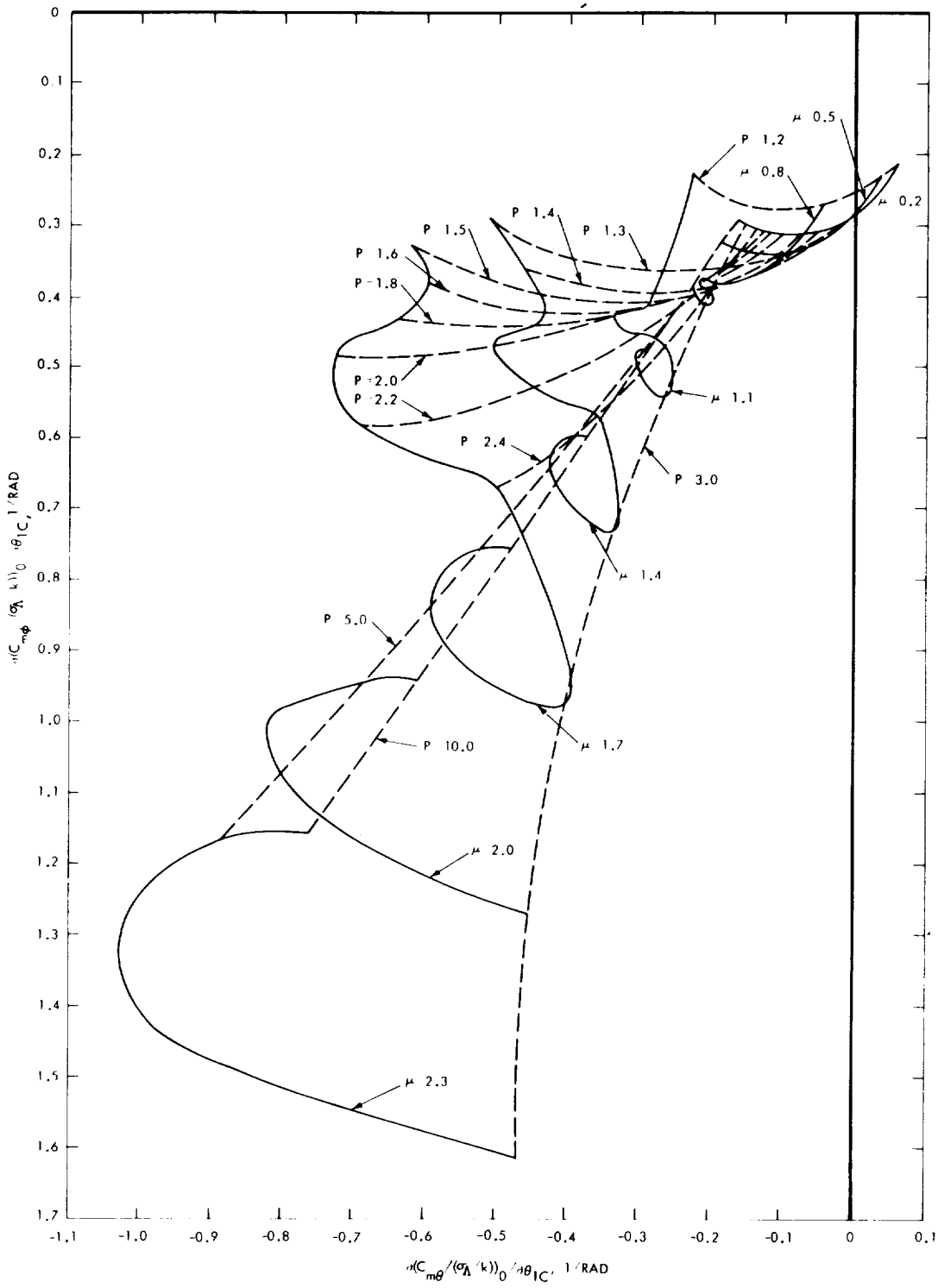

Figure 24. Swashplate Moment Longitudinal Cyclic Pitch Aeroelastic Derivatives, $\gamma = 4.57$

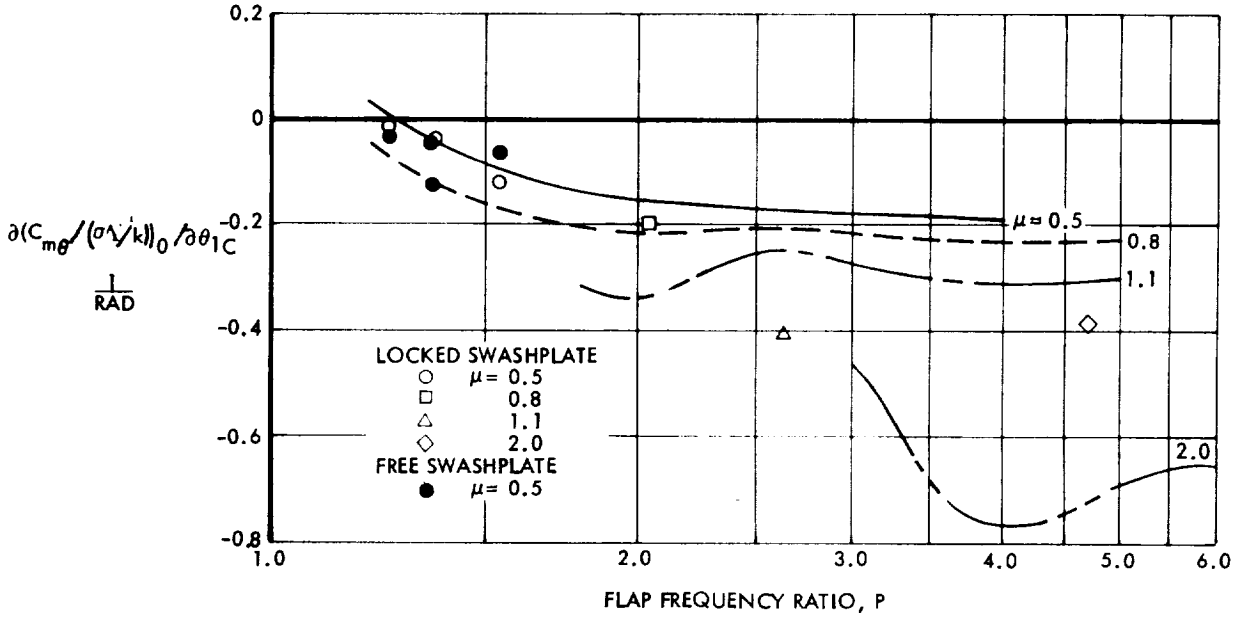

Figure 25. Mean Aeroelastic Swashplate Pitch Moment Derivative With Respect to Lateral Cyclic Pitch, $\gamma = 4.57$

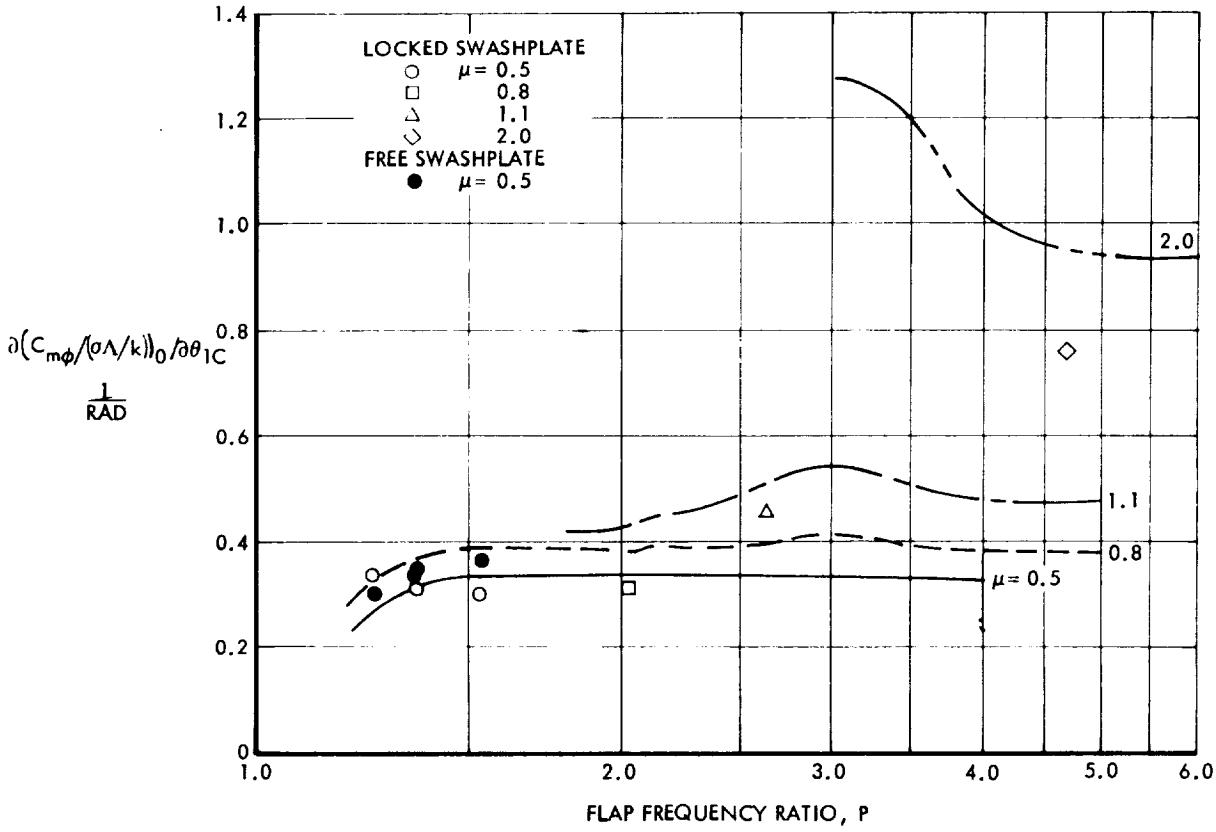

Figure 26. Mean Aeroelastic Swashplate Roll Moment Derivative With Respect to Lateral Cyclic Pitch, $\gamma = 4.57$

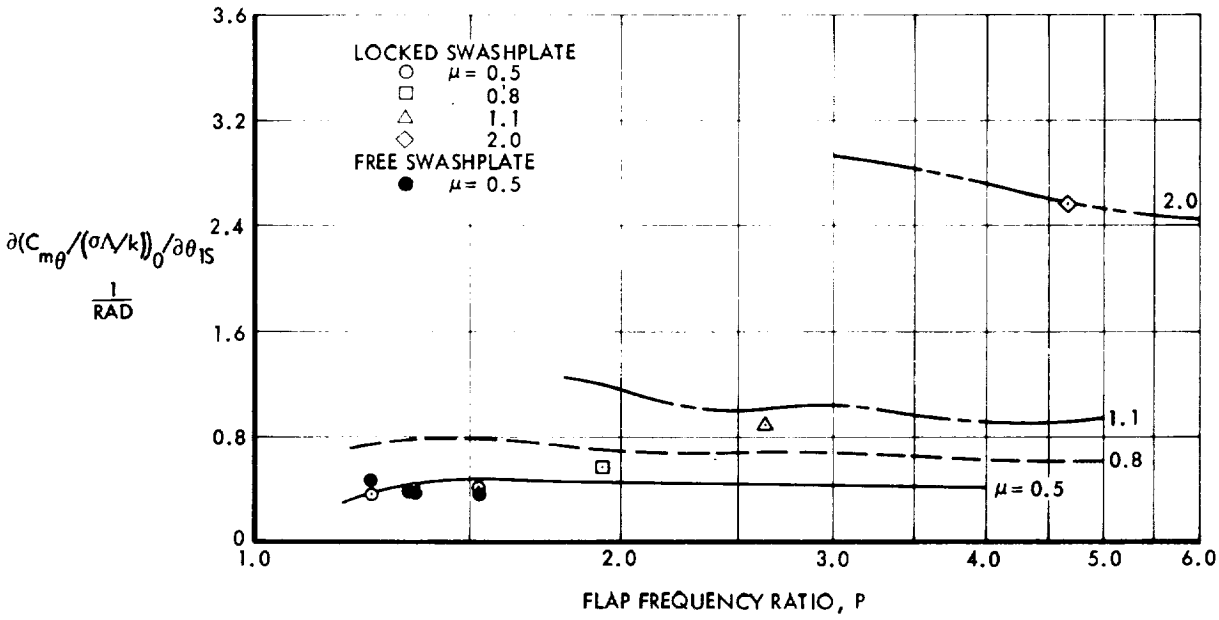

Figure 27. Mean Aeroelastic Swashplate Pitch Moment Derivative With Respect to Longitudinal Cyclic Pitch, $\gamma = 4.57$

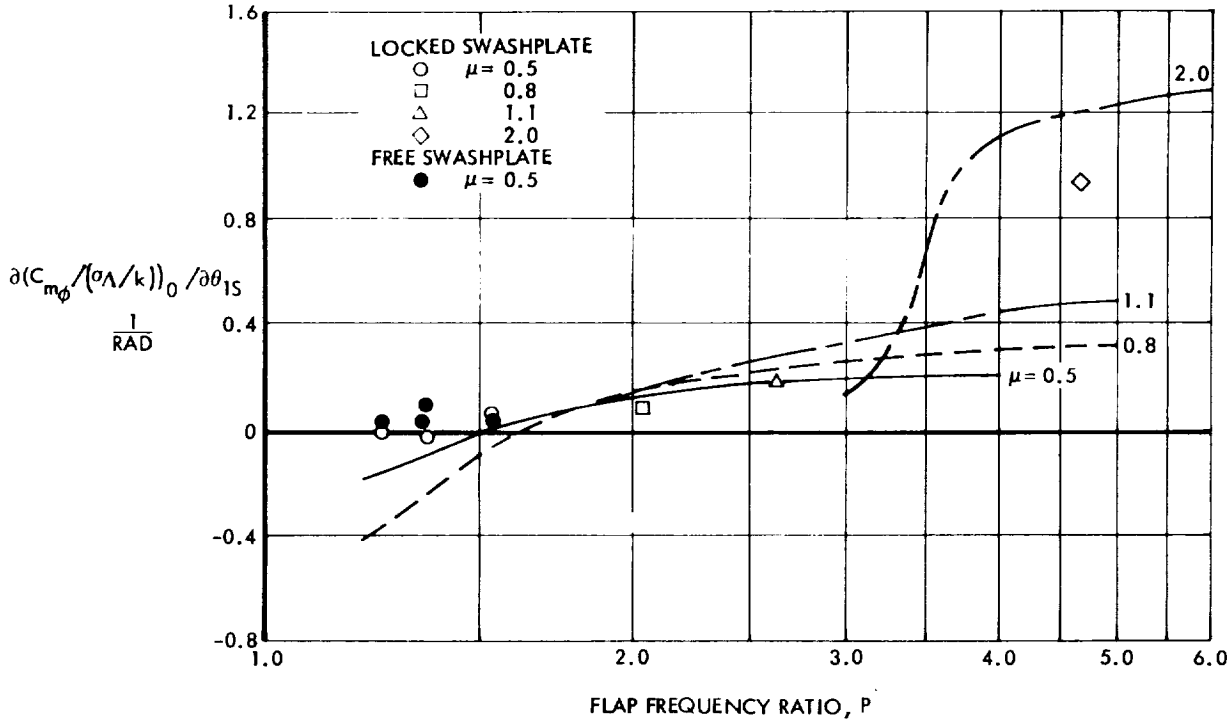

Figure 28. Mean Aeroelastic Swashplate Roll Moment Derivative With Respect to Longitudinal Cyclic Pitch, $\gamma = 4.57$

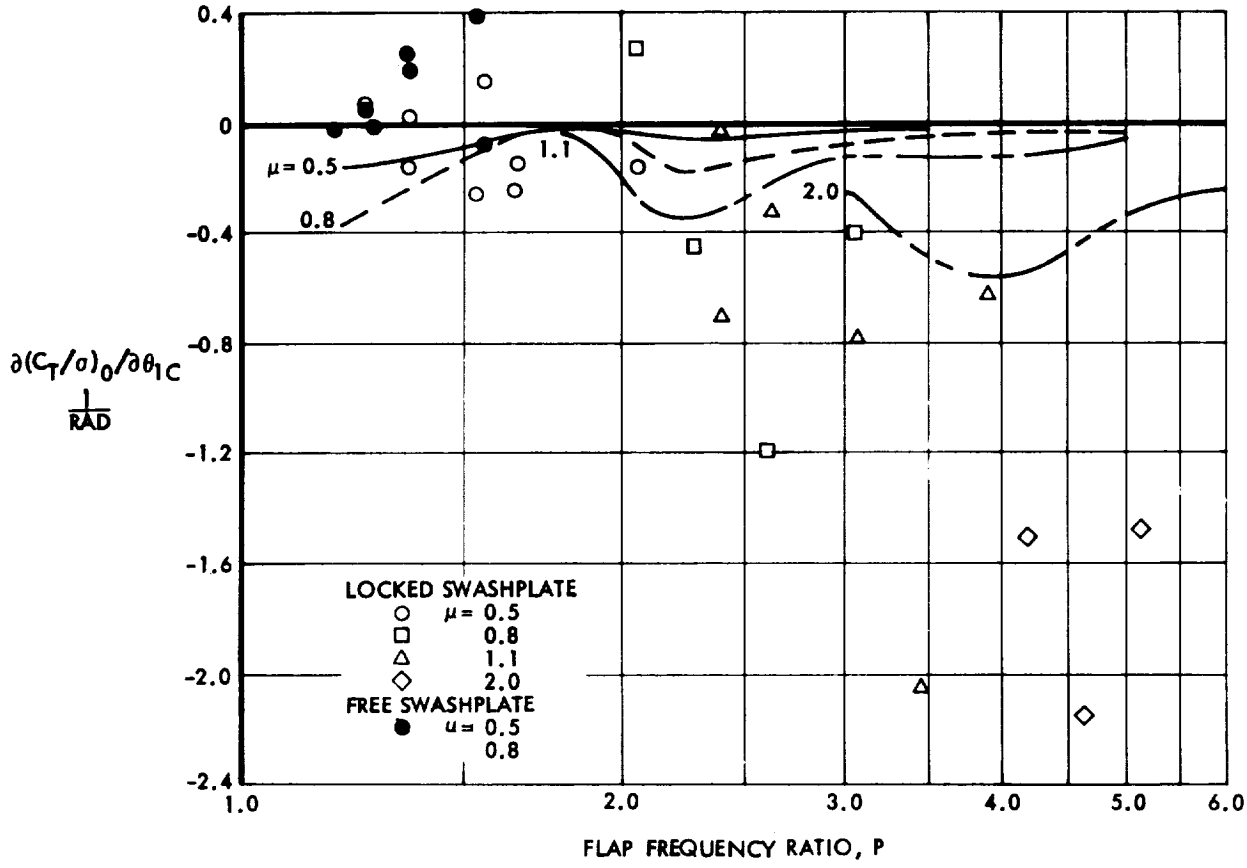

Figure 29. Mean Thrust Aeroelastic Derivative With Respect to Lateral Cyclic Pitch. $\gamma = 4.57$

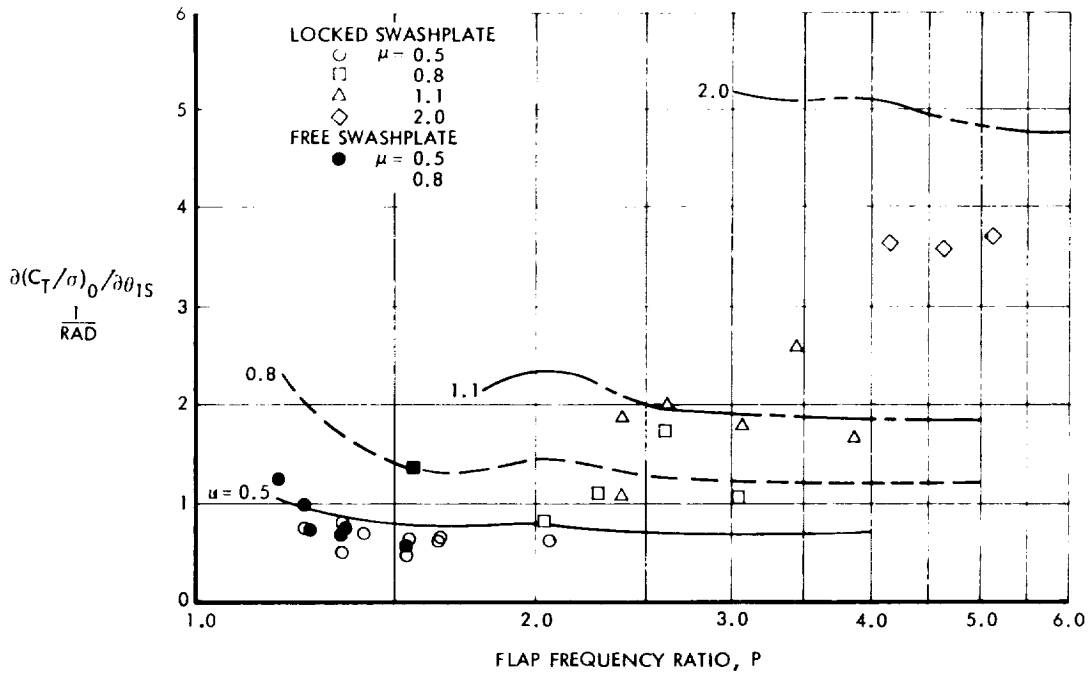

Figure 30. Mean Thrust Aeroelastic Derivative With Respect to Longitudinal Cyclic Pitch. $\gamma = 4.57$

The residual shaft force coefficients for the 33-foot rotor, or those existing at $\theta_{1c} = \theta_{1s} = \alpha = 0$ and $\theta_{.75R} = 1.5^{\circ}$, are needed to reproduce the mean states in which the rotor was tested. Mean shaft force states may be obtained by combining residual force with the forces produced by the two cyclic pitch components of the test conditions desired.

The residual mean force coefficients, hub moment, swashplate moment, and thrust were caused by blade twist, rotor precone, and the small collective pitch angle $\theta_{.75R} = 1.5^{\circ}$. The theoretical variation of them with flap frequency P at the specific values of μ tested are shown in Figures 31 through 35. Experimental values are also shown. Good agreement was not expected and did not occur. The reasons for the poor agreement are thought to be the following:

a. Flow distortion caused by the body

b. Centrifugal flattening of precone not adequately described by one parabolic mode

c. Blade bending in the second flap mode due to blade twist aerodynamics

d. Induced inflow due to blade twist aerodynamics not accounted for

It should be noted that some of the residual forces could not be obtained experimentally without overloading the rotor. They have been obtained by extrapolating best fit plane (or rms plane) data to the zero cyclic condition. To avoid giving a misleading impression, therefore, the residual forces in conjunction with the mean aeroelastic derivatives have been employed to reproduce a mean state of interest - the condition of hub moment trim (or zero hub moment). Cyclic pitch angles needed to trim the 33-foot rotor hub moments to zero are shown in Figures 36. The actual test values of θ_{1c} and θ_{1s} were centered about the trim values and generally did not exceed 3° or 4° amplitude deviation from them.

Residual harmonic aeroelastic forces are discussed later and comparable cyclic pitch values may be found to trim or minimize vibratory loads. The 7.5-foot four-blade rotor hub moment and thrust coefficient aeroelastic derivative theoretical values, divided by solidity, are very similar to those

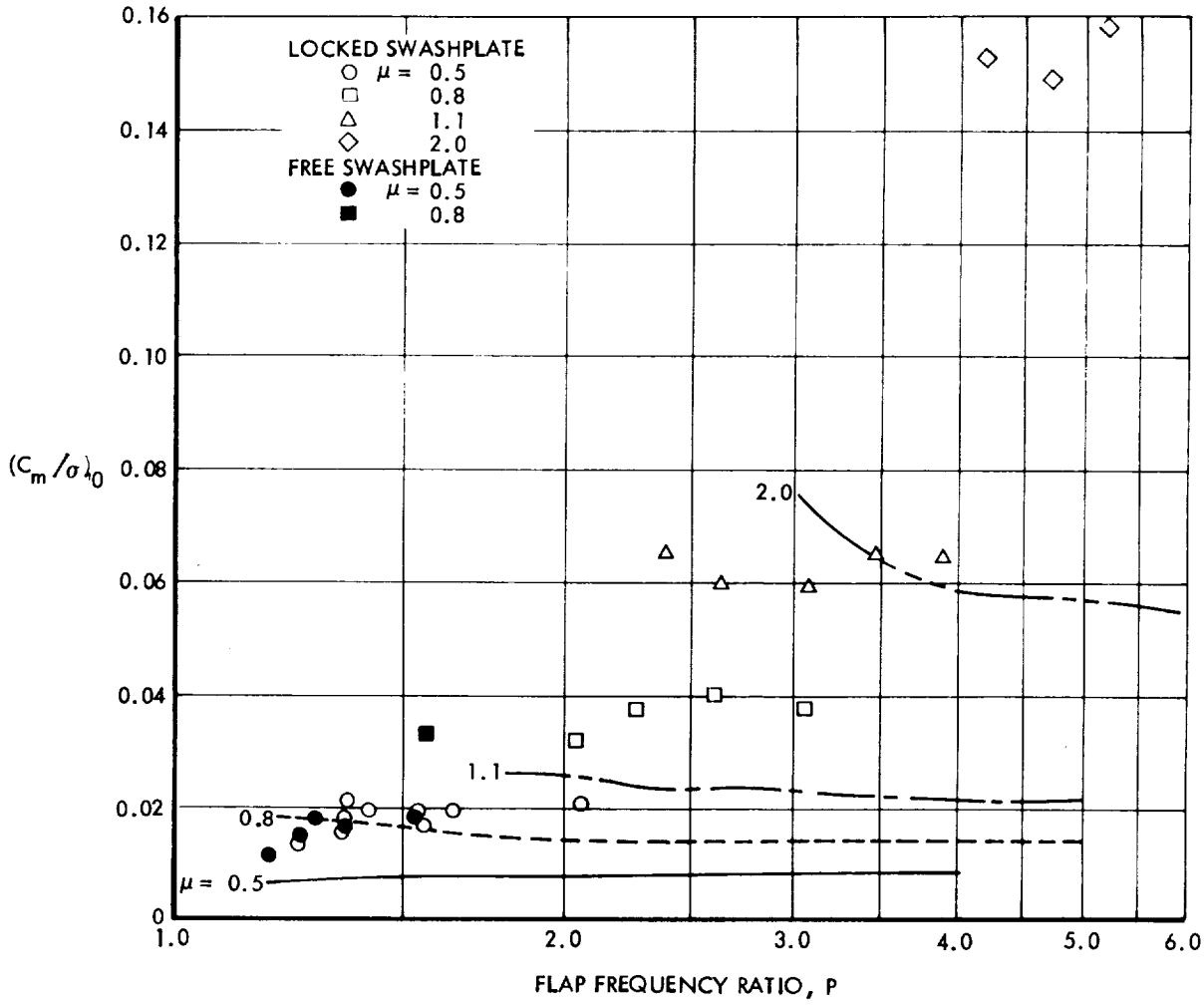

Figure 31. Residual Mean Hub Pitch Moment, $\gamma = 4.57$, $\beta_o = 2.25^o$, $\theta_t R = -9.43^o$, $\alpha = 0$, $\theta_{.75R} = 1.5^o$

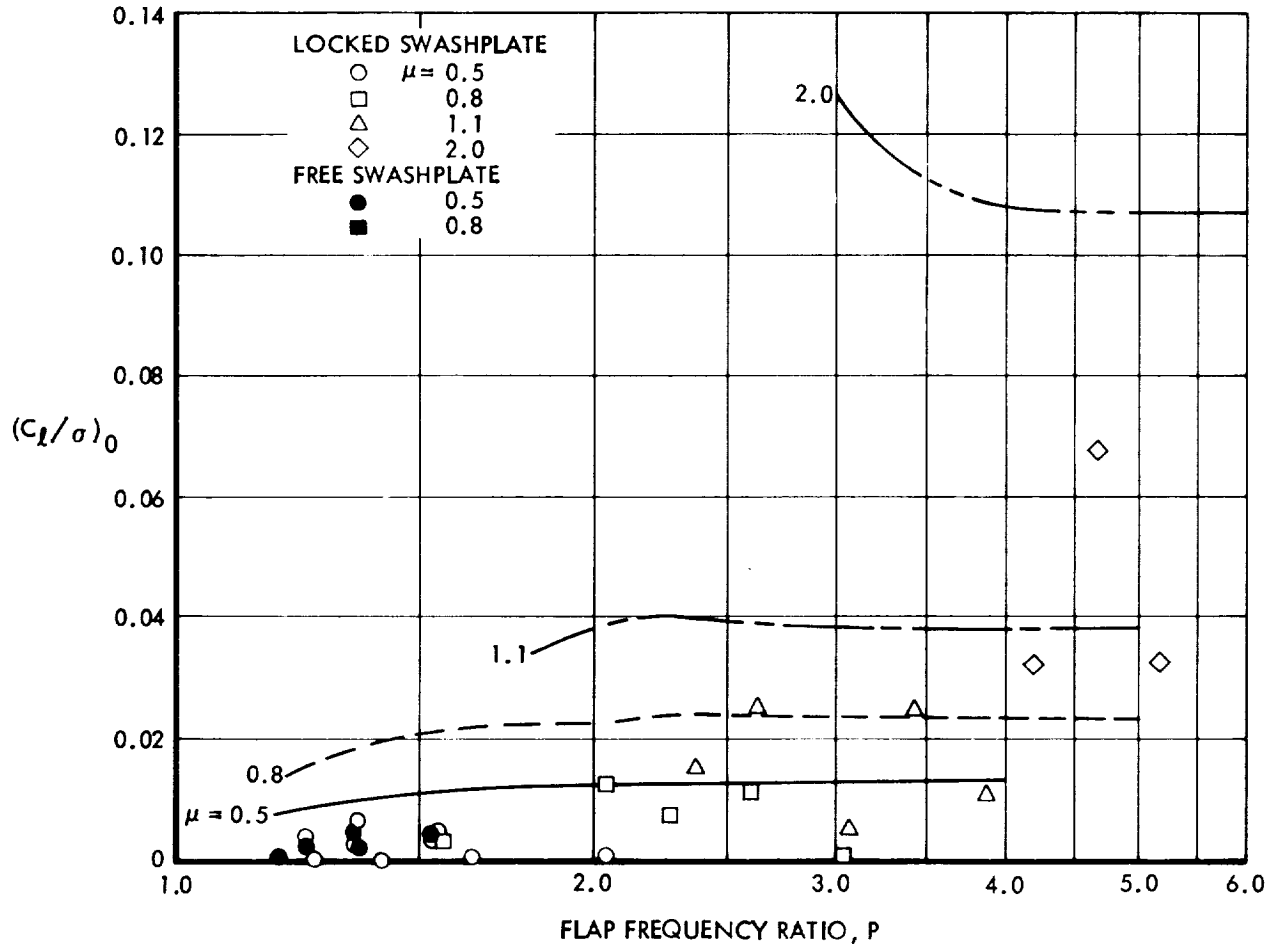

Figure 32. Residual Mean Hub Roll Moment, $\gamma = 4.57$, $\beta_o = 2.25^\circ$, $\theta_t R = -9.43^\circ$, $\alpha = 0$, $\theta_{.75R} = 1.5^\circ$

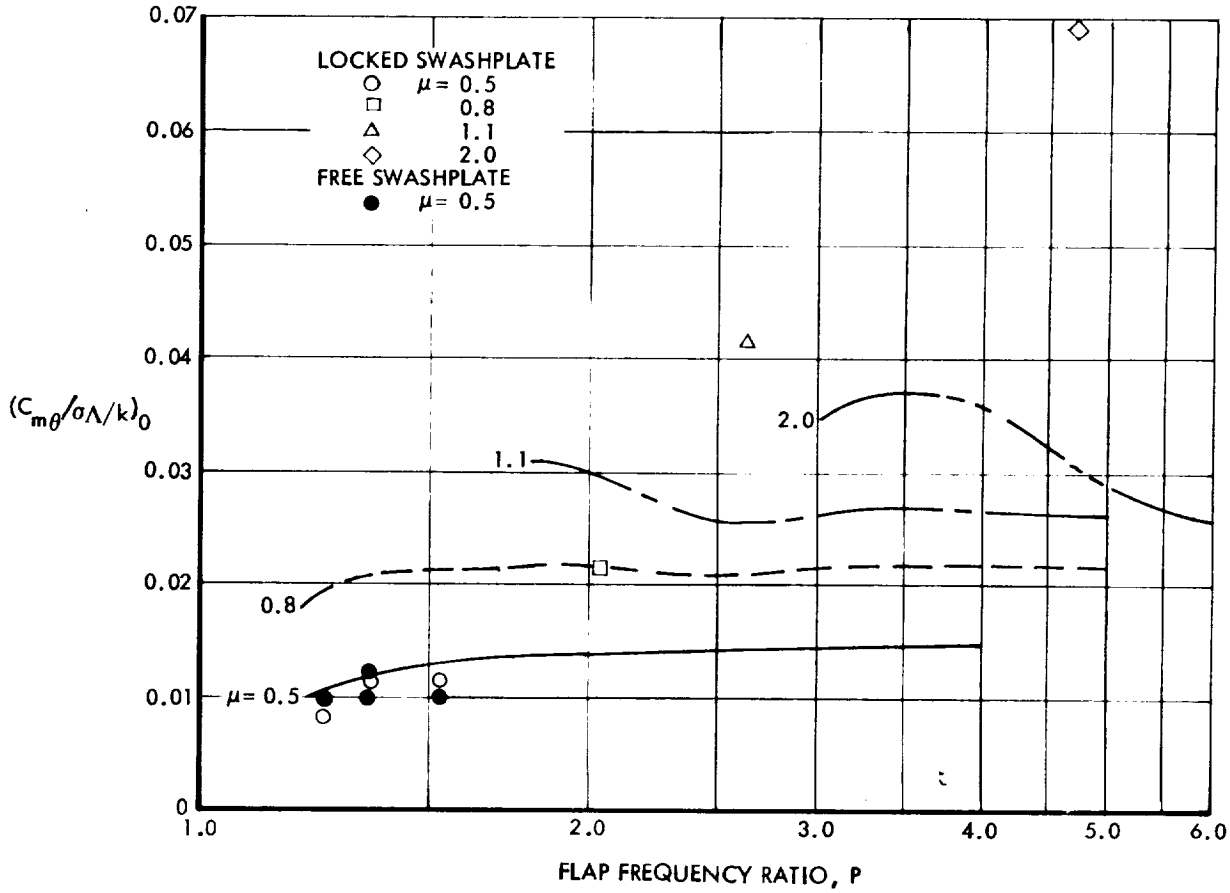

Figure 33. Residual Mean Swashplate Pitch Moment, $\gamma = 4.57$, $\beta_o = 2.25^o$, $\theta_t R = -9.43^o$, $\alpha = 0^o$, $\theta_{.75R} = 1.5^o$

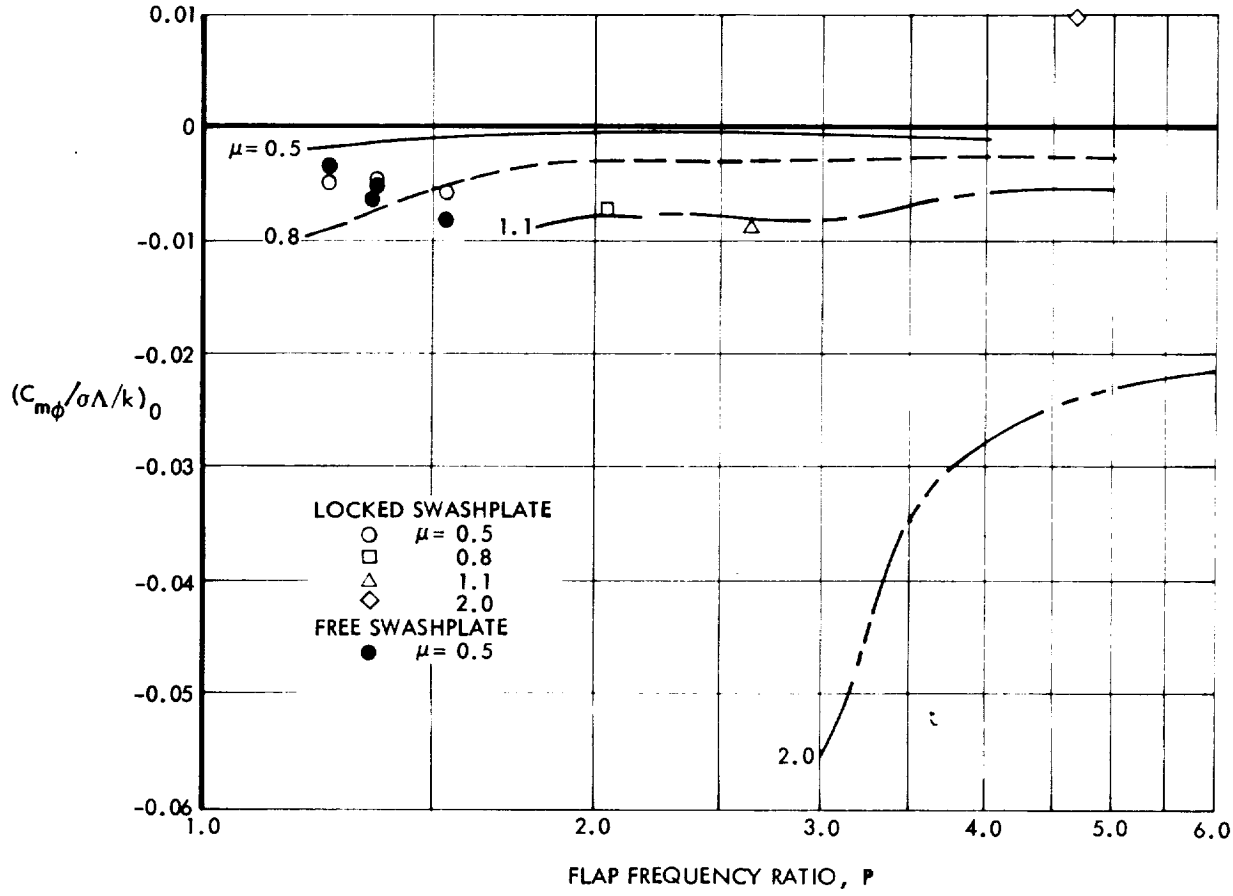

Figure 34. Residual Mean Swashplate Roll Moment, $\gamma = 4.57$, $\beta_o = 2.25^\circ$, $\theta_t R = -9.43^\circ$, $\alpha = 0$, $\theta_{.75R} = 1.5^\circ$

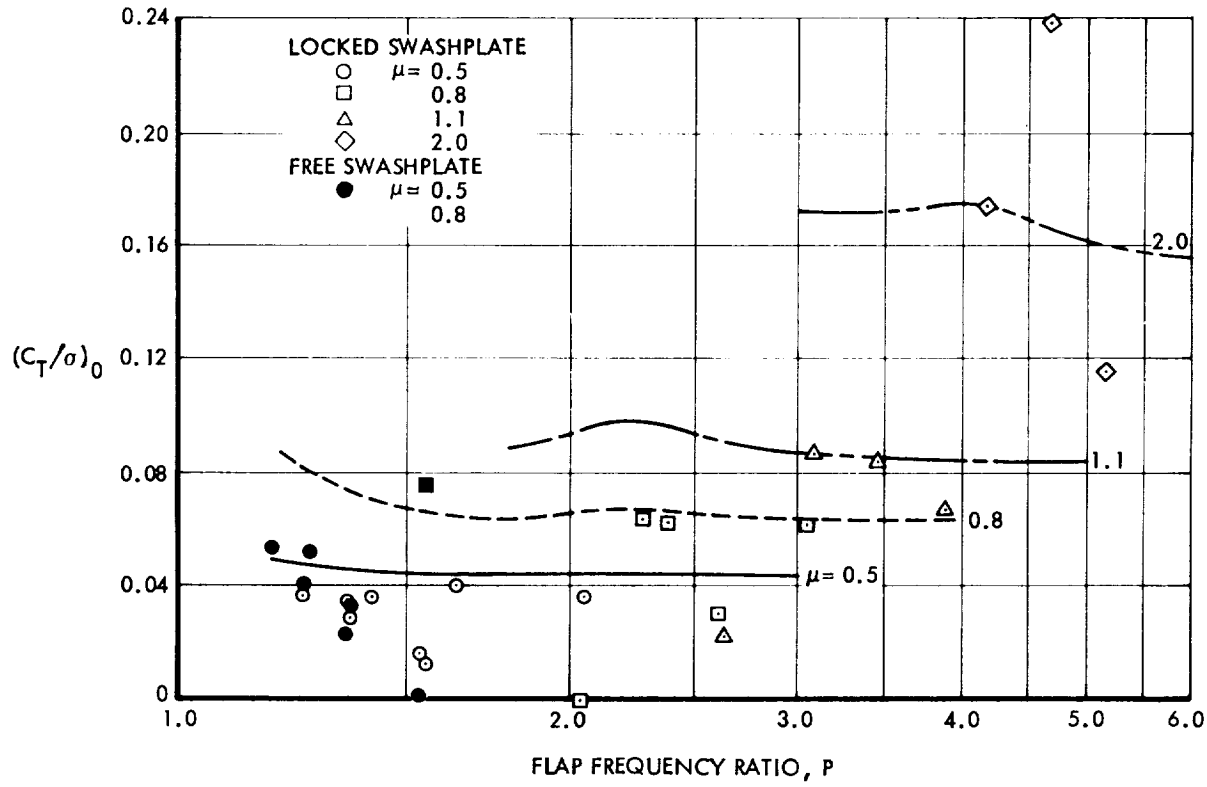

Figure 35. Residual Mean Thrust Force Due to, $\gamma = 4.57$, $\beta_o = 2.25^\circ$, $\theta_t R = -9.43^\circ$, $\alpha = 0$, and $\theta_{.75R} = 1.5^\circ$

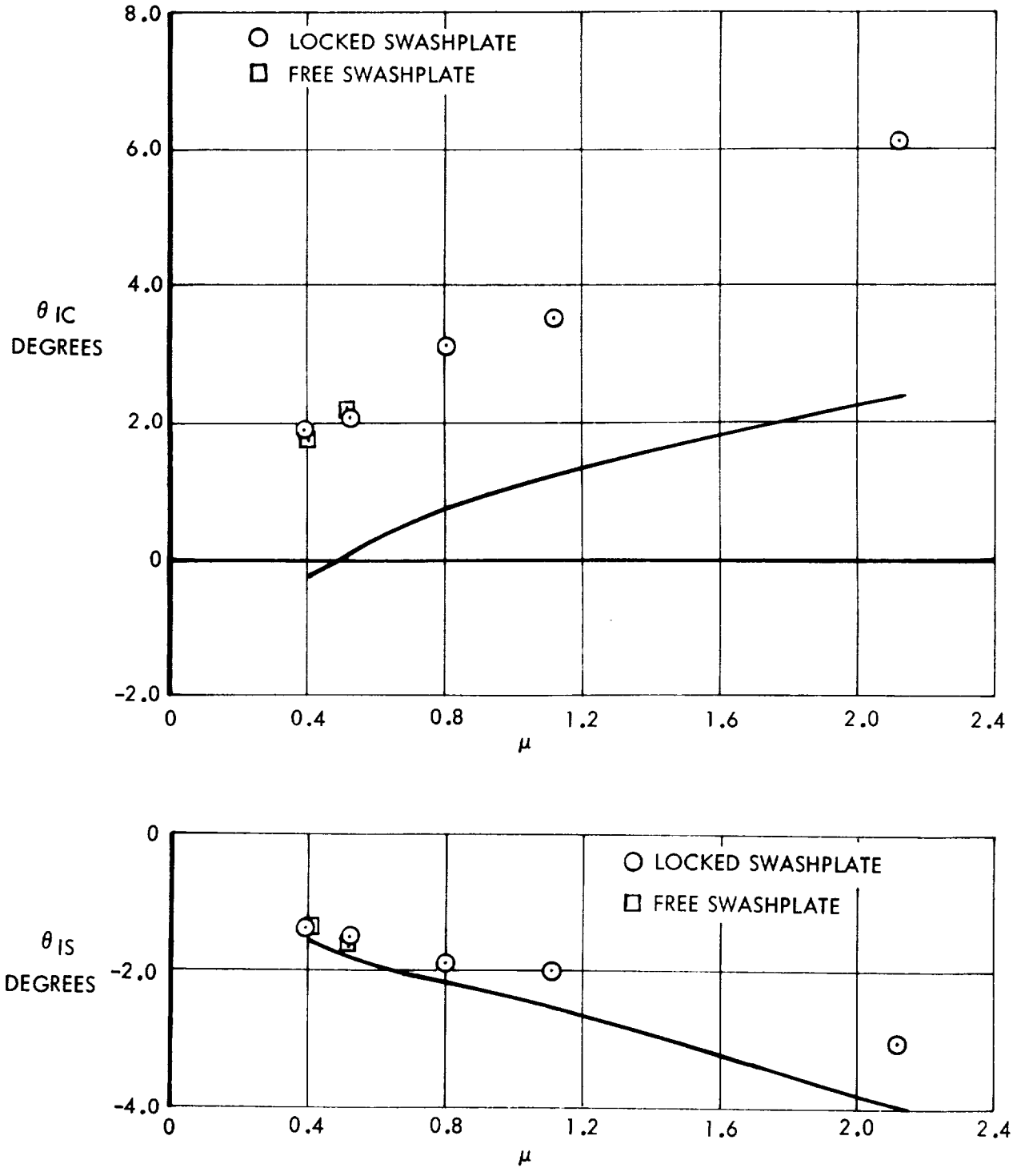

Figure 36. Cyclic Pitch Angles to Trim. $\gamma = 4.57$, $\beta_o = 2.25°$, $\theta_t{}^R = -9.43°$, $\alpha = 0$, $\theta_{.75R} = 1.5°$, 80 Knots.

of the 33-foot three-blade rotor. The difference, about 10%, is due to the larger Lock number, $\gamma = 5.0$, of the four-blade rotor compared to that of the three-blade rotor, $\gamma = 4.57$.

For this reason the theoretical derivatives hub moment vector diagrams with respect to θ_{1c} and θ_{1s} are not repeated. In this section the hub moment derivatives components of the vector diagram are plotted versus advance ratio for the test values of flap frequency P.

The following derivatives are plotted:

$$\frac{\partial C_m/\sigma}{\partial \theta_{1s}} \qquad \frac{\partial C_\ell/\sigma}{\partial \theta_{1s}}$$

$$\frac{\partial C_m/\sigma}{\partial \theta_{1c}} \qquad \frac{\partial C_\ell/\sigma}{\partial \theta_{1c}}$$

$$\frac{\partial C_m/\sigma}{\partial \theta_{o}} \qquad \frac{\partial C_\ell/\sigma}{\partial \theta_{o}}$$

$$\frac{\partial C_m/\sigma}{\partial \alpha} \qquad \frac{\partial C_\ell/\sigma}{\partial \alpha}$$

and comparison with experimental values is shown in Figures 37 through 44.

It should be noted that residual forces for the cantilevered blades with no precone are theoretically zero.

The 7.5 foot 4-blade rotor test procedure and experimental data are discussed in detail in Reference 17.

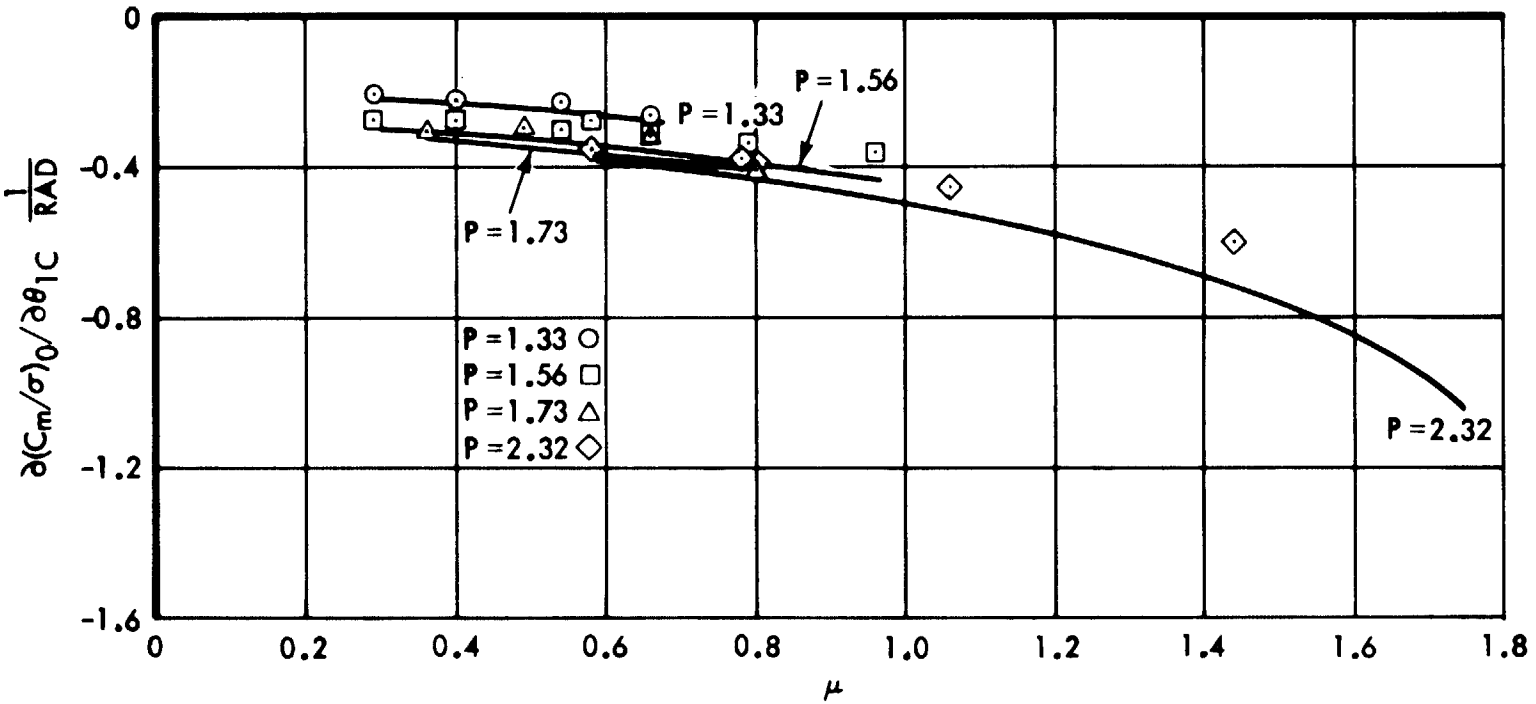

Figure 37. Mean Hub Pitch Moment Aeroelastic Derivative with Respect to Lateral Cyclic Pitch, $\gamma = 5.0$

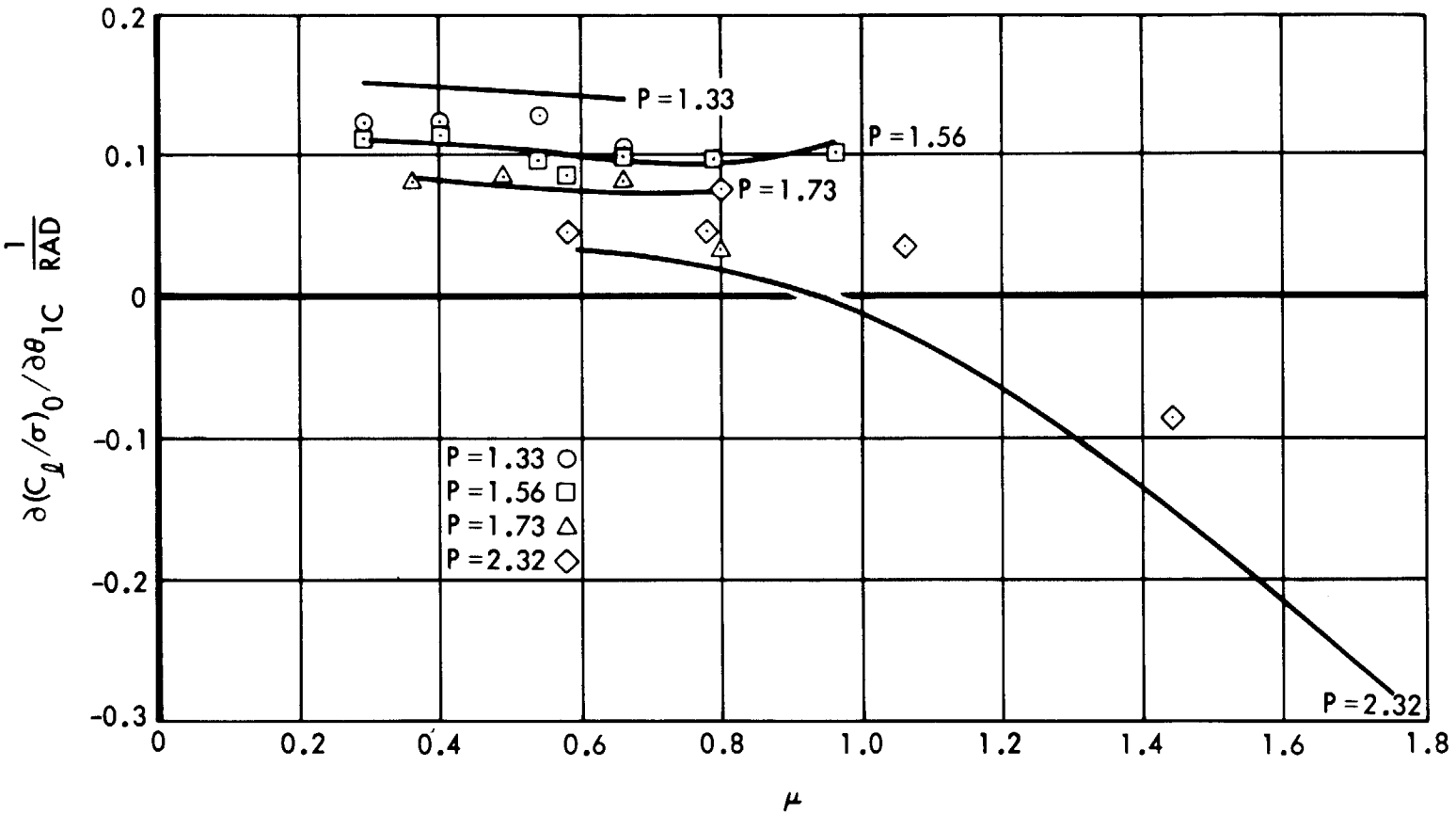

Figure 38. Mean Hub Roll Moment Aeroelastic Derivative with Respect to Lateral Cyclic Pitch, Y = 5.0

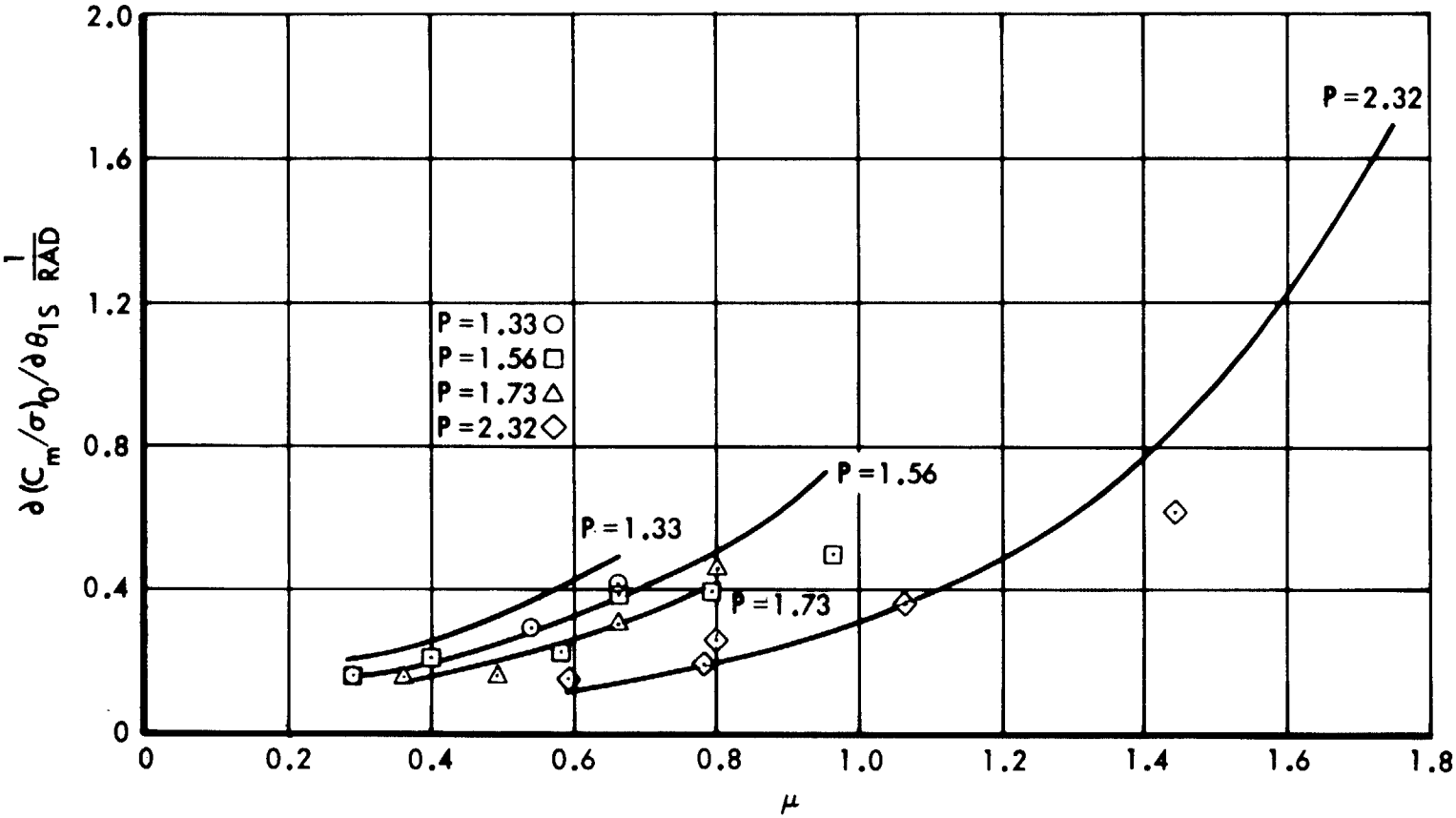

Figure 39. Mean Hub Pitch Moment Aeroelastic Derivative with Respect to Longitudinal Cyclic Pitch, γ = 5.0

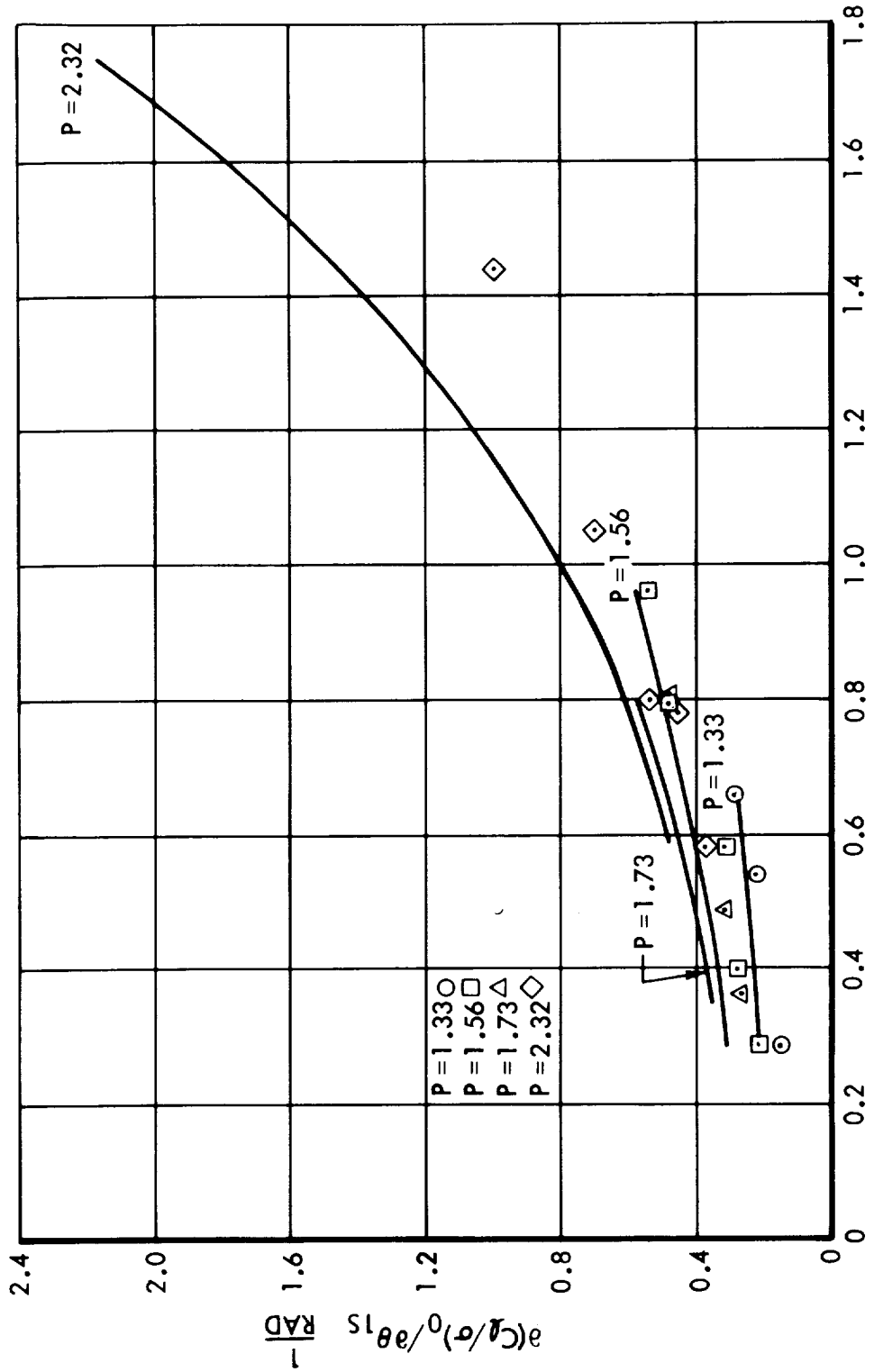

Figure 40. Mean Hub Roll Moment Aeroelastic Derivative with Respect to Longitudinal Cyclic Pitch, γ = 5.0

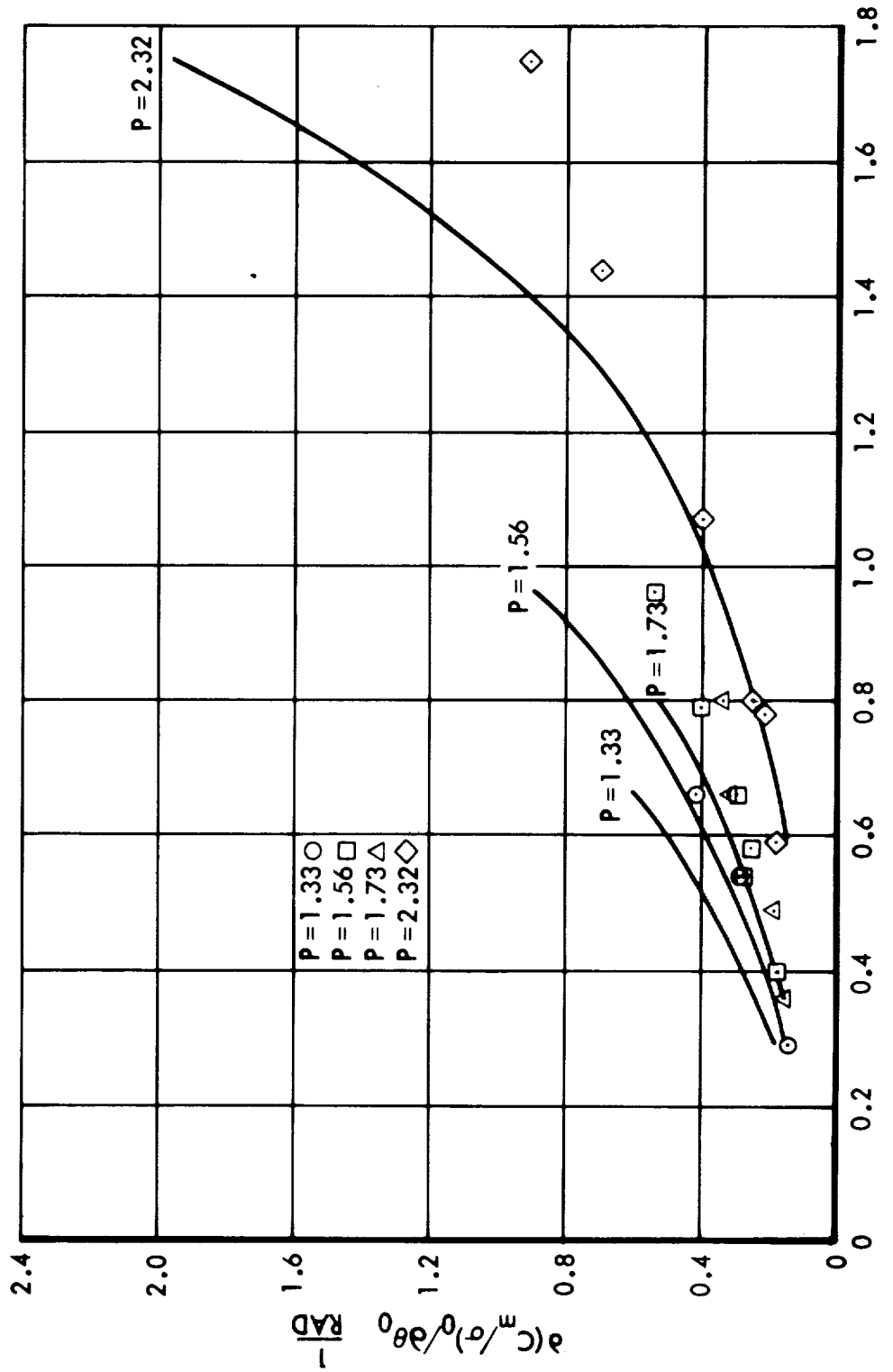

Figure 41. Mean Hub Pitch Moment Aeroelastic Derivative with Respect to Collective Pitch, $\gamma = 5.0$

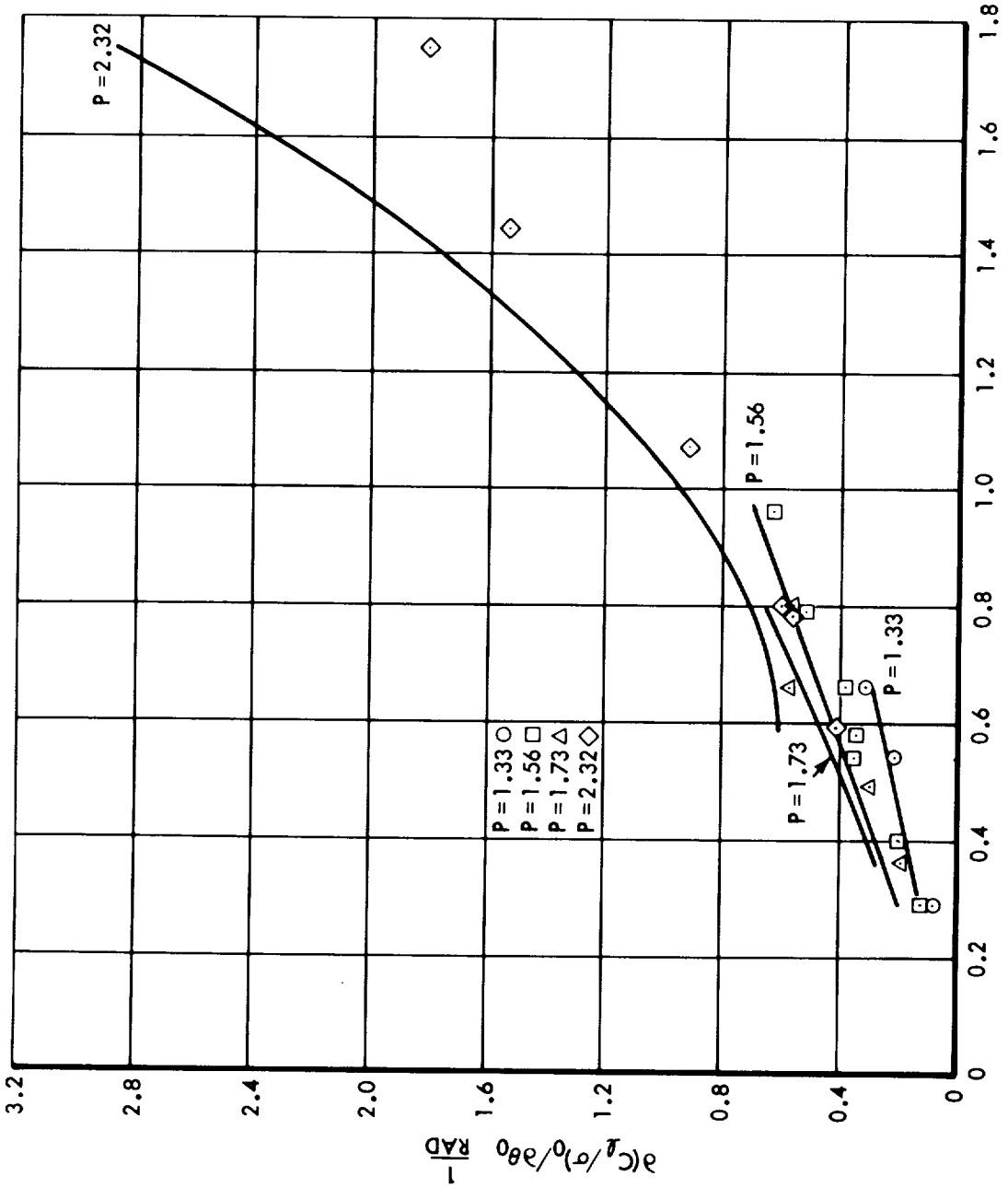

Figure 42. Mean Hub Roll Moment Aeroelastic Derivative with Respect to Collective Pitch, $\gamma = 5.0$

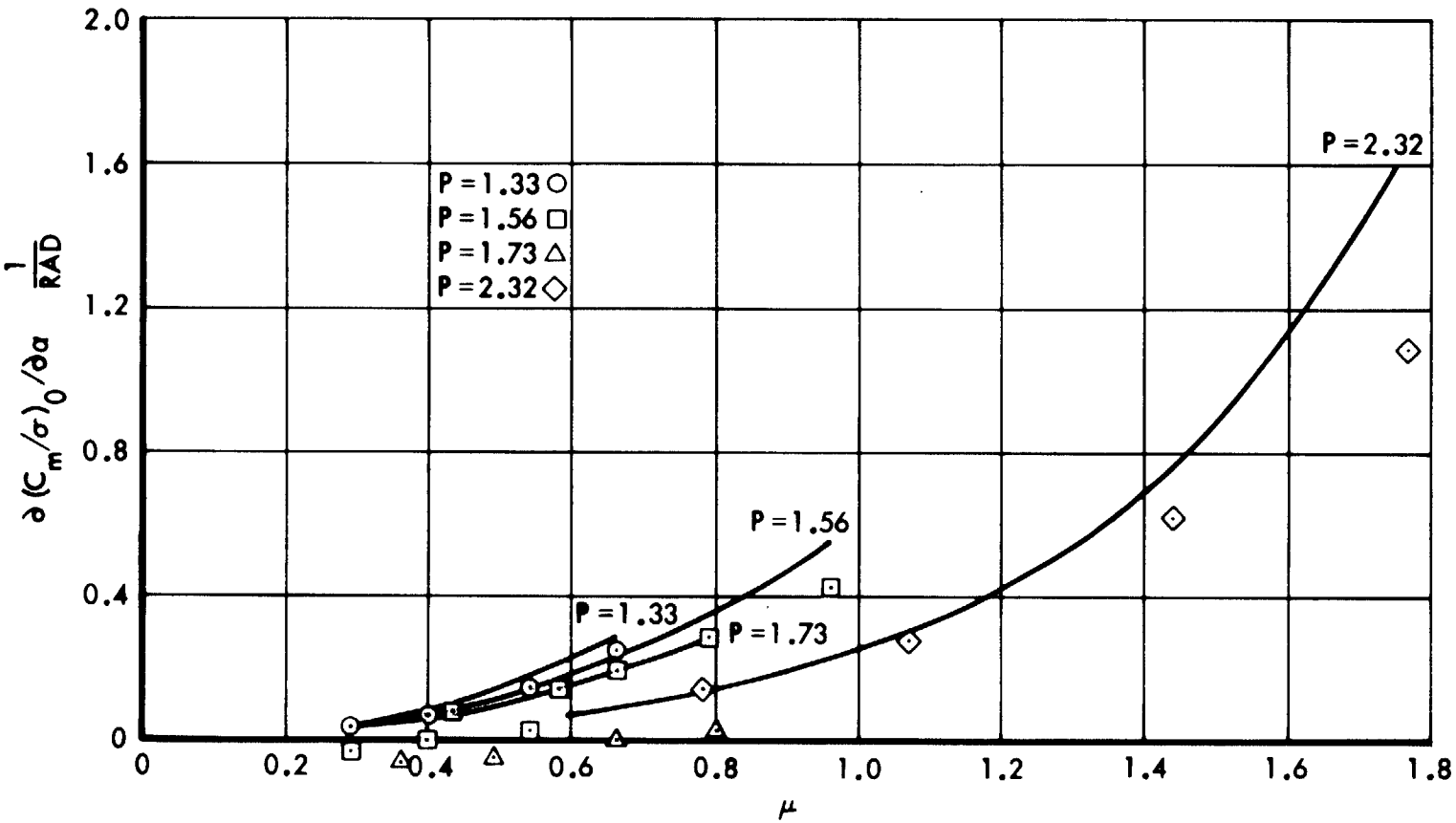

Figure 43. Mean Hub Pitch Moment Aeroelastic Derivative with Respect to Rotor Angle-of-Attack, γ = 5.0

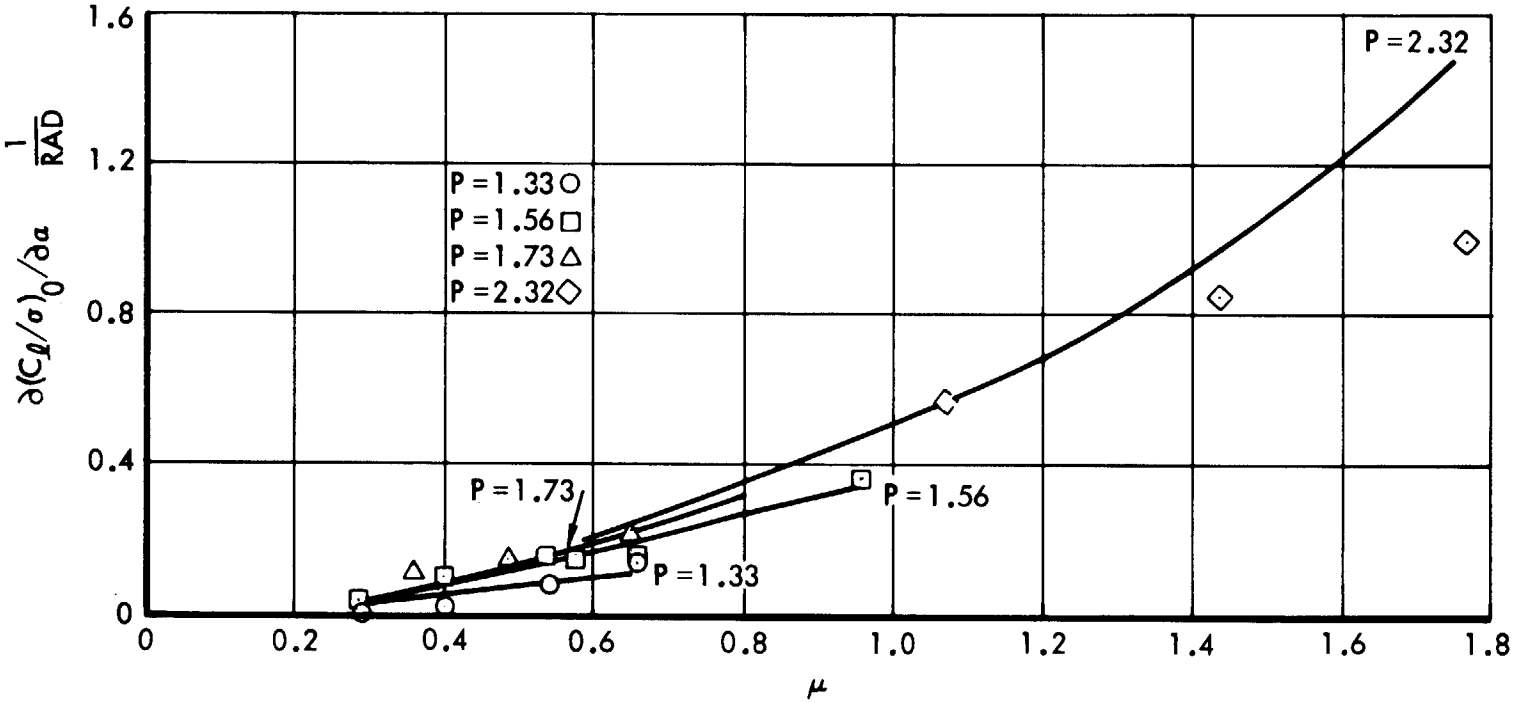

Figure 44. Mean Hub Roll Moment Aeroelastic Derivative with Respect to Rotor Angle-of-Attack, Y = 5.0

Oscillatory aeroelastic derivatives. This section of the report is devoted to the presentation of calculated and experimental values of shaft and swashplate - transmitted oscillatory forces for the fixed-shaft, fixed-swashplate condition. Shaft shear force is a consequence of in-plane motion and is discussed in the section on solutions of in-plane motion equations.

In the section on mean aeroelastic derivatives it was possible to discuss three- and four-blade rotor results together, when suitably nondimensioned, since the results did not depend on the number of blades in the rotor. For oscillatory forces transmitted through the shaft and swashplate however, the number of blades determine the frequency and amplitude of the result. For this reason three-blade and four-blade rotors are treated separately.

The theoretical and experimental results for the 33-foot three-blade rotor are presented first. These are followed by the results for the 7.5-foot four-blade rotor.

The theoretical harmonic response aeroelastic derivatives of hub and swashplate moment coefficient with respect to θ_{1c} and θ_{1s}, divided by solidity, are presented in vector diagrams for the 33-foot three-blade rotor. In stationary axes the hub moment oscillations contain only 3P oscillations but these are conveniently thought of as having been produced by 2P advancing and 4P regressive oscillations relative to coordinates rotating with the rotor. The 2P advancing contributions to the 3P stationary axis hub moment derivatives are shown in Figures 45 and 46, and over the ranges of P and μ for which these analyses are expected to be valid. Figure 46 showing the variations of the hub moment coefficient vectors, divided by solidity, with repect to θ_{1s} shows that at low values of advance ratio, say $\mu = 0.5$ for example, and at low values of rotor blade stiffness ratio, say up to $P = 1.4$, that the 2P contribution to vibratory force is small compared to the mean hub moment produced, as seen in Figure 17. It consists at $P = 1.4$ of nose-down pitch moment of about $\left[\frac{\partial Cm/\sigma}{\partial \theta_{1s}}\right]_{2c} \approx = -.05$ whereas the mean hub moments generated at the same condition are $\left[\frac{\partial Cm/\sigma}{\partial \theta_{1s}}\right]_{o} = .3$ and $\left[\frac{\partial C\ell/\sigma}{\partial \theta_{1s}}\right]_{o} = .34$ or not much more than about $\frac{1}{10}$ of the mean hub moment.

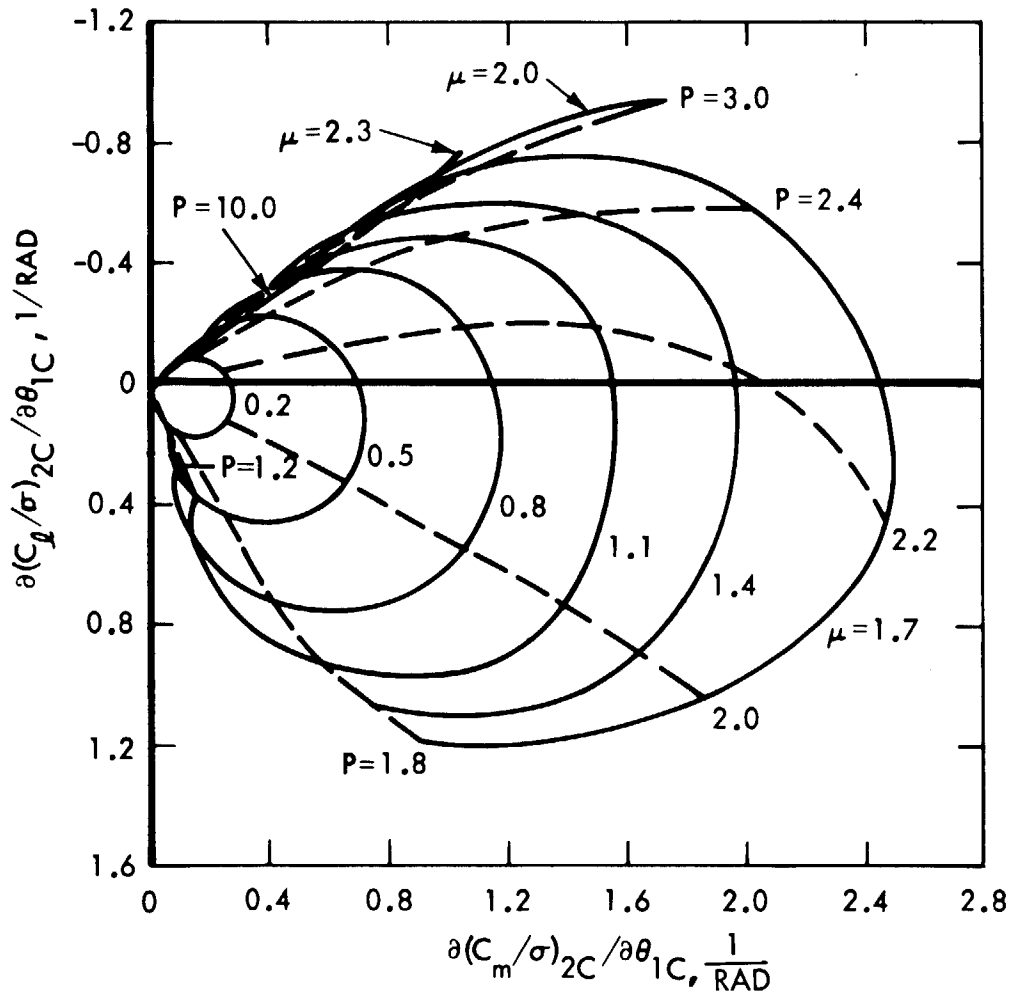

Figure 45. Oscillatory Hub Moment 2P Aeroelastic Derivative With Respect to Lateral Cyclic Pitch, γ = 4.57, Vectors Shown at ψ = 0

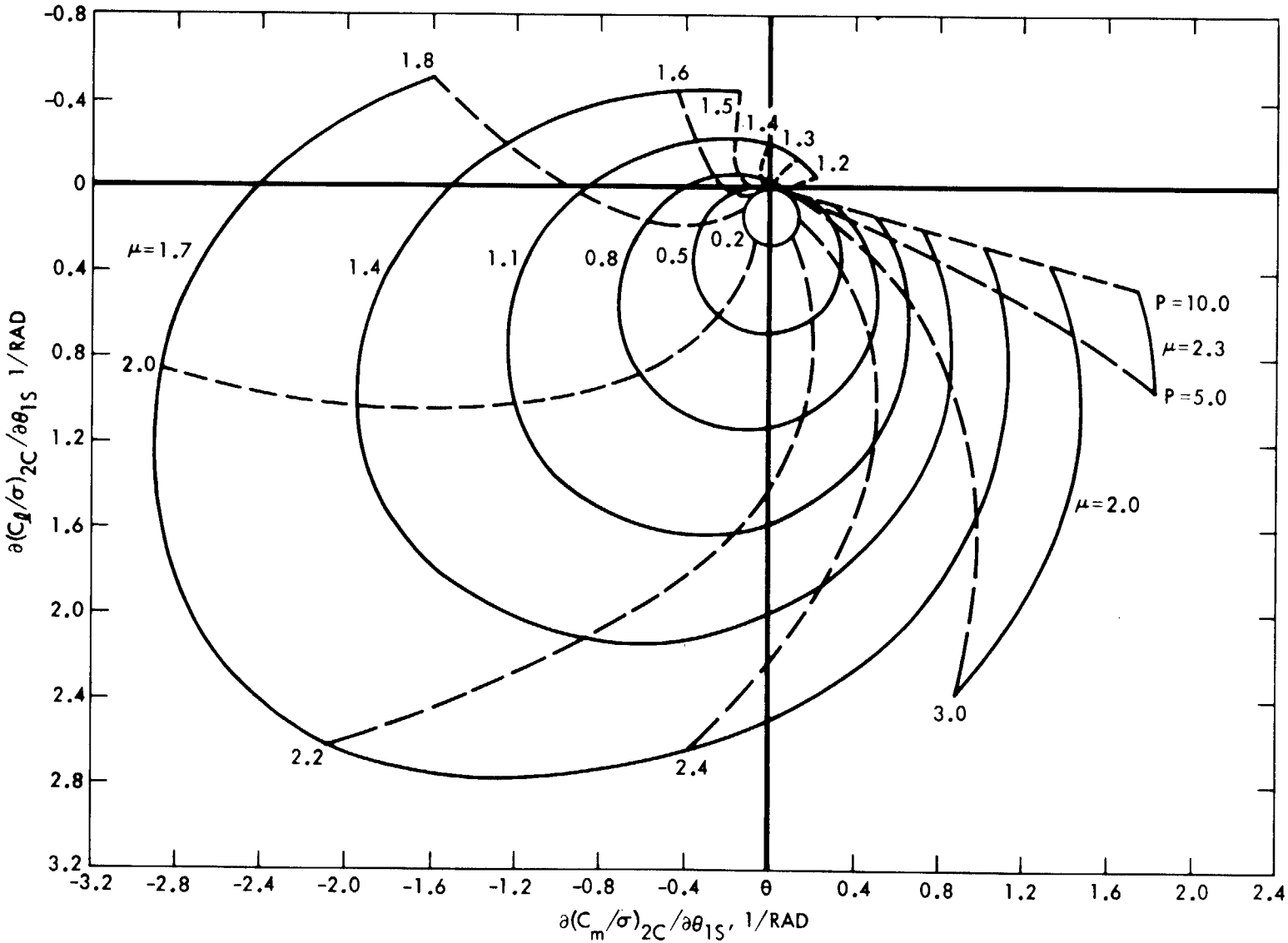

Figure 46. Oscillatory Hub Moment 2P Aeroelastic Derivative With Respect to Longitudinal Cyclic Pitch, $\gamma = 4.57$ Vectors Shown at $\psi = 0$

At P values typically employed in conventional hingeless ratio helicopters, i.e., P = 1.2, the vibratory contribution would be negligible.

It is interesting to note, still at $\mu = .5$, that if P is allowed to reach the neighborhood of 2.0 so that the first flap mode is in resonance, the vibratory contribution can become larger than the mean hub moments produced $\left[\frac{\partial C_m/\sigma}{\partial \theta_{1s}}\right]_{2c} = -.2$ $\left[\frac{\partial C_\ell/\sigma}{\partial \theta_{1s}}\right]_{2c} = .6$

Should the blades be made very stiff, say P = 10, then the vibratory component reduces somewhat but not to as low a value as occurs at low P values.

The same trends continue as advance ratio, μ, increases except that the vibratory contribution grows more rapidly than the mean moment capability.

The 2P vibratory response with respect to θ_{1c} (Figure 45) follows the same general trends as did the component with respect to θ_{1s}.

The theoretical hub moment 2P vibratory derivatives with respect to θ_{1c} and θ_{1s}, shown in Figures 45 and 46, are replotted separately in Figures 47 through 50 versus flap frequency ratio P for the several values of advance ratio μ employed in the wind tunnel tests of the 33-foot rotor. In these plots, comparisons are made with experimental data and it is seen that the general trends are predicted well.

The 4P contributions to the 3P stationary axis hub moment derivatives with respect to θ_{1c} and θ_{1s} are much smaller and less well defined than the 2P contributions. They are displayed in Figures 51 and 52 in general areas for each value of advance ratio, to the same scale as the 2P contributions and are disassembled and displayed versus P in Figures 53 through 56 for the tested values of advance ratio.

The experimental values are very small at low P values and larger at high P values as are the theoretically predicted values, but agreement is erratic.

The swashplate harmonic moment derivatives with respect to θ_{1c} and θ_{1s}, in the 2P contribution to 3P stationary axis moments, display similar behavior

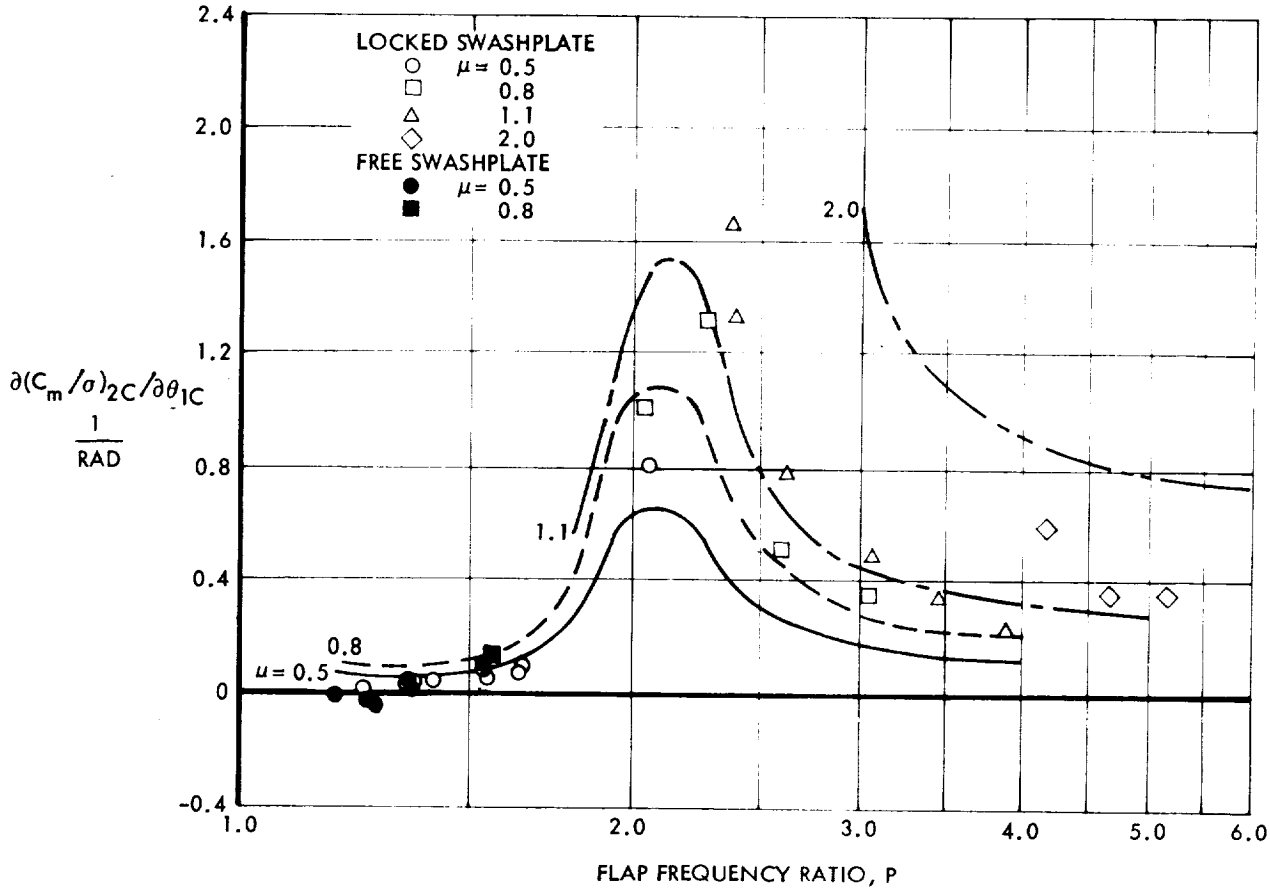

Figure 47. Oscillatory Hub Pitch Moment 2P Aeroelastic Derivative With Respect to Lateral Cyclic Pitch, Vector Component at $\psi = 0$, $\gamma = 4.57$

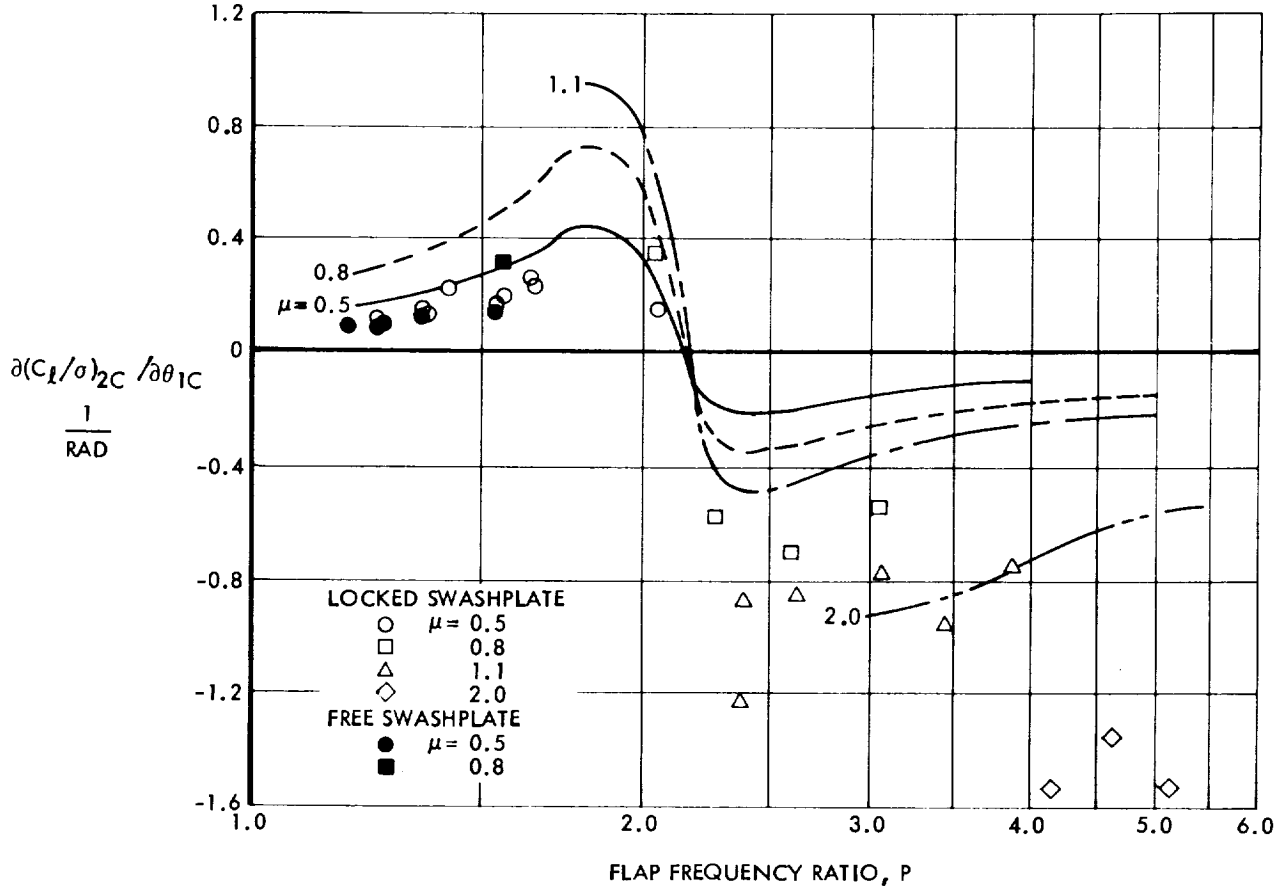

Figure 48. Oscillatory Hub Roll Moment 2P Aeroelastic Derivative With Respect to Lateral Cyclic Pitch, Vector Component at $\psi = 0$, $\gamma = 4.57$

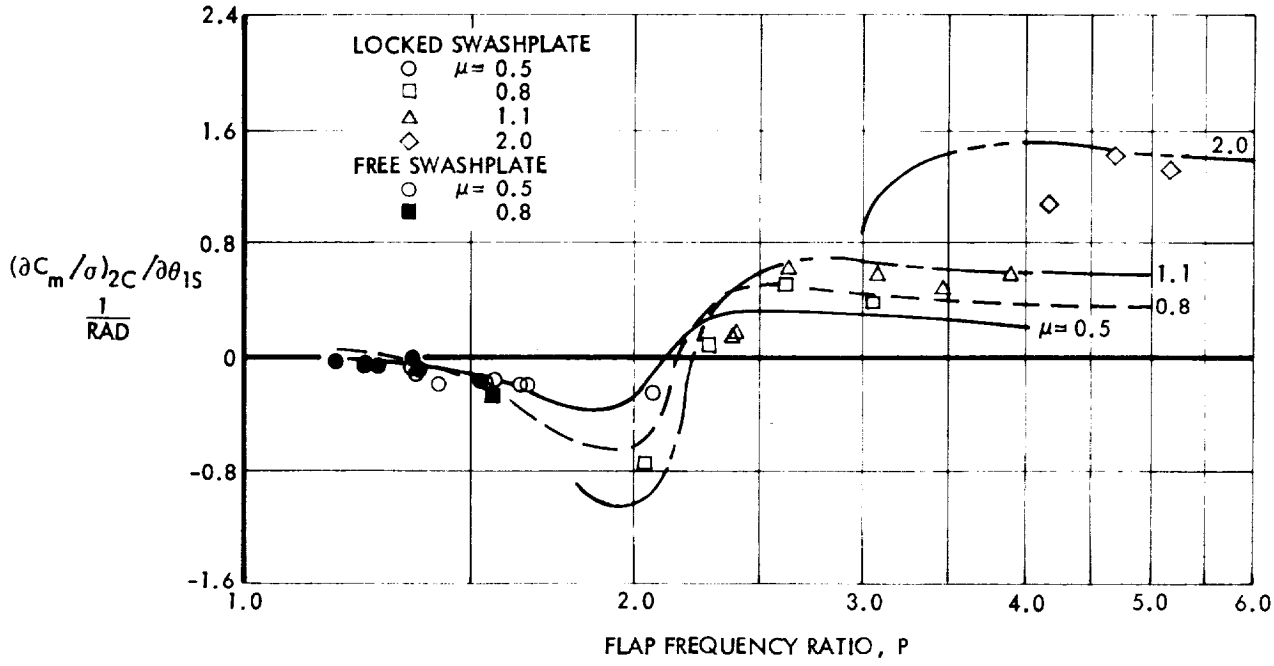

Figure 49. Oscillatory Hub Pitch Moment 2P Aeroelastic Derivative With Respect to Longitudinal Cyclic Pitch, Vector Component at $\psi = 0$, $\gamma = 4.57$

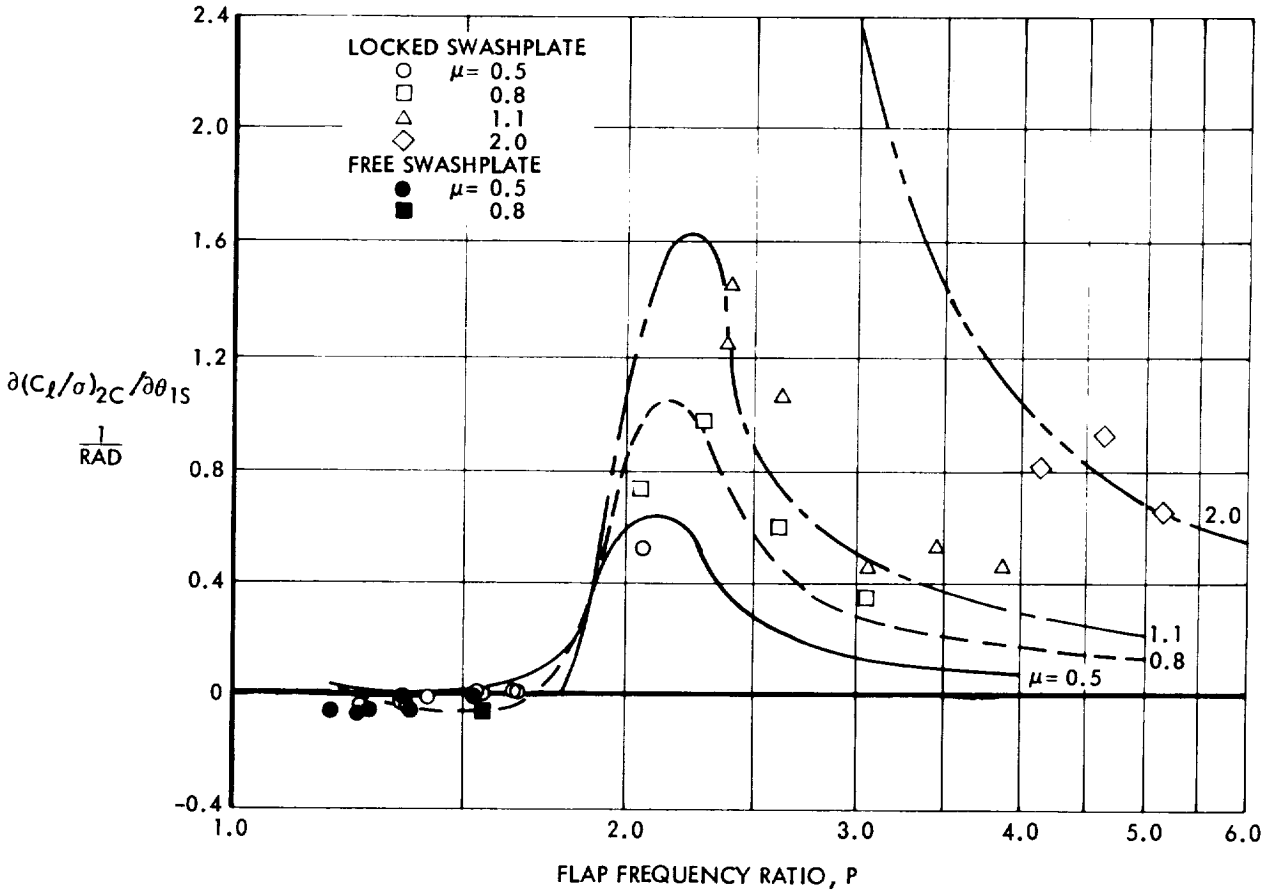

Figure 50. Oscillatory Hub Roll Moment 2P Aeroelastic Derivative With Respect to Longitudinal Cyclic Pitch, Vector Component at $\Psi = 0$, $\gamma = 4.57$

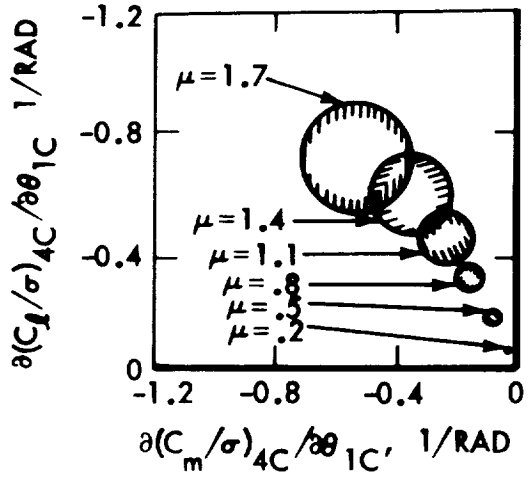

Figure 51. Oscillatory Hub Moment 4P Aeroelastic Derivative with Respect to Lateral Cyclic Pitch, $\gamma = 4.57$.

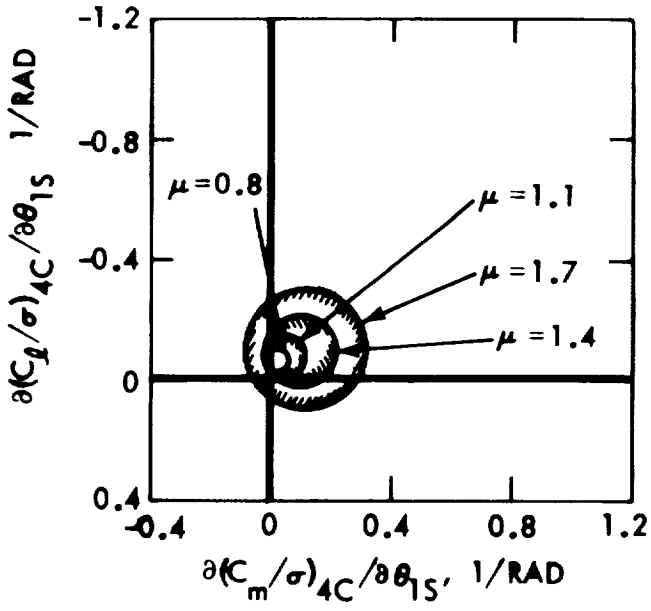

Figure 52. Oscillatory Hub Moment 4P Aeroelastic Derivative with Respect to Longitudinal Cyclic Pitch, $\gamma = 4.57$.

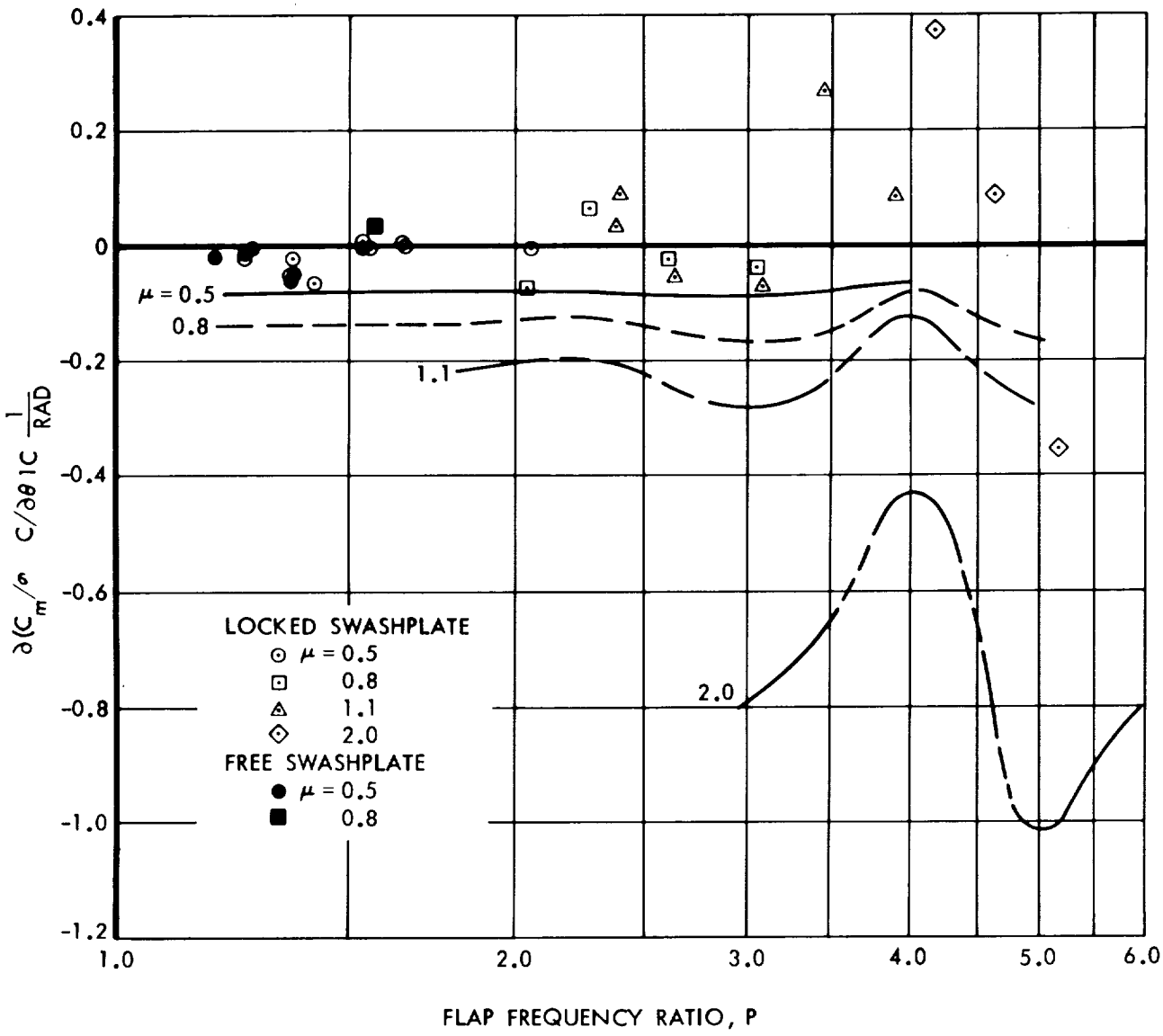

Figure 53. Oscillatory Hub Pitch Moment 4P Aeroelastic Derivative With Respect to Lateral Cyclic Pitch, Vector Component Shown at $\psi = 0$, $\gamma = 4.57$

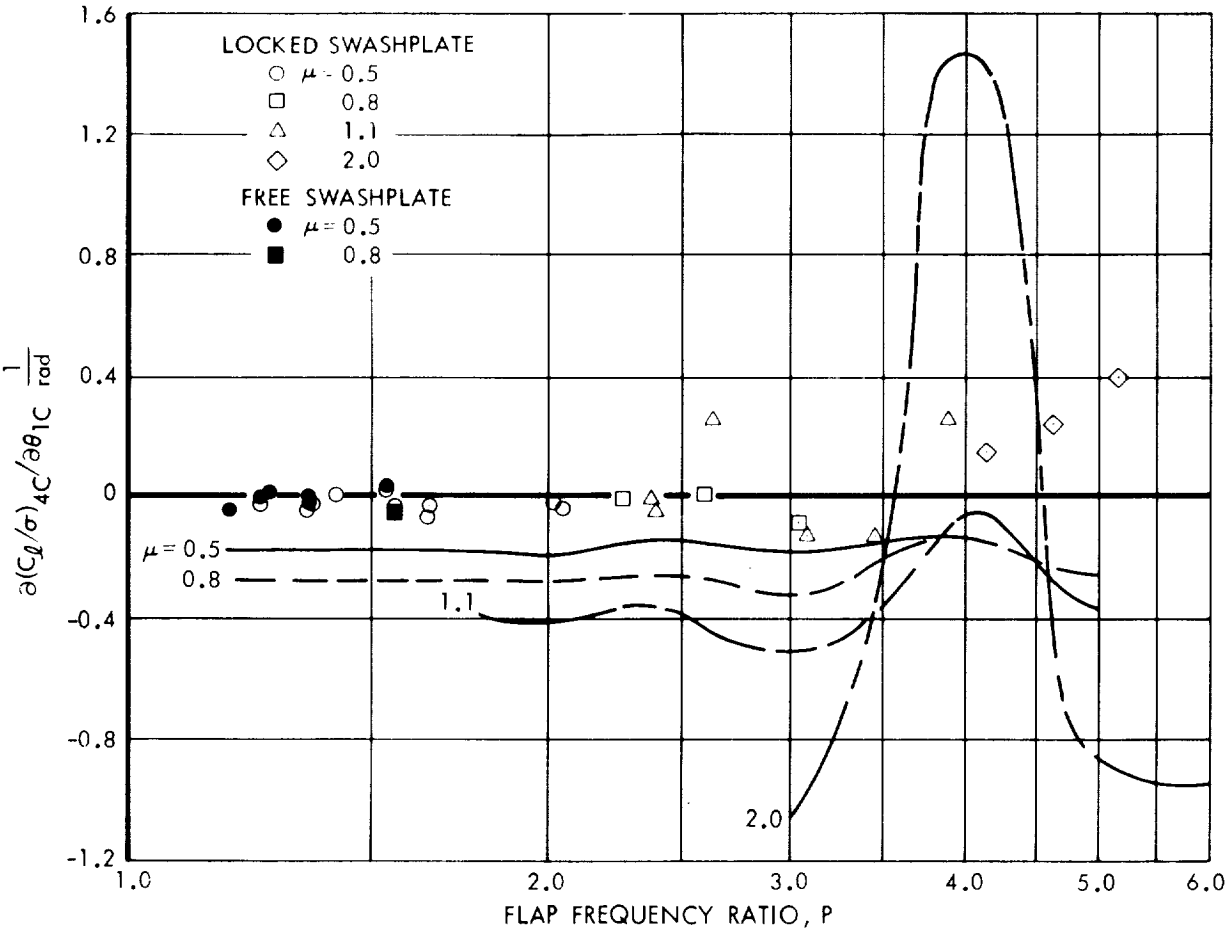

Figure 54. Oscillatory Hub Roll Moment 4P Aeroelastic Derivative With Respect to Lateral Cyclic Pitch, Vector Component Shown at $\psi = 0$, $\gamma = 4.57$

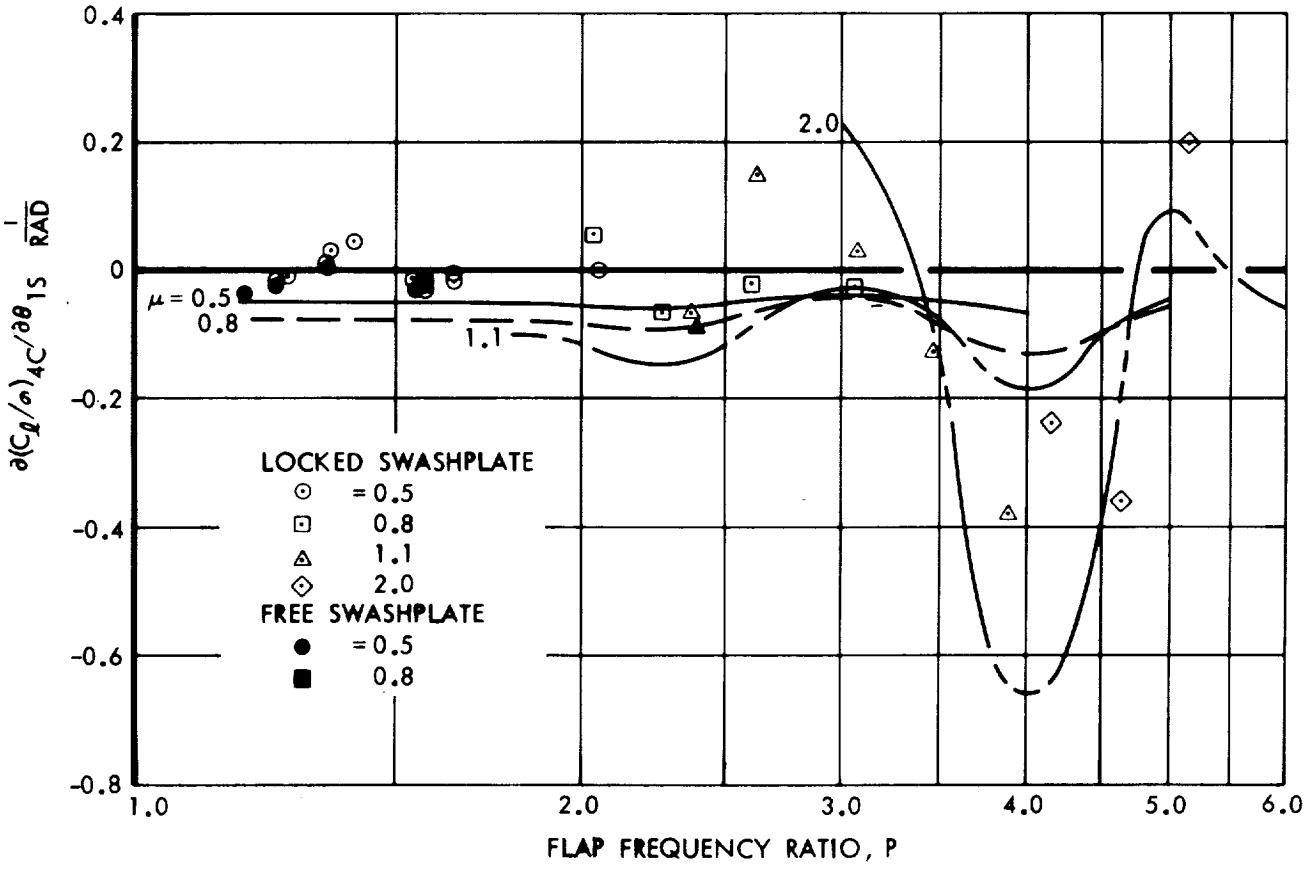

Figure 56. Oscillatory Hub Roll Moment 4P Aeroelastic Derivative With Respect to Longitudinal Cyclic Pitch, Vector Component Shown at $\Psi = 0$, $\gamma = 4.57$

to the hub moment derivatives. As with the mean aeroelastic derivatives, the 60° skewing of the swashplate derivative ahead of the hub values due to the cant angle $\psi_o = 60^{\circ}$ is evident again in Figures 57 and 58.

Figures 59 through 62 show the 2P components of the swashplate derivative vectors plotted versus P at the tested values of μ and compares them with experimental data. Although there are not many experimental points the theory agrees in sign and order of magnitude with the experimental data.

The 4P contribution to the 3P stationary axis swashplate derivatives with respect to θ_{1c} and θ_{1s} are shown in Figures 63 and 64. The detailed variation with P is complicated but within relatively small areas at each value of μ. The areas are shown. The detailed variation with P and μ of each 4P component is shown in Figures 65 through 68 compared to experiment. Agreement is comparable with the 2P swashplate moments.

Rotor thrust oscillation due to cyclic pitch application is next shown theoretically for the 33-foot 3-blade rotor - no experimental data is available. Thrust oscillations occur in stationary axes as harmonics of the product of number of blades and shaft rotation rate $b\Omega$. Harmonics higher than the first are believed to be very small for this rotor; therefore only the first harmonic 3P components are shown.

The sine and cosine components of the thrust coefficient divided by solidity, C_T/σ, aeroelastic derivatives with respect to θ_{1c} and θ_{1s}, are shown in Figures 69 through 72. It should be noted that at $\psi = 0$ the position of number one blade is aft.

It should be noted that the sine component due to θ_{1s} and the cosine component due to θ_{1c} both peak at a flap frequency ratio of P = 3.0.

The residual harmonic forces remaining when $\theta_{1c} = \theta_{1s} = \alpha = 0$ and $\theta_{.75R} = 1.5^{\circ}$ are shown in Figures 73 through 82.

The two components, sine and cosine, of the thrust coefficients, divided by solidity, C_T/σ produced by $\theta_{.75R} = 1.5$, $\theta_t R = -9.43^{\circ}$, and $\beta_o = 2.25^{\circ}$, are shown in Figures 73 and 74 versus flap frequency ratio P for values of advance ratio μ tested. No comparison with test data, however, is available.

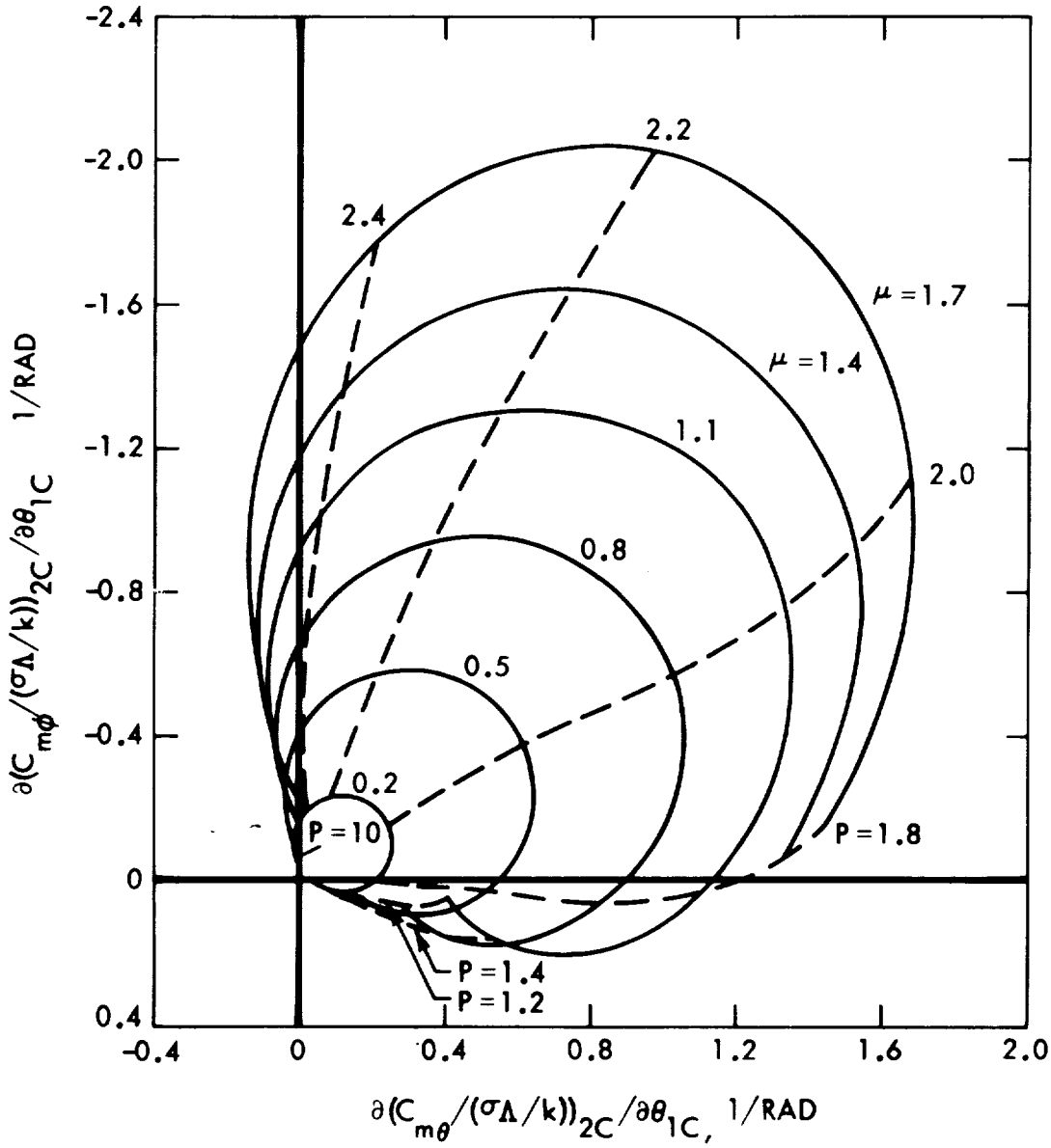

Figure 57. Oscillatory Swashplate Moment 2P Aeroelastic Derivatives With Respect to Lateral Cyclic Pitch. Vectors Shown at $\psi = 0$, $\gamma = 4.57$

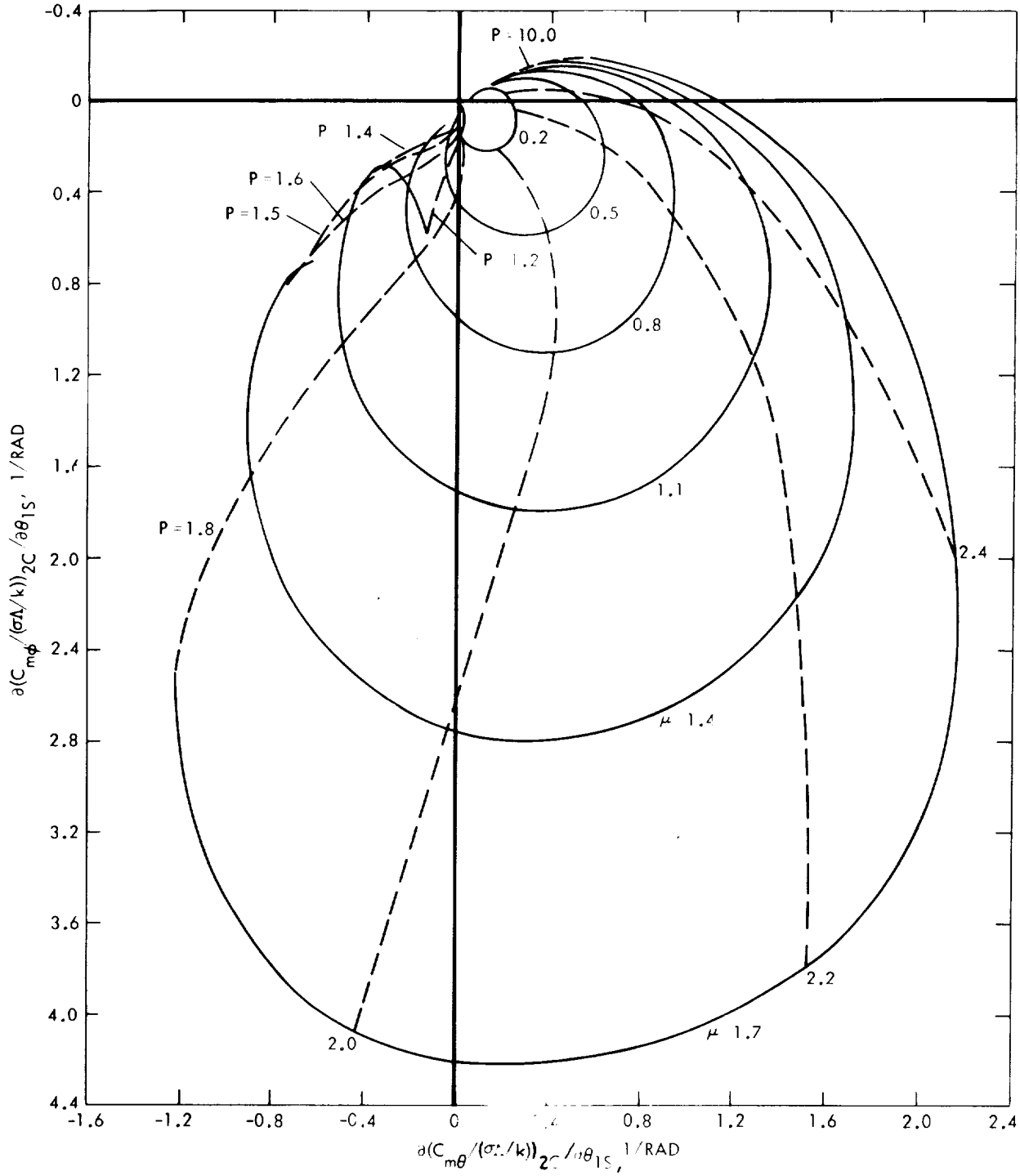

Figure 58. Oscillatory Swashplate Moment 2P Aeroelastic Derivative With Respect to Longitudinal Cyclic Pitch. Vectors Shown at ψ = 0, γ = 4.57

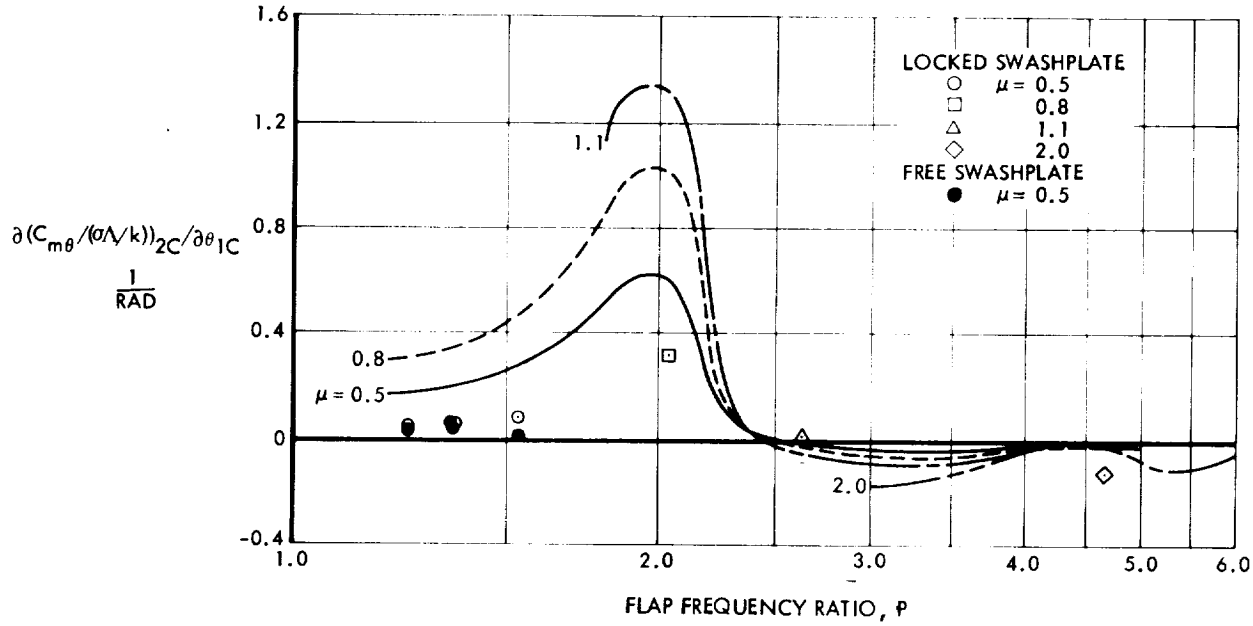

Figure 59. Oscillatory Swashplate Pitch Moment 2P Aeroelastic Derivative With Respect to Lateral Cyclic Pitch. Vector Component at $\psi = 0$, $\Upsilon = 4.57$

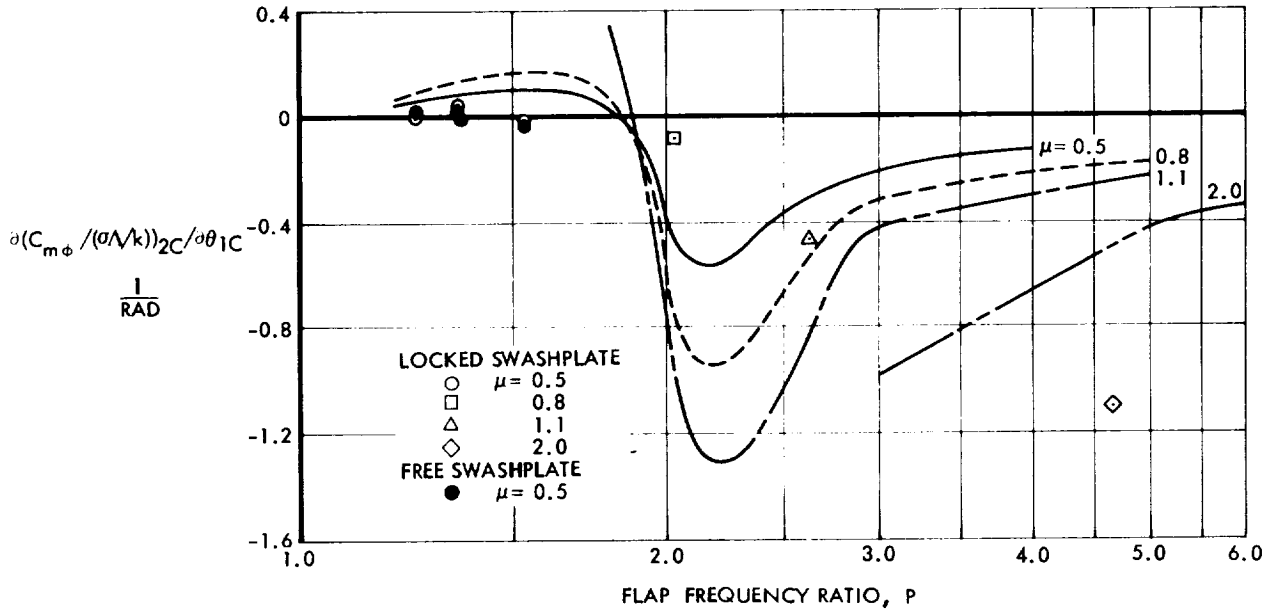

Figure 60. Oscillatory Swashplate Roll Moment 2P Aeroelastic Derivative With Respect to Lateral Cyclic Pitch. Vector Component at $\Psi = 0$, $\gamma = 4.57$

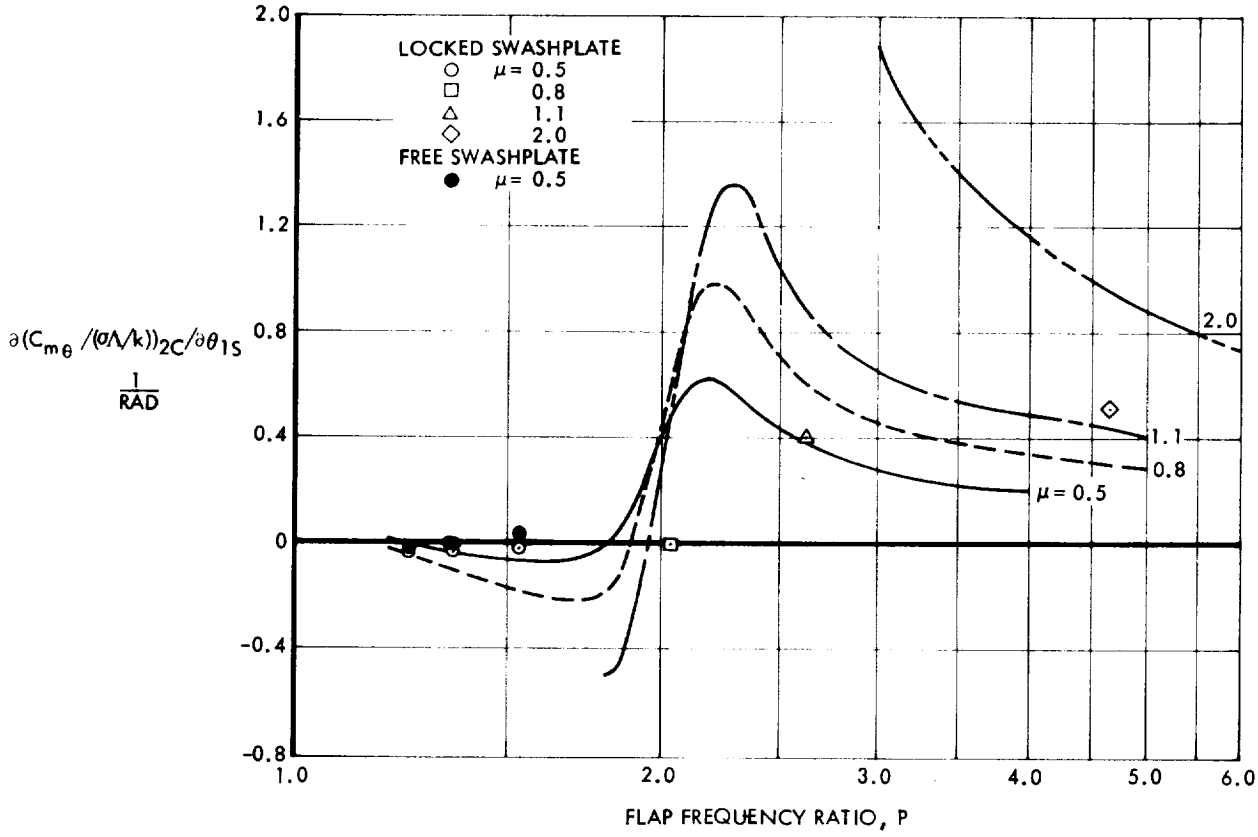

Figure 61. Oscillatory Swashplate Pitch Moment 2P Aeroelastic Derivative With Respect to Longitudinal Cyclic Pitch. Vector Component at $\psi = 0$, $\gamma = 4.57$

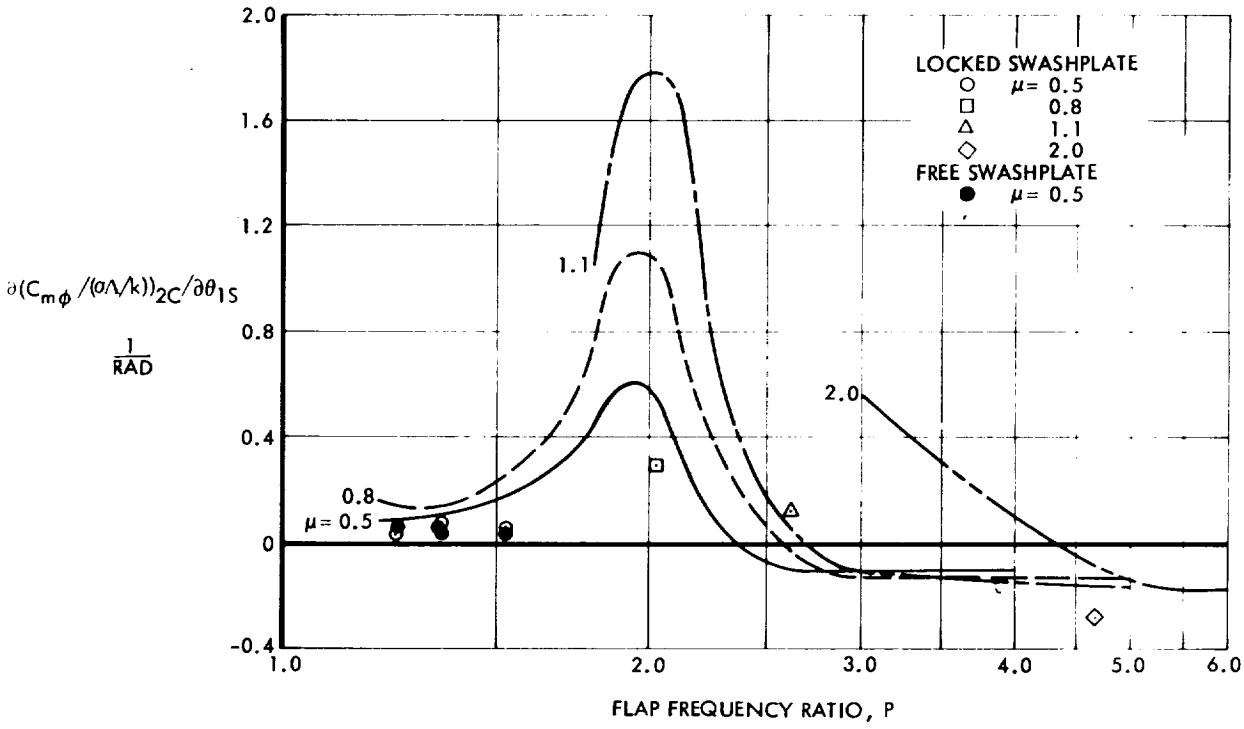

Figure 62. Oscillatory Swashplate Roll Moment 2P Aeroelastic Derivative With Respect to Longitudinal Cyclic Pitch. Vector Component at $\psi = 0$, $\Upsilon = 4.57$

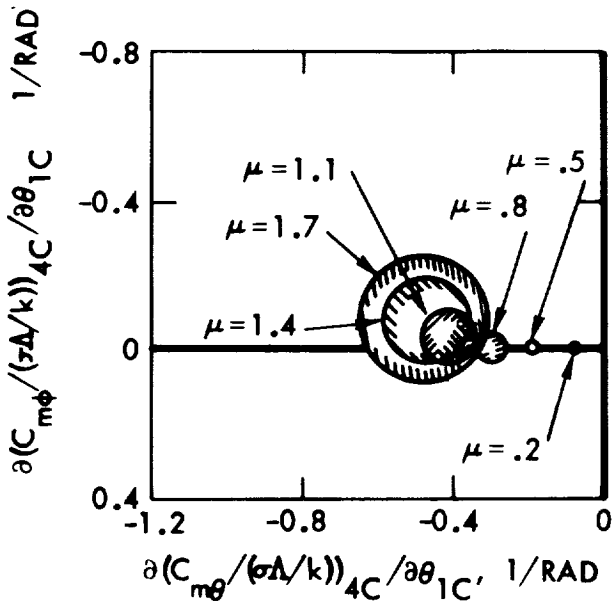

Figure 63. Oscillatory Swashplate Moment 4P Aeroelastic Derivative with Respect to Lateral Cyclic Pitch, $\gamma = 4.57$

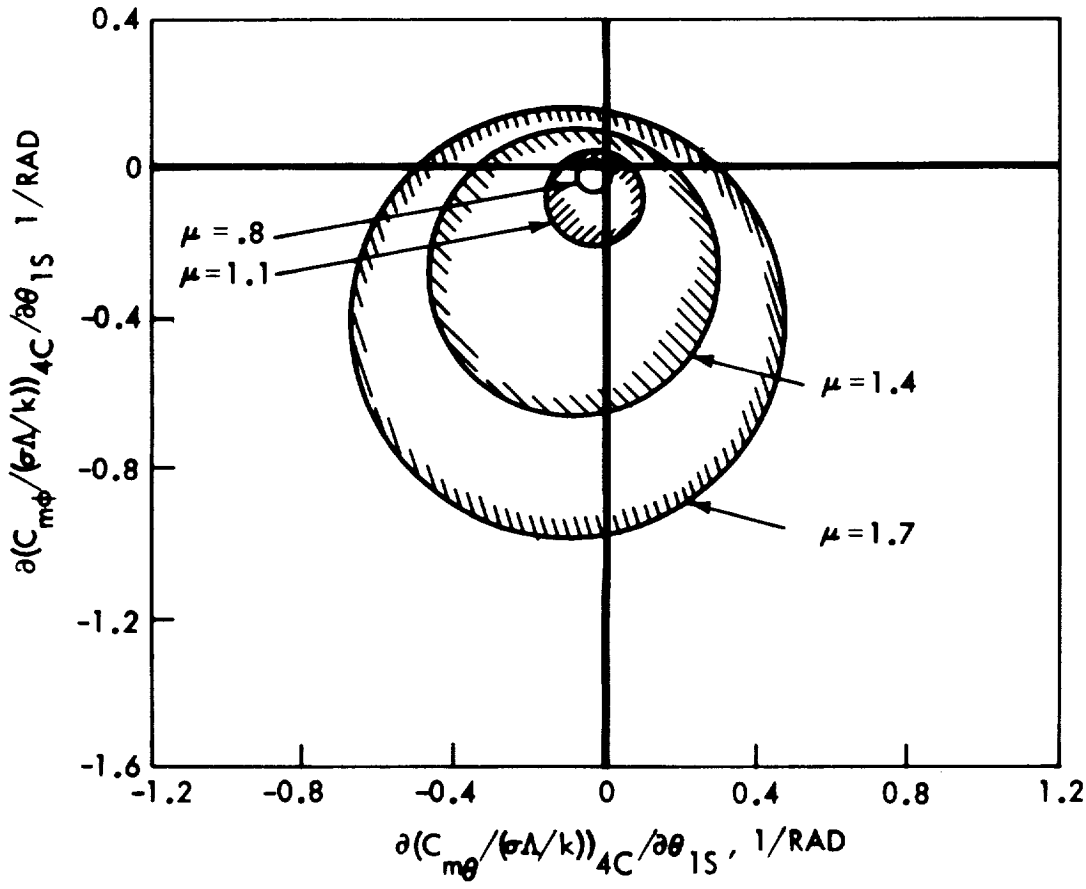

Figure 64. Oscillatory Swashplate Moment 4P Aeroelastic Derivatives with Respect to Longitudinal Cyclic Pitch, $\gamma = 4.57$

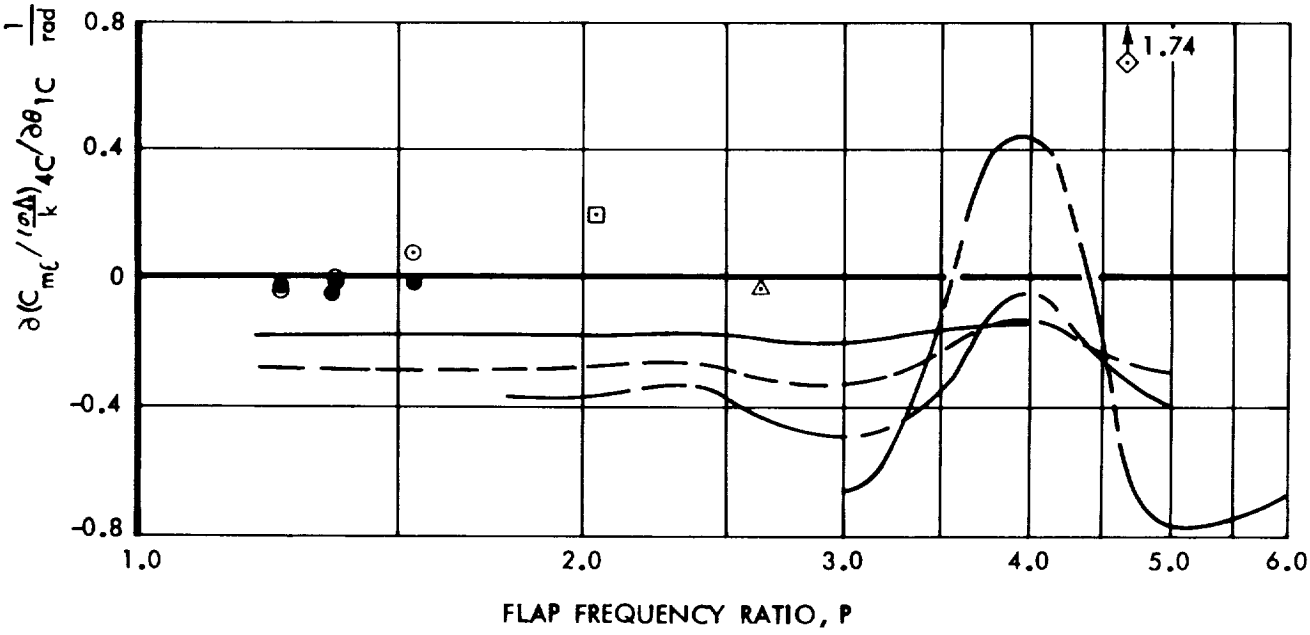

Figure 65. Oscillatory Swashplate Pitch Moment 4P Aeroelastic Derivative With Respect to Lateral Cyclic Pitch. Vector Component at ψ = 0, γ = 4.57

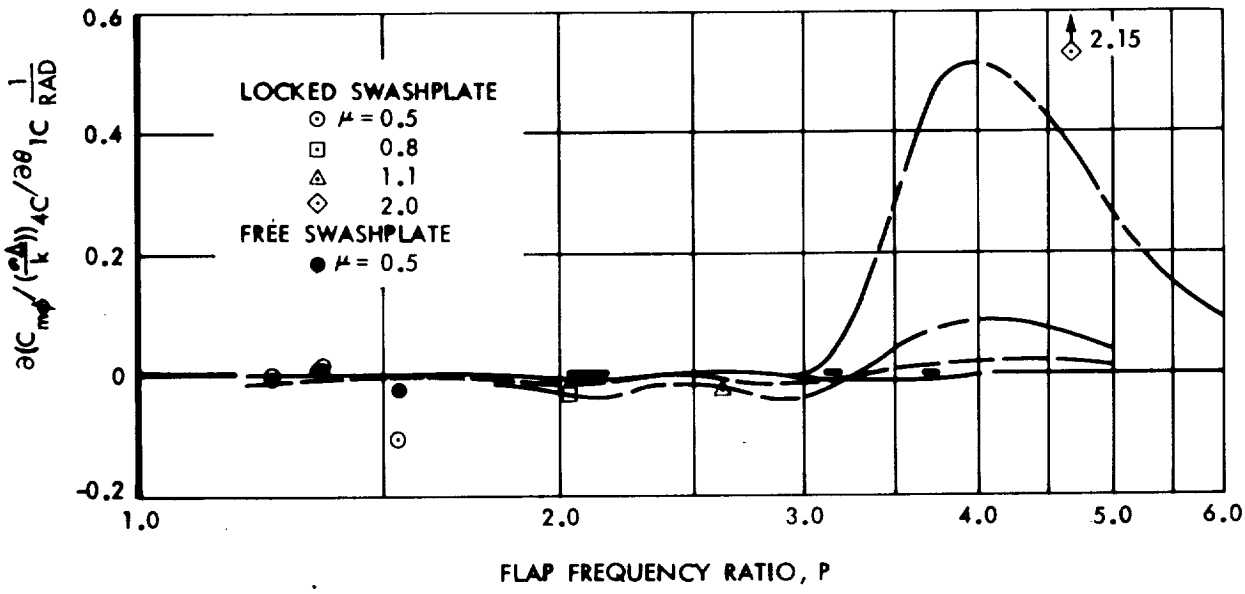

Figure 66. Oscillatory Swashplate Roll Moment 4P Aeroelastic Derivative With Respect to Lateral Cyclic Pitch. Vector Component at $\Psi = 0$, $\gamma = 4.57$

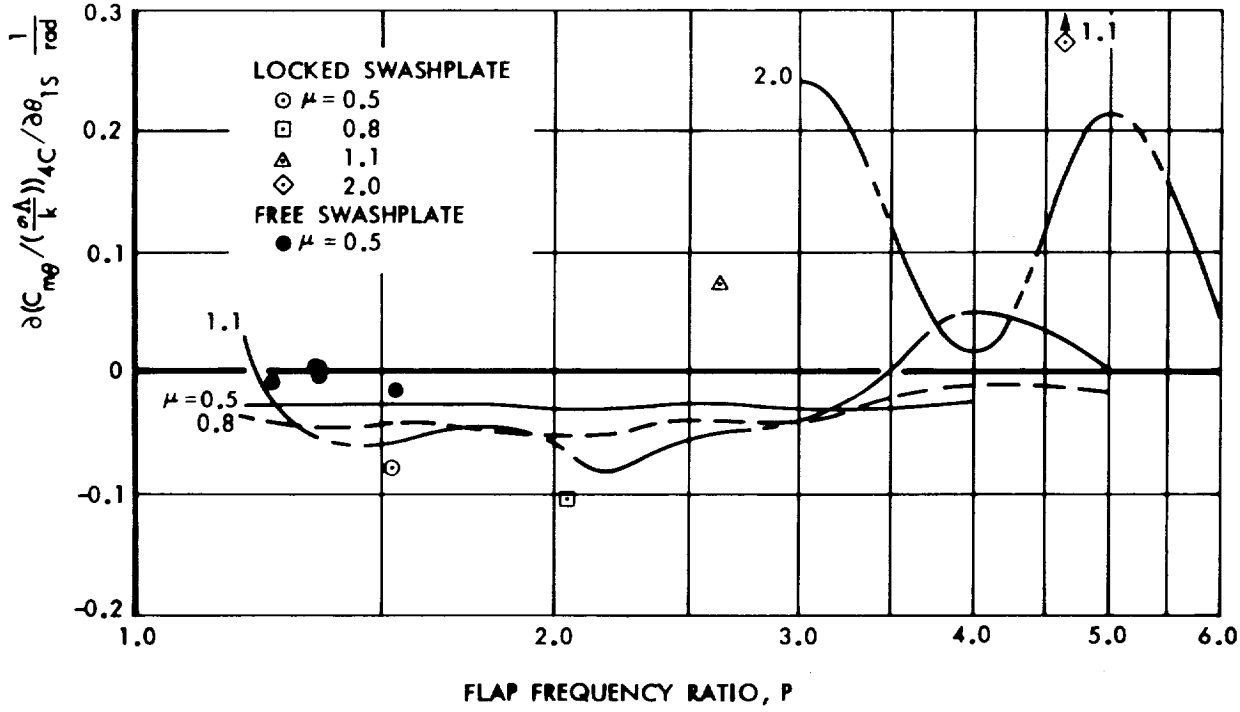

Figure 67. Oscillatory Swashplate Pitch Moment 4P Aeroelastic Derivative With Respect to Longitudinal Cyclic Pitch. Vector Component Shown at $\psi = 0$, $\gamma = 4.57$

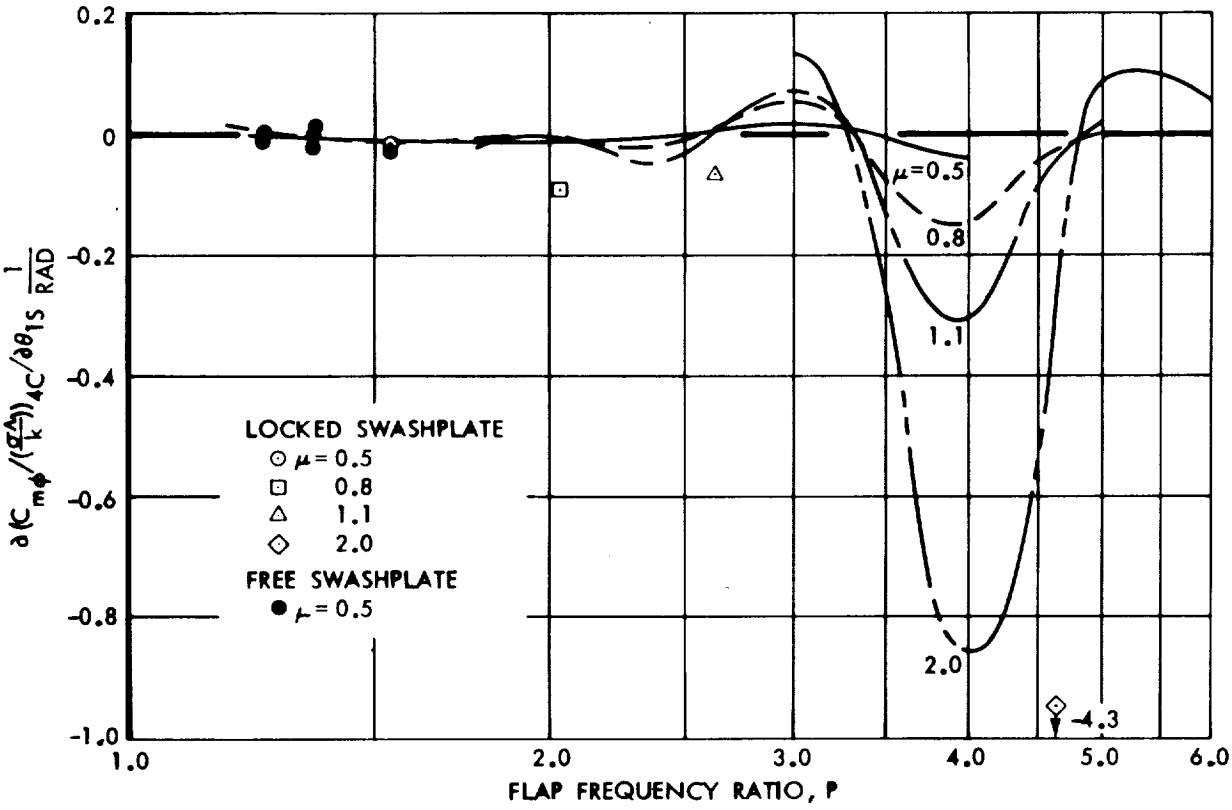

Figure 68. Oscillatory Swashplate Roll Moment 4P Aeroelastic Derivative With Respect to Longitudinal Cyclic Pitch. Vector Component Shown at $\psi = 0$, $\gamma = 4.57$

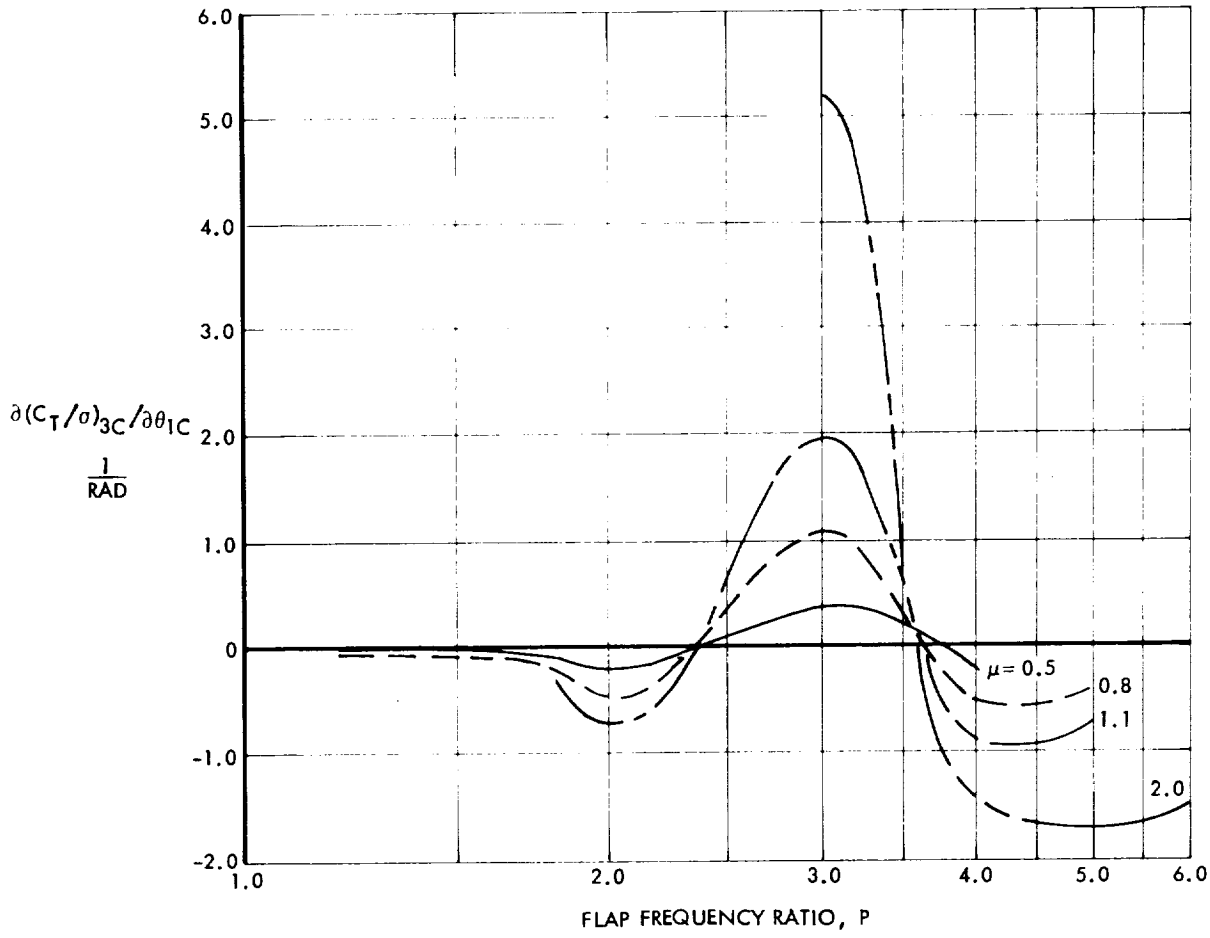

Figure 69. Oscillatory Thrust 3P Aeroelastic Cosine Derivative With Respect to Lateral Cyclic Pitch, $\gamma = 4.57$

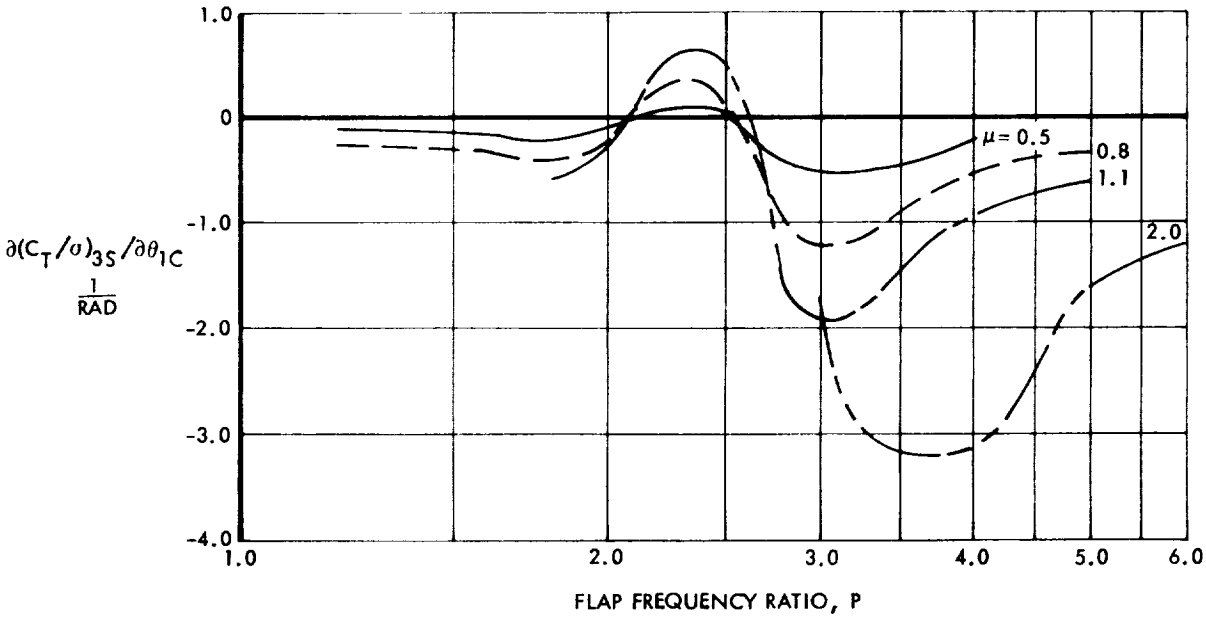

Figure 70. Oscillatory Thrust 3P Aeroelastic Sine Derivative With Respect to Lateral Cyclic Pitch, $\beta = 4.57$

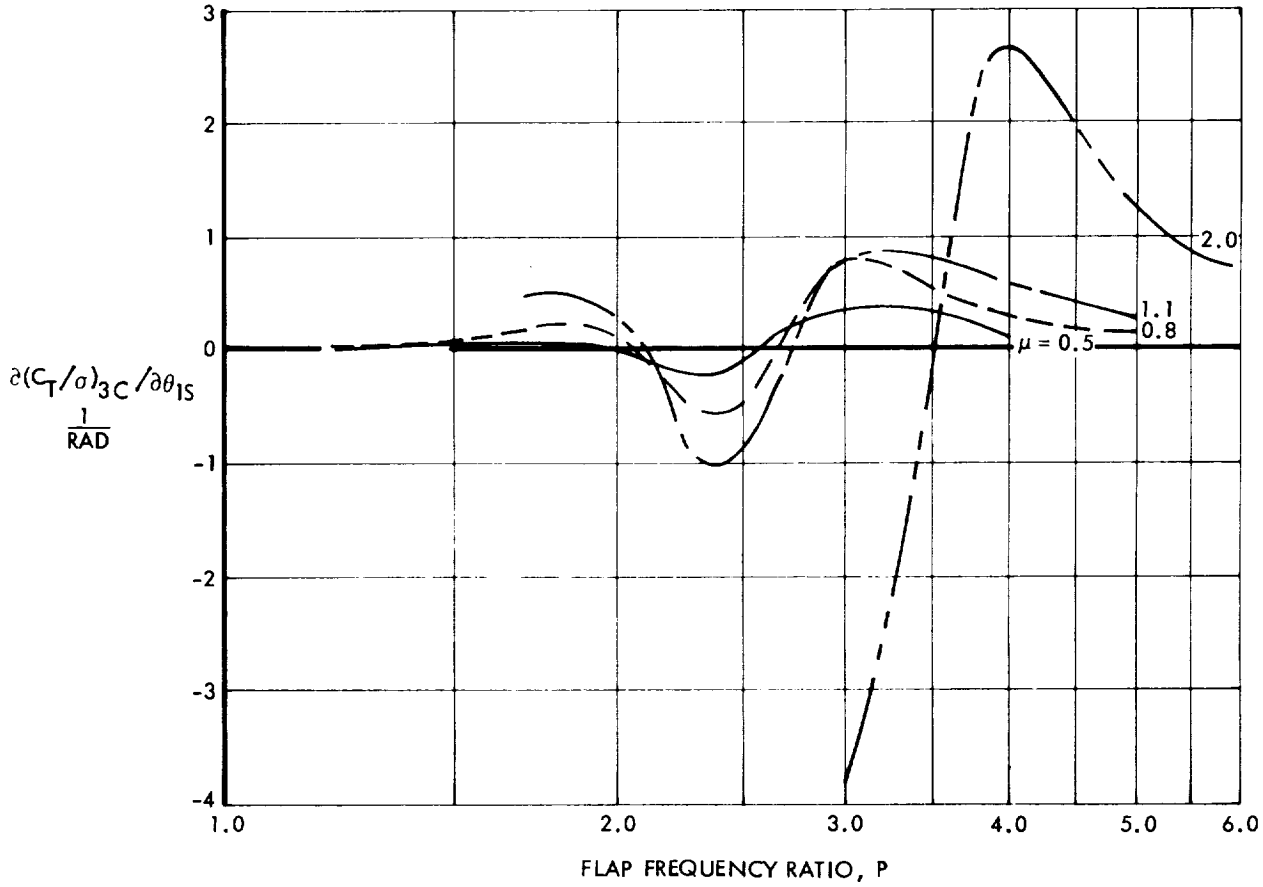

Figure 71. Oscillatory Thrust 3P Aeroelastic Cosine Derivative With Respect to Longitudinal Cyclic Pitch, $\gamma = 4.57$

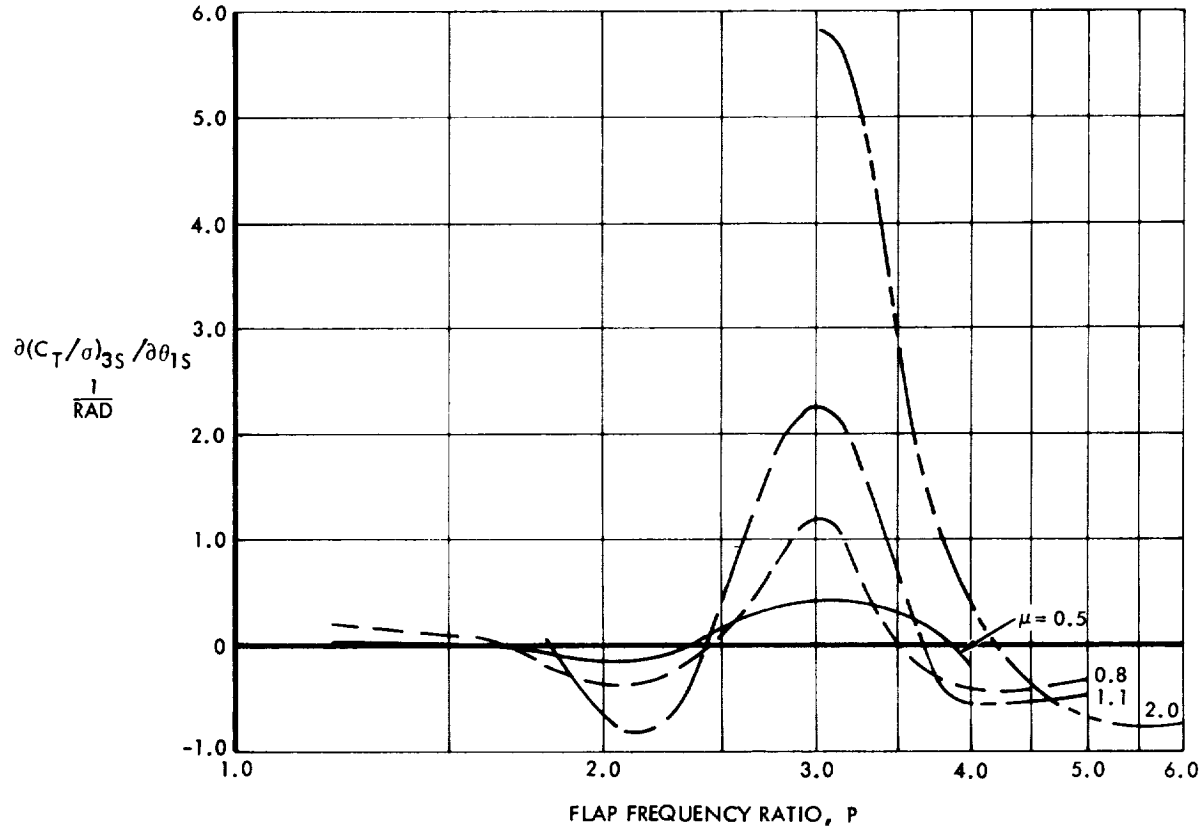

Figure 72. Oscillatory Thrust 3P Aeroelastic Sine Derivative With Respect to Longitudinal Cyclic Pitch, $\gamma = 4.57$

Theoretical hub and swashplate coefficient residual 2P and 4P moments are similarly displayed in Figures 73 through 82, and compared with experimental residual data.

It should be remarked, in concluding the three-blade case, that the residual mean and harmonic rotor shaft forces may be combined with shaft force derivatives factored by the appropriate cyclic pitch angles to fully reproduce the complete dynamic state experienced by the 33-foot 3-blade rotor under any tested condition.

In summary, a complete rotor shaft and swashplate moment and force steady oscillatory state may be assembled for any combination of cyclic pitch components, within the linear range, for the 33-foot 3-blade rotor from plotted coefficients as follows:

$$\frac{Cm}{\sigma} = \left(\frac{Cm}{\sigma}\right)_o + \left[\left(\frac{Cm}{\sigma}\right)_{2c} + \left(\frac{Cm}{\sigma}\right)_{4c}\right] \cos 3\psi + \left[\left(\frac{C\ell}{\sigma}\right)_{2c} - \left(\frac{C\ell}{\sigma}\right)_{4c}\right] \sin 3\psi$$

$$+ \left\{\left(\frac{\partial \frac{Cm}{\sigma}}{\partial \theta_{1c}}\right)_o + \left[\left(\frac{\partial \frac{Cm}{\sigma}}{\partial \theta_{1c}}\right)_{2c} + \left(\frac{\partial \frac{Cm}{\sigma}}{\partial \theta_{1c}}\right)_{4c}\right] \cos 3\psi + \left[\left(\frac{\partial \frac{C\ell}{\sigma}}{\partial \theta_{1c}}\right)_{2c} - \left(\frac{\partial \frac{C\ell}{\sigma}}{\partial \theta_{1c}}\right)_{4c}\right] \sin 3\psi \right\} \theta_{1c}$$

$$+ \left\{\left(\frac{\partial \frac{Cm}{\sigma}}{\partial \theta_{1s}}\right)_o + \left[\left(\frac{\partial \frac{Cm}{\sigma}}{\partial \theta_{1s}}\right)_{2c} + \left(\frac{\partial \frac{Cm}{\sigma}}{\partial \theta_{1s}}\right)_{4c}\right] \cos 3\psi + \left[\left(\frac{\partial \frac{C\ell}{\sigma}}{\partial \theta_{1s}}\right)_{2c} - \left(\frac{\partial \frac{C\ell}{\sigma}}{\partial \theta_{1s}}\right)_{4c}\right] \sin 3\psi \right\} \theta_{1s}$$

$$\frac{C\ell}{\sigma} = \left(\frac{C\ell}{\sigma}\right)_o + \left[\left(\frac{C\ell}{\sigma}\right)_{2c} + \left(\frac{C\ell}{\sigma}\right)_{4c}\right] \cos 3\psi + \left[-\left(\frac{Cm}{\sigma}\right)_{2c} + \left(\frac{Cm}{\sigma}\right)_{4c}\right] \sin 3\psi$$

$$+ \left\{\left(\frac{\partial \frac{C\ell}{\sigma}}{\partial \theta_{1c}}\right)_o + \left[\left(\frac{\partial \frac{C\ell}{\sigma}}{\partial \theta_{1c}}\right)_{2c} + \left(\frac{\partial \frac{C\ell}{\sigma}}{\partial \theta_{1c}}\right)_{4c}\right] \cos 3\psi + \left[-\left(\frac{\partial \frac{Cm}{\sigma}}{\partial \theta_{1c}}\right)_{2c} + \left(\frac{\partial \frac{Cm}{\sigma}}{\partial \theta_{1c}}\right)_{4c}\right] \sin 3\psi \right\} \theta_{1c}$$

$$+ \left\{\left(\frac{\partial \frac{C\ell}{\sigma}}{\partial \theta_{1s}}\right)_o + \left[\left(\frac{\partial \frac{C\ell}{\sigma}}{\partial \theta_{1s}}\right)_{2c} + \left(\frac{\partial \frac{C\ell}{\sigma}}{\partial \theta_{1s}}\right)_{4c}\right] \cos 3\psi + \left[-\left(\frac{\partial \frac{Cm}{\sigma}}{\partial \theta_{1s}}\right)_{2c} + \left(\frac{\partial \frac{Cm}{\sigma}}{\partial \theta_{1s}}\right)_{4c}\right] \sin 3\psi \right\} \theta_{1s}$$

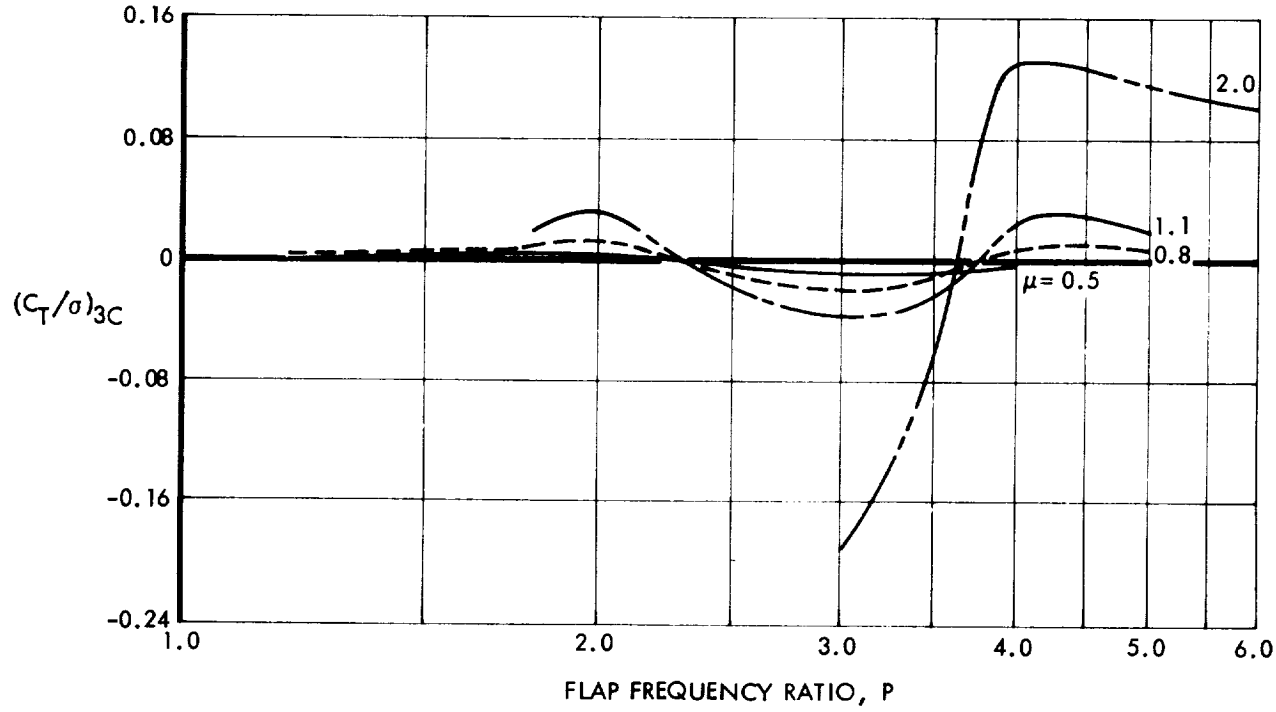

Figure 73. Residual Thrust 3P Cosine Component Due to $\beta_o = 2.25^\circ$, $\theta_t R = -9.43^\circ$ and $\theta_{.75R} = 1.5^\circ$, $\gamma = 4.57$

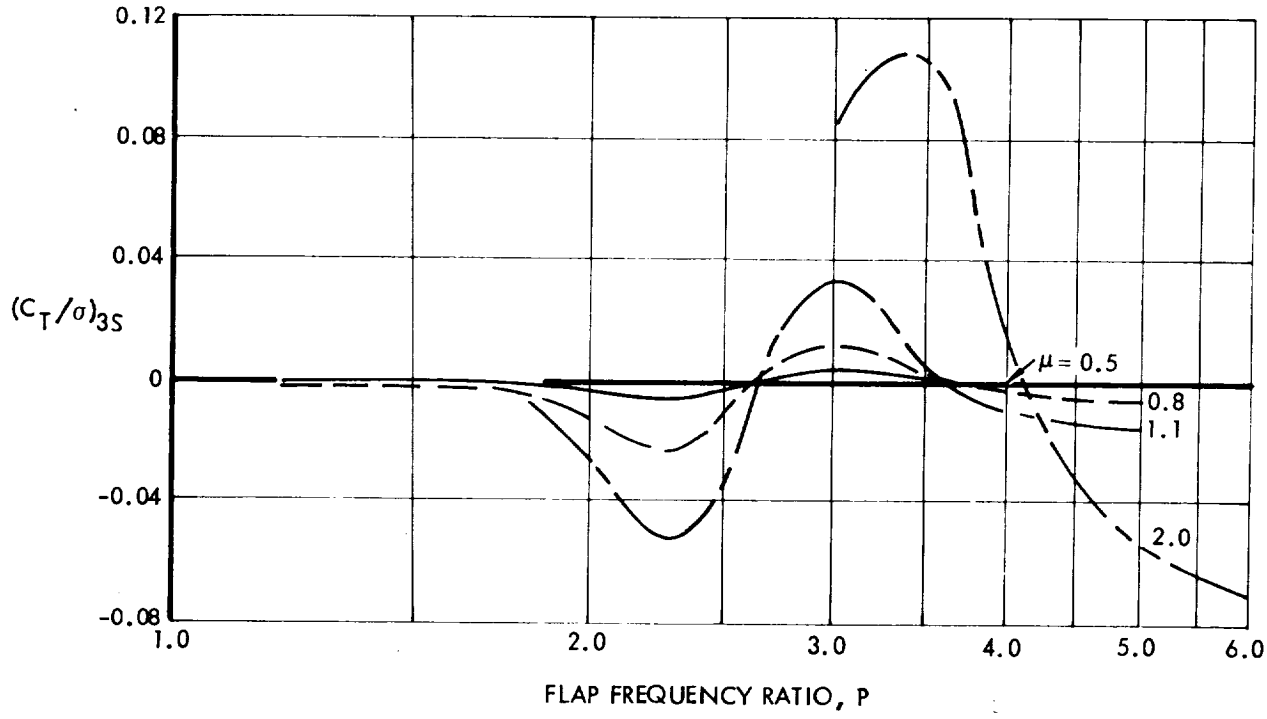

Figure 74. Residual Thrust 3P Sine Component Due to $\theta_o = 2.25^\circ$, $\theta_t R = -9.43^\circ$, and $\theta_{.75R} = 1.5^\circ$, $\gamma = 4.57$

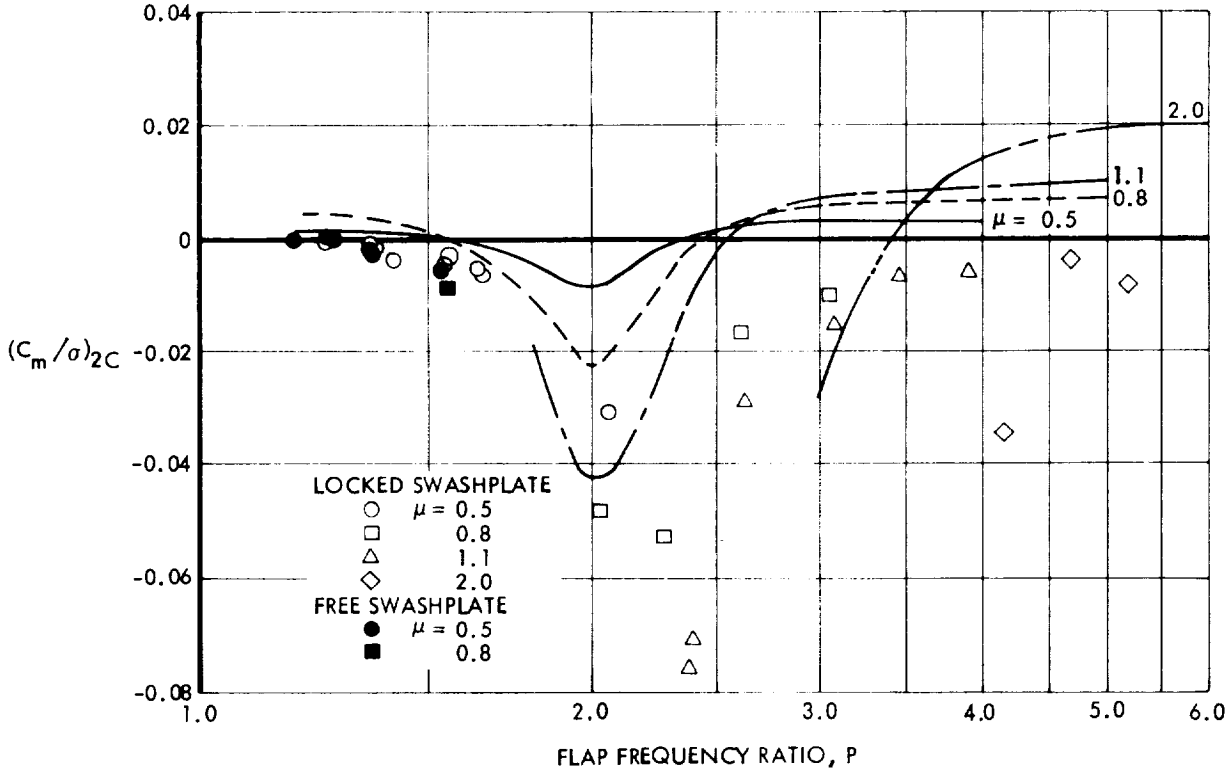

Figure 75. Residual Hub Pitch Moment 2P Component at Zero Azimuth Due to $\beta_o = 2.25^\circ$, $\theta_t R = -9.43^\circ$, $\theta_{.75R} = 1.5^\circ$, $\gamma = 4.57$

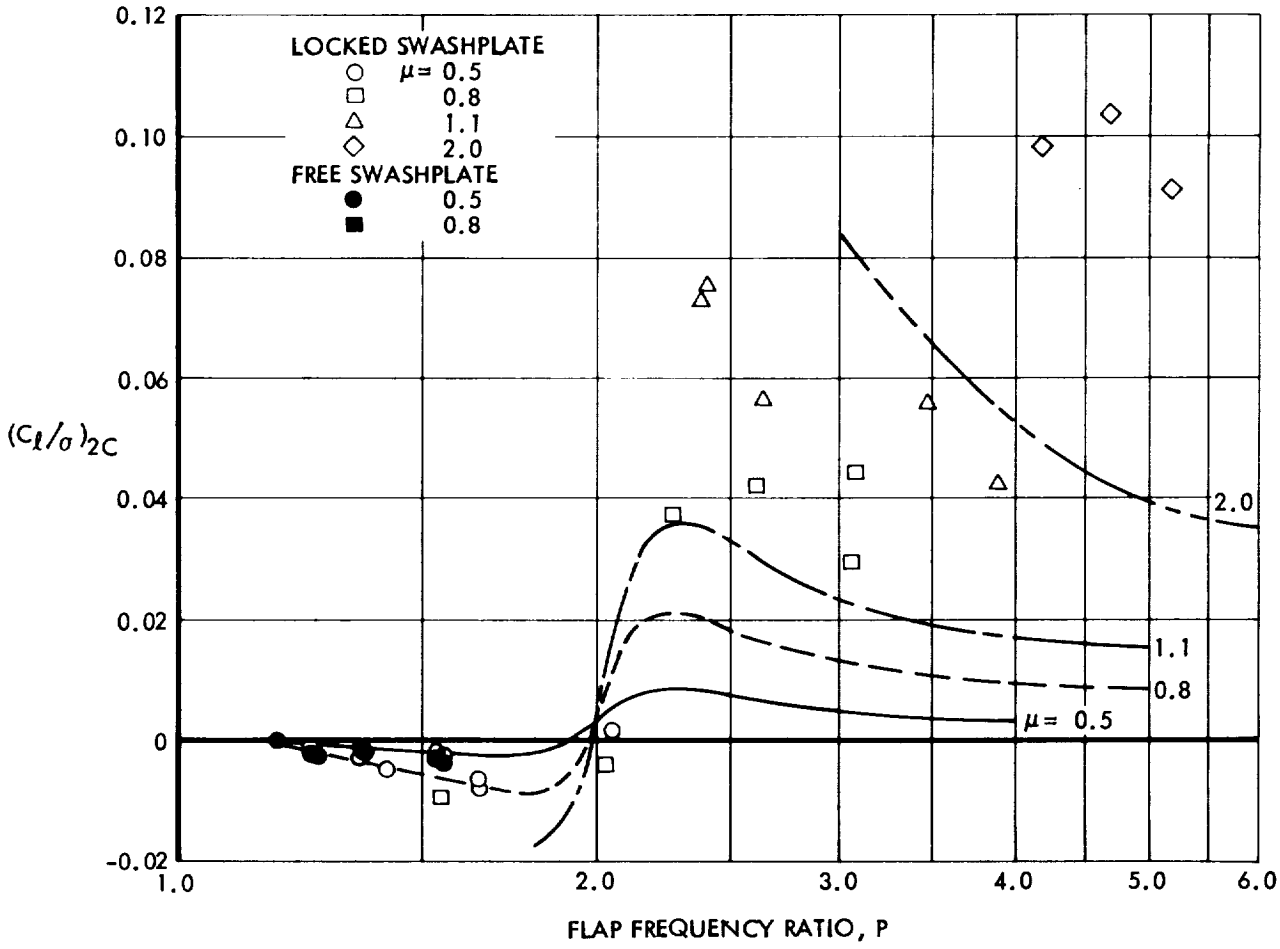

Figure 76. Residual Hub Roll Moment 2P Component at Zero Azimuth Due To $\beta_o = 2.25^\circ$, $\theta_t R = -9.43^\circ$, and $\theta_{.75R} = 1.5^\circ$, $\gamma = 4.57$

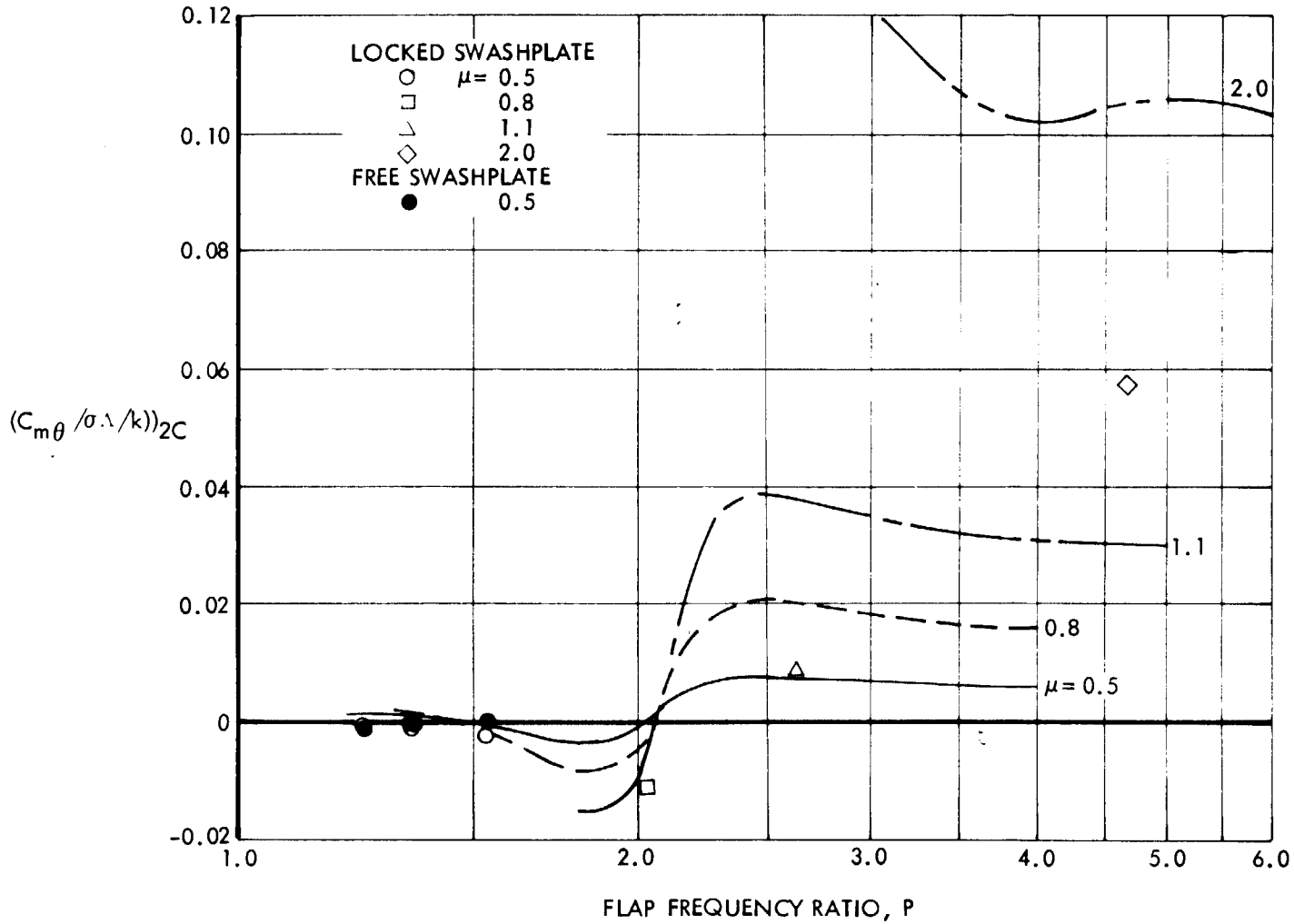

Figure 77. Residual Swashplate Pitch Moment 2P Component at Zero Azimuth Due to $\theta_o = 2.25^\circ$, $\theta_t R = -9.43^\circ$, and $\theta_{.75R} = 1.5^\circ$, $\gamma = 4.57$

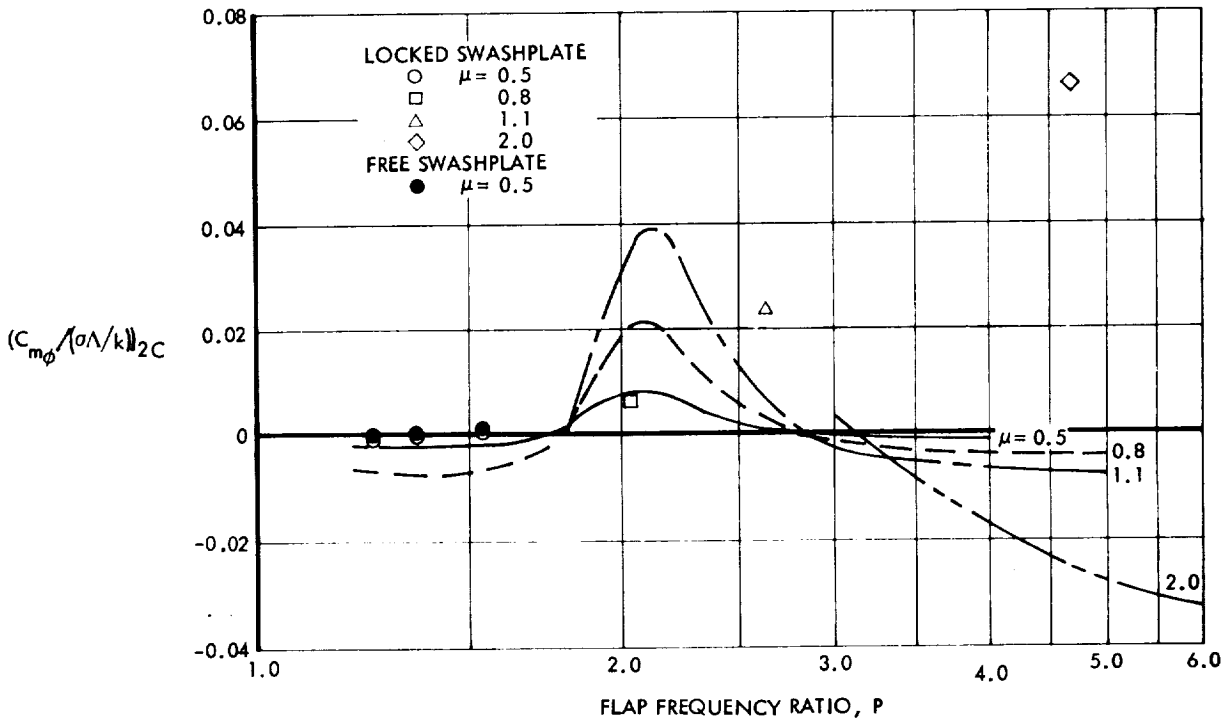

Figure 78. Residual Swashplate Roll Moment 2P Component at Zero Azimuth Due to $\beta_o = 2.25^\circ$, $\theta_t R = -9.43^\circ$, and $\theta_{.75R} = 1.5^\circ$, $\gamma = 4.57$

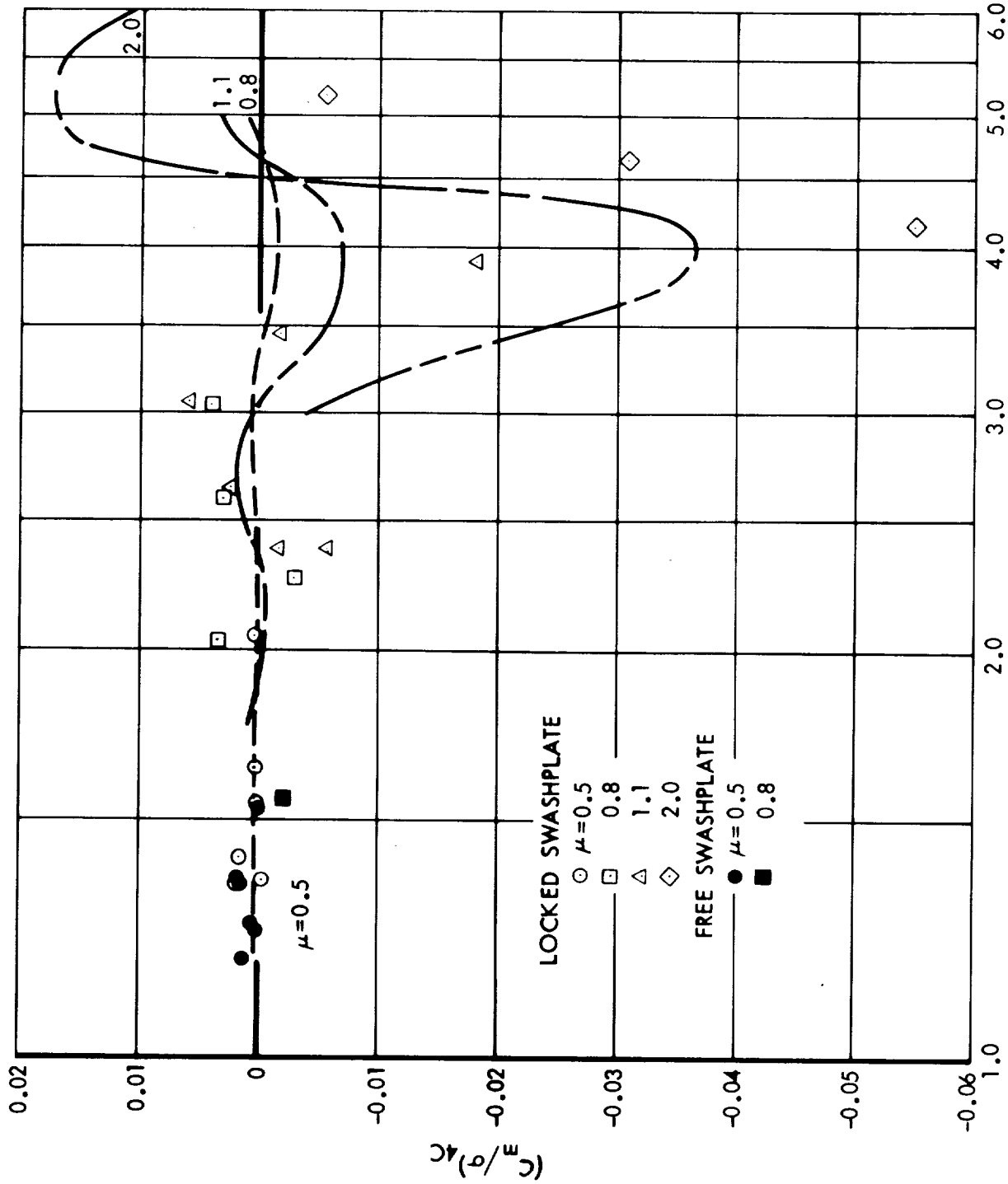

Figure 79. Residual Hub Pitch Moment 4P Component at Zero Azimuth for the 33-Foot, 3-Blade Rotor

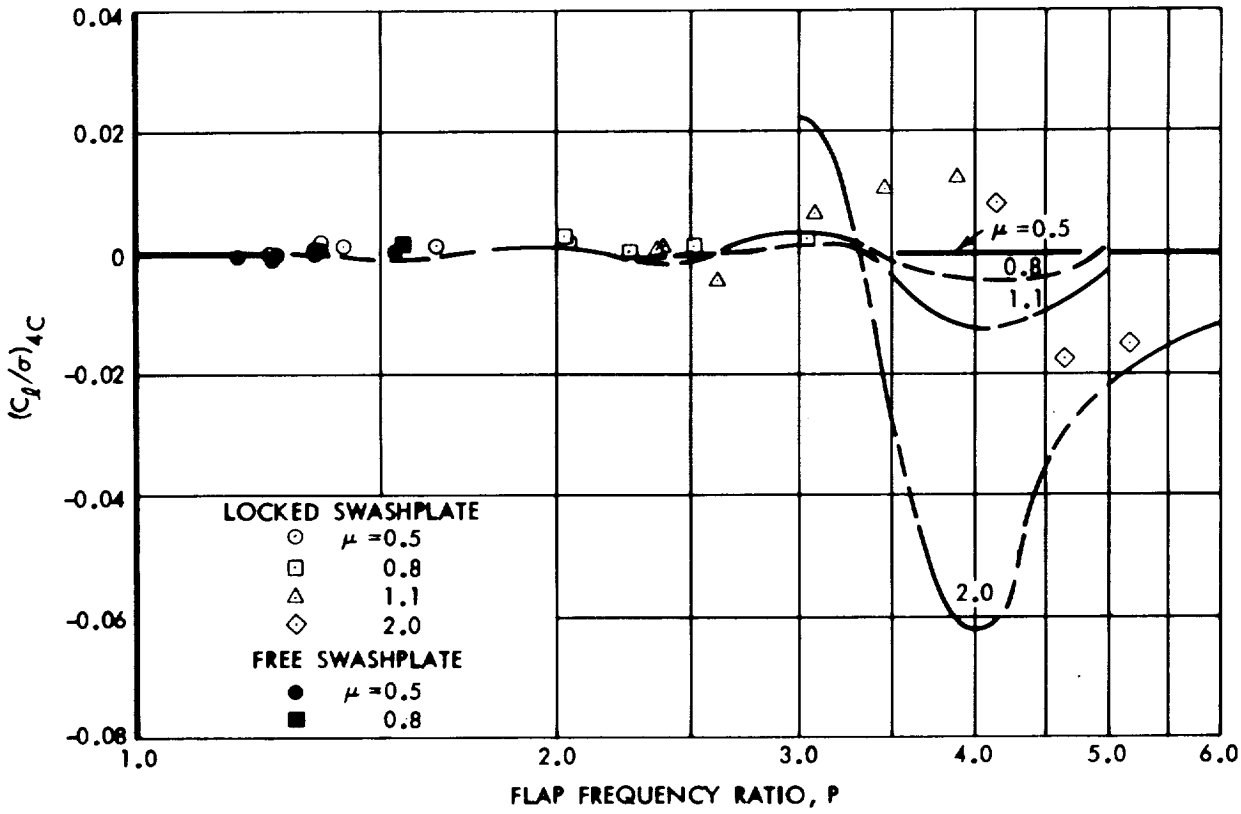

Figure 80. Residual Hub Roll Moment 4P Component at Zero Azimuth for the 33-Foot, 3-Blade Rotor

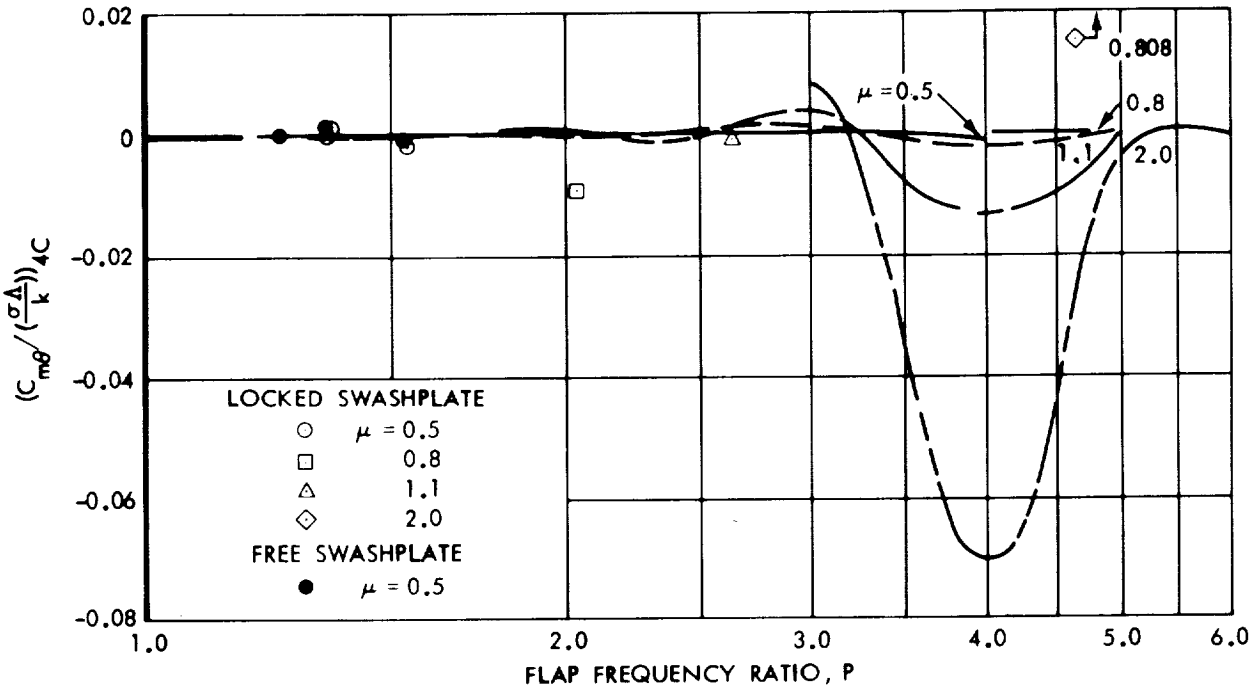

Figure 81. Residual Swashplate Pitch Moment 4P Component at Zero Azimuth for the 33-Foot, 3-Blade Rotor

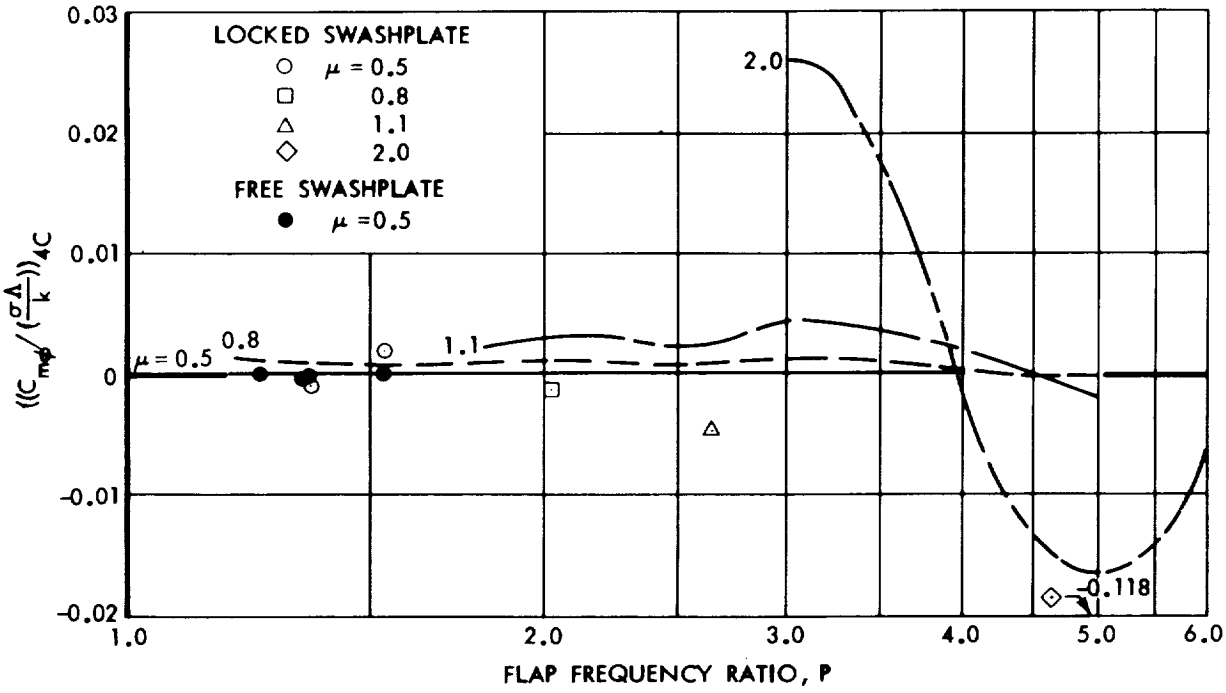

Figure 82. Residual Swashplate Roll Moment 4P Component at Zero Azimuth for the 33-Foot, 3-Blade Rotor

$$\frac{CT}{\sigma} = \left(\frac{C_T}{\sigma}\right)_o + \left(\frac{C_T}{\sigma}\right)_{3c} \cos 3\psi + \left(\frac{C_T}{\sigma}\right)_{3s} \sin 3\psi$$

$$+ \left[\left(\frac{\frac{\partial C_T}{\sigma}}{\partial \theta_{1c}}\right)_o + \left(\frac{\frac{\partial C_T}{\sigma}}{\partial \theta_{1c}}\right)_{3c} \cos 3\psi + \left(\frac{\frac{\partial C_T}{\sigma}}{\partial \theta_{1c}}\right)_{3s} \sin 3\psi\right] \theta_{1c}$$

$$+ \left[\left(\frac{\frac{\partial C_T}{\sigma}}{\partial \theta_{1s}}\right)_o + \left(\frac{\frac{\partial C_T}{\sigma}}{\partial \theta_{1s}}\right)_{3c} \cos 3\psi + \left(\frac{\frac{\partial C_T}{\sigma}}{\partial \theta_{1s}}\right)_{3s} \sin 3\psi\right] \theta_{1s}$$

$$\left.\begin{aligned} \frac{k}{\sigma\Lambda} C_{m_\theta} &= \\ \frac{k}{\sigma\Lambda} C_{m_\phi} &= \end{aligned}\right\} \quad \text{Follow the same rules as} \quad \frac{Cm}{\sigma} \quad \text{and} \quad \frac{C\ell}{\sigma}$$

The nondimensional derivatives are applicable to any three-blade rotor at the same values of γ, P, and μ.

Four-blade rotor oscillatory aeroelastic derivatives, in stationary axes, contain harmonics of the product of number of blades and rotation rate b Ω or 4P. Higher harmonics 8P, 12P ..... are negligible and are not considered in this report. The theoretical variations of the 4P sine and cosine components of thrust coefficient divided by solidity, C_T/σ, derivatives with flap frequency P and advance ratio μ are not shown. The derivatives with respect to θ_{1c} and θ_{1s}, however, are much smaller and center about the 4P resonance of blade flapping instead of the 3P as was the case with the three-blade rotor. No thrust oscillation experimental data is available.

It should be remembered that sines and cosines are relative to $\psi = 0$ with blade number one pointed aft.

The theoretical variations with P and μ of the 3P advancing rotating axes components of the 4P stationary axes hub moment aeroelastic derivatives with respect to θ_{1c} and θ_{1s} are shown in vector form for comparison with the equivalent components of the three-blade rotor, in Figures 83 and 84. Again the components are somewhat smaller and centered about different blade resonances.

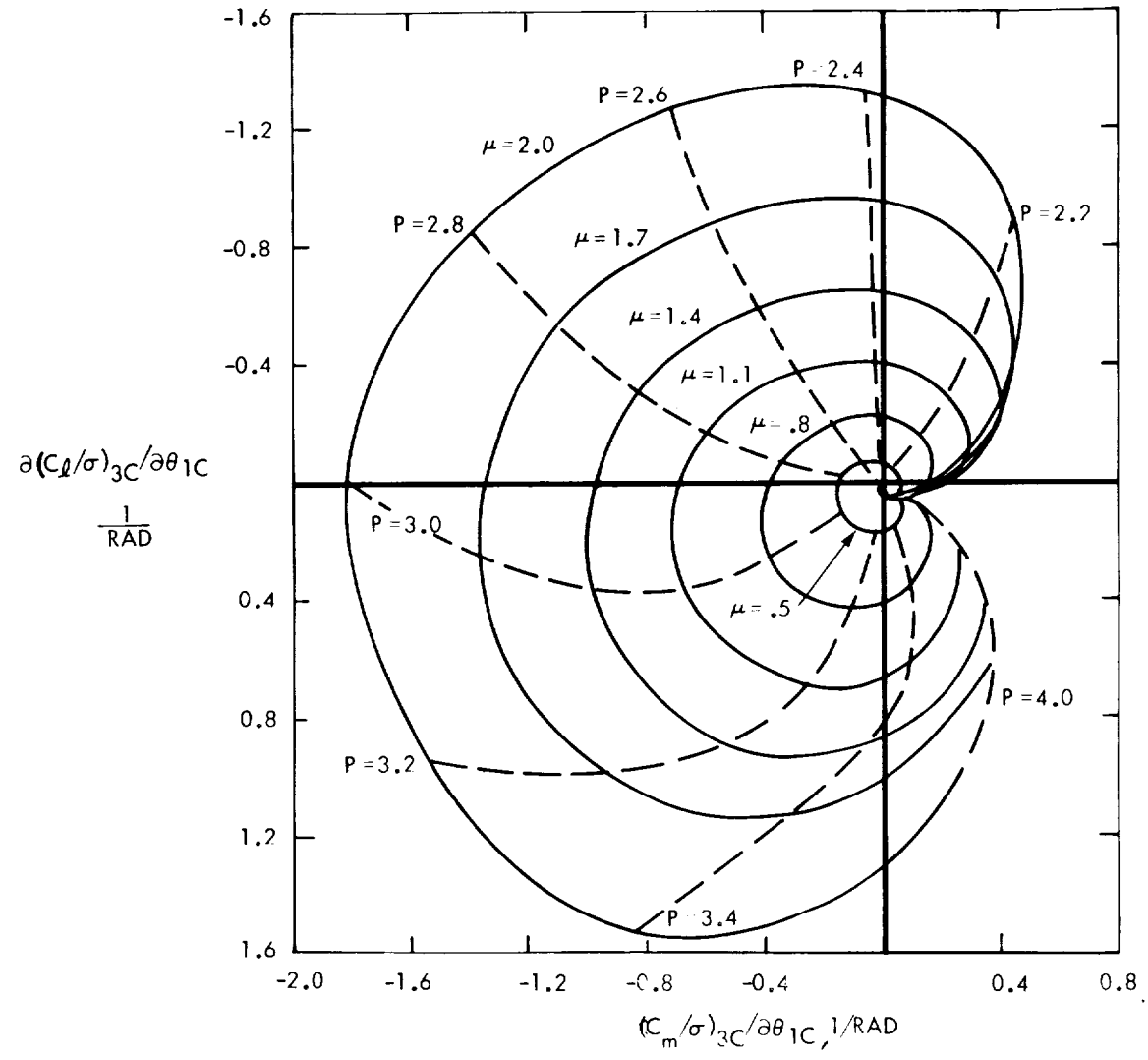

Figure 83. Advancing 3P Hub Moment Vectors at ψ = 0, Due to Unit Lateral Cyclic Pitch, for 4-Blade Rotors with γ = 5.0

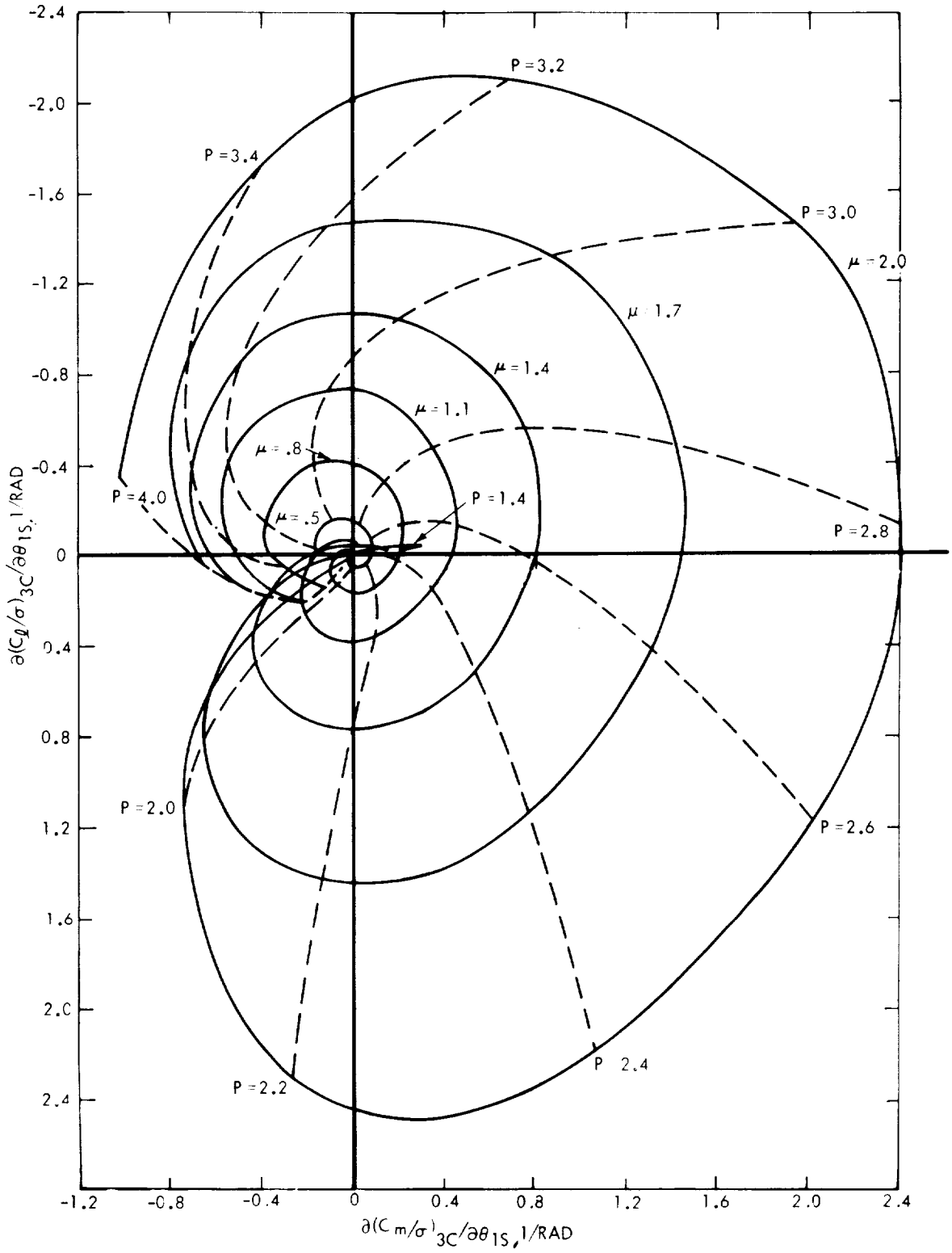

Figure 84. Advancing 3P Hub Moment Vectors Due to Unit Longitudinal Cyclic Pitch, at Ψ = 0, for 4-Blade Rotors with γ = 5.0

For comparison with experimental data, the pitch and roll components of the hub moment cyclic pitch derivatives are replotted versus advance ratio μ at the specific values of P tested and are shown in Figures 85 through 88. All data is for a blade Lock number $\gamma = 5.0$. In addition, the hub moment component derivatives with respect to collective pitch θ_o and rotor angle-of-attack α are also shown in a similar manner and are compared with experimental data in Figures 89 through 92.

Agreement of theory and experiment is quite good where the derivatives are of large magnitude. For the 7.5-foot four-blade rotor, blade twist and precone were zero. Therefore rotor hub force residual harmonic components were theoretically zero.

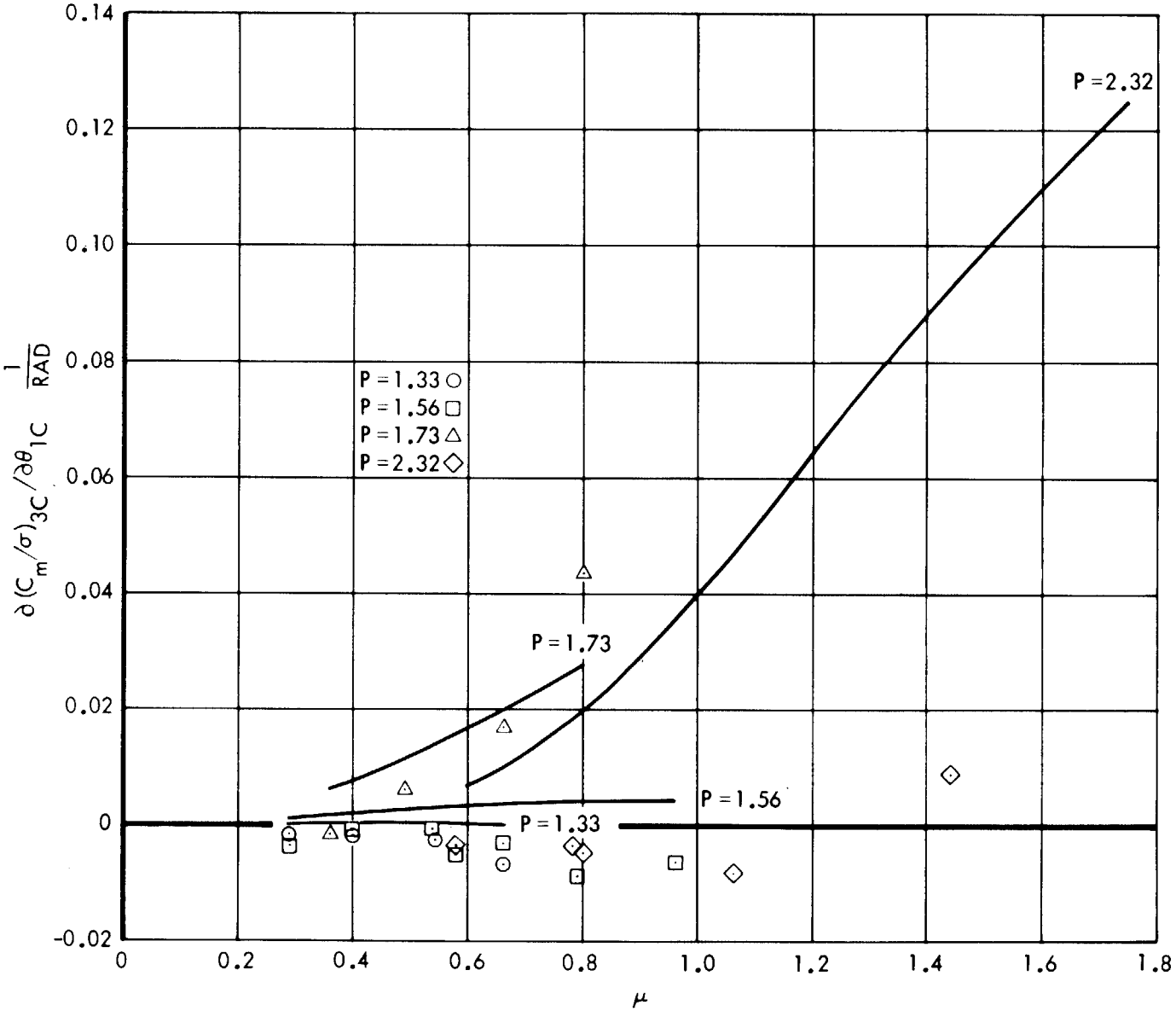

Figure 85. Hub Moment Oscillatory Aeroelastic Derivative With Respect to Lateral Cyclic Pitch, 3P Pitch Component at Ψ = 0 for 4-Blade Rotors With γ = 5.0

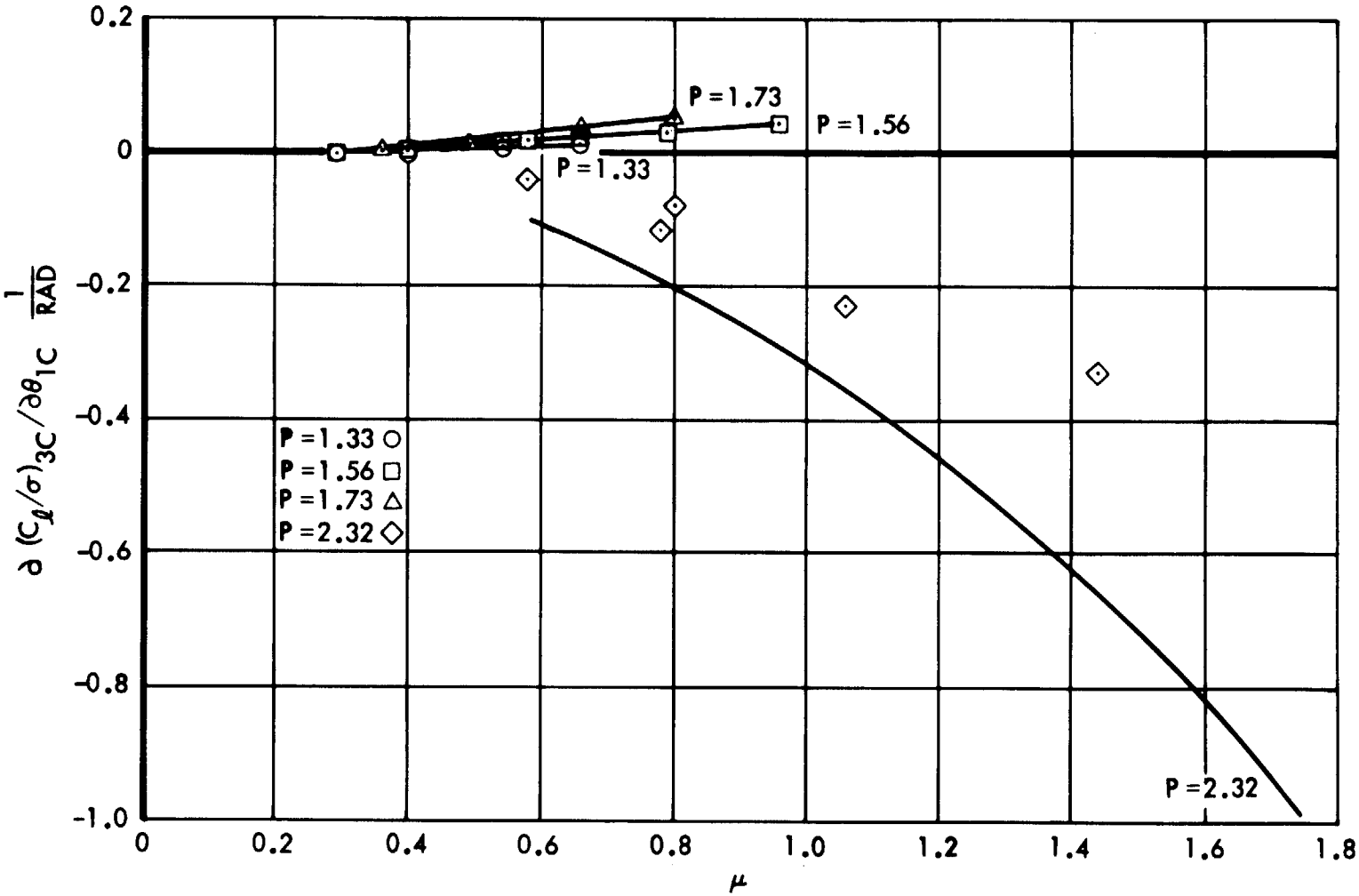

Figure 86. Hub Moment Oscillatory Aeroelastic Derivative With Respect to Lateral Cyclic Pitch, 3P Roll Component at ψ = 0 for 4-Blade Rotors With γ = 5.0

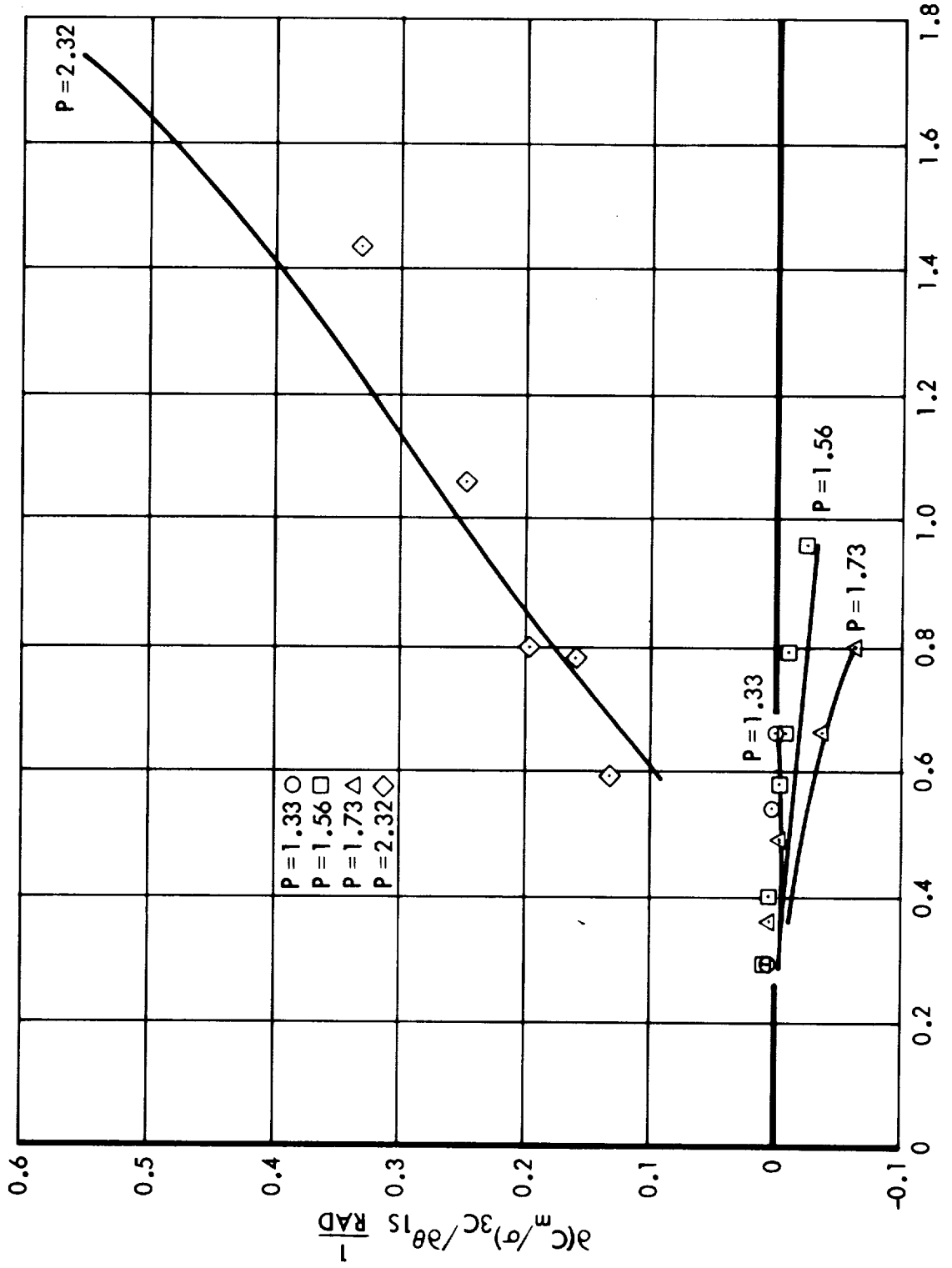

Figure 87. Hub Moment Oscillatory Aeroelastic Derivative With Respect to Longitudinal Cyclic Pitch, 3P Pitch Component at $\psi = 0$ for 4-Blade Rotors with $\gamma = 5.0$

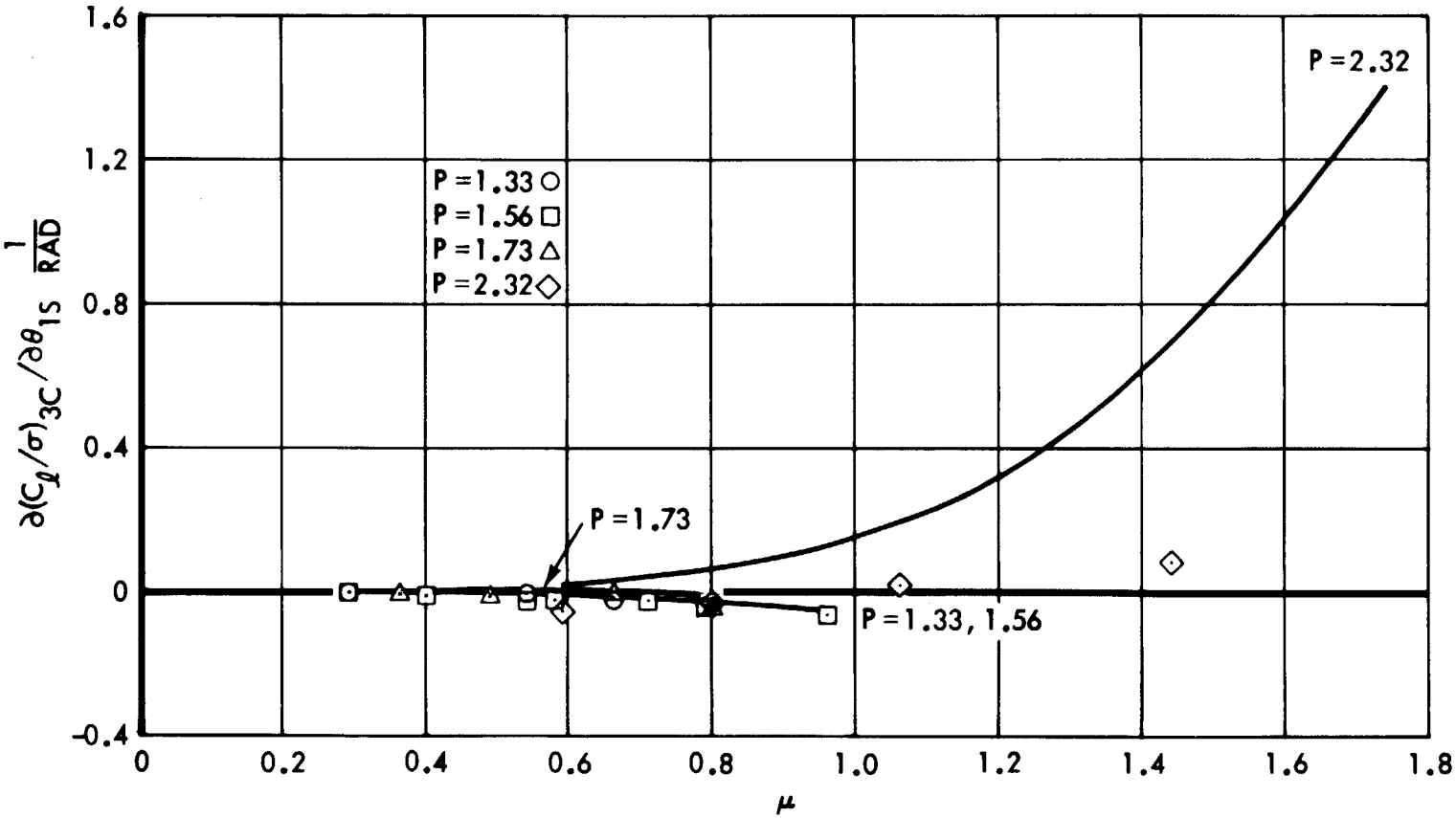

Figure 88. Hub Moment Oscillatory Aeroelastic Derivative With Respect to Longitudinal Cyclic Pitch, 3P Roll Component at Ψ = 0 for 4-Blade Rotors With γ = 5.0

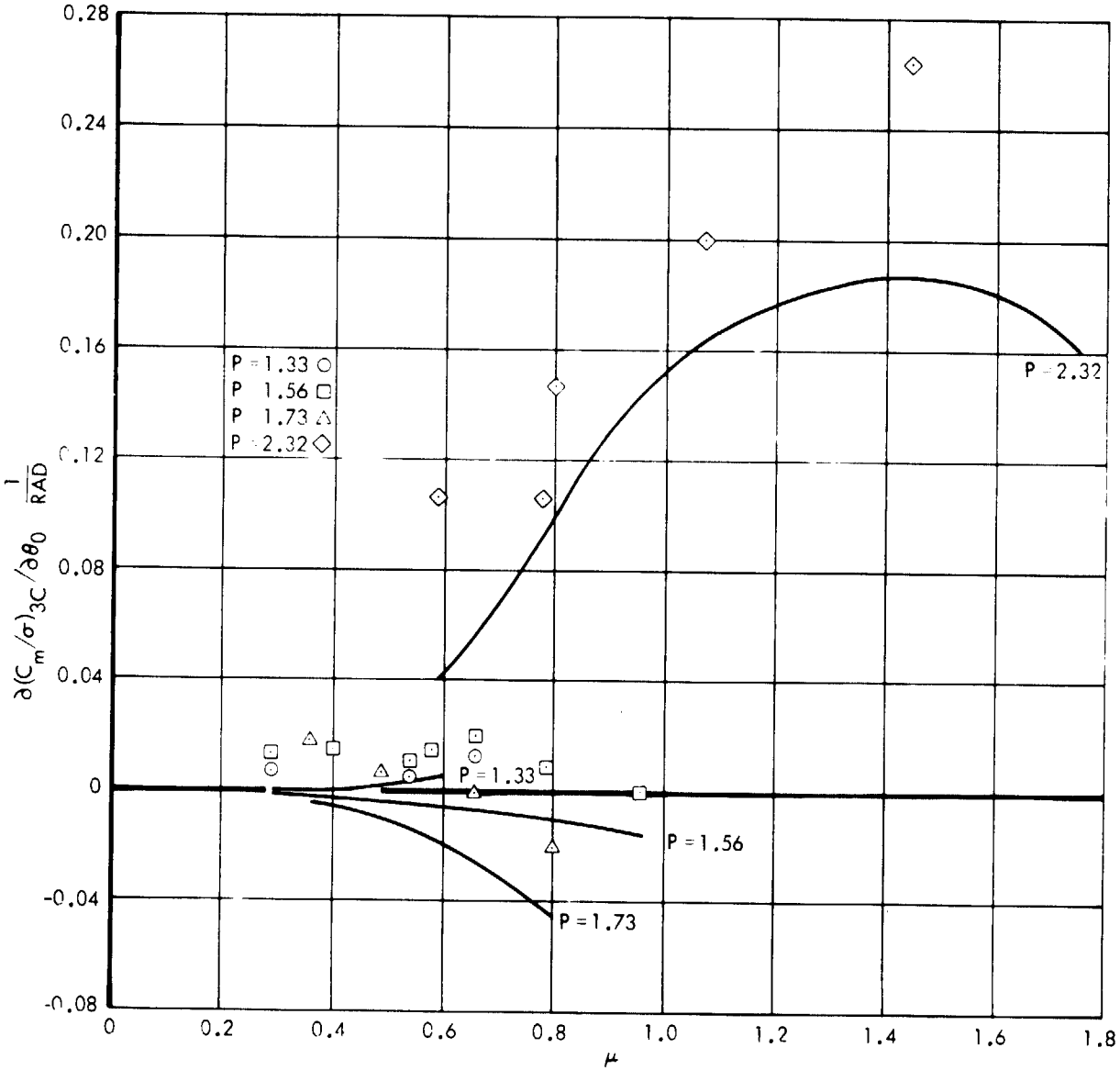

Figure 89. Hub Moment Oscillatory Aeroelastic Derivative With Respect to Collective Pitch, 3P Pitch Component at ψ = 0 for 4-Blade Rotors With γ = 5.0

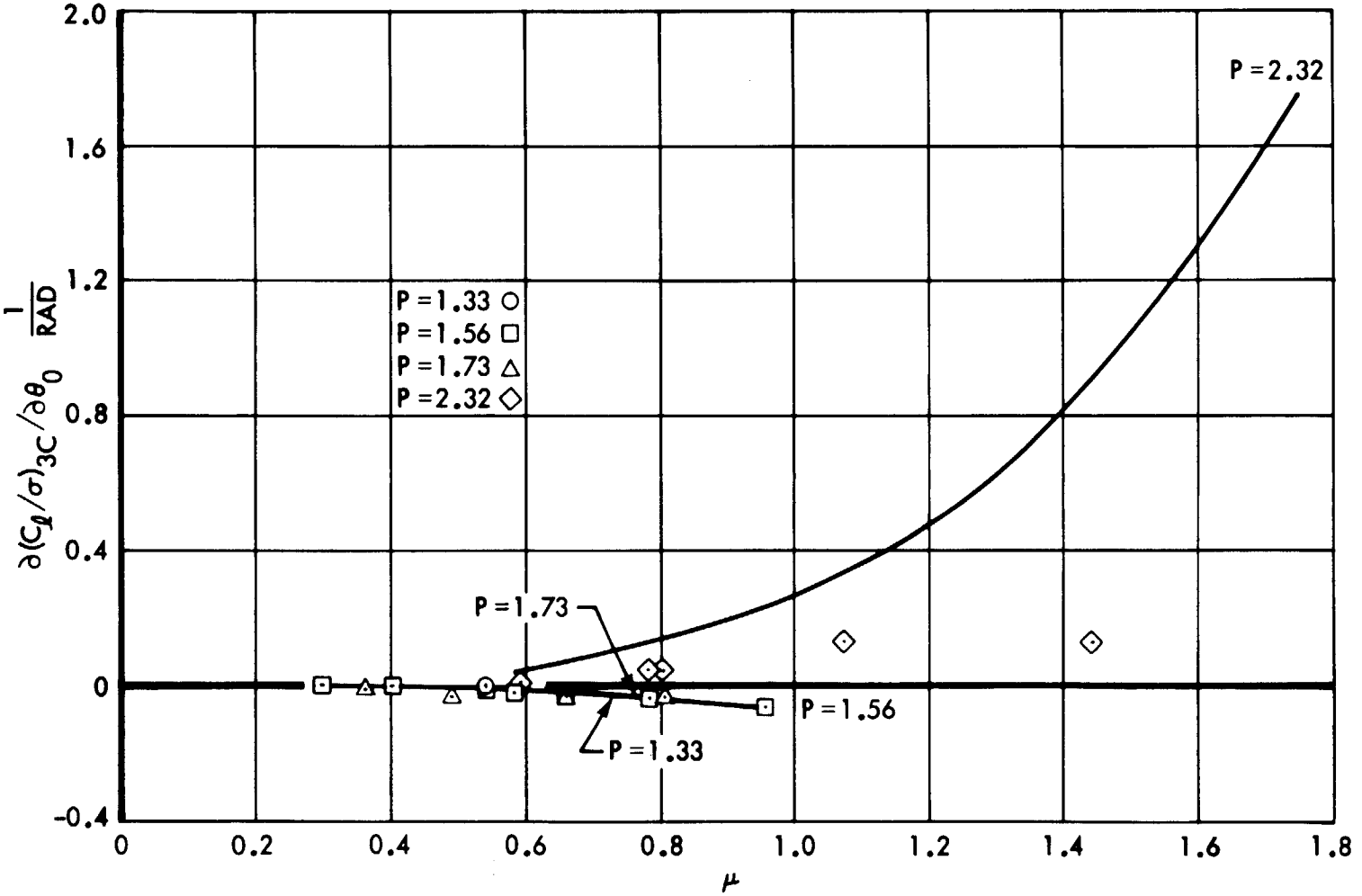

Figure 90. Hub Moment Oscillatory Aeroelastic Derivative With Respect to Collective Pitch, 3P Roll Component at ψ = 0 for 4-Blade Rotors With γ = 5.0

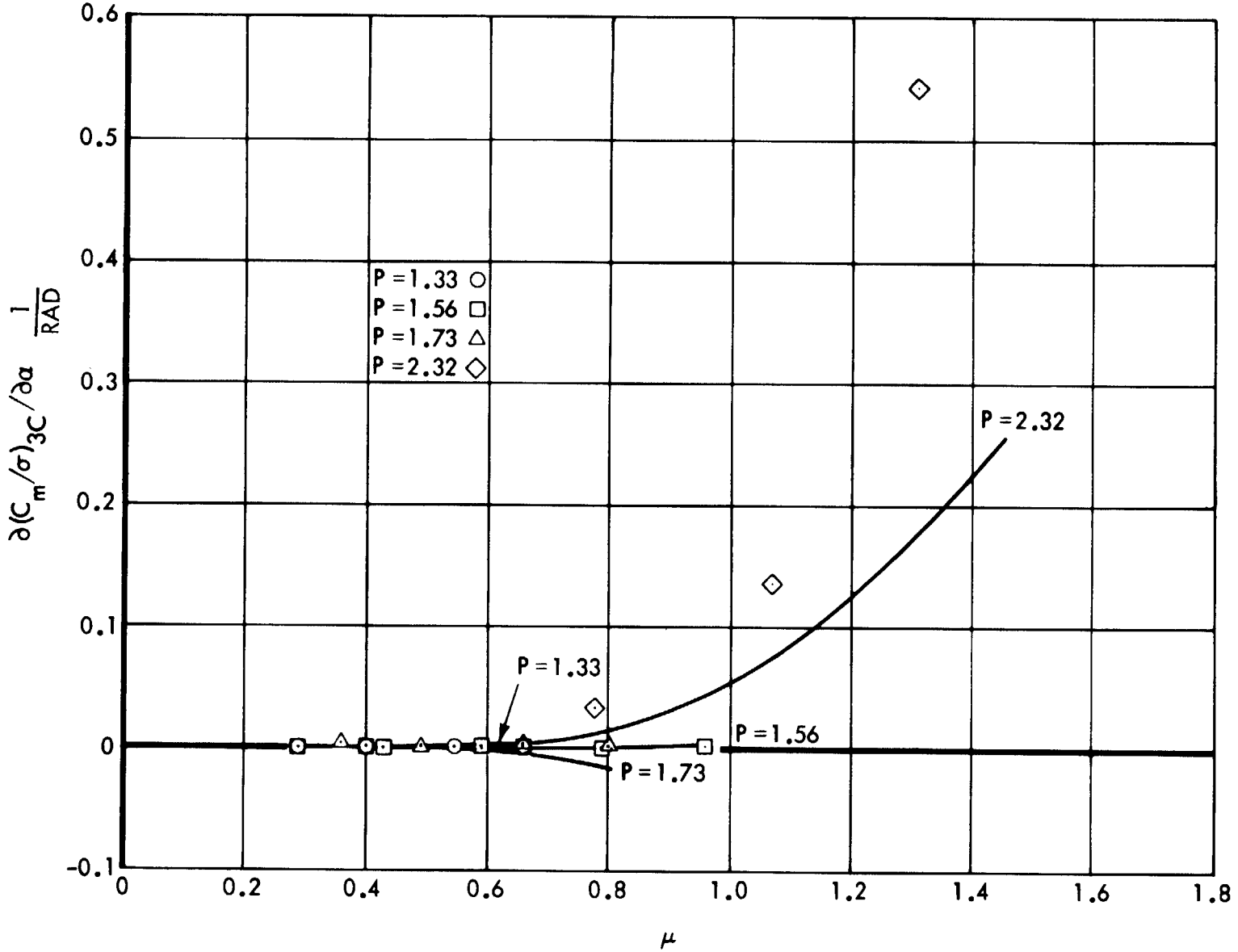

Figure 91. Hub Moment Oscillatory Aeroelastic Derivative With Respect to Rotor Angle of Attack, 3P Pitch Component at Ψ = 0 for 4-Blade Rotors With γ = 5.0

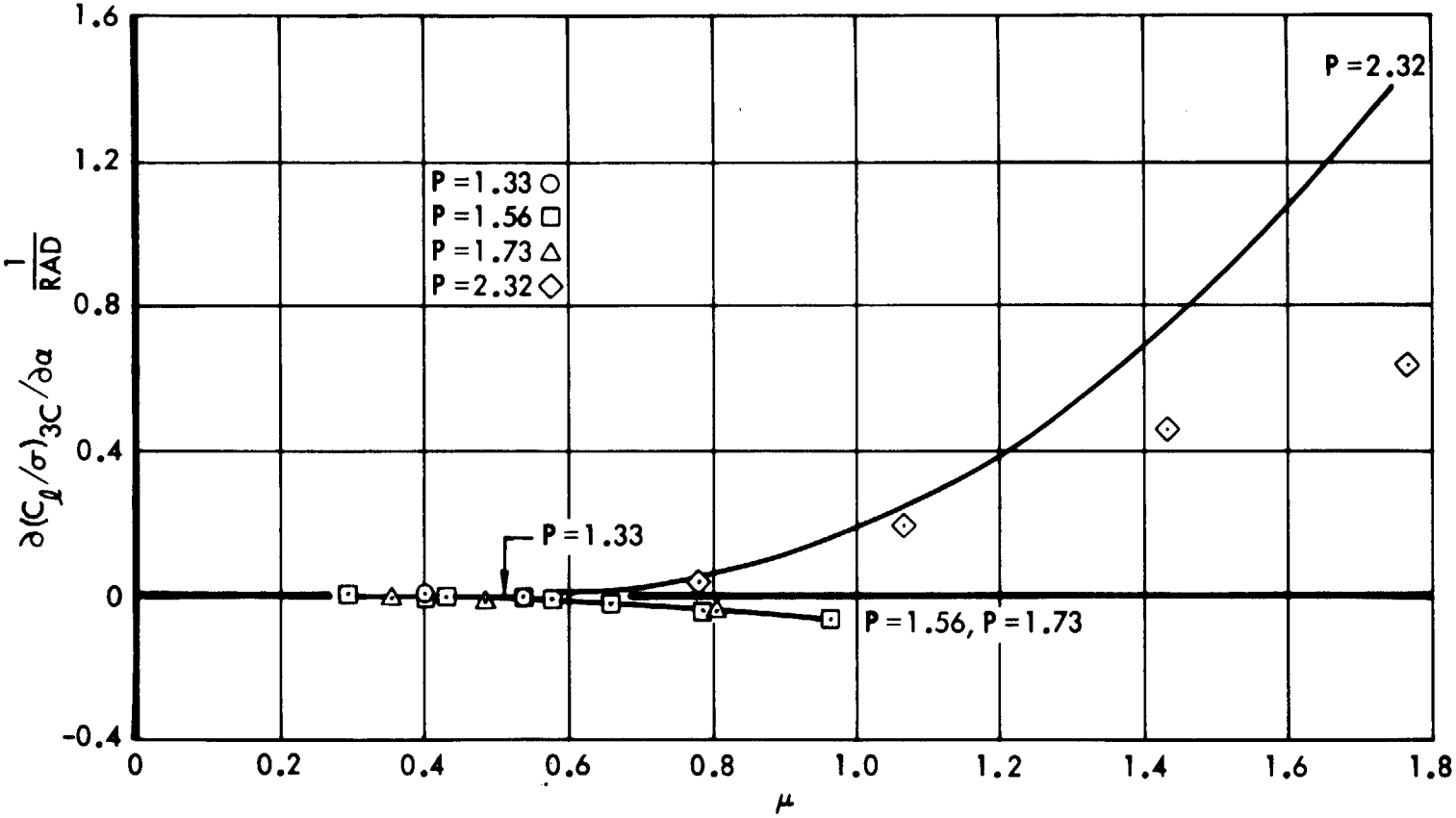

Figure 92. Hub Moment Oscillatory Aeroelastic Derivative With Respect to Rotor Angle-of-Attack, 3P Roll Component at ψ = 0 for 4-Blade Rotors With γ = 5.0

Fixed shaft, free swashplate. - Fixed-shaft, free-swashplate tests at high advance ratio were performed only on the 33-foot 3-blade rotor-gyroscope system. For this reason analyses are limited to this rotor configuration — although the results are couched in a general fashion.

In discussing free-swashplate gyroscope-stabilized systems, it becomes apparent that the rotation rate and size, or diametral inertia, of the gyroscope and the feathering inertia of the blades as well as the blade forward sweep angle become important parameters. That is, as well as advance ratio μ, lock number γ and flap frequency ratio P, the major parameters needed to describe the fixed swashplate, fixed shaft response of the rotor, it is necessary to consider further nondimensional parameters that control the free-swashplate behavior.

The most notable component of the motion of such systems, especially those employing high speed gyroscopes, is the precessive mode of the rotor-gyroscope combination. (The nutating mode natural frequency can be as high as 2OP and is therefore not significantly excited.)

The precessive mode advances and in stationary axes is of low frequency, typically of the order of P-1. If the ratio of its frequency to the shaft rotation rate can be preserved, say in a scaled model test in which the advance ratio, flap frequency ratio, and Lock number of the blades have also been preserved then the nondimensional feathering response, control mode stability, and rotor loads of the full-scale rotor should be faithfully reproduced.

The precessive or control mode natural frequency in stationary axes, neglecting the effects of blade flapping, is given in Reference 15 as:

$$\omega_f = \sqrt{\Omega^2 - \frac{f}{\left(2\frac{\Omega_G}{\Omega} - 1\right) I_G + \frac{bI_f}{2k^2}}}$$

where ω_f = control mode undamped natural frequency rad/sec

Ω = rotor rotation rate rad/sec

Ω_G = gyroscope rotation rate rad/sec

I_G = gyroscope diametral moment of inertia slugs ft^2

$I_f = I_o + \Lambda^2 I_b$ = blade feathering moment of inertia slugs ft^2

k = mechanical advantage

b = number of blades

f = aerodynamic swashplate moment per unit swashplate tilt ft-lb/rad

To preserve the ratio of control mode natural frequency to rotor rotation rate ω_f/Ω, it is only necessary to preserve the ratio,

$$\frac{f}{\Omega^2 \left[\left(2\frac{\Omega_G}{\Omega} - 1\right) I_G + \frac{bI_f}{2k^2}\right]}$$

An approximate expression for f is given in Reference 14 for a three-blade rotor. It may be factored by $\frac{b}{3}$ to make it approximately represent rotors with any numbers of blades.

$$f \approx \frac{b}{3}\frac{\Omega^2}{k^2} \pi \Lambda \rho \, cR^2 \left[\frac{1}{4} + \frac{2}{3}\mu + \frac{1}{2}\mu^2\right]$$

Since μ is separately preserved, no account of it is required in the control mode preserving parameter. In addition, if the slope of the blade section lift curve is expressed as "a" and replaces the 2π in the above expression, then the part of "f" dealing with μ

$$\frac{1}{6}\left[\frac{1}{4} + \frac{2}{3}\mu + \frac{1}{2}\mu^2\right]$$

may be dropped from the expression leaving the parameter which preserves the control mode frequency γ_f

$$\gamma_f = \frac{\Lambda \rho a c R^4}{\left(\rho \frac{\Omega_G}{\Omega} - 1\right) k^2 \frac{I_G}{b} + \frac{I_f}{\rho}}$$ Feathering Lock number

It is also necessary to establish nondimensional ratios for blade feathering friction C_R and swashplate stationary axis damping C_s. These are as follows:

$$k_{C_R} = \frac{C_R}{\frac{\Lambda b}{k} \rho c r R^4}$$

and

$$k_{C_S} = \frac{C_s}{\frac{\Lambda b}{k} \rho c r R^4}$$

where C_R = Swashplate feathering friction in rotating coordinates ft-lb/rad/sec

C_S = Swashplate damping in stationary axes, ft-lb/rad/sec

In summary, the nondimensional motions, stability and response of any free-swashplate, fixed-shaft rotor are defined if the following nondimensional parameters describing the rotor-gyroscope system are known:

Advance ratio	μ
Blade flap frequency ratio	P
Blade Lock number	γ
Blade feathering Lock number	γ_f
Feathering friction coefficient	k_{C_R}
Swashplate damping coefficient	k_{C_S}

It should also be noted that, although not necessary for stability, shaft-transmitted forces and higher harmonic blade motions and loads also depend on the number of blades b.

The solution of the equations of motions of the free-swashplate, fixed-shaft system for motions and shaft transmitted forces follows:

For the free-swashplate solution:

$$\ddot{\Theta} = \dot{\Theta} = \Theta = 0$$

$$\ddot{\Phi} = \dot{\Phi} = \Phi = 0$$

$$\ddot{z} = \dot{z} = z = 0$$

The swashplate tilt angles θ and Φ are degrees of freedom, in contrast to the fixed-swashplate solution of the previous section.

The two solutions differ mainly in the definition of the upper and lower portions of the $\{\beta\}$ vector. Since the swashplate tilt angles are now degrees of freedom, they are included in the $\{\beta_\ell\}$ vector:

$$\{\beta\} = \begin{Bmatrix} \Theta \\ \Phi \\ z \\ \hline \theta \\ \phi \\ \delta_o \\ \delta_\theta \\ \delta_\phi \\ \delta_d \end{Bmatrix} \equiv \begin{Bmatrix} \beta_u \\ \beta_\ell \end{Bmatrix}$$

Note that:

$$\{\beta_u\} = \begin{Bmatrix} 0 \\ 0 \\ 0 \end{Bmatrix}$$

and:

$$\{\beta_\ell\} = \begin{Bmatrix} \theta \\ \phi \\ \delta_0 \\ \delta_\theta \\ \delta_\phi \\ \hline \delta_d \end{Bmatrix} \equiv \begin{Bmatrix} \beta_{\ell u} \\ \hline \delta_d \end{Bmatrix} \equiv \begin{Bmatrix} \delta_u \\ \hline \delta_d \end{Bmatrix}$$

For solution, equation (3) simplifies to:

$$\begin{bmatrix} I_{11} & I_{12} & 0 \\ I_{21} & I_{22} & \\ 0 & 0 & I_{33} \end{bmatrix} \begin{Bmatrix} 0 \\ \ddot{u} \\ \ddot{\beta}_1 \end{Bmatrix} + \begin{bmatrix} B_{11} & B_{12} & B_{13} \\ B_{21} & B_{22} & B_{23} \\ B_{31} & B_{32} & B_{33} \end{bmatrix} \begin{Bmatrix} 0 \\ \dot{u} \\ \dot{\beta}_d \end{Bmatrix} + \begin{bmatrix} F_{11} & F_{12} & F_{13} \\ F_{21} & F_{22} & F_{23} \\ F_{31} & F_{32} & F_{33} \end{bmatrix} \begin{Bmatrix} 0 \\ u \\ \beta_d \end{Bmatrix} = \begin{bmatrix} G_1 \\ G_2 \\ G_3 \end{bmatrix} \{\eta_F\} + \begin{Bmatrix} \eta_1 \\ \eta_2 \\ 0 \end{Bmatrix} \qquad (16)$$

where:

$$\begin{Bmatrix} \eta_1 \\ \hline \eta_2 \end{Bmatrix} = \begin{Bmatrix} M_H \\ L_H \\ T \\ \hline M_\theta \\ M_\phi \end{Bmatrix}$$

The $\{\mathcal{M}_1\}$ vector of rotor loads will be moved to the left-hand side of equation (16) with no change in sign, thereby becoming reaction moments. The $\{\mathcal{M}_2\}$ vector of swashplate moments will be retained on the right-hand side, in which case they remain applied moments. Equation (16) becomes:

$$\begin{Bmatrix} \mathcal{M}_1 \\ 0 \\ 0 \end{Bmatrix} + \begin{bmatrix} I_{12} & 0 \\ I_{22} & 0 \\ 0 & I_{33} \end{bmatrix} \begin{Bmatrix} \ddot{\delta}_u \\ \ddot{\delta}_d \end{Bmatrix} + \begin{bmatrix} E_{12} & E_{13} \\ E_{22} & E_{23} \\ E_{32} & E_{33} \end{bmatrix} \begin{Bmatrix} \dot{\delta}_u \\ \dot{\delta}_d \end{Bmatrix} + \begin{bmatrix} F_{12} & F_{13} \\ F_{22} & F_{23} \\ F_{32} & F_{33} \end{bmatrix} \begin{Bmatrix} \delta_u \\ \delta_d \end{Bmatrix} = \begin{bmatrix} G_1 \\ G_2 \\ G_3 \end{bmatrix} \{\eta_F\} + \begin{Bmatrix} 0 \\ \mathcal{M}_2 \\ 0 \end{Bmatrix} \tag{17}$$

The preceding equation may be separated into two uncoupled parts. The lower portion becomes:

$$\begin{bmatrix} I_{22} & 0 \\ 0 & I_{33} \end{bmatrix} \begin{Bmatrix} \ddot{\delta}_u \\ \ddot{\delta}_d \end{Bmatrix} + \begin{bmatrix} E_{22} & E_{23} \\ E_{32} & E_{33} \end{bmatrix} \begin{Bmatrix} \dot{\delta}_u \\ \dot{\delta}_d \end{Bmatrix} + \begin{bmatrix} F_{22} & F_{23} \\ F_{32} & F_{33} \end{bmatrix} \begin{Bmatrix} \delta_u \\ \delta_d \end{Bmatrix} = \begin{bmatrix} G_2 \\ G_3 \end{bmatrix} \{\eta_F\} + \begin{Bmatrix} \mathcal{M}_2 \\ 0 \end{Bmatrix} \tag{18}$$

from which the displacement vectors may be determined. The known displacement vectors may then be used to get the response loads in the upper part of equation (17), as follows:

$$\{\mathcal{M}_1\} = - \begin{bmatrix} I_{12} \end{bmatrix} \{\ddot{\delta}_u\} - \begin{bmatrix} E_{12} & E_{13} \end{bmatrix} \begin{Bmatrix} \dot{\delta}_u \\ \dot{\delta}_d \end{Bmatrix} - \begin{bmatrix} F_{12} & F_{13} \end{bmatrix} \begin{Bmatrix} \delta_u \\ \delta_d \end{Bmatrix} + \begin{bmatrix} G_1 \end{bmatrix} \{\eta_F\} \tag{19}$$

The solution of equations (18) and (19) proceeds in like manner to the prior section. The differences are minor and are due only to the differing matrix sizes and the somewhat different forcing functions of equations (6) and (18).

Free-swashplate effects may be compared with those of the locked swashplate only if the calculated cases are similar. It would not be reasonable, for example, to compare rotor shaft force derivatives, fixed and free, due to collective pitch or rotor angle-of-attack. They would be basically different due to the trimming effect of the free swashplate.

For a valid determination of the higher harmonic effects of the free swashplate on the shaft transmitted vibratory forces, the fixed-shaft free-swashplate system should be caused to change cyclic pitch, one component at a time, by judicial application of swashplate control moments. A comparison could then be made between the rates of change of shaft and swashplate forces with respect to unit changes in cyclic pitch for the fixed and free swashplates. Differences could then be logically ascribed to freeing the swashplate.

The speculation that the swashplate motions, which should have occurred during the tests, were suppressed by high values of swashplate stationary axis damping was also investigated by calculating results with $k_{C_R} = k_{C_S} = 0$ as well as with the nominal values observed during bench testing.

Tip path motions and swashplate wobble: — The rates of change of non-dimensional tip path motions with respect to each of the cyclic pitch components were not measurably affected by freeing the swashplate, even in the absence of swashplate damping and feathering friction. In addition, the swashplate wobble was very small.

This calculated result occurred at all conditions of rotor rpm and forward speed for which the system was stable. Inspections of the experimental data tended to confirm this theoretical finding. However, directly comparable cases were difficult to find and the result was obscured by the free swashplate's ability to neutralize random very low frequency perturbations in the flow field.

The theory and experimental data indicated that mean and oscillatory aeroelastic force and moment derivatives for the stable rotor-gyroscope system were not significantly affected by freeing the swashplate.

It should not be inferred from these results that no swashplate parameter γ_f (feathering Lock number) and gyroscope inertia and rpm values exist which will reduce vibration. Preliminary studies by Dr. G. J. Sissingh (Reference 16) suggest that careful tuning of rotor-gyroscope systems can result in reduced vibration. No attempt, however, is made in this study to verify his predictions.

Free shaft, free swashplate. – Solution of the complete rotor-gyroscope-airframe equations for the motions, shaft-transmitted loads, and blade section forces is the objective of the free-shaft, free-swashplate calculations. These calculations are somewhat simpler than the previous analyses since none of the degrees of freedom are suppressed.

The solution produces loads on free-flying aircraft in steady flight. The body degrees of freedom of the system are not restricted.

This solution is the simplest of the three types of application. Again, it differs from its predecessors mainly in the definition of the $\{\beta\}$ vector. In this instance, $\{\beta_u\}$, which is a vector of the locked-out degrees of freedom, does not exist. Thus:

$$\{\beta\} = \{\beta_\ell\} = \left\{\begin{array}{c} \Theta \\ \Phi \\ Z \\ \theta \\ \phi \\ \delta_o \\ \delta_\theta \\ \delta_\phi \\ \hline \delta_d \end{array}\right\} = \left\{\begin{array}{c} \beta_{\ell u} \\ \hline \delta_d \end{array}\right\} \equiv \left\{\begin{array}{c} \delta_u \\ \hline \delta_d \end{array}\right\}$$

The solution will simplify to the form of equation (4) without the top row and first column, which is:

$$\begin{bmatrix} I_{22} & 0 \\ 0 & I_{33} \end{bmatrix} \begin{Bmatrix} \ddot{\delta}_u \\ \ddot{\delta}_d \end{Bmatrix} + \begin{bmatrix} E_{22} & E_{23} \\ E_{32} & E_{33} \end{bmatrix} \begin{Bmatrix} \dot{\delta}_u \\ \dot{\delta}_d \end{Bmatrix} + \begin{bmatrix} F_{22} & F_{23} \\ F_{32} & F_{33} \end{bmatrix} \begin{Bmatrix} \delta_u \\ \delta_d \end{Bmatrix} = \begin{bmatrix} G_2 \\ G_3 \end{bmatrix} \{\eta_F\} + \begin{Bmatrix} m \\ 0 \end{Bmatrix} \quad (20)$$

For the present applications, the vehicle will be controlled by moment inputs to the swashplate. Consequently there will be no loads applied to the hub such that the loads vector becomes:

$$\{m\} = \begin{Bmatrix} 0 \\ 0 \\ 0 \\ M_\theta \\ M_\phi \\ 0 \\ 0 \\ 0 \end{Bmatrix}$$

Equation (19) is solved for the displacement vectors in like manner to equations (5) and (18) of prior sections.

No aeroelastic response derivatives may be determined for the free-flight cases.

SOLUTION OF IN-PLANE MOTIONS EQUATIONS

Stability of In-Plane Motions

Before undertaking the calculation of the steady oscillatory response of the in-plane blade-hub-body-spring system to its external forcing functions, it is advisable to examine its stability and modal behavior in the unforced state. This is done by arbitrarily letting the right-hand side (RHS) of the equation be zero. The left-hand set (LHS) or homogeneous equations may then be solved for its eigenvalues, or frequency and damping, and eigenvectors, or mode shapes.

The damping characteristic of each mode of the system must be negative for stability and the system must be stable for realistic calculations of the oscillatory response to forcing functions. The natural or unforced frequencies of the modes vary with rotor rpm and since the modes are stable but lightly damped they experience resonance with rotor forces when their frequencies coincide with the Ωb or 3 per revolution harmonics. The rpm's at which the in-plane modes intersect the 3P line are therefore important since they may lead to severe rotor loads.

The following sections present the values of the rotor in-plane parameters employed in the 33-foot 3-blade rotor analyses. Then the types of modes such a system possesses and how its frequencies vary with rpm is discussed.

In-plane parameters for the 33-foot rotor. –

Blade mass	M_b	=	2.52 slugs
Blade c.g. radial position	$r_{c.g.}$	=	9.00 ft
Position of blade pivot	e	=	2.50 ft
Blade moment of inertia, about shaft	$I_{b_{shaft}}$	=	253 slugs ft^2
Blade moment of inertia, about its pivot	$I_{b_{pivot}}$	=	156 slugs ft^2
Blade natural frequency, nonrotating	$\omega_{ip.}$	=	53.2 rad/sec

Blade section drag coefficient	C_{d_o}	= 0.011
Rotating hub mass	M_R	= 17.8 slugs
Rotating hub moment of inertia	I_R	= 6.72 slugs ft^2
Structural damping fraction	γ	= 0
Body effective lateral mass	M_y	= 66 slugs
Body effective longitudinal mass	M_x	= 110 slugs
Body lateral spring	K_y	= 682,000 lb/ft
Body longitudinal spring	K_x	= 235,000 lb/ft

In-plane modes and frequencies. — The number of modes equals the number of degrees of freedom since the body is attached to the wind tunnel by springs and is therefore not free.

The modes of the system at zero rpm consist of one rigid body rotation of zero frequency, one collective in-plane mode of high frequency, in which the blades and hub rotate in opposite directions and four blade-body lateral and longitudinal modes.

The four blade-body modes are of greatest interest and at zero rpm are real, or all elements in each mode keep the same relationship to one another throughout the period of oscillation. The elements change amplitude and sign but keep the same distribution. The four modes are sketched in Figure 93.

The modes resemble two of those measured; however, the frequencies calculated are somewhat higher.

Modes of the rotating rotor, in stationary axes, contain real and imaginary parts. That is, the modes have different shapes at different times during the period of oscillation. This variation can best be seen by examining the modal vectors in the imaginary plane. The actual shape at any instant of time is given by the projection of the vector components in the real axis. A construction of the real shape at regularly spaced intervals of time provides a "moving picture" of the mode throughout its period.

The four rotor modes are shown in Figure 94 at rotor rpm of 250. Two modes are practically uncoupled body modes and two are the rotor advancing

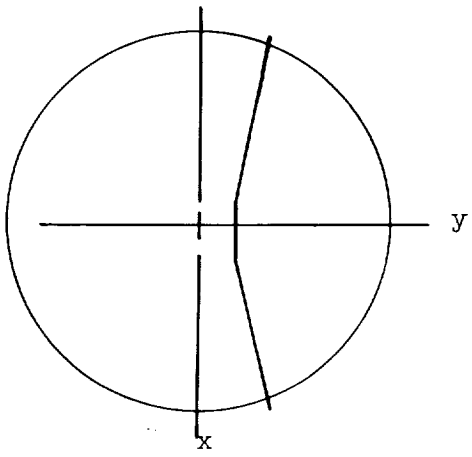

f = 7.63 cps

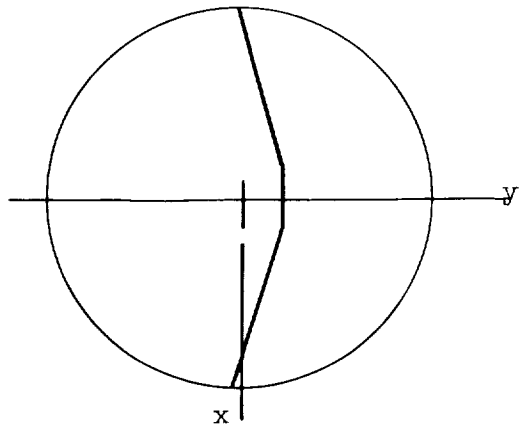

f = 9.10 cps

LATERAL MODES

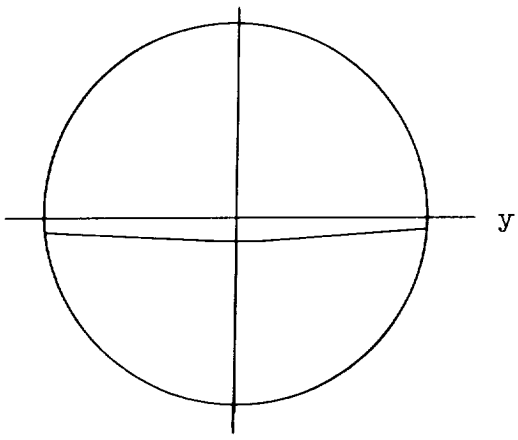

f = 11.56 cps

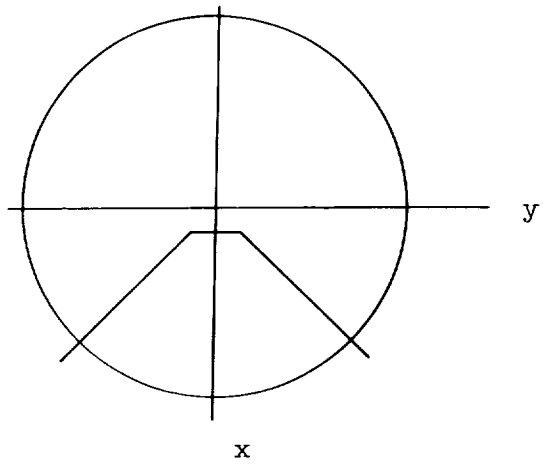

f = 8.37 cps

LONGITUDINAL MODES

Figure 93. In-plane Modes at Zero RPM for the 33-foot 3-Blade Rotor. Shaft Motion Exaggerated. Shapes Show Deformation of Disk.

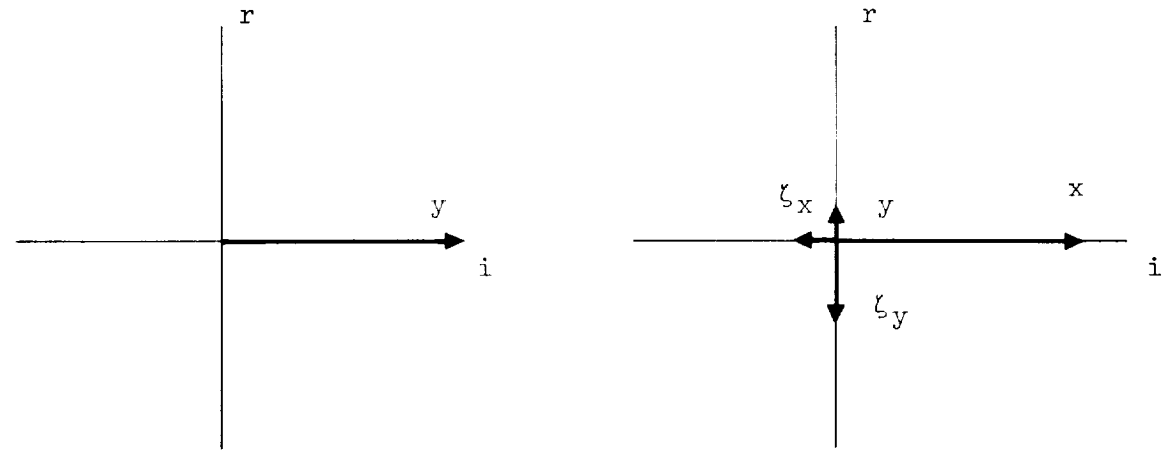

f = 8.07 cps

f = 11.16 cps

BODY MODES

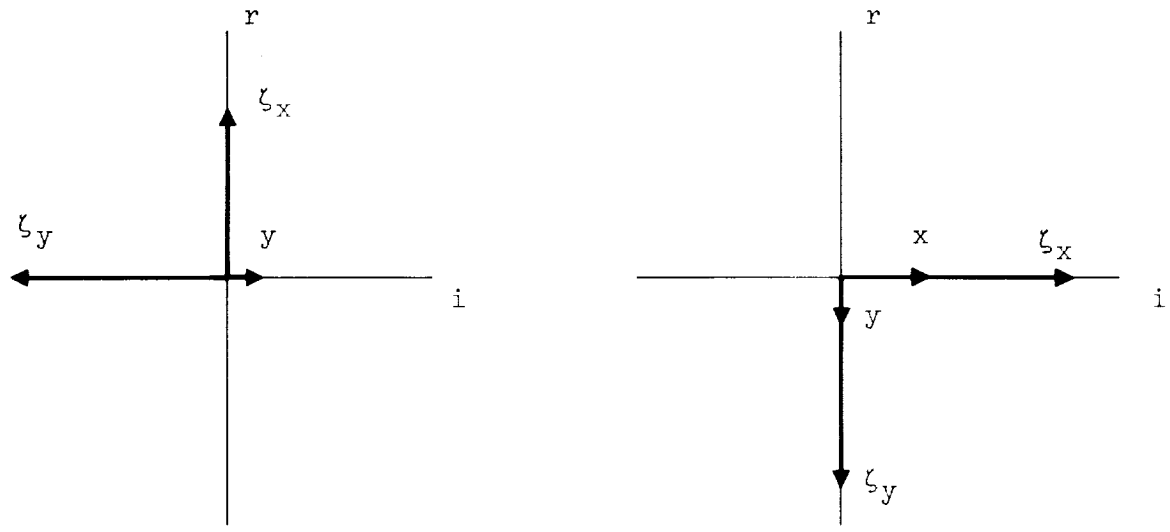

f = 4.55 cps

f = 13.45 cps

ROTOR MODES

Figure 94. In-plane Modes at 250 RPM for the 33-Foot 3-Blade Rotor. Shaft Motion Exaggerated.

and regressing modes. The fact that modes are advancing or regressing can be determined from the vectors in the imaginary (i-r) plane by noting that they keep constant magnitude while rotating counterclockwise or clockwise through the period of oscillation. The projection in the real axis of the advancing mode, for example, shows $_x$ to be positive at the initial time so that the mode essentially appears as follows:

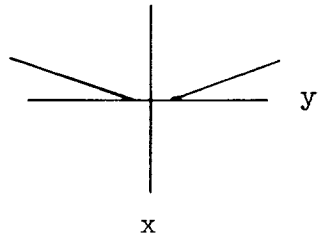

One quarter of the period later ζ_y is positive and $\zeta_x = 0$ and the mode shape appears as follows:

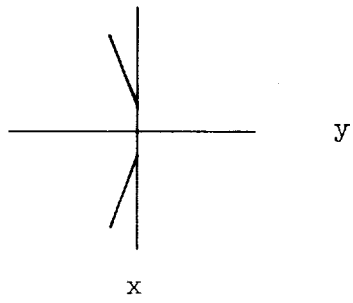

It is obvious that the blades are precessing in the same direction as the rotor rotation or are advancing.

The variation of the unforced rotor frequencies with rpm is shown in Figure 95. It should be noted that modes intersect the 3P line at rpm = 128, 160, 220, and 275. Only the regressive mode intersection of 3P did not excite measurable oscillations in the rotor. Large chordwise oscillations of the blades were noted at the other intersecting values of rpm.

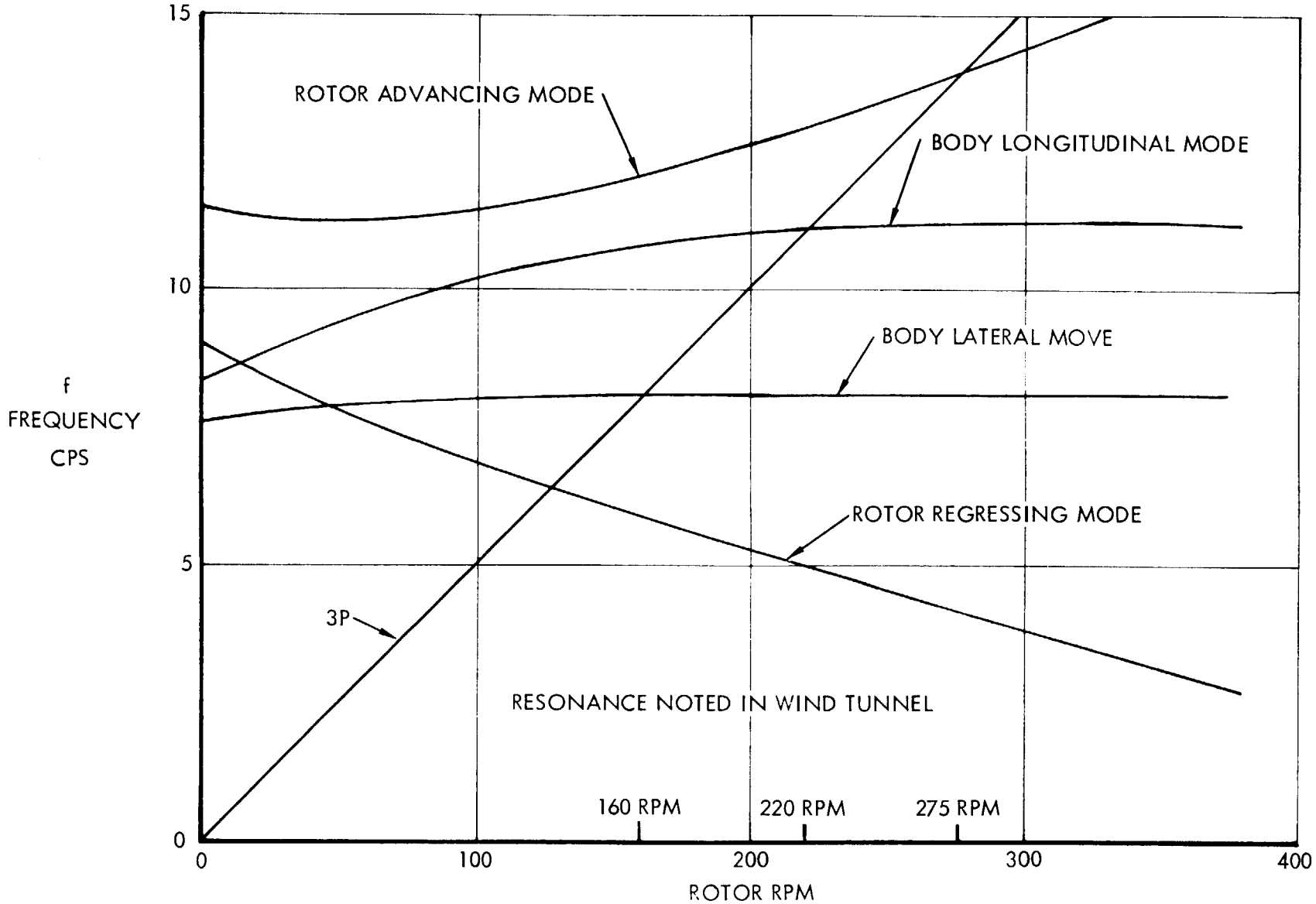

Figure 95. Unforced Body and Rotor Vibration Mode Frequency Variation with RPM for the 33-Foot 3-Blade Rotor

BLADE LOADS

The determination of blade section lift and flapping bending moment azimuthal distributions from calculated rotor external forces and response motions is discussed in this section. Theoretical flap bending distributions are shown compared to experiment at two radial stations on the 33-foot, 3-blade rotor.

For the fixed-shaft 33-foot rotor both experimental data and theoretical results are analyzed so as to provide the rates of change of flap bending distribution with respect to cyclic pitch components and the residual bending distributions due to rotor fixed geometric parameters when cyclic pitch is zero.

For the XH-51A rotor, experimental azimuthal distributions are available from existing flight test conditions. These provided net or combined effects of cyclic pitch and rotor fixed geometry for comparison with theory. Correlation with the present theory was very poor and is not shown.

Principles Involved in Blade Loads Determination

Blade section lift and flap bending are found from the displacements, velocities, and accelerations of the degrees of freedom produced by the vertical motions differential equations when solved for steady oscillatory response to external forcing functions.

Bending moments at blade stations are not found from the curvatures of the blade. Far too few modes are employed to make this a reasonable procedure. Bending moments are found by integrating the aerodynamic and inertia section forces factored by the moment arms to the station from the station to the blade tip. The blade mode shape primarily affects inertia acceleration and centrifugal forces. The aerodynamic forces are largely independent of mode shape. For these reasons fairly accurate flapping bending moments

were predicted at blade stations near the root at high rpm and at all stations at low rpm despite the fact that only one flap bending mode was employed.

The actual procedure employed to calculate the blade loads azimuthal distributions is indicated below for the three-blade rotor. A similar procedure was used for the four-blade case. The blade-force-at-station-r column matrix is defined as follows:

$$\left\{F_b\right\}_r = \begin{Bmatrix} BM \\ V \\ PM \\ FM \\ SL \end{Bmatrix} = \begin{matrix} \text{bending moment at station r} \\ \text{shear at station r} \\ \text{pitching moment} \\ \text{feathering moment} \\ \text{section lift at station r} \end{matrix}$$

$$\left\{F_b\right\}_r = \left[\left[Q_\eta(r,\Psi)\right] + \left[CF_b(r)\right]\right]\left\{\eta_b\right\} + \left[Q_{\dot\eta}(r,\Psi)\right]\left\{\dot\eta_b\right\}$$
$$+ \left[I_b(r)\right]\left\{\ddot\eta_b\right\} + \left[Q_F(r,\Psi)\right]\left\{\eta_F\right\}$$

Blade forces are calculated from blade deflections, velocities, and accelerations and external forces. The matrices in the blade force equation contain the following terms

$Q_\eta(r,\Psi)$	aerodynamic, displacement contribution to blade section forces
$Q_{\dot\eta}(r,\Psi)$	aerodynamic velocity contribution to blade section forces
$Q_F(r,\Psi)$	aerodynamic and inertia external forces
$CF_b(r)$	centrifugal contribution to section forces
$I_b(r)$	acceleration contribution to section forces

Elements in the blade forces matrices are calculated in a way parallel to that employed in calculating coefficients in the differential equations.

The vectors of blade b deflections η_b and fixed geometric shapes η_F are defined as follows:

$$\eta_b = \begin{Bmatrix} \beta \\ z \\ \theta \\ \delta \end{Bmatrix}_b \qquad \eta_F = \begin{Bmatrix} \beta_o \\ \theta_o \\ \theta_t \\ \dot{z}_g \end{Bmatrix}$$

The blade "b" vector and its derivatives are determined from the overall rotor displacements, velocities, and accelerations relative to rotor coordinates through the use of the restraining transformation matrices.

$$\eta_b = \left[D_{zb}\right] \beta_R$$

$$\dot{\eta}_b = \left[D_{zb}\right] \dot{\beta}_R$$

$$\ddot{\eta}_b = \left[D_{zb}\right] \ddot{\beta}_R$$

and the motions in rotating coordinates depend on the motions in stationary axes through the time dependent transformation $\left[T\right]$.

$$\beta_R = T \beta_S$$

$$\dot{\beta}_R = T \dot{\beta}_S + \dot{T} \beta_S$$

$$\ddot{\beta}_R = T \ddot{\beta}_S + 2\dot{T} \dot{\beta}_S + \ddot{T} \beta_S$$

and β_S is the vector of degrees of freedom of the equation in stationary axes; the output of the steady oscillatory calculations.

$$\beta_S = \begin{Bmatrix} \theta \\ \phi \\ \delta_o \\ \delta_\theta \\ \delta_\phi \end{Bmatrix}$$

and is itself a function of azimuth.

$$\beta = \beta_o + \beta_{3c} \cos 3\psi + \beta_{3s} \sin 3\psi + \beta_{6c} \cos 6\psi + \beta_{6s} \sin 6\psi$$

Blade Flap Bending Moments, 33-Foot Rotor

On the 33-foot 3-blade rotor, flap bending moments were measured at $\frac{r}{R}$ = .217 and .596 (stations 43 and 118 inches respectively) at 80 knots forward speed over a range of rpm. At $\frac{r}{R}$ = .217, moments on the three blades were analyzed and presented in nondimensional form. The measurements showed a common basic behavior and provided a check on each other despite fairly large differences between the blades. At $\frac{r}{R}$ = .596, bending moment measurements were available only on blade number 2.

The test cases analyzed are shown in the following table.

Forward Speed (Knots)	RPM	μ	P	ν
80.59	197.2	.399	1.35	4.57
82.76	153.2	.528	1.53	4.57
82.78	100.2	.808	2.03	4.57
82.68	72.1	1.121	2.64	4.57
82.88	38.0	2.132	4.67	4.57

At each radial station for each test condition, bending moment distributions caused by approximately a dozen combinations of cyclic pitch were analyzed. Best fit planes (rms fit) of each harmonic component versus the two cyclic pitch angles supplied rates of change of bending moment harmonic component with respect to each cyclic pitch component and a residual value at $\theta_{lc} = \theta_{ls} = 0$.

From these, bending moment azimuthal distributions per unit value of each cyclic pitch component and the residual were prepared. These were then compared with theoretical values. All bending moments were presented in the form $\frac{b}{\sigma} C_{b.m.}$ where $C_{b.m.}$ is defined:

$$C_{b.m.} = \frac{\text{bending moment}}{\rho(\Omega R)^2 \pi R^2 R}$$

For purposes of comparison the azimuthal distributions of bending moment at the two radial stations due to longitudinal cyclic pitch θ_{1s} are shown in Figures 96 through 105 for the five tested cases in the order given in the table.

It is interesting to note, at high rpm, in the first two cases, that the bending moment at $\frac{r}{R} = .596$ is not correctly predicted at all, where, as the rpm reduces over the last three cases, the agreement between theory and experiment improves. This is thought to be due to the single parabolic mode shape employed to represent blade flapping deflection. The tip region, at high rpm, would theoretically be deflected upward too far and would induce a negative bending moment at a point in the azimuth where a positive bending moment occurred physically.

At low rpm, on the other hand, tip deflections and centrifugal forces are very small and most of the blade bending moment is produced by aerodynamics.

Figures 96 through 105 also show the transition of the distribution from an almost sinusoidal form at P = 1.35 and 1.53 to heavy two-per-revolution oscillations at P = 2.03. At the latter condition the blade is in damped resonance with its 2P exciting forces. At the P = 2.64 condition light three per revolution oscillations become evident and at P = 4.67 four per revolution become evident.

Figures 106 through 115 show the variation of the azimuthal distribution pro- bending moment at $\frac{r}{R} = .217$ and .596 due to unit lateral cyclic pitch θ_{1c} over the range of tested cases. Remarks regarding the variations with longitudinal cyclic pitch apply in general. However, the change in phase due to the change in cyclic pitch component may be noted.

Figures 116 through 125 show the bending moment azimuthal distribution produced by precone $\beta_o = 2.25$ degrees, blade twist $\theta_t R = -9.43$ degrees, and collective pitch $\theta_{.75R} = 1.5$ degrees, with cyclic pitch and angle of attack zero $\theta_{1c} = \theta_{1s} = \alpha = 0$. These plots include the centrifugally induced bending moment due to precone and collective blade flapping, δ_o, and at high rpm, the first

two cases, are suspected of causing the deviation of the mean bending moment from the experimental values. At low rpm the effect is not quite as pronounced.

The residual flap bending moment distribution roughly resembles the negative of the bending moment due to θ_{1c}. Trimming bending moments to zero therefore could be approximately accomplished by an application of positive θ_{1c}.

Reference 3, Figure 5 show $+\theta_{1c}$ to be the larger of the cyclic pitch components required to trim hub moment to zero, although fairly large values of $-\theta_{1s}$ are also required.

In summary, the theory predicted the essential features of the bending moment distributions at the inboard station at the five combinations of Γ and μ tested at a Lock number $\gamma = 4.57$.

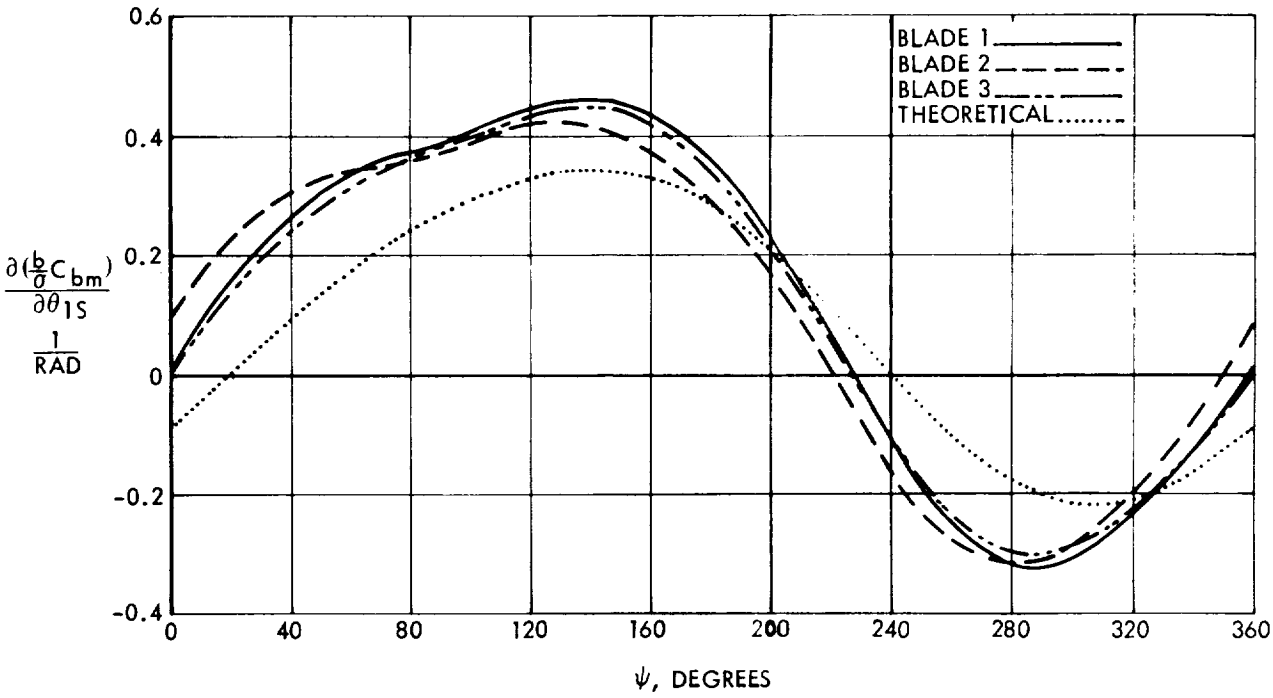

Figure 96. Blade Flap Bending Moment per Unit θ_{1s}, 33-Foot Rotor, μ = .399, P = 1.35, = 4.57. r/R = .217

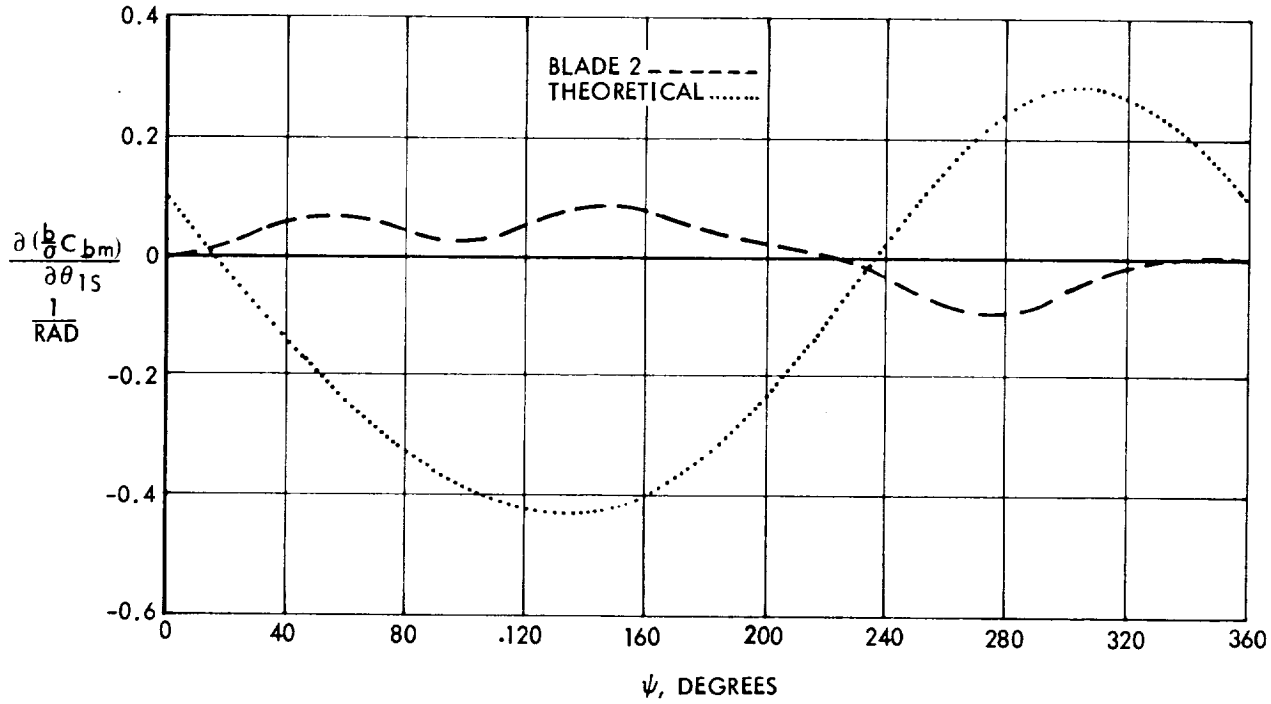

Figure 97. Blade Flap Bending Moments per Unit θ_{1s}, 33-Foot Rotor, μ = .399, P = 1.35, = 4.57. r/R = .596

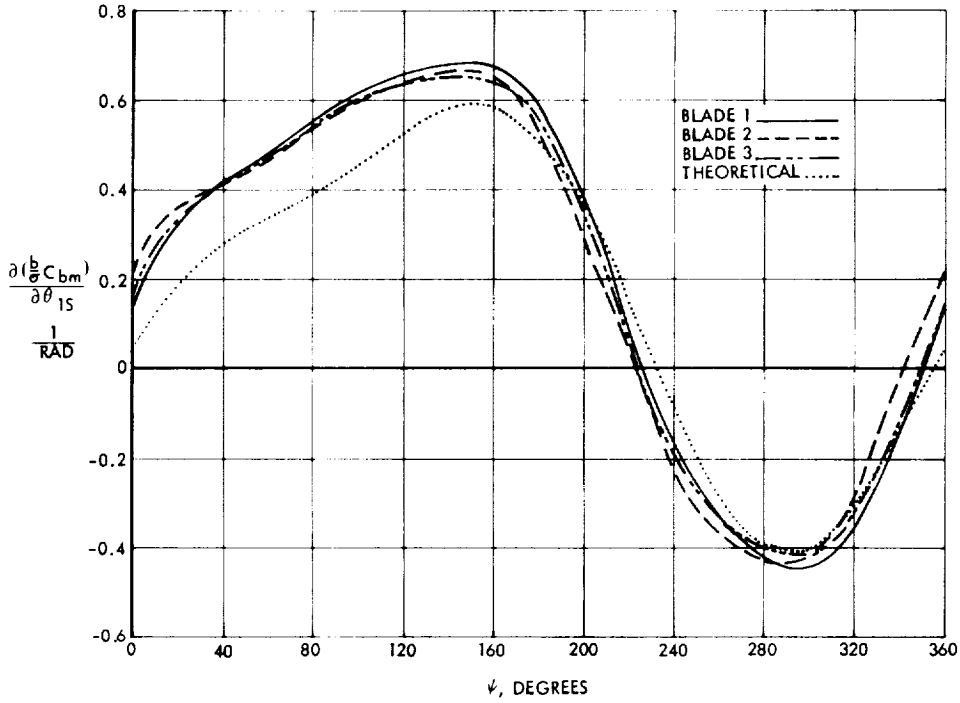

Figure 98. Blade Flap Bending Moment per Unit θ_{1s}, 33-Foot Rotor, μ = .528, P = 1.53, γ = 4.57. r/R = .217

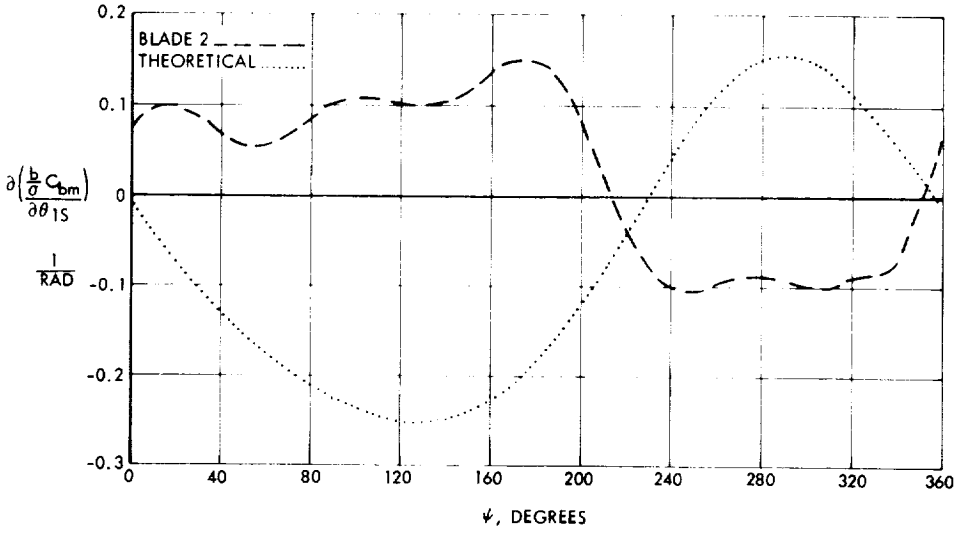

Figure 99. Blade Flap Bending Moment per Unit θ_{1s}, 33-Foot Rotor, μ = .528, P = 1.53, γ = 4.57. r/R = .596

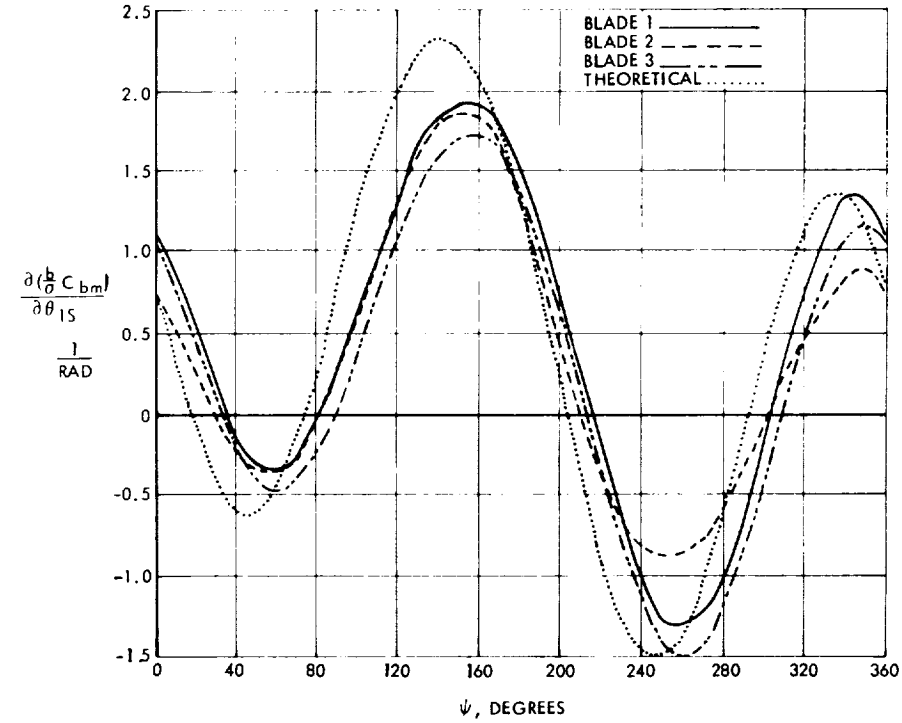

Figure 100. Blade Flap Bending Moment per Unit θ_{1s}, 33-Foot Rotor, μ = .808, P = 2.03, γ = 4.57. r/R = .217

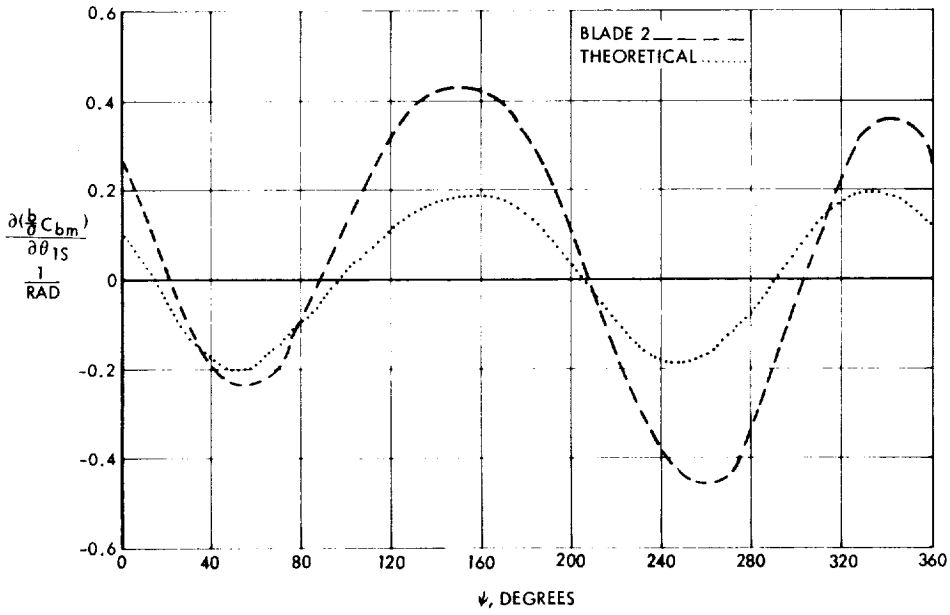

Figure 101. Blade Flap Bending Moment per Unit θ_{1s}, 33-Foot Rotor, μ = .808, P = 2.03, γ = 4.57. r/R = .596

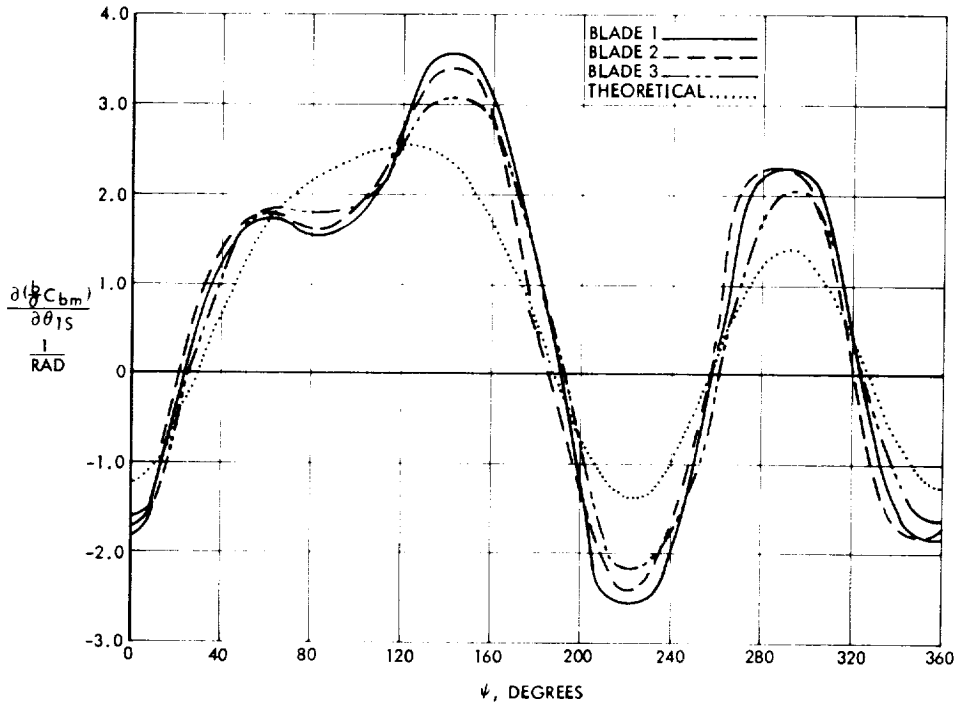

Figure 102. Blade Flap Bending Moment per Unit θ_{1s}, 33-Foot Rotor, μ = 1.121, P = 2.64, γ = 4.57. r/R = .217

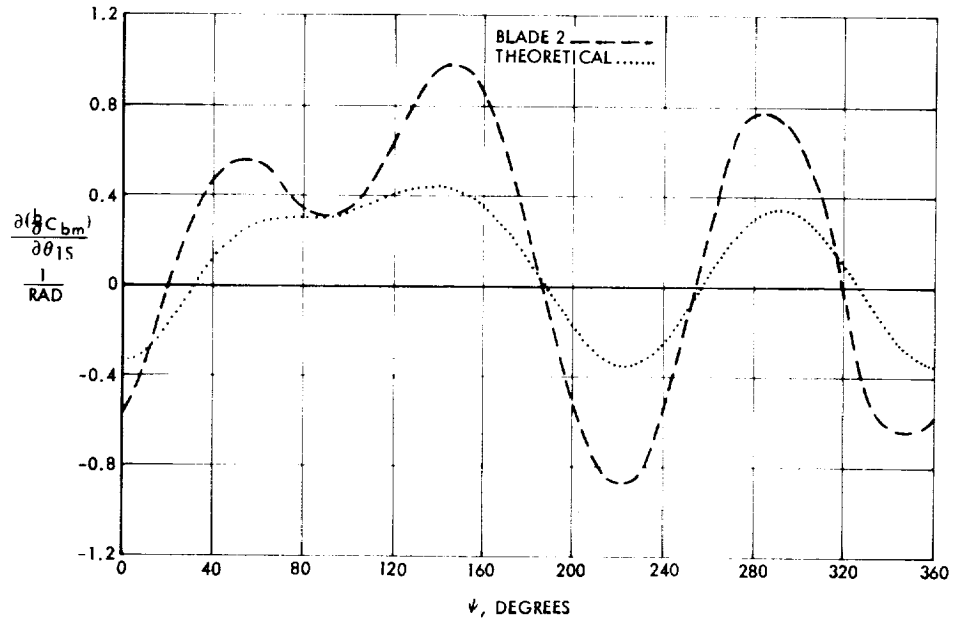

Figure 103. Blade Flap Bending Moment per Unit θ_{1s}, 33-Foot Rotor, μ = 1.121, P = 2.64, γ = 4.57. r/R = .596

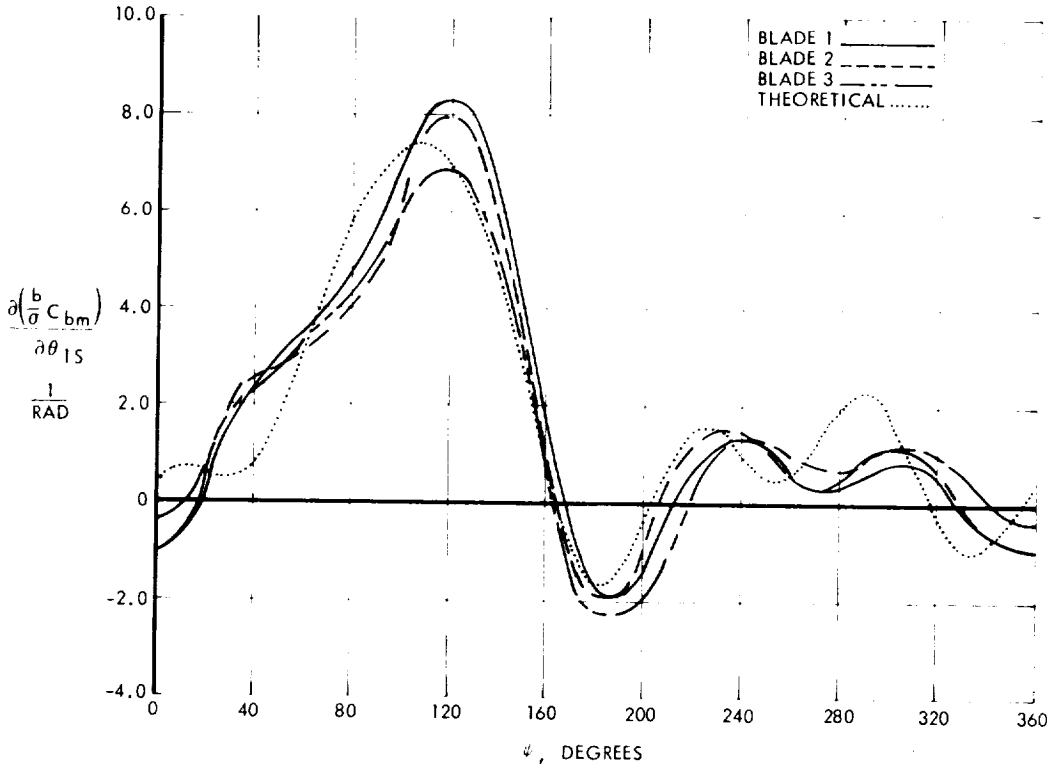

Figure 104. Blade Flap Bending Moment per Unit θ_{1s}, 33-Foot Rotor, $\mu = 2.132$, $P = 4.67$, $\gamma = 4.57$ $r/R = .217$

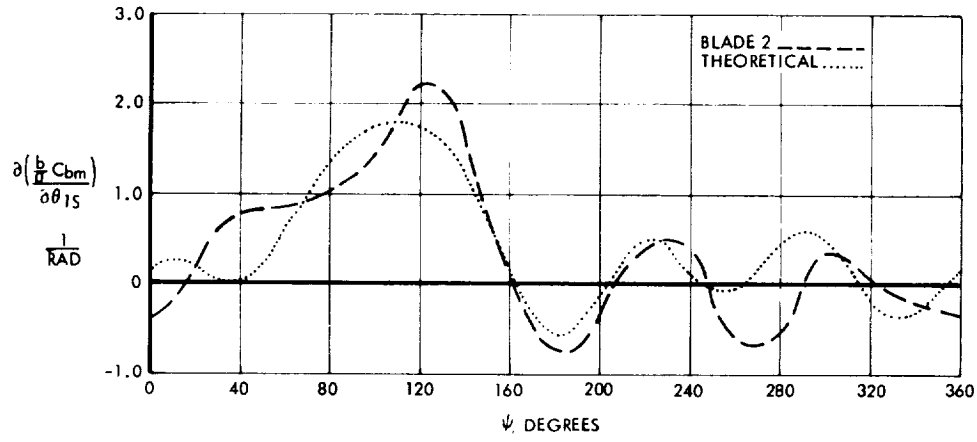

Figure 105. Blade Flap Bending Moment per Unit θ_{1s}, 33-Foot Rotor, $\mu = 2.132$, $P = 4.67$, $\gamma = 4.57$ $r/R = .596$

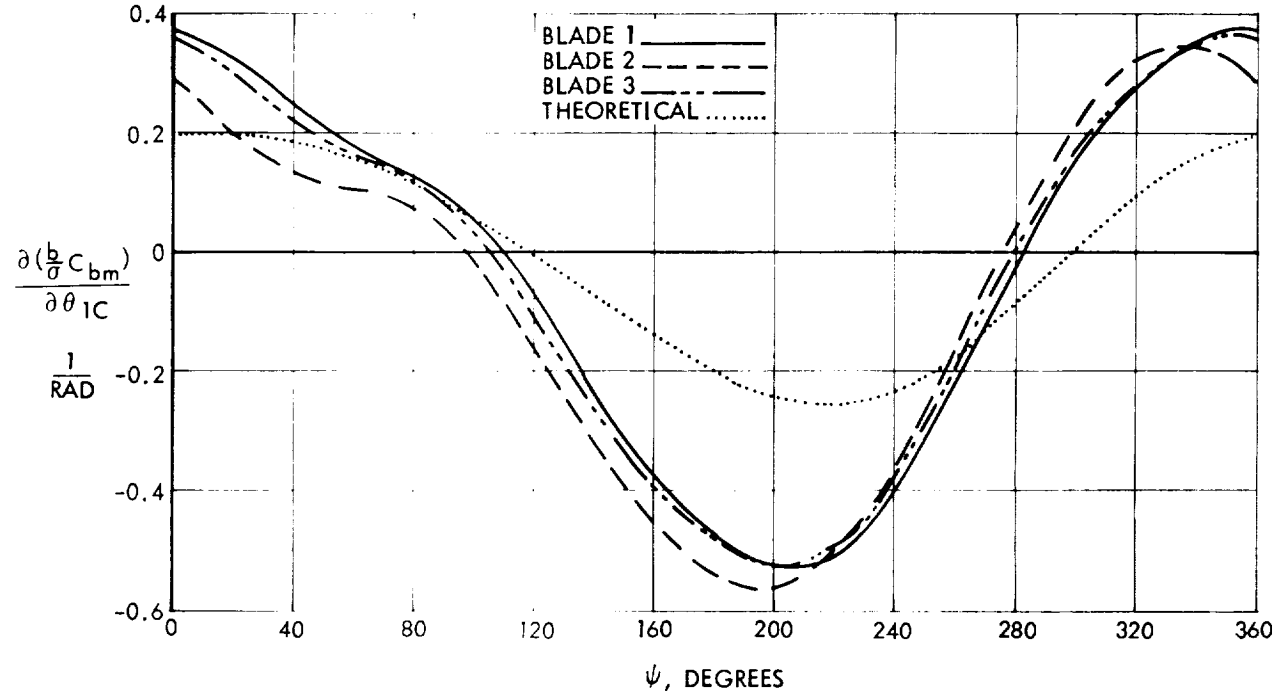

Figure 106. Blade Flap Bending Moment Per Unit θ_{1c}, 33-Foot Rotor, μ = .399, P = 1.35, γ = 4.57. r/R = .217

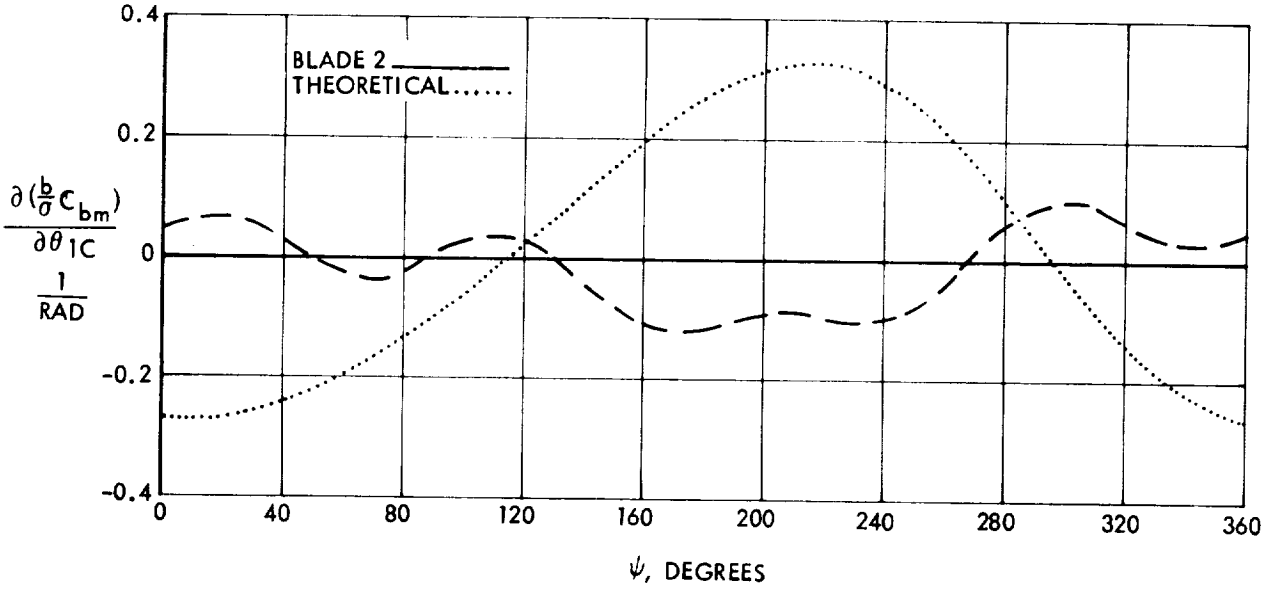

Figure 107. Blade Flap Bending Moments Per Unit θ_{1c}, 33-Foot Rotor, μ = .399, P = 1.35, γ = 4.57. r/R = .596

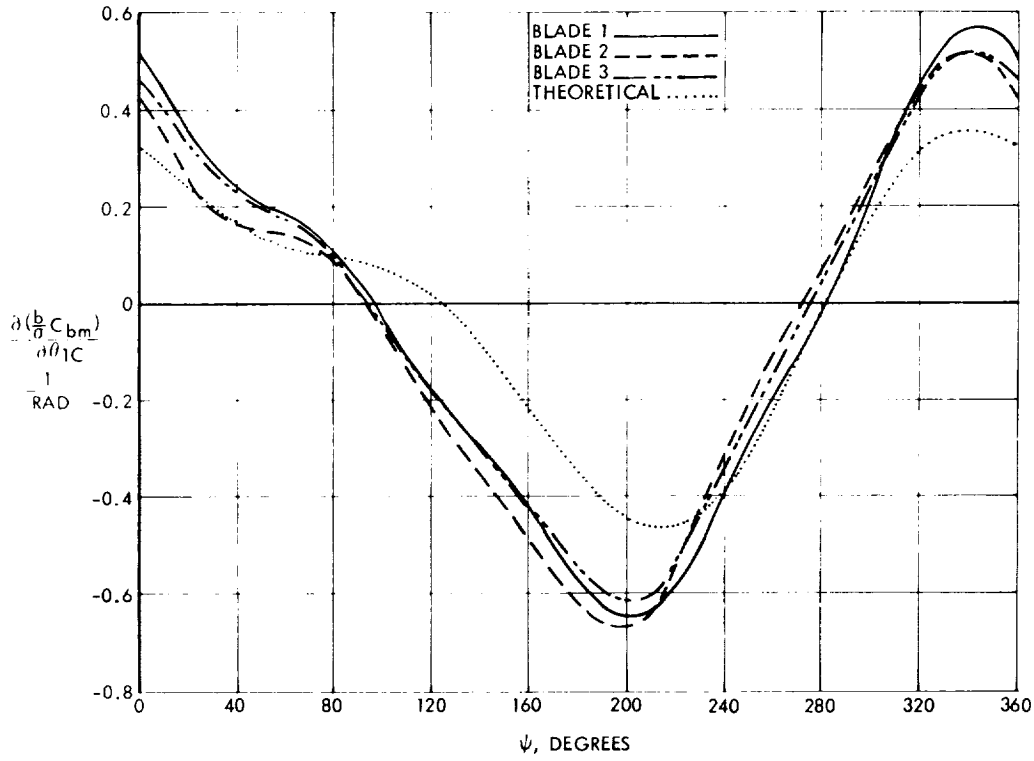

Figure 108. Blade Flap Bending Moments Per Unit θ_{1c}, 33-Foot Rotor, μ = .528, P = 1.53, γ = 4.57. r/R = .217

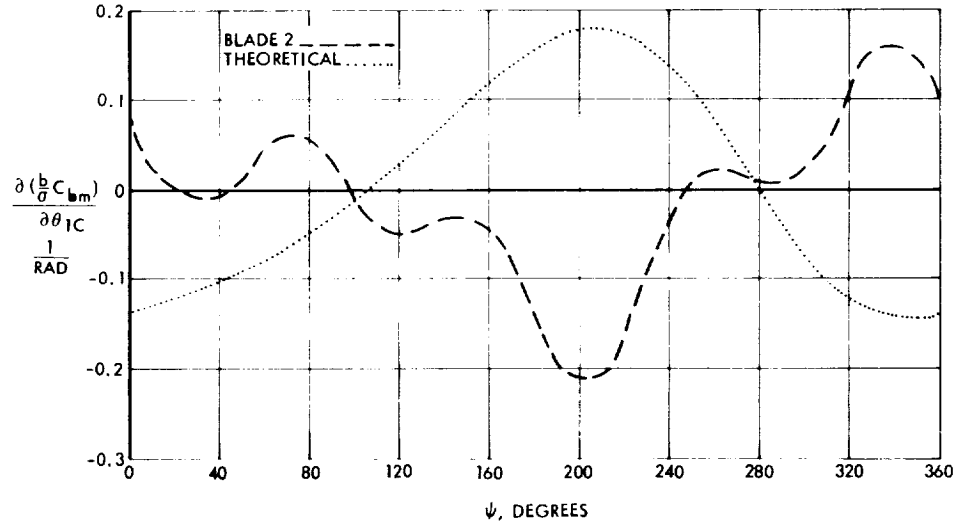

Figure 109. Blade Flap Bending Moments Per Unit θ_{1c}, 33-Foot Rotor, μ = .528, P = 1.53, γ = 4.57. r/R = .596

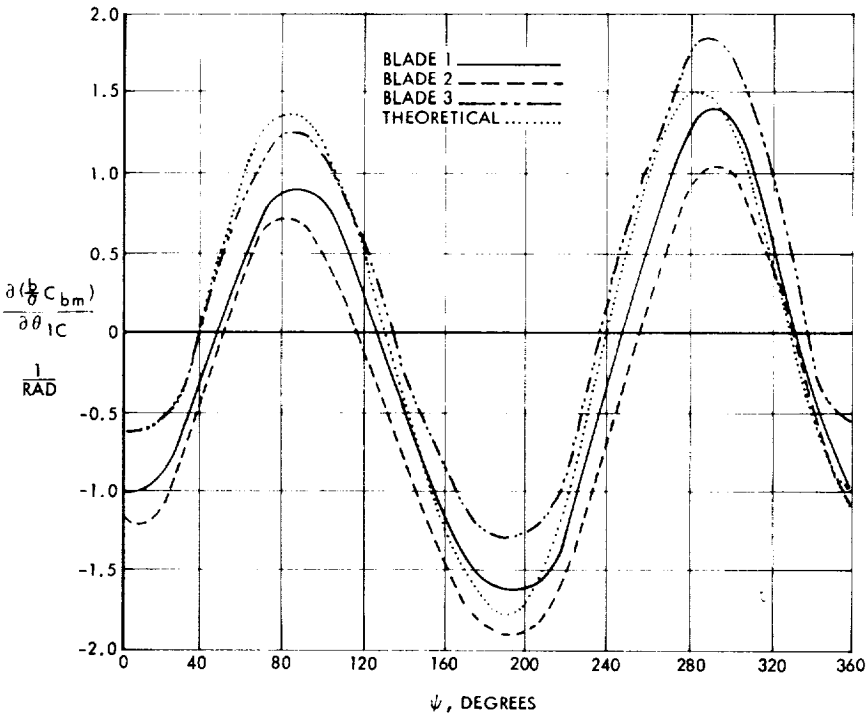

Figure 110. Blade Flap Bending Moments Per Unit θ_{1c}, 33-Foot Rotor, μ = .808, P = 2.03, γ = 4.57. r/R = .217

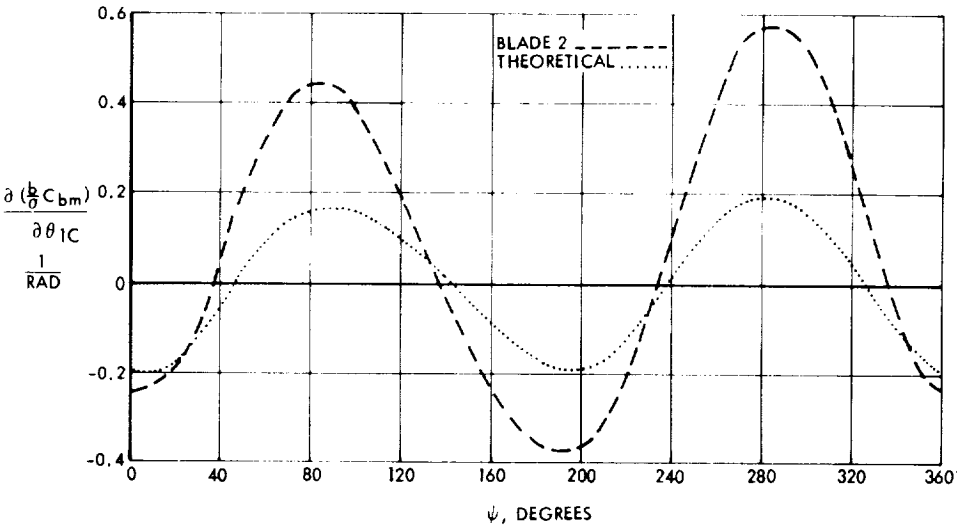

Figure 111. Blade Flap Bending Moments Per Unit θ_{1c}, 33-Foot Rotor, μ = .808, P = 2.03, γ = 4.57. r/R = .596

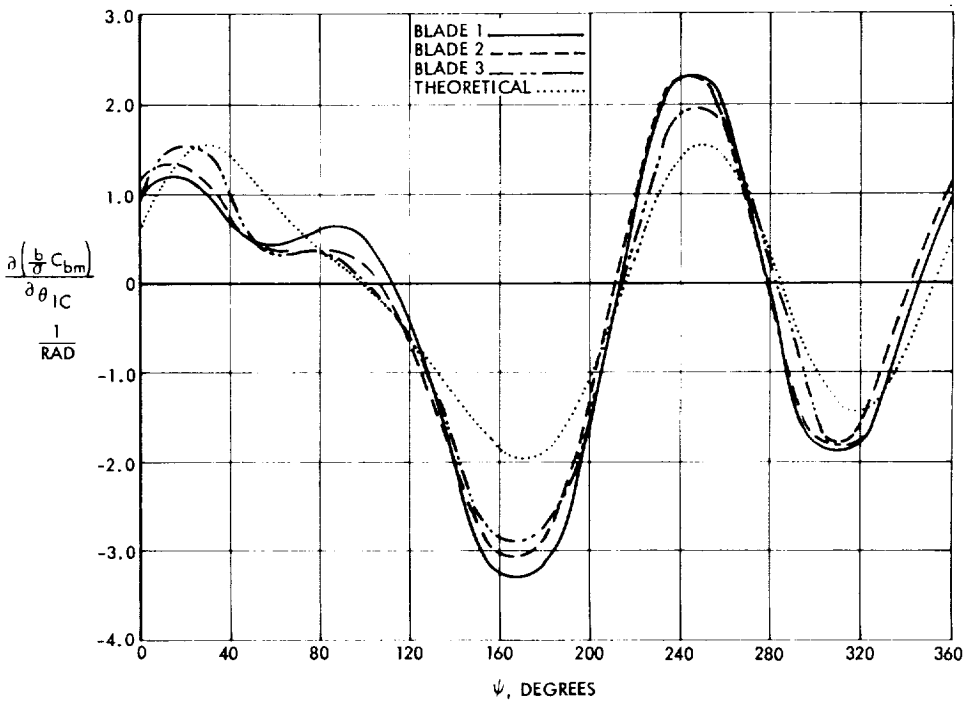

Figure 112. Blade Flap Bending Moments Per Unit θ_{1c}, 33-Foot Rotor, μ = 1.121, P = 2.64, γ = 4.57. r/R = .217

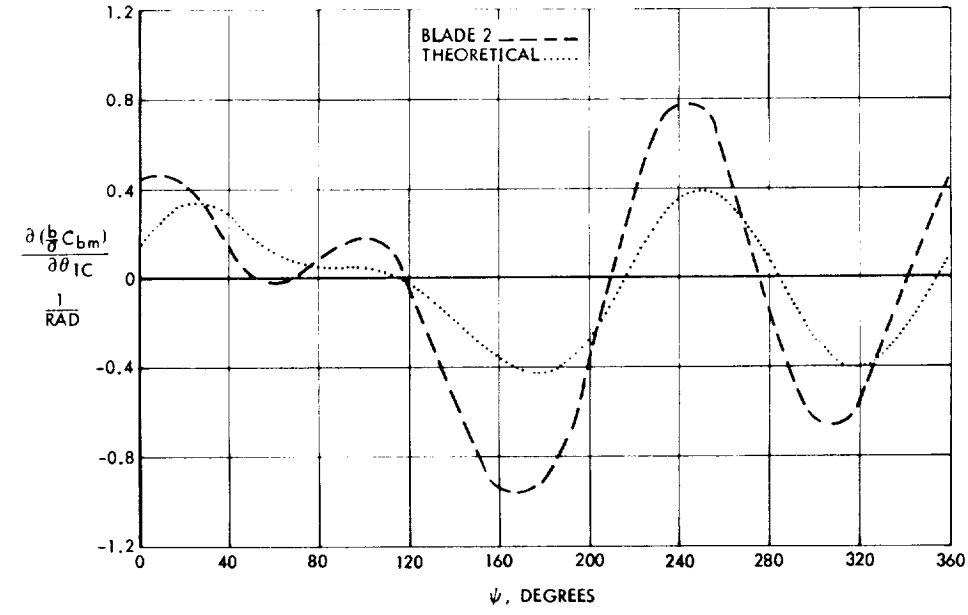

Figure 113. Blade Flap Bending Moments Per Unit θ_{1c}, 33-Foot Rotor, μ = 1.121, P = 2.64, γ = 4.57. r/R = .596

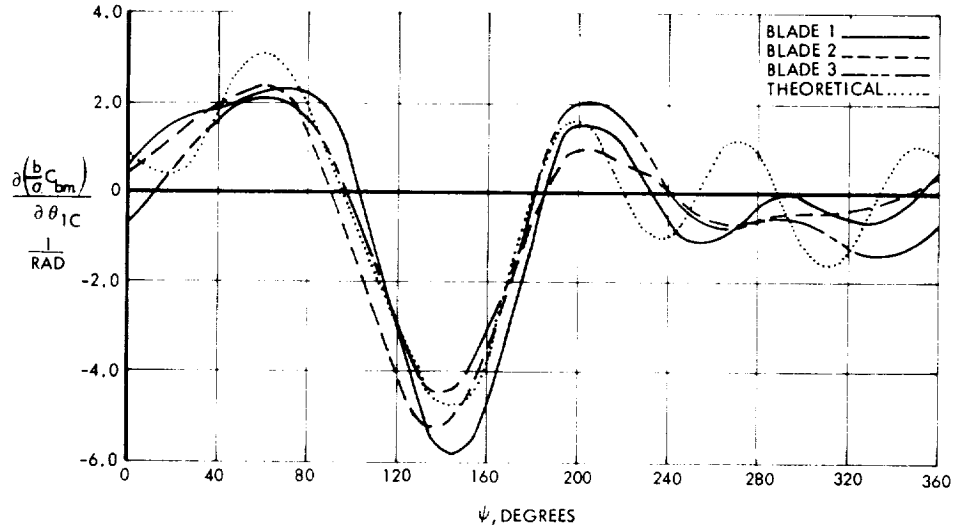

Figure 114. Blade Flap Bending Moments Per Unit θ_{1c}, 33-Foot Rotor, $\mu = 2.132$, $P = 4.67$, $\gamma = 4.57$. $r/R = .217$

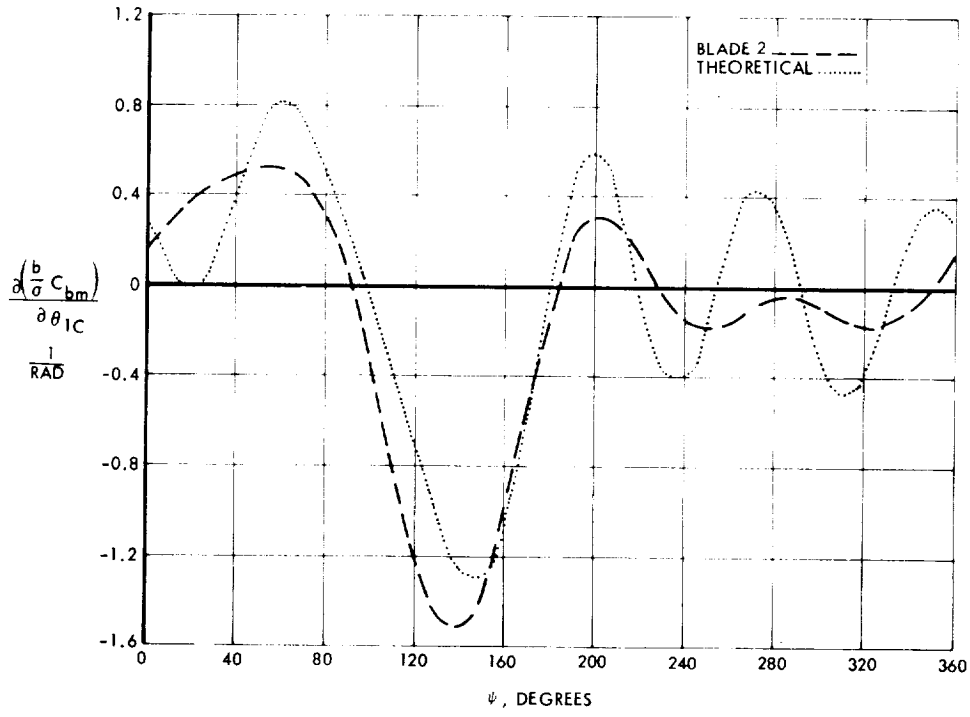

Figure 115. Blade Flap Bending Moments Per Unit θ_{1c}, 33-Foot Rotor, $\mu = 2.132$, $P = 4.67$, $\gamma = 4.57$. $r/R = .596$

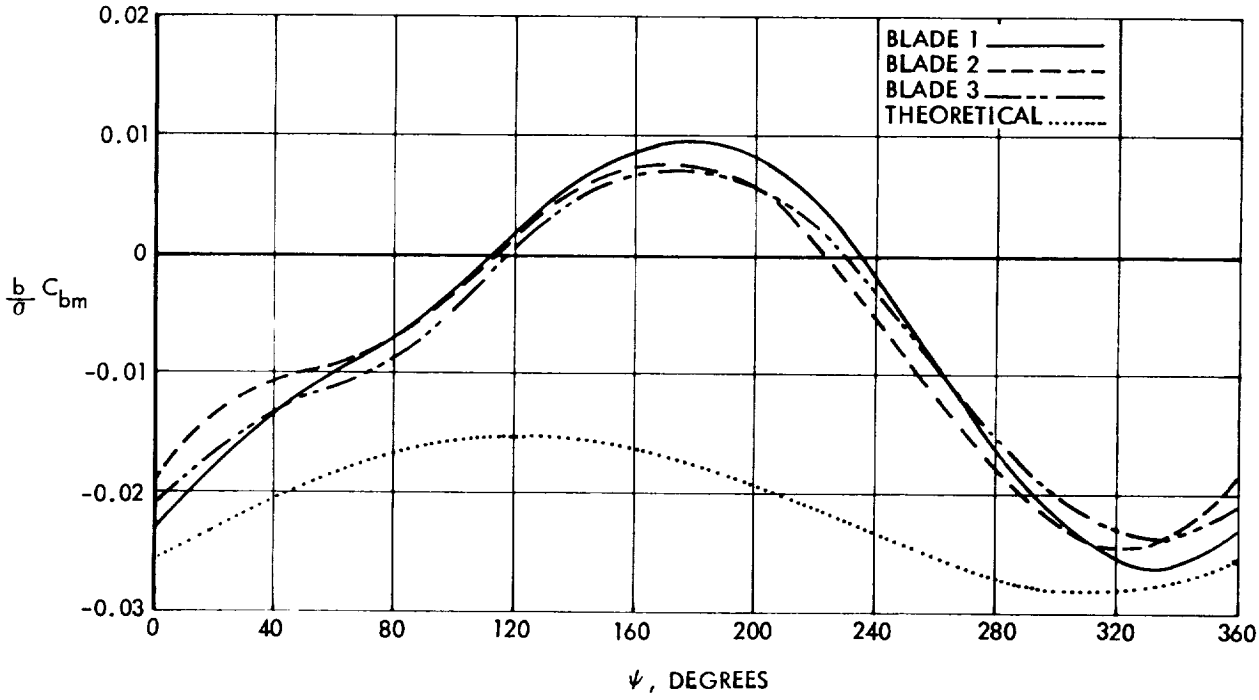

Figure 116. Blade Residual Flap Bending Moments, 33-Foot Rotor, μ = .399, P = 1.35, γ = 4.57. r/R = .217

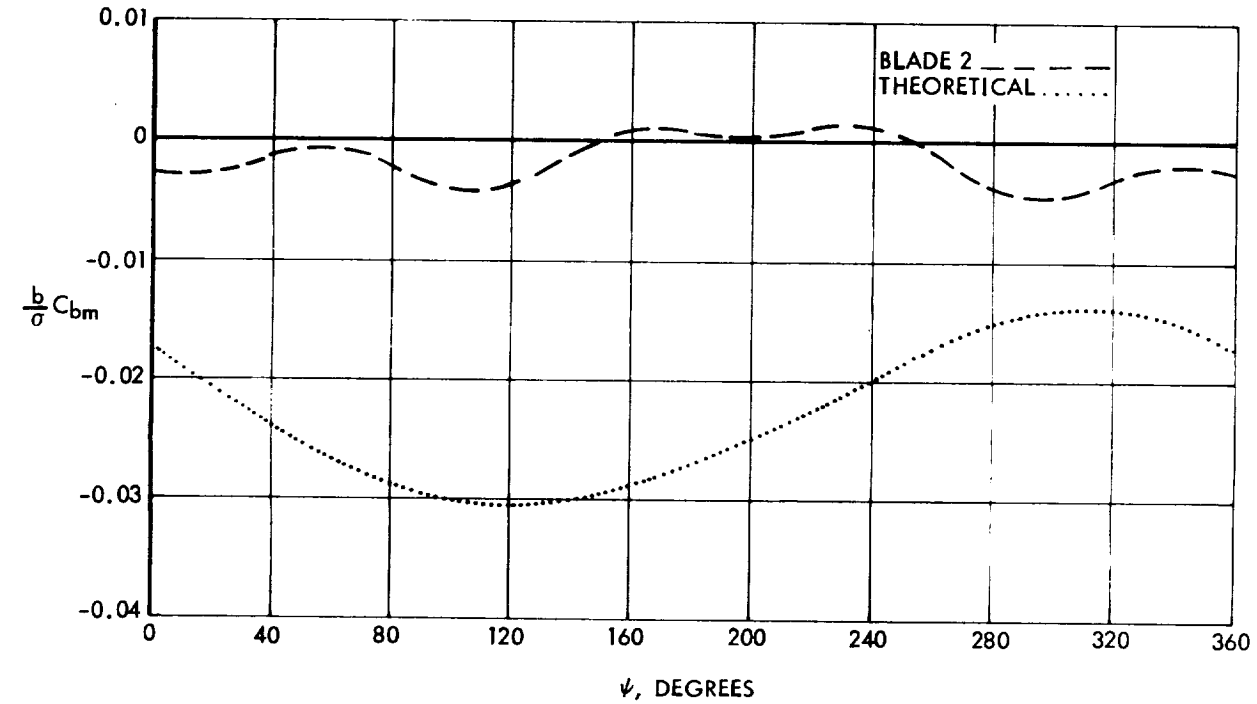

Figure 117. Blade Residual Flap Bending Moments, 33-Foot Rotor, μ = .399, P = 1.35, γ = 4.57. r/R = .596

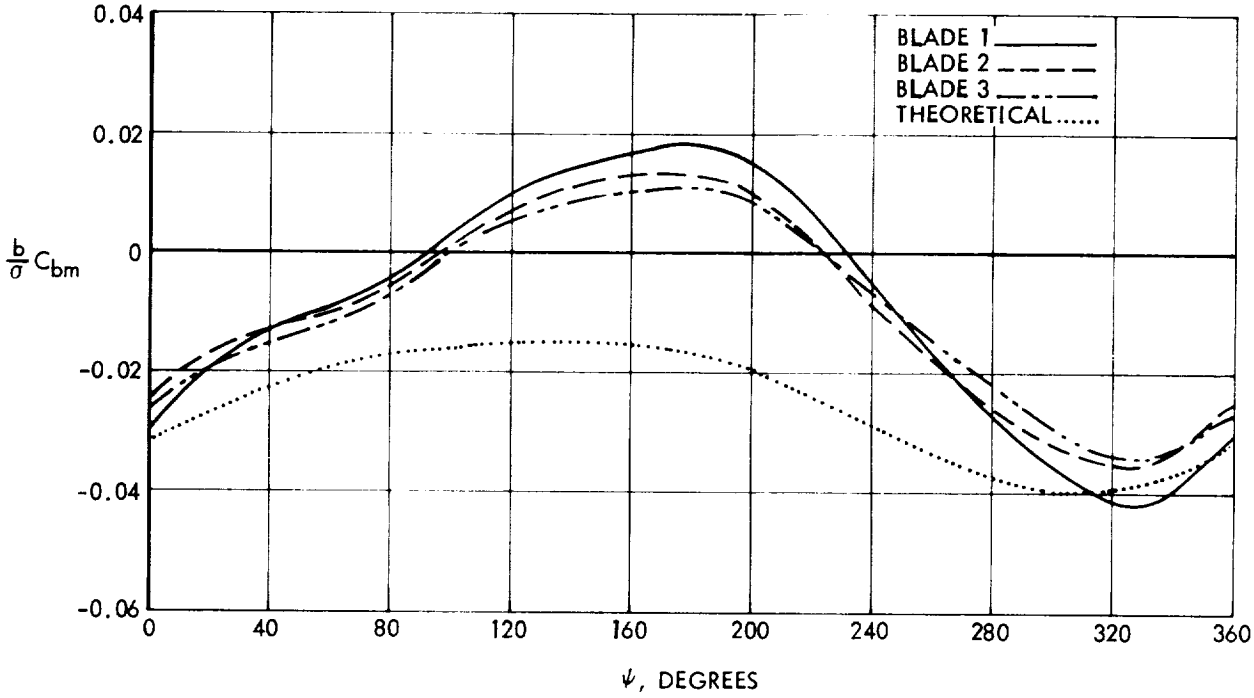

Figure 118. Blade Residual Flap Bending Moments, 33-Foot Rotor, μ = .528, P = 1.53, γ = 4.57. r/R = .217

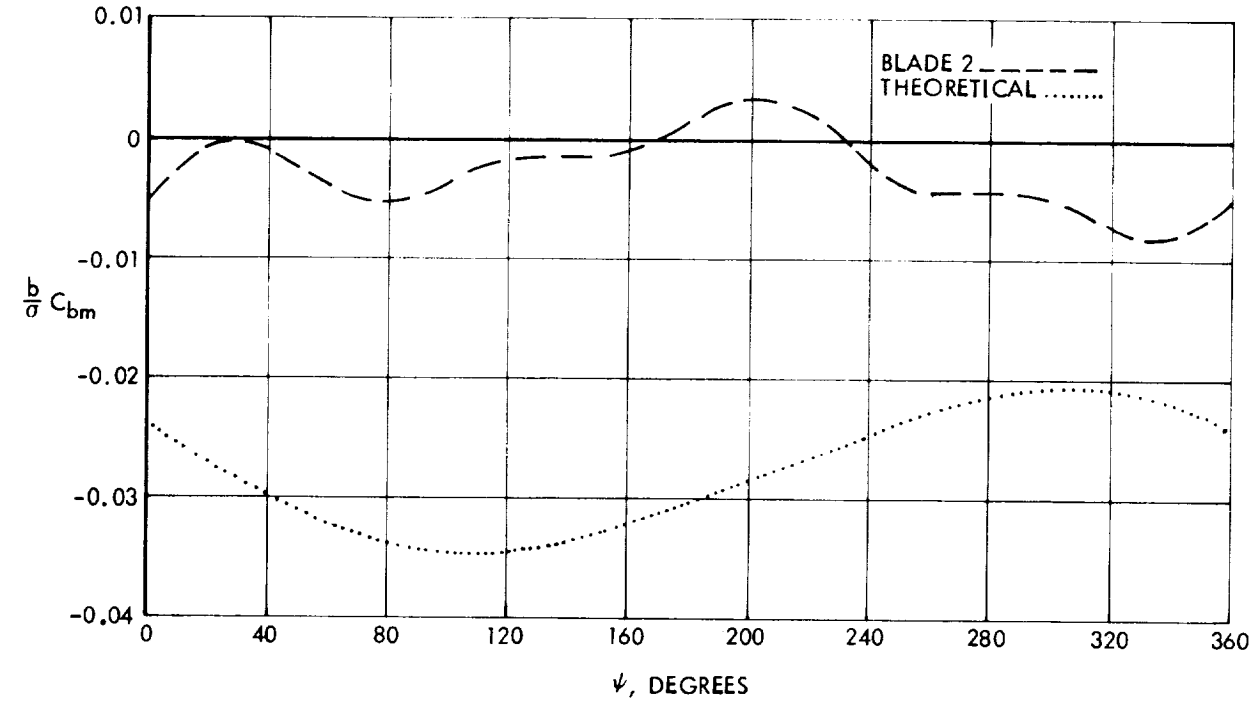

Figure 119. Blade Residual Flap Bending Moments, 33-Foot Rotor, μ = .528, P = 1.53, γ = 4.57. r/R = .596

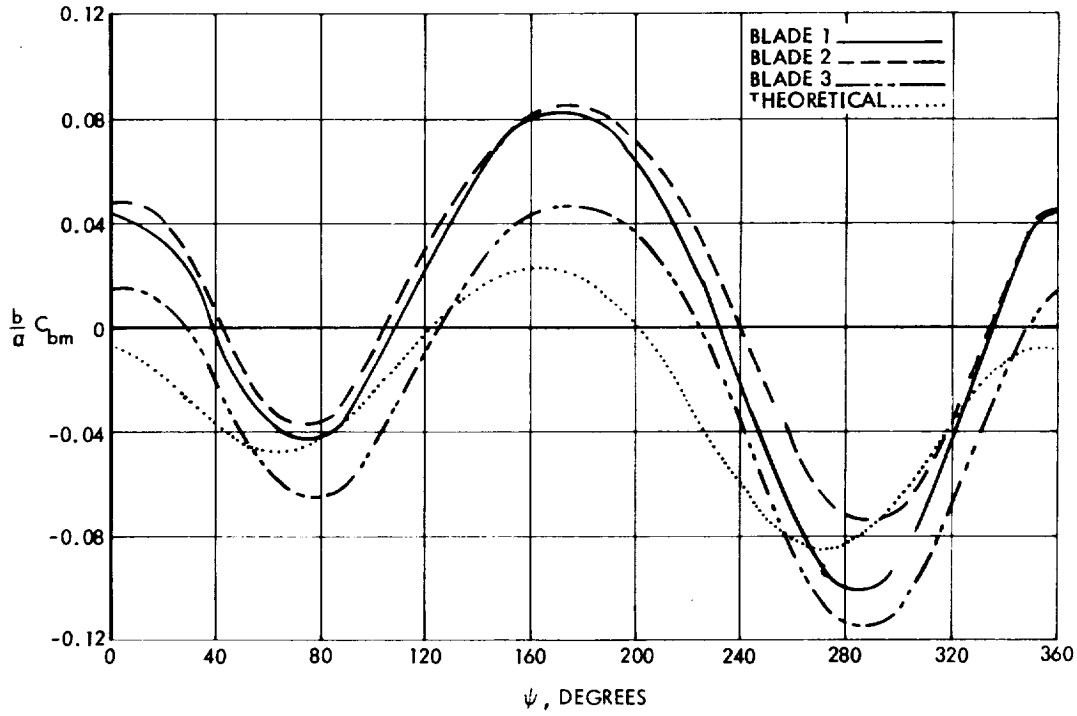

Figure 120. Blade Residual Flap Bending Moments, 33-Foot Rotor, μ = .808, P = 2.03, γ = 4.57. r/R = .217

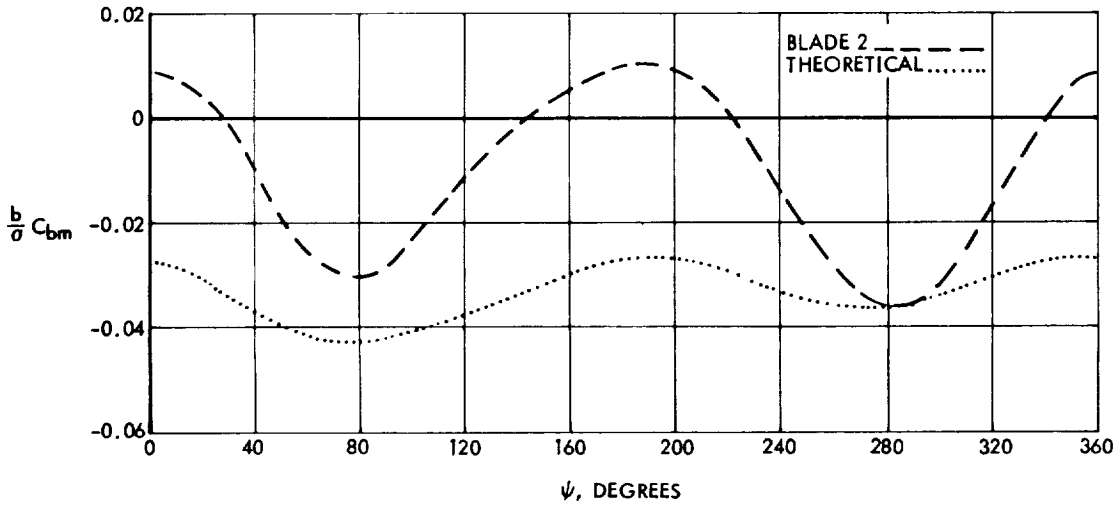

Figure 121. Blade Residual Flap Bending Moments, 33-Foot Rotor, μ = .808, P = 2.03, γ = 4.57. r/R = .596

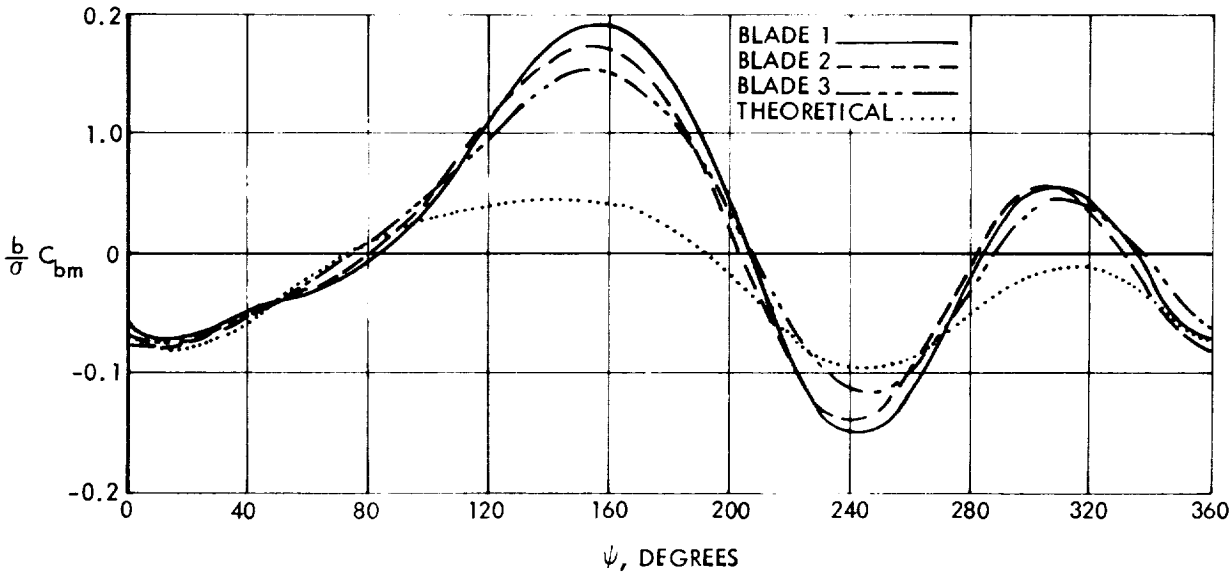

Figure 122. Blade Residual Bending Moments, 33-Foot Rotor, μ = 1.121, P = 2.64, γ = 4.57. r/R = .217

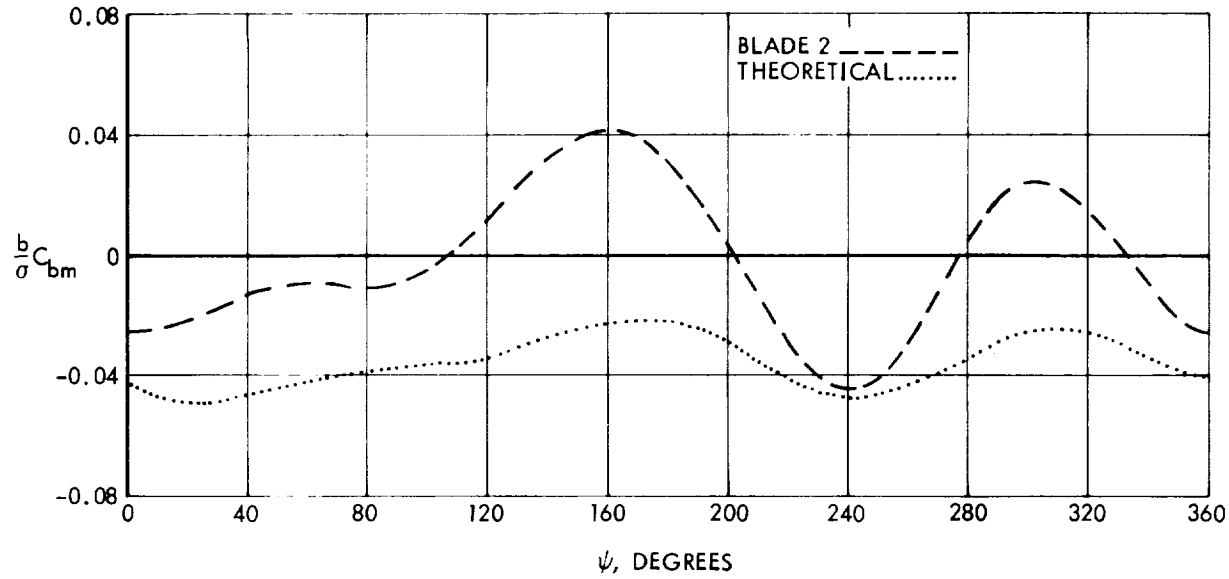

Figure 123. Blade Residual Bending Moments, 33-Foot Rotor, μ = 1.121, P = 2.64, γ = 4.57. r/R = .596

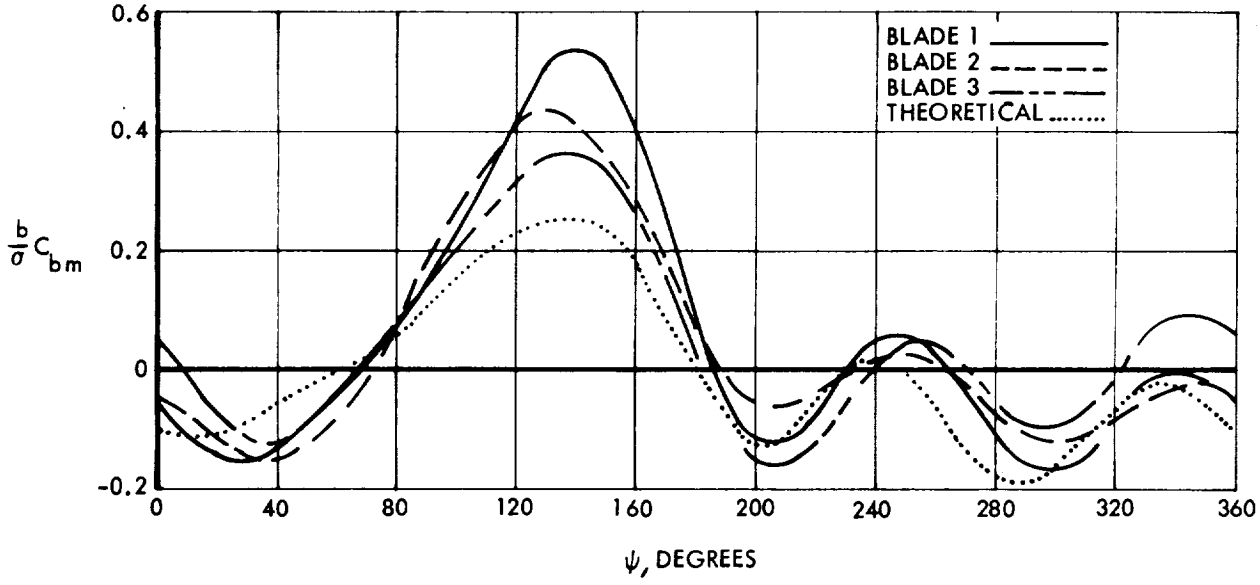

Figure 124. Blade Residual Flap Bending Moments, 33-Foot Rotor, $\mu = 2.132$, $P = 4.67$, $\gamma = 4.57$. $r/R = .217$

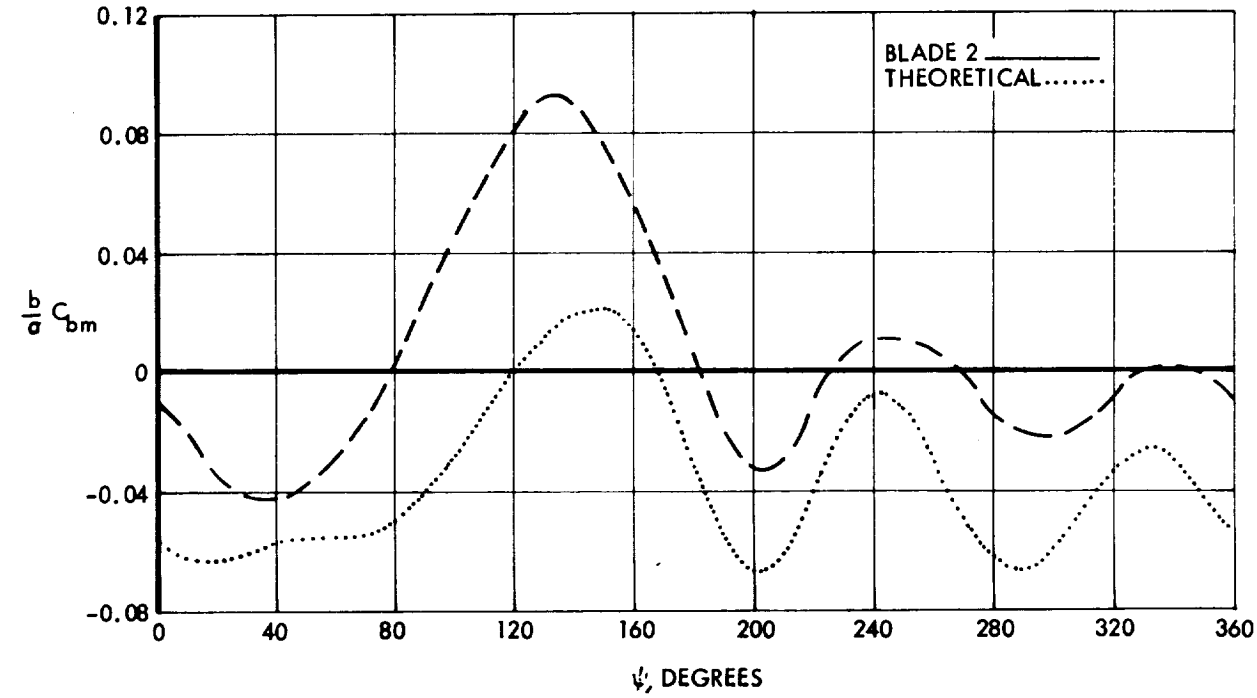

Figure 125. Blade Residual Flap Bending Moments, 33-Foot Rotor, $\mu = 2.132$, $P = 4.67$, $\gamma = 4.57$. $r/R = .596$

CONCLUDING REMARKS

1. A system of linear ordinary differential equations with periodically varying coefficients, forced by functions containing oscillation of the same period, has been derived to represent the flapping and associated motions of a hingeless rotor, free-swashplate, free-airframe configuration operating at advance ratio greater than .3 ($\mu > .3$) and with its ratio of blade flap frequency to rotor rotation rate greater than 1.3 ($P > 1.3$).

2. The system of equations has been solved for its steady oscillatory response to the periodic forcing produced by cyclic pitch, collective pitch and angle-of-attack, with some of its degrees of freedom suppressed. The shaft-transmitted moments obtained from the response were resolved into mean and oscillatory aeroelastic derivatives and approximately agreed with experimental data reduced and analyzed so as to provide equivalent derivatives.

3. Shaft moment oscillatory aeroelastic derivatives agreed best with experimental data when the blade natural flap frequency was in the vicinity of the two-per-revolution excitation, in rotating axes, for the three-blade rotor and in the vicinity of the three-per-revolution excitation for the four-blade rotor.

4. Omission of the harmonic components of the coefficients in the differential equation of vertical motion yielded approximately correct mean aeroelastic derivatives, at all values of flap frequency ratio provided the advance ratio was less than about .8 ($\mu < .8$).

At advance ratio greater than .8 omitting the periodic components of the coefficients caused the mean aeroelastic derivatives to be greatly in error.

5. In addition to shaft forces, the equations of motion have been solved for the azimuthal distribution of blade flapping bending moment. The bending moment distributives were computed for unit values of cyclic

pitch and compared with experimental distribution deduced from measured data in an equivalent form.

Despite the fact that blade flap bending moments are sensitive to the shape of deflection modes employed in the theory, and the theory of this report used only a single parabolic deflection degree of freedom, bending moment distributions calculated were quite similar to those deduced from the experimental data.

Blade root region flap bending was approximated correctly at all tested values of blade flap frequency ratio ($1.3 < P < 5$) at advance ratio greater than .5 ($\mu > .5$). Blade outer region bending moments, however, became realistic only at large values of flap frequency ratio ($P > 3$).

6. A set of linear ordinary differential equations describing the in-plane motion of hingeless rotor blade-hub-body-spring system were derived and applied to the 33-foot 3-blade rotor. Theoretical modal characteristics were compared with experimental.

Means of determining the in-plane forcing functions based on the motions and forces of the vertical equations were discussed.

REFERENCES

1. Ormiston, R.A. and Hodges, D.H., "Linear Flap-Lag Dynamics of Hingeless Helicopter Rotor Blades in Hover", Journal of the American Helicopter Society, April, 1972.

2. Watts, G.A., London, R.J., and Kokorowski, S.A., "Conversion Aerodynamics of the Horizontally Stoppable Rotor", Lockheed Report LR 23864, December, 1970.

3. Watts, G.A. and Biggers, J.C., "Horizontal Stoppable Rotor Conversion", Preprint 502, 27th Annual National AHS Forum, May, 1971.

4. Watts, G.A., London, R.J., and Snoddy, R.J., "Trim, Control, and Stability of a Gyro-Stabilized Hingeless Rotor at High Advance Ratio and Low Rotor Speed", NASA CR 114362, May, 1971.

5. Sissingh, G.J., "Dynamics of Rotors Operating at High Advance Ratios", Journal of the American Helicopter Society, July, 1968.

6. Sissingh, G.J., and Kuczynski, W.A., "Investigations at the Effect of Blade Torsion on the Dynamics of Flapping Motion", Journal of the American Helicopter Society, April, 1970.

7. Ormiston, R.A. and Peters, D.A., "Hingeless Rotor Response with Non-Uniform Inflow and Elastic Blade Bending — Theory and Experiment", AIAA paper 72-65, 10th Aerospace Sciences Meeting, January, 1972.

8. Heimbold, R.L. and Griffith, C.D., "Synthesis of an Electromechanical Control System for a Compound Hingeless Rotor Helicopter", Preprint No. 536, 27th Annual National AHS Forum, May, 1971.

9. Bartsch, E.A. and Sweers, J.E., "In-Flight Measurement and Correlation with Theory of Blade Airloads and Responses on the XH-51A Compound Helicopter Rotor" Volumes I, II and III, USAAVLABS Technical Report 68-22A, B & C, May, 1968.

10. Deckert, W.H., and McCloud, J.L., III "Considerations of the Stopped Rotor V/STOL Concept", Journal of the American Helicopter Society, January, 1968.

11. Gessow, A., and Myers, G.C. "Aerodynamics of the Helicopter" Frederick Ungar Publishing Co., New York, 1952.

12. Abbott, I.H., and Von Doenhoff, A.E., "Theory of Wing Sections" Dover Publications, New York, 1959.

13. Harris, F.D., Tarzanin, F.J., and Fisher, R.K. "Rotor High Speed Performance, Theory vs. Test", Proc. V/STOL Tech. and Planning Conference, Las Vegas, 1969.

14. Fung, Y.C., "The Theory of Aeroelasticity", John Wiley and Sons, Inc. New York.

15. Donham, R.E.; Watts, G.A.; Cardinale, S.V., "Dynamics of a Rigid Rotor Controlled by a High-Speed Gyro as it Slows/Stops at High Forward Speed," Preprint No. 343, 25th Annual National AHS Forum, May 1969.

16. Sissingh, G.J., "Dynamic Characteristics of Dual Speed Gyros" Lockheed Report LR 24298, January, 1971.

17. Kulzynski, W.A. and Sissingh, G.J. "Research Program to Determine Rotor Response Characteristics at High Advance Ratios" Lockheed Report LR 24122, February 1971.